Numerical, Analytical and Experimental Analysis of Combined Extrusion Forging Processes Applied to Collet Chuck Holders

Srikar Potnuru

Department of Mechanical Engineering
National Institute of Technology Rourkela

Numerical, Analytical and Experimental Analysis of Combined Extrusion Forging Processes Applied to Collet Chuck Holders

Dissertation submitted in partial fulfilment

of the requirements of the degree of

Doctor of Philosophy

in

Mechanical Engineering

by

Srikar Potnuru

(Roll No. 512ME121)

Based on research carried out

under the supervision of

Prof. Susanta Kumar Sahoo

and

Prof. Santosh Kumar Sahoo

Department of Mechanical Engineering
National Institute of Technology Rourkela
December 2016

Department of Mechanical Engineering
National Institute of Technology Rourkela

December 07, 2016

Declaration of Originality

Roll Number: 512ME121

Name: *Srikar Potnuru*

Title of Dissertation: *Numerical, analytical and experimental analysis of combined extrusion forging processes applied to collet chuck holders*

We the below signed, after checking the dissertation mentioned above the official record book (s) of the student, hereby state our approval of the dissertation submitted in partial fulfilment of the requirements for the degree of *Doctor of Philosophy* in *Mechanical Engineering* at *National Institute of Technology Rourkela.* We are satisfied with the volume, quality, correctness and originality of the work.

Prof. Santosh Kumar Sahoo Co-supervisor	Prof. Susanta Kumar Sahoo Principal Supervisor
Prof. Chandan Kumar Biswas Member, DSC	Prof. Saroj Kumar Patel Member, DSC
Prof. Archana Mallick Member, DSC	External Examiner Prof. Pinaki Talukdar NIFFT, Ranchi
Prof. Kalipada Maity Member, DSC	Head of the Department Prof. Siba Sankar Mohapatra

Department of Mechanical Engineering
National Institute of Technology Rourkela

Prof. Susanta Kumar Sahoo
Professor

Prof. Santosh Kumar Sahoo
Assistant Professor

December 07, 2016

Supervisors' Certificate

This is to certify that the work presented in this dissertation entitled "Numerical, analytical and experimental analysis of combined extrusion forging processes applied to collet chuck holders" by "*Srikar Potnuru*", Roll Number 512ME121, is a record of original research carried out by him under our supervision and guidance in partial fulfilment of the requirements of the degree of *Doctor of Philosophy in Mechanical Engineering*. Neither the thesis nor any part of it has been submitted for any degree or diploma to any institute or university in India or abroad.

Santosh Kumar Sahoo
Assistant Professor
(Co-supervisor)

Susanta Kumar Sahoo
Professor
(Principal Supervisor)

Dedicated to My Parents
Kasi Viswanatham and Susila

Declaration of Originality

I, Srikar Potnuru, Roll Number 512ME121 hereby declare that this thesis dissertation entitled Numerical, analytical and experimental analysis of combined extrusion forging processes applied to collet chuck holders presents my original work carried out as a doctoral student of NIT Rourkela and, to the best of my knowledge, it contains no material previously published or written by another person, nor any material presented for the award of any other degree or diploma of NIT Rourkela or any other institution. Any contribution made to this research by others, with whom I have worked at NIT Rourkela or elsewhere, is explicitly acknowledged in the dissertation. Works of other authors cited in this dissertation have been duly acknowledged under the sections ‘‘Reference’’ or "Bibliography". I have also submitted my original research records to the scrutiny committee for evaluation of my dissertation.

I am fully aware that in case of any non-compliance detected in future, the Senate of NIT Rourkela may withdraw the degree awarded to me on the basis of the present dissertation.

December, 2016 *Srikar Potnuru*
NIT Rourkela

ACKNOWLEDGEMENTS

I would like to express my sincere appreciation to my Supervisor, **Dr. Susanta Kumar Sahoo**, Mechanical Engineering Department, National Institute of Technology Rourkela. I am really thankful to Prof. Sahoo for the way he taught me to be cool and explore the depths of research, and standing by during tough times at work. I am grateful to his unwavering support and inspiration. I am also thankful to him for giving me sufficient time so I could perform to my best level. I would also like to thank my Co-supervisor **Dr. Santosh Kumar Sahoo**, Metallurgical and Materials Engineering Department, National Institute of Technology, Rourkela for his constant guidance and encouragement without which this work would not have been possible.

I would also like to extend my sincere gratitude to **Prof. S. S. Mahapatra**, Head of the Department, Mechanical Engineering, National Institute of Technology Rourkela for his constant guidance and support.

I am also thankful to Lab. technicians **Mr. Kumar**, **Mr. Ali**, **Mr. S. Murmu**, **Mr. S.S. Samal** and **Mr. R.N. Jena** for their guidance at central workshop. Mr. Bhanjo Naik, Mr. Tanti and Mr. Amit for their technical guidance/in conducting Optical Microscopy.

I am ever thankful to my senior **Mr. Sushant kumar sahoo** for helping me and providing necessary insight during experimentation. I am thankful to **Mr Rudra Narayana Kandi** for his support during Numerical analysis. I feel grateful to have juniors like **Mr. Raviteja Vinjamuri**, **Mr. B.A.G Yuvaraju** and **Mr. Tukuraj Tudu** who have helped me during experimental analysis. I use this opportunity to express my deep sense of gratitude to my friends **Mr. Racha Harish**, **Mrs Rukmini Dey**, **Mr. Vivekananda Kukkala**, **Mr. D. Narsimhachary**, **Mr. K Anand Babu**, **Mr. Muddu Alaparthi**, **Mr. S Sravan Kumar**, **Mr. V.B. Shaibu**, **Mr. Bikash Ranjan Moharana**, **Mr. Mantra Prasad Satpathy**, **Mr. Kasinath Mohapatra** and **Mr. Trinath Talapaneni**, **Ms. Sharmila** and **Ms. Chandran** for their support in my difficult times.

I am really thankful to my family in particular my parents deserve a special mention for mammoth support and standing with me during my hard times. Words fail me to express my appreciation to my siblings **Mr Himakar Potnuru**, **Mrs. Sharath Dhruthi Kodam** and **Mr. Sri Harsha Potnuru** for their understanding, patience and active cooperation throughout the course of my doctoral dissertation. I thank them for being supportive and caring.

Thanks are due to my co-scholars at NIT Rourkela for their constant encouragement during my research period.

I am forever indebted to my parents who work and live for my well-being.

Srikar Potnuru

Abstract

The material flow in the combined extrusion/forging process is an important phenomenon which controls the mechanical and metallurgical properties of any manufactured component. Collet chuck holder is a tool holding device used in different types of CNC milling machines. The chuck holder is described by a flange at the middle to fit into the machine, taper portion which is conical shaped area present at the bottom which enters the spindle for changing holder and collet pocket which fits the collet for holding the cutting tool. For manufacturing the tool holder an enormous amount of material is being wasted by the machining process which is almost equal to the volume of the product. Some manufacturer use casting, subsequently by machining to get the final shape. Both the used processes have their limitations as discussed earlier. To secure our material resources and to get better mechanical properties it is proposed to adopt the combined extrusion/forging and/or multi-stage processes for the production of different types of collet chuck holders.

In general, it is found challenging to predict the metal flow by 3D combined extrusion/forging process of complicated sections, collet chuck holder in particular, due to its complexity nature of analysis. From experiments it is observed that the complete process to get the first three components can be assumed to compose of four stages and fourth one of two stages with regard to forward/backward extrusion, forging, die corner filling, and flash formation. The mechanical, microscopic, micro hardness and residual stress analyses are performed for all the four components manufactured under different frictional conditions and ram velocities. The results confirm the advantage of the proposed processes to manufacture collet chuck holder. In the present investigation, upper bound method is used to analyze the combined extrusion/forging process of different types of collet chuck holders. A set of kinematically admissible velocity field is proposed to predict the metal flow pattern and the forging load. This work also employed 3D finite element formulation to simulate the combined extrusion/forging process for axisymmetric collet chuck holders. The forming loads obtained by proposed upper bound technique is in good agreement with the numerical and experimental results and lies in the range of 0-15%, 5-20%, 0-15% and 12-20% for first, second, third and fourth products respectively.

Experimental observations indicate that the collet chuck holder can be effectively manufactured by metal forming route of combined and/or multi-stage extrusion/forging to

get its inherent advantages instead of following the present practice of machining and/or casting. The estimated loads obtained using proposed kinematically admissible velocity fields effectively take care of work hardening, friction effects and redundant work and are remain within engineering accuracy when compared with that obtained from FEA and experiments. The results confirm the suitability of the proposed techniques (FEA and upper bound) for the prediction of load in combined extrusion-forging processes studied in the present work applied to collet chuck holder.

Keywords: ***CEF; material flow; finite element; UBET; microscopy; micro hardness and residual stress***

Contents

Certificate of Examination **ii**

Supervisor's Certificate **iii**

Dedication **iv**

Declaration of Originality **v**

Acknowledgment **vi**

Abstract **vii-viii**

List of Figures **xii-xvii**

List of Tables **xviii-xix**

Nomenclature **xi-xxi**

1 Introduction **1**

1.1 Backgrounds 1

1.1.1 Different types of extrusion processes 1

1.1.2 Different types of forging processes 4

1.1.3 Combined extrusion forging processes 6

1.2 Existing Manufacturing & Modern Industry Demand 7

1.3 Conventional Dies 8

1.3.1 Types of Dies 8

1.4 The Present Problem 9

1.4.1 Importance of the problem 10

1.4.2 Combined extrusion-forging processes in the present problem 11

1.5 Research Objective 11

1.6 Outline of Thesis 12

1.7 Closure 13

2 Literature Review **14**

2.1 Introduction 14

2.2 Previous Work 14

2.2.1 Numerical analysis 14

2.2.2 Experimental analysis 18

2.2.3 Analytical analysis 22

2.2.4 Tribological analysis 26

2.3 Research Gaps Identified from the Literature Review 29

2.4 Novelty of the Present Investigations and Methodology 30

2.5 Summary 31

3 Solutions to Metal Forming Problems 33

3.1 Introduction 33

3.2 Solution of a Plastic Deformation Problem 33

3.3 Techniques for Deriving the Kinematically Admissible Velocity Fields in 3-D Metal Deformation Problems 39

3.3.1 Dual stream function method 40

3.3.2 Conformal transformation technique 40
3.3.3 Generalized velocity field technique 41
3.3.4 The SERR technique 42
3.4 The Continuity Condition of a Discontinuous Velocity Field 42
3.5 Solution of a Plane Strain Problem 44
3.6 Closure 48

4 Analytical Analysis 49
4.1 Introduction 49
4.2 Modelling of the Process 50
4.3 Analysis of Single Collet Chuck Holder by CEF Process 51
4.3.1 Kinematically admissible velocity fields for stage I 52
4.3.2 Kinematically admissible velocity fields for stage II 55
4.3.3 Kinematically admissible velocity fields for stage III 57
4.3.4 Kinematically admissible velocity fields for stage IV 60
4.4 Analysis of Double Collet Chuck Holder by CEF Process 61
4.5 Analysis of Double Collet Chuck Holder by CE Process 67
4.6 Analysis of Single Collet Chuck Holder by Multi-stage Extrusion/forging Process 71
4.7 Upper Bound Solution 74
4.7.1 Internal power, W_P 74
4.7.2 Shear power, W_S 75
4.7.3 Friction power, W_f 78
4.8 Results and Discussion 80
4.8.1 CEF process for single collar collet chuck holder 80
4.8.2 CEF process for double collar collet chuck holder 82
4.8.3 CEF process for double collar collet chuck holder 84
4.8.4 Multi-stage extrusion/forging process for single collar collet chuck holder 86
4.9 Conclusions 87

5 Numerical Analysis 89
5.1 Introduction 89
5.2 Modelling of the System 90
5.2.1 Interface formulation 91
5.2.2 Simulation control 92
5.2.3 Simulation modelling 92
5.2.4 Formulation 93
5.2.5 Simulation for the present problem 94
5.3 Results and Discussions of the Simulations 98
5.3.1 CEF process for single collar collet chuck holder 98
5.3.2 CEF process for double collar collet chuck holder 107
5.3.3 CEF process for double collar collet chuck holder 116
5.3.4 Multi-stage extrusion of single collar collet chuck holder 125
5.4 Conclusions 128

6 Experimental Analysis 130
6.1 Introduction 130
6.2 The Test Rig 131

6.3 Dies 133
6.4 Specimen 134
6.5 Experimental Procedure 134
6.6 Stress-Strain Characteristics of Specimen Al 1070 135
6.7 Ring Test for Determination of Friction Factor 137
6.8 Manufacturing of Collet Chuck Holders 139
6.9 Results and Discussions of Experimental Analysis 140
6.9.1 CEF process for single collar collet chuck holder 140
6.9.2 CEF process for double collar collet chuck holder 155
6.9.3 CEF process for double collar collet chuck holder 166
6.9.4 Multi-stage extrusion of single collar collet chuck holder 177
6.10 Conclusions 182

7 Comparison of Results and Discussion 183
7.1 Introduction 183
7.2 Comparison of Results for SCCCH by CEF Process 183
7.2.1 Metal flow pattern at different punch movements 187
7.2.2 Deformed product shape at different punch movements 188
7.3 Comparison of Results for DCCCH by CEF Process 188
7.3.1 Metal flow pattern at different punch movements 190
7.3.2 Deformed product shape at different punch movements 191
7.4 Comparison of Results for DCCCH by CE Process 192
7.4.1 Metal flow pattern at different punch movements 194
7.4.2 Deformed product shape at different punch movements 194
7.5 Multistage CEF Process 195
7.5.1 Metal flow pattern at different punch movements 196
7.5.2 Deformed product shape at different punch movements 197
7.6 Conclusions 198

8 Conclusions 199
8.1 Introduction 199
8.2 Summary of Findings 199
8.3 Conclusions 201
8.4 Contribution to Knowledge Enhancement 201
8.5 Scopes for Future Work 202

References 203
Appendix A Detail Drawings of Die-Punch Set-up 211

List of Figures

S. No		
1.1	Direct extrusion	2
1.2	Indirect extrusion	2
1.3	Radial extrusion	3
1.4	Impact extrusion	3
1.5	Hydrostatic extrusion	4
1.6	Upset forging	4
1.7	Open die forging	5
1.8	Closed die forging	5
1.9	Flashless forging	6
1.10	Forward-backward extrusion process	6
1.11	Extrusion-forging process	7
1.12	Square die	9
1.13	Taper die	9
1.14	Curved die	9
1.15	Various stages of CEF process of collet chuck holder	11
2.1	Methodology of the present investigation	31
3.1	A general surface separating two rigid regions	43
3.2	Plane strain extrusion problem	45
4.1	Single collar collet chuck holder	51
4.2	Different zones in stage I of SCCCH	52
4.3	Different zones in stage II of SCCCH	56
4.4	Different zones in stage III of SCCCH	57
4.5	Different zones in stage IV of SCCCH	60
4.6	Double collar collet chuck holder processed by CEF process	62
4.7	Different zones in stage I of DCCCH	62
4.8	Different zones in stage II of DCCCH	63
4.9	Different zones in stage III of DCCCH	64
4.10	Different zones in stage IV of DCCCH	66
4.11	Double collar collet chuck holder processed by CE process	67
4.12	Different zones in stage I of DCCCH	67
4.13	Different zones in stage II of DCCCH	68
4.14	Different zones in stage III of DCCCH	69
4.15	Different zones in stage IV of DCCCH	71
4.16	Single collar collet chuck holder processed by multi-stage CEF process	72
4.17	Different zones in stage I of SCCCH	72
4.18	Different zones in stage II of SCCCH	73
4.19	Variation of punch load with ram displacement at m = 0.13	81
4.20	Variation of punch load with ram displacement at m = 0.19	81
4.21	Variation of punch load with ram displacement at m = 0.38	82
4.22	Variation of punch load with ram displacement at m = 0.13	83

4.23	Variation of punch load with ram displacement at m = 0.19	83
4.24	Variation of punch load with ram displacement at m = 0.38	84
4.25	Variation of punch load with ram displacement at m = 0.13	85
4.26	Variation of punch load with ram displacement at m = 0.19	85
4.27	Variation of punch load with ram displacement at m = 0.38	86
4.28	Variation of punch load with ram displacement	87
5.1	Major input parameters for FEM simulation for CEF and CE of collet chuck holders	90
5.2	Schematic view of combined extrusion-forging process	95
5.3	Input parts required for the simulation process	95
5.4	Grid independence test result	96
5.5	Single collar collet chuck holder	98
5.6	Variation of punch load with punch travel at friction factor of 0.13	99
5.7	Variation of punch load with punch travel at friction factor of 0.19	99
5.8	Variation of punch load with punch travel at friction factor of 0.38	100
5.9	Die filling at different punch movement with 0.13 friction factor at 0.5 mm/min ram velocity	101
5.10	Flow pattern of SCCH with varying frictional condition with ram velocity 0.5 mm/min	102
5.11	Flow pattern of SCCH with varying ram velocities at 0.13 frictional condition	103
5.12	Effective strain, effective stress and total velocity with varying friction factor at 0.5mm/min punch movement	105
5.13	Effective strain, effective stress and total velocity with 0.13 friction factor at varying punch movements	106
5.14	Double collar collet chuck holder	107
5.15	Variation of punch load with punch travel at friction factor of 0.13	108
5.16	Variation of punch load with punch travel at friction factor of 0.19	108
5.17	Variation of punch load with punch travel at friction factor of 0.38	109
5.18	Die filling at different punch movement	110
5.19	Flow pattern of DCCH with varying frictional condition with ram velocity 1 mm/min	111
5.20	Flow pattern of DCCH with varying ram velocities at 0.19 frictional condition	112
5.21	Effective strain, effective stress and total velocity of DCCH with varying frictional condition with ram velocity 1 mm/min	114
5.22	Effective strain, effective stress and total velocity of DCCH with varying ram velocities at 0.19 frictional conditions	115
5.23	Double collar collet chuck holder	116
5.24	Variation of punch load with punch travel at friction factor of 0.13	117
5.25	Variation of punch load with punch travel at friction factor of 0.19	117
5.26	Variation of punch load with punch travel at friction factor of 0.38	118
5.27	Die filling at different punch movement	119
5.28	Flow pattern of DCCH by CE process with varying frictional	120

	condition with ram velocity 2 mm/min	
5.29	Flow pattern of DCCH by CE process with varying ram velocities at 0.38 frictional condition	121
5.30	Effective strain, effective stress and total velocity DCCH by CE process with varying frictional condition with ram velocity 2 mm/min	123
5.31	Effective strain, effective stress and total velocity DCCH by CE process with varying ram velocities at 0.38 frictional condition	124
5.32	Multistage single collar collet chuck holder	125
5.33	Variation of punch load with punch travel at friction factor of 0.13	126
5.34	Die filling at different punch movement	126
5.35	Flow pattern at different punch movement	127
5.36	Mean stress, effective strain and velocity at a 0.19 friction factor with 1mm/min punch movement	128
6.1	Extrusion-forging die set up assembly	132
6.2	Photograph of UTM machine with assembled set-up	135
6.3	Compression test setup with aluminium specimen	136
6.4	Compression test for determination of flow stress	137
6.5	Stress-Strain (Flow stress) curves for aluminium specimen	137
6.6	Setup for ring test	138
6.7	comparing the ring test curves with theoretical standard calibration curve (6:3:2)	139
6.8	Single collar collet chuck holder manufactured by CEF process	140
6.9	Variation of punch load with ram displacement at m = 0.13	141
6.10	Variation of punch load with ram displacement at m = 0.19	142
6.11	Variation of punch load with ram displacement at m = 0.38	142
6.12	Punch load Vs Rate of ram displacement for single collar collet chuck holder	143
6.13	Die filling at different punch movement	143
6.14	Product shape at different punch position	144
6.15	Flow pattern at different punch movement	145
6.16	Optical Microscope	145
6.17	Microscopic analyses of CCH with friction factor 0.19 at 0.5 mm/min ram displacement	147
6.18	Microscopic analyses of CCH with friction factor 0.19 at 1 mm/min ram displacement viewed at 500 µm	148
6.19	Microscopic analyses of CCH with friction factor 0.19 at 2 mm/min ram displacement	148
6.20	Microscopic analyses of CCH with friction factor 0.13 at 0.5 mm/min ram displacement	149
6.21	Microscopic analyses of CCH with friction factor 0.38 at 0.5 mm/min ram displacement	149
6.22	Vickers Micro-Hardness Tester	150
6.23	Micro hardness analyses of CCH with friction factor 0.19 at 0.5 mm/min ram displacement	151

6.24	Micro hardness analyses of CCH with friction factor 0.19 at 1 mm/min ram displacement	151
6.25	Micro hardness analyses of CCH with friction factor 0.19 at 2 mm/min ram displacement	152
6.26	Micro hardness analyses of CCH with friction factor 0.13 at 0.5 mm/min ram displacement	152
6.27	Micro hardness analyses of CCH with friction factor 0.38 at 0.5 mm/min ram displacement	153
6.28	X-Ray Powder Diffractometer	154
6.29	Residual stress indicating at various positions for SCCCH	154
6.30	Double collar collet chuck holder manufactured by CEF process	155
6.31	Variation of punch load with punch travel at m = 0.13	156
6.32	Variation of punch load with punch travel at m = 0.19	156
6.33	Variation of punch load with punch travel at m = 0.38	157
6.34	Punch load vs Rate of ram displacement for double collar collet chuck holder	158
6.35	Die filling at different punch movement	158
6.36	Product shape at different punch position	159
6.37	Flow pattern at different punch movement	160
6.38	Microscopic analyses of double collar CCH with friction factor 0.13 at 0.5 mm/min ram displacement	161
6.39	Microscopic analyses of double collar CCH with friction factor 0.13 at 1 mm/min ram displacement	162
6.40	Microscopic analyses of double collar CCH with friction factor 0.13 at 2 mm/min ram displacement	162
6.41	Microscopic analyses of double collar CCH with friction factor 0.19 at 2 mm/min ram displacement	163
6.42	Microscopic analyses of double collar CCH with friction factor 0.38 at 2 mm/min ram displacement	163
6.43	Micro hardness analyses of double collar CCH with friction factor 0.13 at 0.5 mm/min ram displacement	164
6.44	Micro hardness analyses of double collar CCH with friction factor 0.13 at 1 mm/min ram displacement	164
6.45	Micro hardness analyses of double collar CCH with friction factor 0.13 at 2 mm/min ram displacement	165
6.46	Micro hardness analyses of double collar CCH with friction factor 0.19 at 2 mm/min ram displacement	165
6.47	Micro hardness analyses of double collar CCH with friction factor 0.38 at 1.0 mm/min ram displacement	165
6.48	Residual stress indicating at various positions for DCCCH	166
6.49	Double collar collet chuck holder manufactured by CE process	167
6.50	Variation of punch load with ram displacement at m = 0.13	167
6.51	Variation of punch load with ram displacement at m = 0.19	168
6.52	Variation of punch load with ram displacement at m = 0.38	168

6.53	Punch load Vs Rate of ram displacement for single collar collet chuck holder	169
6.54	Die filling at different punch movement	169
6.55	Product shape at different punch position	170
6.56	Flow pattern at different punch movement	171
6.57	Microscopic analyses of double collar CCH with friction factor 0.38 at 0.5 mm/min ram displacement	172
6.58	Microscopic analyses of double collar CCH with friction factor 0.38 at 1 mm/min ram displacement	172
6.59	Microscopic analyses of double collar CCH with friction factor 0.38 at 2 mm/min ram displacement	173
6.60	Microscopic analyses of double collar CCH with friction factor 0.13 at 1 mm/min ram displacement	173
6.61	Microscopic analyses of double collar CCH with friction factor 0.19 at 1 mm/min ram displacement	174
6.62	Micro hardness analyses of double collar CCH with friction factor 0.38 at 0.5 mm/min ram displacement	175
6.63	Micro hardness analyses of double collar CCH with friction factor 0.38 at 1 mm/min ram displacement	175
6.64	Micro hardness analyses of double collar CCH with friction factor 0.38 at 2 mm/min ram displacement	175
6.65	Micro hardness analyses of double collar CCH with friction factor 0.13 at 1 mm/min ram displacement	176
6.66	Micro hardness analyses of double collar CCH with friction factor 0.19 at 1 mm/min ram displacement	176
6.67	Residual stress indicating at various positions for DCCCH by CE process	177
6.68	Single collar collet chuck holder manufactured by multistage CEF process	177
6.69	Variation of punch load with ram displacement	178
6.70	Die filling at different punch movement	178
6.71	Product shape at different punch position	179
6.72	Flow pattern at different punch movement	179
6.73	Microscopic analyses of Multistage CEF of single collar CCH with friction factor 0.19 at 1 mm/min ram displacement	180
6.74	Microscopic analyses of single collar CCH with friction factor 0.19 at 1 mm/min ram displacement	181
6.75	Residual stress indicating at various positions for SCCCH	181
7.1	Comparison of loads at 0.13 frictional conditions at varying ram velocities	185
7.2	Comparison of loads at 0.19 frictional conditions at varying ram velocities	185
7.3	Comparison of loads at 0.38 frictional conditions at varying ram velocities	186

7.4	Flow pattern at different punch movement	187
7.5	Die filling at different punch movement at ram velocity of 1 mm/min and m = 0.19	188
7.6	Comparison of loads at 0.13frictional conditions at varying rams velocities	189
7.7	Comparison of loads at 0.19 frictional conditions at varying rams velocities	189
7.8	Comparison of loads at 0.38 frictional conditions at varying rams velocities	190
7.9	Flow pattern at different punch movement	190
7.10	Die filling at different punch movement	191
7.11	Comparison of loads at 0.13 frictional conditions at varying rams velocities	192
7.12	Comparison of loads at 0.19 frictional conditions at varying rams velocities	193
7.13	Comparison of loads at 0.38 frictional conditions at varying rams velocities	193
7.14	Flow pattern at different punch movement	194
7.15	Die filling at different punch movement	195
7.16	Comparison of loads at 1mm/min ram velocity with 0.19 frictional condition	196
7.17	Flow pattern at different punch movement	196
7.18	Die filling at different punch movement	197
A.1	Container	211
A.2	Cover plate for container	212
A.3	Sleeve	213
A.4	Extrusion-forging die holder	214
A.5	Punch with punch plate	215
A.6	Base plate	216
A.7	Split die 1	217
A.8	Split die 2	217
A.9	Split die 3	218
A.10	Split die with flash	218
A.11	Split die with flash	219
A.12	Taper die	219
A.13	Split die 4	220
A.14	Split die 5	220
A.15	Large punch	221
A.16	Small punch	221
A.17	Punch head	222

List of Tables

S. No		
3.1	Summary of discontinuity lines and velocity vectors on their sides	46
3.2	Summary of velocity discontinuities across the lines	47
4.1	Kinematically admissible velocity fields for stage II	56
4.2	Strain rates for stage II	57
4.3	Kinematically admissible velocity fields for stage III	58
4.4	Strain rates for stage III	59
4.5	Kinematically admissible velocity fields for stage IV	60
4.6	Strain rates for stage IV	61
4.7	Kinematically admissible velocity fields stage I	63
4.8	Kinematically admissible velocity fields stage II	64
4.9	Kinematically admissible velocity fields for stage III	65
4.10	Kinematically admissible velocity fields for stage IV	66
4.11	Kinematically admissible velocity fields for stage I	68
4.12	Kinematically admissible velocity fields stage II	69
4.13	Kinematically admissible velocity fields for stage III	70
4.14	Kinematically admissible velocity fields for stage IV	71
4.15	Kinematically admissible velocity fields for stage I	72
4.16	Kinematically admissible velocity fields stage II	73
4.17	Velocity discontinuity surfaces for stage I of product 1	75
4.18	Velocity discontinuity surfaces for stage II of product 1	75
4.19	Velocity discontinuity surfaces for stage III of product 1	76
4.20	Velocity discontinuity surfaces for stage IV of product 1	77
4.21	Frictional surfaces for stage I of product 1	78
4.22	Frictional surfaces for stage II of product 1	78
4.23	Frictional surfaces for stage III of product 1	79
4.24	Frictional surfaces for stage IV of product 1	79
5.1	Composition of specimen (Aluminium 1070)	94
5.2	Process parameters used in the simulation	96
5.3	Forming load at different ram velocities and friction conditions	100
5.4	Forming load at different ram velocities and friction conditions	109
5.5	Forming load at different ram velocities and friction conditions	118
6.1	List of components	133
6.2	Composition of specimen (Aluminium 1070)	134
6.3	Components considered for microscopic analysis	146
6.4	Residual stress values at various positions of SCCCH	154
6.5	Various conditions considered for experimentation of double CCH	160
6.6	Residual stress values at various positions of DCCCH	166
6.7`	Various conditions considered for experimentation of Single CCH	171
6.8	Residual stress values at various positions of DCCCH by CE process	177
6.9	Residual stress values at various positions of SCCCH	181
7.1	Variation of forming loads for different analysis obtained for SCCCH	186

by CEF process
7.2 Variation of forming loads for different analysis obtained for DCCCH by CEF process 188
7.3 Variation of forming loads for different analysis obtained for DCCCH by CE process 192
7.4 Variation of forming loads for different analysis obtained for SCCCH by Multistage CEF process 195

Nomenclature

A	Area of a triangle
A_b, A_e	Area of the billet and product cross section
A_i	Area of the i^{th} face of the tetrahedral rigid region
A_x, A_y, A_z	X-, Y-, Z-projections of triangle in space
a	Half width of the product
B	Length of side of the triangle section
c	Overall width of product cross section
d	Overall length of product cross section
F, G	Functions of die cavity parameters
H, L	Optimization parameters
i, j, k	Unit vectors along the axis of a Cartesian co-ordinate frame
J	Upper bound energy consumption
J_1	Internal power dissipated due to plastic deformation
J_2	Power for shear deformation against velocity discontinuity
J_3	Frictional power dissipated at tool/work interface
J_{min}	Minimum value of J
J_{Si}	Power of shear deformation on the plane *S,*
L	Height/length of deformation zone
m	friction factor on the die surface
M	Height of the floating point on the extrusion axis from origin
$\hat{n}$	Unit vector normal to a surface
P_{av}	Average extrusion pressure
R	Shaft radius/Radius of extruded shaft
N	Number of sides of approximating polygon
s	Length of each side of the approximating polygon
S_i	i^{th} surface of velocity discontinuity
S_{Di}	I^{th} interface of tool/work
t_1, t_2	Relevant widths in section dimensions
u_r u_θ u_z	Component of velocity in Cylindrical coordinates
V	Velocity vector in general
V_o	Volume of deformation one
V_1, V_2	Velocity vectors on both sides of a surface
V_k	Velocity vector in tensor notation
$/\Delta V/$	Velocity discontinuity
$/\Delta V/S_i$	Velocity discontinuity across the i^{th} surface
$/\Delta V/S_{Di}$	Velocity discontinuity across the surface S_{Di}
$/\Delta V/_i$	Velocity discontinuity across the i^{th} face

V_b , V_p	Billet and product velocity
V_{1n}, V_{2n}	Components of V_1 and V_2 along $\hat{n}$
V_x, V_y, V_z	Component of velocity in Cartesian coordinates
W	Half width of the billet
x, y, z	Axes of general Cartesian coordinates
r, θ, z	Axes of general Cylindrical coordinates
σ_o	Yield stress in uniaxial tension or compression
f	Function representing the equation of a planer surface
ε_{ij}	Components of strain rate tensor
k	Yield stress in simple shear
$\varepsilon_{rr}\varepsilon_{\theta\theta}\varepsilon_{zz}$	Strain rate components (direct)
$\varepsilon_{r\theta}\varepsilon_{rz}\varepsilon_{\theta z}$	Strain rate components (shear)
ζ, η, Z	Transformed co-ordinate system
ψ_1, ψ_2	Dual stream functions
θ	Internal angle of the polygon

Chapter 1

Introduction

1.1 Backgrounds

Conventional manufacturing processes such as machining, casting, assembly (fabrication), and metal forming finds applications in major automobile and aircraft industries. Among them metal forming as a technique has advantages over other manufacturing processes due its high precision in production of complex shapes with minimal material wastage and better mechanical properties. It has gained lot of importance in the past decade [1-2]. Metal forming is a process in which a metal block is being plastically deformed to a desired geometry. In order to obtain the deformation a force higher than the yield strength of the material is applied. Metal forming is a broad concept, can be classified into two major sections: bulk metal working processes and sheet metal working processes. Bulk metal deformation processes can be broadly of four types, namely, rolling, forging, extrusion and drawing. Forging and extrusion are frequently used forming processes since early 18^{th} century [3]. Extrusion and forging having many advantages such as high dimensional accuracy, minimal or complete elimination of machining, good surface finish, better mechanical properties, quick production process and economic in comparison with other conventional manufacturing processes [4]. Extrusion and forging processes can be carried out under three working temperatures, namely, hot, cold and warm linked to recrystalization tempurature. Cold forging and extrusion processes have more advantages compared to hot and warm processes with respect to geometrical accuracy, surface finish and mechanical properties of the final component [5].

1.1.1 Different types of extrusion processes

Basically, cold extrusion is classified into four types depending on the relative movement of the punch and extruded product [6]. They are: forward (Direct) extrusion, backward (indirect) extrusion, radial (lateral) extrusion and impact extrusion [7].

Direct (Forward) extrusion

Forward extrusion process, represented in Figure 1.1, is the most common method used in the industries to manufacture long products of uniform cross-section. In this type of

extrusion, the ram moves in the same direction of the extruded product. There is a relative movement between the billet and container, leading to high frictional forces. Friction at the die and container wall increases the extrusion load requirements than that for indirect extrusion.

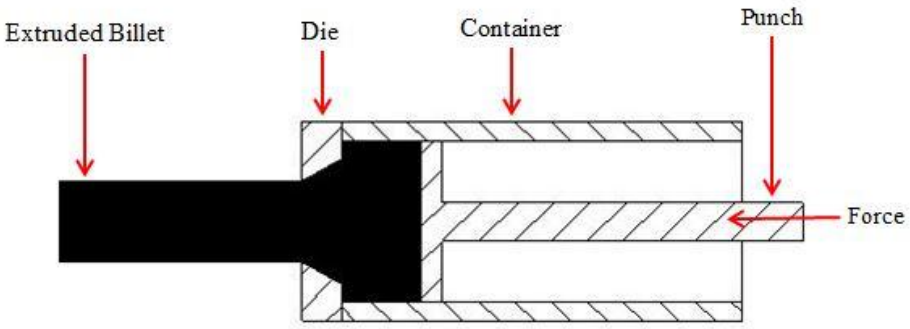

Figure 1.1: Direct extrusion

Indirect (Backward or Reverted) extrusion

In this type of extrusion, the billet does not move relative to the container. A die fixed on a hollow ram which is pushed against the billet, leading to flow of the extruded section in opposite direction to the ram movement shown in Figure 1.2. Frictional force between billet and container interface is thus eliminated during indirect extrusion. Alternatively, the closed container end in backward extrusion can be forced to move against die and ram assembly.

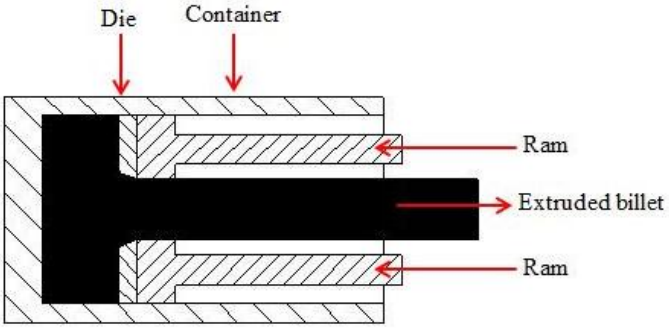

Figure 1.2: Indirect extrusion

Radial (Lateral) extrusion

In this type of extrusion, the material flow perpendicularly to the direction of the punch movement as shown in Figure 1.3. Due to the change in metal flow direction additional power is required to overcome the friction at the die-billet interface. These types of extrusions are commonly used for production of flange type components.

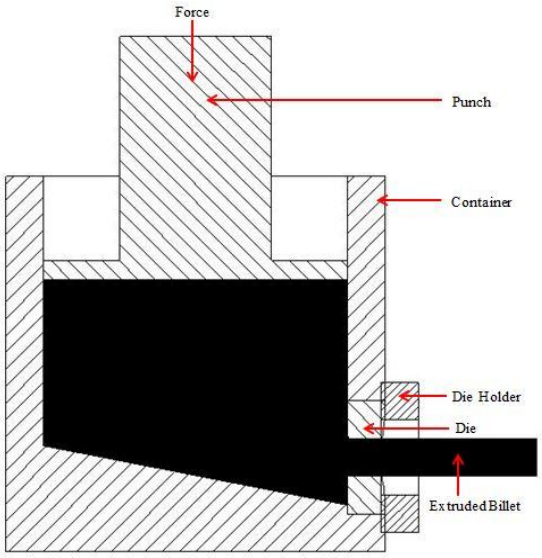

Figure 1.3: Radial extrusion

Impact extrusion

This process (illustrated in Figure 1.4) is similar to backward/indirect extrusion process represented in Figure 1.2. The punch runs down quickly on the blank which gets revert extruded the punch to obtain a tubular section. The length of the tube depends on the size of the blank. Toothpaste tubes are an excellent example of this process.

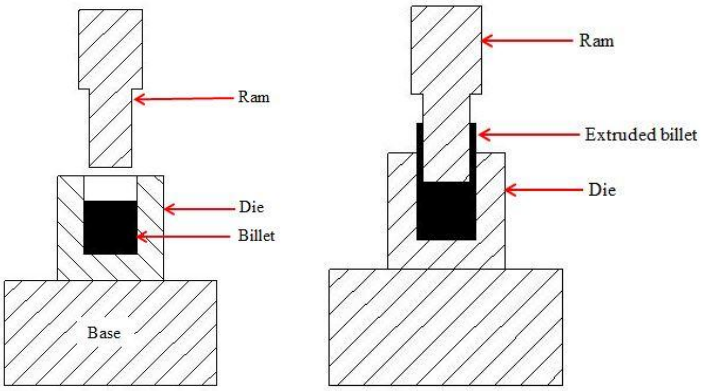

Figure 1.4: Impact extrusion

Hydrostatic extrusion

Besides these four types of extrusion processes, we also have hydrostatic extrusion method in which the billet in the container is extruded through the die by the action of a hydrostatic liquid pressure medium rather than by direct application of the load with a ram represented in Figure 1.5. The billet is surrounded by a hydrostatic fluid, which is sealed off and is pressurized sufficiently to extrude the billet through the die. This process can be

done hot, warm, or cold, however; the temperature is limited by the stability of the fluid used. This method can be used to extrude brittle materials that cannot be processed by conventional extrusion since ductility of the material is improved by applying hydrostatic pressure.

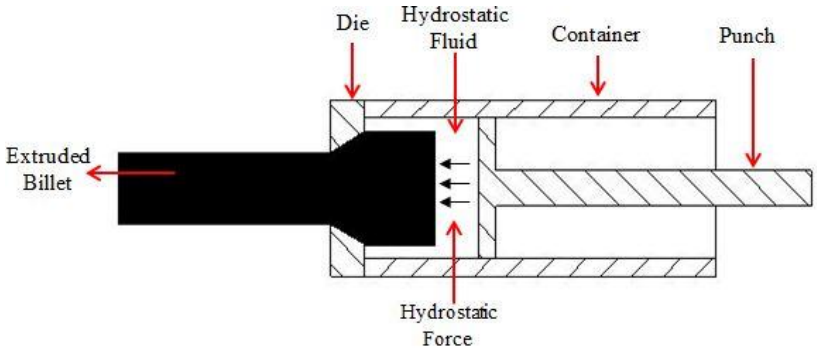

Figure 1.5: Hydrostatic extrusion

1.1.2 Different types of forging processes

According to the nature of the applied force, forging is classified as:

Hammer/drop forging: The applied force is impact type.

Press forging: Load is applied gradually.

Based on the nature of material deformation or direction of applied force forging process is divided as:

Upset forging

In this process, force is applied parallel to the length direction**.** This is the operation of increasing the cross section at the expense of length. Heads of nails, bolts and other hardware products are formed through this technique as shown in Figure 1.6.

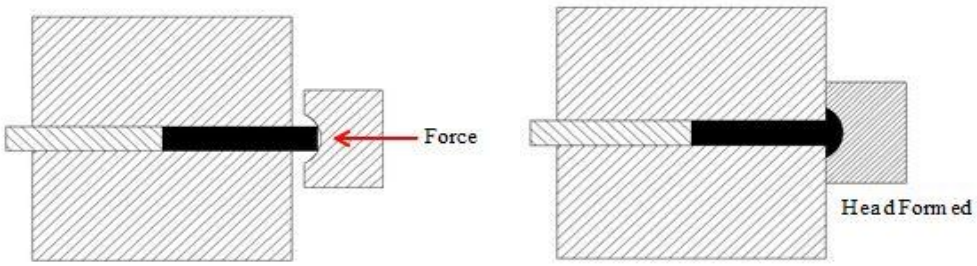

Figure 1.6: Upset forging

Drawing out: In this process, force is applied perpendicular to the length axis of the billet**.** This is the operation in which cross section area decreases with increase of length.

Based on the geometry of the dies by which material is compressed to get a shape forging process is divided as:

Open die forging

In this type, the work is compressed between two flat dies, allowing metal to flow freely laterally with minimum constraint which is shown in Figure 1.7. These types of operations are performed for initial breakdown of the billet.

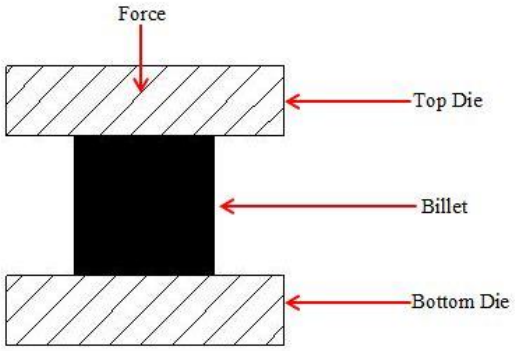

Figure 1.7: Open die forging

Closed die or Impression die forging

In this type of process, the work piece is compressed between two die halves which carry the impressions of the desired shape that is to be imparted on the work piece shown in Figure 1.8. Metal flow is constrained and we get a multidirectional unbroken grain flow inside the product giving better mechanical properties. The extra metal is expelled out as flash mostly at parting line.

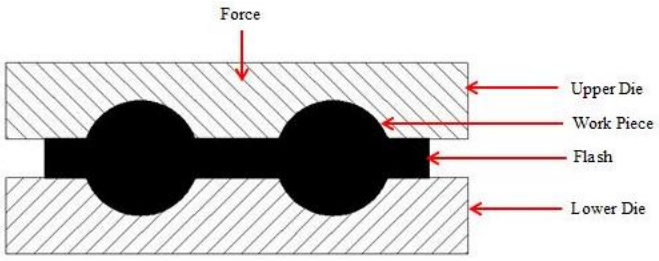

Figure 1.8: Closed die forging

Flashless forging

In this type of forging the volume of the workpiece is equal to the volume of the die cavity, with no requirement of flash arrangement as shown in Figure 1.9.

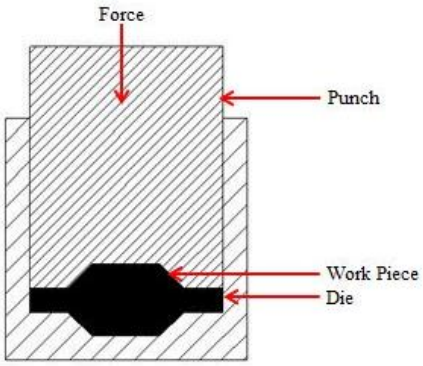

Figure 1.9: Flashless forging

1.1.3 Combined extrusion forging processes

Because of industrial requirements various operation's, such as, direct and indirect extrusion and forging are combined to get complex shapes.

Combined forward and backward extrusion (CE)

In this combine process backward and forward extrusion takes place simultaneously as shown in the Figure 1.10.

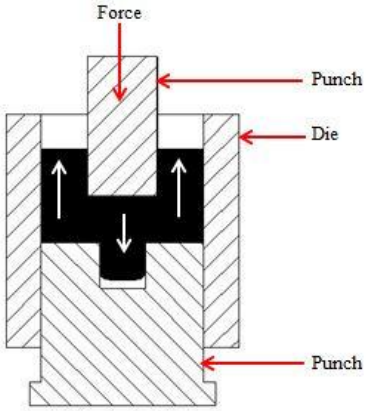

Figure 1.10: Forward-backward extrusion process

Combined extrusion-forging (CEF)

In this type of operation both extrusion and forging takes place simultaneously. As shown in Figure 1.11, forward extrusion takes place for forming of the shaft and forging takes place to form a flange. This process is also called cold heading with forging.

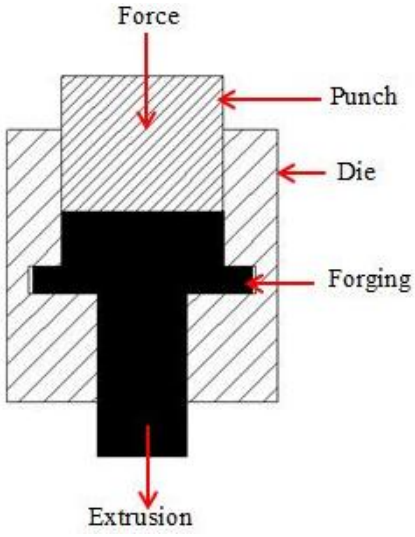

Figure 1.11: Extrusion-forging process

1.2 Existing Manufacturing and Modern Industry Demand

The conventional metal extrusion and forging routes have gained importance involving single process (forward or backward extrusion, upsetting or closed die forging) for its manufacturing ability of components with better mechanical properties because of unbroken and multidirectional grain flow directions. The major hindrances encountered by the present manufacturing industries are to produce complex profiles with better surface finish, near net shape in one pass and improved mechanical properties. Due to the ever increasing demand of components with intricacy features single route is not sufficient to manufacture those parts, which lead to the significance of the combined extrusion-forging process.

In combined extrusion-forging technique, a billet is forced by a ram through the dies to flow in the same, opposite and perpendiclar directions with respect to ram movement to obtain the desired shape. The beauty of this process is that two or more forming processes (different type of extrusion and forging) takes place simultaneously. Thereby, reducing the capital investment and we can obtain net or near-net shape product can be obtained by single ram movement at single station. Combined extrusion-forging (CEF) has drawn the attention of automobile, aircraft industries and received industrial significance due to higher productivity, decrease in material wastage, better mechanical properties when compared to the existing conventional processes. Along with that,

complex shapes can also be manufactured with ease, otherwise casting and machining are the present routes of manufacturing.

In the current market requirements, the use of complex aluminium sections are getting larger scope due to its properties of durability, wear resistance, low weight, etc. [8]. Combined extrusion–forging plays a very vital role for the production of near-net shaped products [9]. Metals like aluminium and aluminium based alloys play a predominant role in the cold CEF & CE processes. Due to the presence of high compressive stress, it minimizes cracks in the material in the initial breakdown of the ingot. Further, cold CEF is commercially preferred as it avoids complex tooling.

Although combined extrusion-forging has the ability to represent a better solution, analysis of this process has gained less importance till date due to its complexity nature.

1.3 Conventional Dies

Dies are the replica of the profile which is to be extruded or forged. Those are used as mould/tooling device in manufacturing process for the extrusion, forging and combined extrusion-forging of profiles. The dies used should have higher mechanical characteristics, should be strong enough and have the ability to hold the dimensional accuracy during elevated stresses. In general, tool steels are used as metal extrusion/forging dies. High-grade alloy steels with coatings having higher wear resistance are also used for dies. For higher accuracy and wear resistance sometime carbides are also used as die materials. The essential technical requirements for fabrication of dies are:

- Die angle is an important factor for the material flow, which influences the force requirement. Although, accurate die angle is difficult to establish due to the influence of temperature and lubrication.
- The die design should consider the flash formation for the finishing operations, fillet, corner radii, and shrinkage.

1.3.1 Types of Dies

In general, dies are of three types, namely, flat faced dies, conical dies and curved dies.

Flat faced or square dies (Figure 1.12)

- These dies are most preferred in the industry due to its simple design and low cost.
- Flat faced dies are used to extrude simple designs of hard and tough metal.

- These dies form dead metal zones due to which the metal shears internally which form its own dies angle.
- Difficult for lubrication.

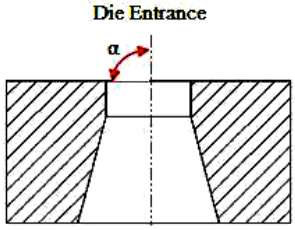

Figure 1.12: Square die

Taper or conical dies (Figure 1.13)

- These dies have an entrance angle for metal flow.
- Dead metal zones are not present in these dies.
- Low frictional force is present when compared to the flat faced dies.
- Lubrication is easy.

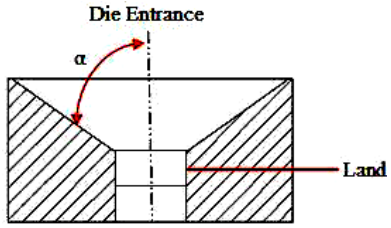

Figure 1.13: Taper die

Curved dies (Figure 1.14)

- Friction loss and redundant work can be minimized
- It can be cosine, sine, elliptic, circular, hyperbolic, polynomial etc.

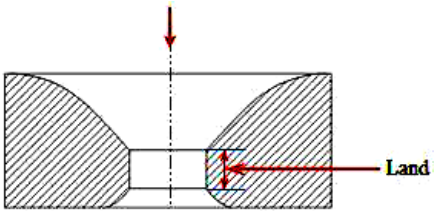

Figure 1.14: Curved die

1.4 The Present Problem

Collet chuck holder is a tool holding device used in different types of CNC milling machines. Face milling, drilling, tapping, boring are some of the suitable operations which are performed on CNC machines for accuracy and precision, where this device holder is

used to hold the cutting tool. It is a specialized type of clamp to hold the rotating cutting tool with the help of a spring collet which is used for its higher level of precision and accuracy. The chuck holder is described by a flange at the middle to fit into the machine, taper portion which is conical shaped area present at the bottom which enters the spindle for changing holder and collet pocket which fits the collet for holding the cutting tool. Depending upon the taper portion the holders are divided into three types namely, CAT (Caterpillar), SK (Long Taper), and HSK (Hollow Taper Face). The flanges may be single or dual which is called V-flange. It is a type of chuck where the sleeve being inner cylindrical surface and conical surface at the outer. The chuck holder can grip different types of collets such as ER Collet, R8 Collet, and 5C Collet.

For manufacturing the tool holder an enormous amount of material is being wasted by the machining process which is almost equal to the volume of the product. Some manufacturer use casting, subsequently by machining to get the final shape. Both the used processes have their limitations as discussed earlier. To secure our material resources and to get better mechanical properties it is essential for us to adopt the proposed CE and CEF processes for the production of different types of collet chuck holders.

1.4.1 Importance of the problem

The present work emphasizes on manufacturing of collet chuck holders with intricate corners by combined extrusion-forging & combined extrusion processes in cold working condition. Because of complex shape of the product metal flow during punch movement is multifarious. The influencing parameters for the combined extrusion–forging process includes

a) Percentage area reduction,

b) Die & product geometry,

c) Strain rate,

d) Lubrication between the split dies and the billet, etc., which influences

i) Load and stress, ii) microstructure, iii) hardness, etc. of the final product. Many times, industries follow ‘thumb rule’ to predict the load and estimate the capacity /strength of machine/tooling.

Hence, it is imperative to investigate the metal flow, load & stress calculations for this product in a much scientific way to get reasonable results by numerical and analytical methods and get validated by the experiments.

1.4.2 Combined extrusion-forging processes in the present problem

Experimental observations of CEF applied to collet chuck holder indicate that the full process can be visualized consists of four stages as shown in Figures 1.15 (a-d).

The initial step (stage I) of the process is backward extrusion which takes places after the initial compression of ram to the billet as shown in Figure 1.15 (a), which is responsible to create the collet pocket (Detail explanation is given in subsequent chapters).

During the second step (stage II), forward and lateral extrusion takes place (Figure 1.15 (b)). In this stage metal flows starts to fill the die cavity for the collar formation.

The third step (stage III), corner filling takes place for the formation of complete component which is required to fix in the spindle. In this stage, minimal amount of forward, lateral extrusion and forging occurs. Figure 1.15 (c) shows the corner filling stage with final formation of pull stud (used to fix the collet chuck holder in the spindle).

Flash is formed during the final step (stage IV), shown in Figure 1.15 (d). The flash is encrypted to the die design, which works as a reservoir for storing the extra left out metal after filling the cavities.

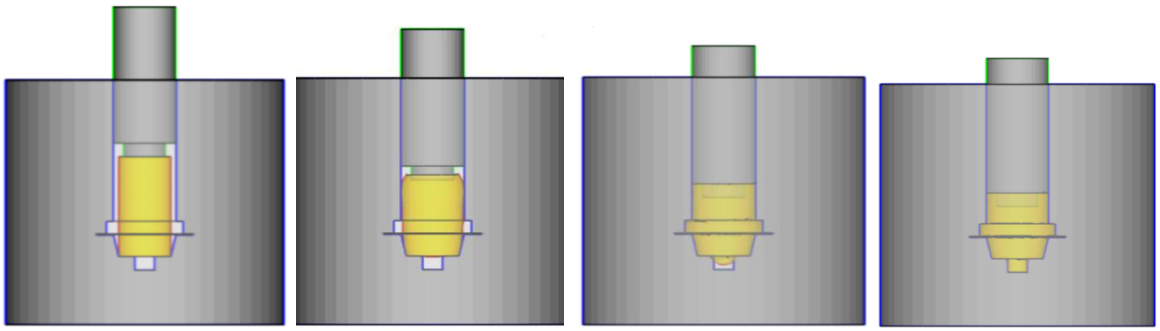

(a) (b) (c) (d)

Figure 1.15: Various stages of CEF process of collet chuck holder

1.5 Research Objective

The present work highlights on production of collet chuck holders with complex corners by combined extrusion-forging process in cold working condition. The objectives of the present work can be summarized as follows:

- The present work proposes to manufacture a collet chuck holders using combined extrusion-forging and combined extrusion processes to obtain better mechanical properties, less material wastage and by an economical way in comparison to other conventional methods currently followed by industries.
- To derive kinematically admissible velocity fields using upper bound analysis and further comparing the same with numerical and experimental results to estimate the forming load at different punch movements.
- To perform numerical analysis based on finite element method using commercially available software for plastic deformation to compare the results with that obtained from analytical and experimental methods.
- To design and fabricate an experimental setup with required dies for combined extrusion-forging of collet chuck holder to be made of aluminium. Further, to perform exhaustive experiments to create a database for the product and to compare the observations with the analytical and numerical results.
- Determining the forming loads using various lubricants and to find out the effect of friction and ram velocity on the components.
- Characterisation of the manufactured components using optical microscopy for validating the results mentioned above along with the determination of microhardness and residual stress data.

1.6 Outline of Thesis

The remaining chapters of the thesis are outlined as follows:

Chapter 2: Literature review

This section summarises the different extrusion and forging techniques used till date. The chapter also gives us a brief idea about the various types of analysis performed with their future scope of work. A short understanding of the objective is also obtained.

Chapter 3: Solutions to metal forming problems

Include a description of the metal forming analysis, types of available solutions and brief description and application of upper bound technique.

Chapter 4: Analytical analysis

This section contains a brief report of the upper bound technique and its application to different types of collet chuck holders. Different kinematically admissible

velocity fields are proposed for different products for different stages to calculate the upper bound load. Further provides us with the database of various parameters obtained mathematically under the influence of different lubricated and ram velocity conditions.

Chapter 5: Numerical analysis

This section contains a brief report on the numerical analysis of collet chuck holder manufactured by CEF and CE processes. It also provides us with the database of various parameters obtained by DEFORM 3D® under different lubricated and ram velocity conditions.

Chapter 6: Experimental analysis

This section contains a brief report on die design and manufacturing of different types of collar chuck holders by CEF and CE processes. Further, the section provides the database obtained by experimentation under different lubricated and ram velocity conditions. This chapter also includes a concise report on the metallographic analysis with microhardness and residual stress results.

Chapter 7: Comparison of results and discussion

This chapter deals with the comparison of results obtained from numerical, mathematical and experimental analyses applied to different types of collar chuck holders manufactured by CEF and CE processes under different lubricated and ram velocity conditions.

Chapter 8: Conclusions and future recommendations

The conclusions of the present work along with the future scopes are presented.

1.7 Closure

The present chapter highlights the significance of combined extrusion-forging and combined extrusion processes of collet chuck holders. The chapter also briefs:

- Existing manufacturing process and industry demands for new technology.
- The importance of CEF and CE for collet chuck holder manufacturing.
- Stages of CEF process during collet chuck holder production.
- Objectives of the present investigation.

In context with the objective of current work an exhaustive literature review is presented in the next chapter.

Chapter 2

Literature Review

2.1 Introduction

Present manufacturing industries are facing tremendous challenges to produce components at a cheaper cost with superior mechanical properties such as high strength, resistance to fatigue & heat, anti-corrosion, surface finish, etc. Metal forming is one such process which has gained a lot of importance in recent years due to its ability to give those required properties. As discussed earlier the combined extrusion–forging (CEF) and combined extrusion processes (CE), comes under metal forming group, has been selected for the present investigation to manufacture a collet chuck holders. Due to the presence of various influencing parameters such as frictional condition at the interface of the die/billet, strain rate, elevated working temperature, intricate shape of the product, etc. it becomes complex to analyse the practical situation to estimate the forming load. Many researchers have applied different techniques to predict the metal flow & load requirement at different working conditions and reported their findings at different forums.

2.2 Previous Works

In the context of present investigation the previous works can be discussed in four groups.

- Numerical analysis
- Analytical analysis
- Experimental analysis
- Tribological analysis

2.2.1 Numerical analysis

The numerical analyses of the metal forming processes came into existence during the 1950s which were developed for the elastic analysis of airplane. In the year 1967, Zienkiwitcz and Cheung [10] published a book in which a software written in FORTRAN language was described briefly. With the advent of digital computers and popularity of finite element method (FEM) many researchers from different countries explored different

methodologies to analyse the metal forming processes. From the early 20th century many FEM based software's were developed, such as HYPEREXTRUDE®, DEFORM 3D®, FORGE®, etc. that can be applied to the different metal forming processes.

Shin et al. [11] presented experimental and numerical analysis of non-axisymmetric extrusion for square, hexagonal and T-sections from a round billet. The numerical analysis was carried out initially followed to validate with experimental results. The investigation performed to predict the metal flow, heat transfer, friction, material tool interaction to minimise the material wastage. The analysis was performed at 40%, 50%, and 60% of area reductions. Kim and Altan [12] proposed a generalised plane-strain condition using FEM for a rigid plastic material. Plasticine is used to validate their prediction. The error between numerical and experimental analysis was found to remain within the range of 23-28%. Martins and Marques [13] performed an exercise substituting Gaussian rule of numerical interrogation to deviatoric components based on FEM for the implementation of existing formulation to the 3D hexagonal closed die forging. A brief theoretical and experimental analysis is performed to calculate the punch load for 1050A aluminium alloy with lithium base grease as lubricant. Balaji et al. [14] presented a viscoplastic model for extrusion through an axisymmetric streamlined die. The investigation was focused to predict the metal flow using a die with optimal profile and deformation enclosed by plastic boundaries. Low carbon steel material was taken as a billet for evaluation of geometry for a third–order polynomial profile. They found that friction between die/container with billet decreases the axial velocity along the lateral direction and distorts the grain flow direction. Hirai and Ishise [15] found a solution to the metal forming problem regarding the metal flow pattern and pressure distribution on tool surface using numerical analysis. A Galerkin FEM formulation is used for calculation of stress distribution for the axisymmetric product made of lead. To observe the transient progress of metal flow, the deformation zone is divided into five regions. They found the effect of friction along the tool and workpiece and observed horizontal and lateral cracks on the die due to the hoop stress at the corner points. Park et al. [16] proposed a recurrent boundary condition in the twisted helical extrusion of clover and trochoidal gear sections. They showed that extrusion pressure increased significantly with friction factor and total twist angle is decreased with increase in friction factor. It was found that the effective strain is larger near the minor axis of the die surface due to relatively higher local reduction in radial direction than any

other part of the cross-section. Finally, the experimental and computational results are found to been in good agreement.

Mori et al. [17] in their analysis, used a method for determining an optimum position of die orifice product by finite element simulation. A three-dimensional analysis for the extrusion of the arbitrarily shaped section is simulated using iso-parametric hexahedral elements by rigid–plastic FEM. They showed that the curvature of the extruded billet due to the axisymmetric shape of die opening decreased with increase of taper length. In general, the curvatures of the products with T, L-shaped sections were predicted by FEM simulation. For a plasticine billet, it was found that the curvature obtained from numerical modelling is in rational agreement with the experimental result. Kang and Yang [18] presented a finite element analysis based on arbitrary Lagrangian–Eulerian method for hot extrusion of AA 2014-76 to derive square sectioned shape. Here the metal flow pattern was found greatly influenced by the variation of die bearing length. It was found that extrusion load and local temperature were increased with die bearing length and appropriate design of die bearing area was required for uniform velocity distribution to improve product quality.

In an attempt to minimize the material usage Khumann et al. [19] adapted a CAD technique based on FEM for helical and spur gears to minimise the trial and error experimentations. The forming load, friction factor at the die and billet interface and die geometry were considered to minimise failures. The load predicted using FEM was very well validated by them with that obtained by slab method. Osakada et al. [20] proposed a FEM based on elastoplasticity analysis for the hydrostatic extrusion. It was found that computed plastic zone based on FEM spreads wider than obtained by the slip line field analysis. Authors' also observed that die pressure was high near the die entry and exit. It was also observed that the plastic zone was increased with ram displacement, hydrostatic pressure and flow stress was homogenously distributed under plane strain condition. Hwang et al. [21] developed a finite element model to analyse the effect of various process variables such as semi-cone angle of the die, reduction area, ram speed, extrusion force, etc. for semi-solid extrusion of Al 2024. It was found that due to the shear deformation, the large gradient of liquid pressure was associated with the large gradient of the solid fraction at conical part of the die. To attain the uniform microstructure in the semi-solid forming process, closed die process should be preferred than open die. The study suggests

that with the increase of ram speed, the liquid segregation decreases at the contact point of the die.

Gouveia et al.'s [22] research suggest that the upper bound method has the limitation to explain the design of the die for minimum stress and load calculation for complicate 3D profile extrusion. They have tried two different numerical formulations, i.e., updated Lagrangian and combined Eulerian–Lagrangian. The study was performed to predict the material flow and validate it with the experimental results. For the analysis, extrusion of a round section to square section was opted. The FEM base software PLAST3® was used to compare the results with that obtained from experiments. Lee et al. [9] carried out 3D analysis using thermo-rigid-viscoplastic approach and automatic remeshing module applied to flat die hot extrusion. It was found that to obtain high quality extruded product there should be the proper design of bearing length. In the simulation, it was found that deflection of extruded part is not influenced by punch velocity or by variation of workpiece temperature.

Minami et al. [23] simulated the forging process using transient two and three-dimensional steady and unsteady state temperature fields. Their analysis revealed that maximum temperatures, depth of softened layer and hardness of forging dies can be well estimated. Behrens [24] proposed a numerical model for tool wear to improve the versatility of hot forging process. This model was introduced to find the amount of die wear influenced by thermal effects and hardness of tool material. A lot of data was taken for development and calibration of this approach from different experiment and industrial processes. The calibrated wear model allows comparison between hot wear of die made of steels using FEA. The numerical approach was found to be valid in wear estimation of hot forging dies. Zuyan and Zhongjin [25] have drawn load curves for lateral extrusion process using experimental and numerical models. The curves were drawn and calculated for H62 alloy and LY12 alloy. They have approached a finite element software Forge 2D® using a rigid – plastic method for the same. During deformation, it was found that the friction force was much larger than the deformation forces; hence maximum load was applied to overcome the friction. In this article, both curves are compared with experiments and found to be in good agreement. Meidert et al. [26] cold forged a bevel gear using a self-prepared lubricant (glycerine mixed with little liquid soap followed by a talcum powder coating). They have performed 2D simulation to predict load & flow

pattern and obtained load of 2500 MPa. They have used three approaches to find optimal filling of dies, which includes:

1. Die cavity filled by moving both punches (top & bottom),
2. Only top punch moves to fill the cavity,
3. Only bottom punch moves to fill the cavity.

They concluded that the die filling was optimal by bottom punch movement. The numerical and experiments are validated and found that they are in good agreement. Im et al. [27] studied the friction conditions using FE simulations and compared results with the experiments. Similarly Li et al. [28] used three formulations based on FEM, i.e., transient updated Lagrangian (UL) formulation, Steady state (SS) Eulerian approach and the Arbitrary Lagrangian-Eulerian (ALE) for extrusion. Zhao et al. [29] also used the ALE approach and it effectively predicts the defects in the extrusion process. On an another report, Zhou et al. [30] claimed that updated-lagrangian approach was the best suited to perform simulations on aluminium extrusion. Prasad and Rao [31] conducted experiments on isothermal forging of electrolytic copper to manufacture rib-webs. They modelled the process using finite element simulation and materials models involving kinetic analysis and processing maps with a view to validate their predictions. Lee et al. [32] reported on numerical characteristics of triangular and tetrahedral elements applied to forging simulation. Haghighat and Mahdavi [33] studied a bi-metallic tube extrusion process to find out the internal power, power dissipated on frictional, and velocity discontinuity surfaces using analytical and numerical methods. Gavrus et al. [34] examined two step inverse analysis method applied to an extrusion process. The main concern of the process was to identify the tribological properties in relation with real contact conditions for a forward extrusion process. Wang et al. [35] investigated a novel simulative friction test with respect to DAE (Double Action Extrusion) process. Two commonly used friction models are considered for the numerical analysis.

2.2.2 Experimental analysis

Experimental analysis is a fundamental route to predict the forming load, flow characteristics and state of stress and strain for metal forming processes. Huge amounts of research have been performed from the early 18^{th} century till date for the same. The present section tries to give a consolidated picture of experiments carried out by different researchers for extrusion-forging processes.

Jafarzadeh et al. [8] performed an experimental analysis of the extrusion process to predict the deformation behaviour of Al-1050 subjected to combination of backward-radial-forward extrusion processes. They have investigated forming characteristics with respect to die design geometry parameters. The findings suggest that friction has an influence on the flow pattern of material in the radial direction which is significant. Increase of friction factor may lead to a good near net shaped product, but the die wear and increased forming load should be minimized. Ultra fine-grained material's presence in the product obtained by metal forming signifies with higher mechanical properties of the product. In this context Hosseini et al. [36] proposed a novel backward extrusion process for aluminium material, performed at higher strain rate. They have shown microstructural grains distributed homogeneously throughout the final product, giving better strength. A 3.5% higher plastic strain was observed and the microhardness values yield 52% improvement. FEM analysis results have shown good correlation with the experimental product. Zhuang et al. [37] found a solution based on FEM to analyse micro tubes with low wall thickness to diameter ratio that cannot be predicted by the macro mechanics. In his analysis, they have used a CPFE (Crystal Plasticity Finite Element) model where the localised thinning can be captured. The FE analysis used VGRAIN® system in ABAQUS® to perform the analysis in the subroutine VMAT. From the results predicted that the localised thinning occurs at the angle between crystal slip system and hoop stress direction. The analysis has also been performed on single-crystal and multi-crystal metal and concluded that localised thinning can be predicted using CPFE for single crystal only. Lee and altan [38] approached a numerical modelling for prediction of flow stress and friction influence on the metal flow during the upset forging of rings. The program developed by them has the ability to calculate strain, strain-rate, flow pattern and forming load of the upset forging. To validate with the numerical analysis, experimental analysis was performed for an annealed aluminium billet. The paper concludes that lower friction conditions show good correlation with the forming load. The upset forming load was not in good agreement at higher friction conditions, may be due to redundant metal flow and strain hardening at interfaces.

Lin and Wang [39] investigated the possibilities to design the die depending on varying draft angle and radii using FEM analysis. To validate the FEM results two sets of dies are fabricated for experimental study. Narayanasamy and Pandey [40] conducted

good number of experiments to generate results on upset forging with annealed aluminium as material. The findings of their works suggest that the stresses increase with the increase in the metal deformation. The hoop stress and axial stresses are found to be linearly related to each other. Further, the calculated and experimentally obtained radius of curvature was found to be in good agreement. The authors' Hirt et al. [41] undergone deep research on designing a die to avoid premature failures. After experimentation, it was found that the work hardening and frictions were the most influencing parameters which should be considered during die design. They have investigated a prototype die for forging an aluminium billet with different area of reductions and further with varying lubrication conditions. Finally, it has been concluded that the lubricant is supportive in reducing the forming load compared to the unlubricated case.

Kuzman et al. [42] performed an experimental and numerical analysis of combined extrusion (backward can and forward rod extrusion) process. The article deals with the die geometry and friction, which are interconnected with type of lubrication for combined extrusion. The primary objective of the FEM analysis was to find a way to reduce the effort for die designing, along with reducing the cost and wastage of material. It was concluded that the FEM analysis gave more accurate results related to the metal forming. In this context Shan et al. [43] investigated an experimental analysis for forging an aluminium alloy rotor. A female die was made with exact replica which consists of 23 radial twist blades. The experiments are performed in a fully isothermal closed die condition. The conclusions drawn from the article tells us that by an improved mechanical forging process, manufacturing of complex components is easier which reduces the machining cost and time. Experimental, numerical and analytical analyses were performed for a component of staggered branches by Monaghan [44]. The process was carried out using lead as the elasto–plastic material at room temperature. A two half split billet was used to understand the metal flow patterns during the filling of dies. Experimentally observed flow pattern also matched with that obtained by FEM analysis and they also used the upper bound analysis for load prediction. The conclusion drawn from the article said that either FEM or upper bound analysis can be used to predict the parameters for this type of metal forming processes.

Authors Farhoumand and Ebrahimi [4] used FEM based ABAQUS® software for analysing metal forming process which involves forward, backward and radial flow of

metal, i.e., gears, flanges, hollow shafts, etc. They have found the effect of parameters such as the die corner radius and friction on forging load. They have designed the die apparatus taking the results obtained from FEM for the experimental analysis. They observed that the cup formed by forward extrusion is smaller than that is formed by backward extrusion, which can be controlled by changing the friction factor. In the recent times, Lee et al. [45] explored the geometrical parameters which were assumed to be least importance till date. In the DCEP (Double Cup Extrusion Process) surface expansion, contact pressure, sliding velocity and distance are focussed. The surface stresses generated during the backward extrusion and forward extrusion are measured. The results concluded that the maximum extrusion force has an insignificant dependence on the thickness ratio.

Uyyuru and Valberg [46] made special tubes with contrast materials of the intrinsic pattern by backward extrusion and studied the flow characteristics using FE simulation. They used soap film as a lubricant with a conversion coating. They proposed a new circle method, found to be usefulway to predict the frictional conditions. Dong and Xianghuai [47] investigated the radial forging process numerically, analytically and experimentally. An upper bound approach was applied; where the geometry coordinates system and velocities are mapped to straight lines. The analysis was compared with FE simulation and experimental results. Rayes and Danaf et al. [48] redesigned a die to manufacture T-shape products at different friction conditions by the metal forming process. Experiments were conducted using copper billets and concluded that friction have very marginal effects.

Rokni et al. [49] conducted an experimental analysis to study the microstructural characteristics of 7075 aluminium alloy. The experiments were performed at various strain rates in room temperature. From results they concluded that during backward-thixo forming the grain are elongated due to higher strain rate, may be due to a higher temperature. They also observed that higher the ram speed better the product with good/enhanced mechanical properties. Garbacz et al.'s [50] article gave us a glimpse of surface inspection, multimodal analysis and thermography analysis. The thermography analysis gave an idea of the different temperature regions of the extrusion profile. Further, the proposed hybrid method is found to predict appreciable results that can be used for inspection of defects arising in extruded products.

A novel backward extrusion process was investigated with the reduced billet size by shatermashhadi [51]. The experimental and numerical analysis was performed and

results were compared. In the novel backward technique, it was found that the product was manufactured at the $3/4^{th}$ of the load that was required for the general backward process. He claimed that the load was decreased due to plastic strain that is two times the conventional backward extrusion process. It was also found that the ultrafine-grained particles may be expected. A kinematically velocity field for upper bound elemental technique (UBET) has been developed and applied to forward spiral extrusion by khoddam et al. [52]. The axisymmetric forward spiral extrusion was performed using lead billets and experiments are conducted to validate with the analytical results. It was noticed that the die reaction torque and extrusion force increased due to increase in die-helix angle. Lee et al. [7] studied a forward-backward extrusion process applied to hexagonal and trochoidal wrench bolts experimentally and using UBET. The parameters, namely forming load, extruded length, deformation pattern, are taken into consideration taking lead billet as material. Further, the experimental and analytical results are used for comparison. Ranatunga et al. [53] approached a UBET to design the flash gap in a forging process to generate an axisymmetric shape. They assumed that the entire forging process took place in different sub-stages, like, extrusion stage, back-filling stage, etc. Finally, the total analysis was examined by the FEM simulation results with analytical results. Ishikawa et al. [5] proposed an optimal ram motion to control the heat generation in the cold backward extrusion of an aluminium alloy. They found that inhomogeneous temperature distribution due to differential strain causes local heat shrinkages. It was found that temperature ultimately affects the accuracy of the product; due to this, a optimal ram motion was proposed. As the heat is generated locally, it was difficult to avoid the local deformation due to heat contraction. Finally, it was found that to get a precise product during deformation, cooling process with an oscillatory motion is most suitable.

2.2.3 Analytical analysis

A significant trend has been observed in the extrusion-forging industry towards the production of precision components with minimal lead time. Metal forming in general, extrusion-forging in particular requires sever compressive load, which makes the design of die very critical. In this context, many methods have been developed to calculate the load requirement. Various researchers have proposed different analytical methods to predict the metal flow and extrusion-forging load at different time.

Choi et al. [2] proposed a new kinematically admissible velocity field for forging of spur gears using a hollow billet with flat punch by upper bound analysis. It was found that hollow billet preferably decreased the forging load than solid billet for the production of gears. The forging pressure was found to be increased with reduction of height and number of teeth. It was also found that for a given module hollow gears were more work hardened than solid gears. Choi et al. [54] investigated the forging of helical gears by two forging processes, guiding type and clamping type, using UBET. The billet was phosphate coated and MoS_2 sprayed for lubrication. It was found that the predicted forging loads by UBET were in good agreement with experimental results. It was seen that relative forging pressure increased with the number of teeth for guiding type forging but for clamping type it decreased. The relative average forging pressure dropped with increase in helix angle for both type processes. The punch pressure of guiding type was found to be lower than clamping type. Can et al. [3] proposed a kinematically admissible velocity field with various parameters to determine the punch pressure & extrusion load for lateral extrusion of spline and spur gears. It was found that average punch pressure components to overcome friction portion and internal deformation part increased with increase in punch displacement. Due to the complexity of non-uniform metal flow, Kim et al. [55] investigated the extrusion of square shape from a round billet mathematically and experimentally. They have used upper bound analysis to predict the extrusion load and extruded length under different friction conditions. This article concluded that the theoretical predicted extruded length was in good agreement with the experimental result.

Kwan [56] has shown a mathematical/numerical analysis on extrusion and forging processes using the upper bound elemental technique for axisymmetric shaped products. He applied the proposed technique to estimate extrusion load and velocity field for trochoidal and elliptical shaped products. The lubricant was taken as MoS_2 mixed with grease. The estimated values for both shapes were found to be in good agreement when the friction factor was considered as 0.2. Choi et al. [57] considered a phosphate coated aluminium alloy Al 2218 as a billet for their analysis to get trochoidal gear and used upper bound elemental technique. Two types of billets (solid and hollow) were taken and found that the results are matching with the obtained experimental data. Kumar and Prasad [58] proposed an upper bound rigid plastic element (UB - RPE) model for axisymmetric cold and hot forging to determine the optimal power. The results predicted that various

parameters like higher ram velocity and friction between die-billet interface increase the power requirement for the process. Also, it was found that extrusion ratio and die length has a significant effect on the extrusion power. The results obtained by UB- RPE are found to be in good agreement with the experiment. Kim and Yang [59] proposed a kinematically admissible velocity field to describe the 3D deformation for upset forging. A square section was considered to find the forging load. The effect of friction was tested using Teflon sheet lubrication and dry lubrication. It was found that bulging along thickness was negligible in lubrication condition. The upset forging experiment of square blocks was carried on a hydraulic press at room temperature. Jung et al. [60] proposed a three-dimensional kinematically admissible velocity field for the extrusion of helical shape from a round billet using different lubrication condition. Upper bound solution was formulated from the derived velocity fields for rigid-perfectly plastic material and various parameters were analysed. It was found that the extrusion pressure increases with increases in helix angles. Alvir et al. [61] Proposed a limit analysis method for drawing process of solid components under plastic strain condition. They analysed multi-block models to study the process comparing different velocities with compatible boundary conditions. Various process parameters like die semi-angle, friction coefficient (μ) and reduction (r) were considered. It was found that $\sigma/2K$ value for partial friction model is larger than cold friction model for reduction over 20%.

Ranatunga et al. [53] investigated UBET to design the flash gap for forging operation applied to axisymmetric shapes. The parameters such as forging load, die cavity filling, and effective stress-strain were considered for the analysis. A C-program was developed where the material followed Von-Mises yields criteria to fill the cavity in extrusion and back filling stages. The UBET technique was validated with the results obtained using FEM for the back-filling stages. It was found that the load increases as the flash gap decreases. Lee et al. [7] proposed a kinematically admissible velocity field to analyse the combined forward-backward extrusion in hexagonal and trochoidal shaped wrench bolt. The billet was chosen as antimony lead. Various parameters like punch load, extruded length, flow pattern, etc. were taken into consideration. It was found that forming load increases slowly upto certain punch displacement, subsequently load increases rapidly for both bolts. Bramley [62] used upper bound analysis for realistic flow simulation dividing deformation zone by tetrahedral blocks for extrusion and forging processes. The author analysed the process to find the approximate forming load using

UBET and TEUBA (Tetrahydral Element Upper Bound Analysis). Bhattacharya et al. [63] predicted the metal flow pattern of extrusion by developing an algorithm. The algorithm solved the metal flow applying hydrodynamic formulation. The slip-line theory was adapted to the mathematical analysis and compared with experiments.

Chitkara and Yohngjo [1] focused on the application of upper bound analysis to forge gears with straight tapered teeth. They have proposed a kinematically admissible velocity field to predict forging pressure and deformation at different stages. They also compared their results with that of experiments performed taking plasticine as working material at various frictional conditions. They also performed experiments using aluminium alloy LY12 (AISI 2024) as workpiece with castor oil as the lubricant. A new technique has been applied by the combination of an energy formulation with the upper bound elemental technique by Moller et al. [64]. The technique was used to predict the effective strain and temperature during the forging process of an axisymmetric product. Further, the performed analysis was compared with the effective stress-strain obtained using FEM. The new technique provides a new route to predict the hardening at different strain rate for the temperature dependent materials. Finally, it was found that the theoretically augmented UBET was in good correlation with FEM results. The monotonic loading technique has led the interest for Macijewski and Mroz [65] in metal forming processes. Their work was mainly concentrated on the cyclic rotating of the die at varying amplitude and frequency. During the process of cyclic torsion on the die, the extrusion pressure at different strain rates was observed. An upper bound analysis was performed assuming a rigid plastic material model using a proposed kinematically admissible velocity field. The results concluded that the plastic flow is higher at the bottom region with higher rotational frequency of the die. Lee and Kwan [66] considered UBET to find out the load on the upper die for convex circular parallelepiped and convex spherical shapes. The velocity field is determined by assuming a kinematically admissible velocity field. Along with the UBET analysis, experimental analysis was performed for the same using lead billet at room temperature. The results showed increase of load with the flash height. Further, the experimental and UBET analysis also support the same.

Yang et al. [67] proposed a fourier transformation formulation for the prediction of die profile required for a complicated shapes and a kinematically admissible velocity was also proposed for finding the effective forging load. The material was taken as rigid plastic

for both theoretical and experimental investigations. Aluminium billet is used for experimentations to extrude rectangle section from round section. The flow pattern and load predicted by theoretical analysis were found to be in good agreement with the experimental results. Han et al. [68] performed analytical and numerical analyses to get clover section from round billet. They have approached an analytic function with upper bound technique using a proposed the kinematically admissible velocity field. The analytical and numerical analysis predicted the flow pattern and forming load required for the extrusion process. Yang and Han [69] have used AISI 4140 steel billets for cold extrusion of the axisymmetric shapes using arbitrarily curved dies. Interest was shown to predict the extrusion load and flow pattern of the material by optimizing the parameters obtained by upper bound technique. Further, an FEM analysis was performed using a bi-quadratic polynomial for die profile to check out the correlation. Sahoo et al. [70] investigated on extrusion for the round-to-triangle section using a discontinuous velocity field called SERR (spatial elementary rigid region) technique. The study was focused on the remodelling the UBET technique to handle round billets. Patra et al. [71] focused on the experimental and analytical analysis of lateral extrusion using SERR technique. The investigation was performed using round billets to get different section heads by means of square/flat dies. Similar kind of works have been carried out by many researchers [72–74] to remodel the SERR technique to accommodate the round billet to get hexagonal, square and T-sections. Hsu [75], Choi and Choi [76] and Choi et al. [77] used the upper bound method for forging of spur gears. Subsequently, the results were compared with that obtained from FEM-based numerical analysis and/or experimental observations.

2.2.4 Tribological analysis

The forming load is an important parameter in cold extrusion process which depends mainly on lubrication. A lubricant can direct metallic contact and reduces the forming load which inturn offers improved product quality and better die life. The present section deals with past work carried out by different researchers using various lubricants and their effects on the metal forming parameters.

Jayaseelan et al. [78] carried out experiments with and without lubrication conditions and studied the effect of friction on tool & work piece in the extrusion process. Graphite powder with molybdenum disulphide (MoS_2) & zinc stearate (ZnS) was used as lubricants for the extrusion of AA6063 material. The experimental and numerical

extrusion loads were compared and found to be in good agreement. A Prototype experimentation was conducted by fereshtehsanill et al. [79] to gain knowledge on effect of lubricant on metal forming processes. To analyse the same, a gravity drop hammer test was conducted at various strain rates along with numerous ring tests. Three types of lubricants were used to determine the friction factor for plasticine and lead specimens by means of a double cup extrusion process. Sawamura et al. [80] proposed a new method by which friction coefficient can be measured in the backward extrusion process. The method deals with a combined measurement of load and torque. For the study, they have used a die set to rotate the punch at very slow angular velocity. Four types of lubricants were taken, namely, mineral oil, cold forging oil, bonderzing and dry-in-place. It was found that friction coefficient for dry-in-place had higher values than other lubrication condition at all testing temperatures. The friction coefficient was found to be less than 0.1 when adhesion occurred in punch load.

Asai and Kitamura [81] summarized various lubricants used for hot forging of steel by ring compression test. Experiments were conducted in mechanical and hydraulic press. It was found that coefficient of friction was varying depending upon the type of press used. Higher coefficient of friction was observed during ring test when the hydraulic press was used for the non-graphite type of lubricants at high or low speed of ram. The study revealed that non-graphite type of lubricants predicts similar value when compared with graphite type of lubricant. The coefficient of friction was low when graphite type lubricant was applied in a small amount. Finally, it was found that lubricants were retaining their lubrication property when the temperature is less than 450^{o}C. Hafis et al. [82] analysed the deformation of aluminium billet with Paraffinic mineral palm oil as lubricant for the cold forward extrusion process. Paraffinic mineral palm oil used were taken in the range of coefficient of friction 0.12 to 0.9. It was found that contact pressure and load in cold forward extrusion were reduced due to the use of lubricant. Wang et al. [83] investigated and compared the different friction testing methods for extrusion of aluminium to study their effects on forming characteristics. Among all the used friction testing methods, it is found that combined extrusion friction test and sliding distance ball on the disc are most suitable. The contact pressure was found to be increased when ball size decreased and decreased when sliding distance increased.

Arentoft et al. [84] developed a new lubricant carrier for cold forging process. The surfaces were generated by electrochemical deposition of two immiscible metals by etching. These surfaces acted as lubricant carrier. The deposited layers are evaluated by ring compression and double cup extrusion tests. It was found that mineral oil lubricant had a low viscosity which leads to low friction and increase in resistance toward galling compared to non-coated surfaces. It was observed that when coating and soap lubrication was applied the friction and resistance towards galling shows better results.

Sagisaka et al. [85] proposed a new friction test based on combined forward spline-backward extrusion. Aluminium fluoride coating got replaced by a double-layer solid film lubricant for its eco-friendly nature. It was found that the double-layer solid film showed high lubrication performance in comparison to aluminium fluoride coating. Matsumoto et al. [86] proposed a new forming method, where a servo press pushed a ram with high aspect ratio to combine pulsed and step-wise modes. The analysis was carried out for combined forward-backward extrusion process. The shear friction coefficient was determined by experiments and numerically by FEA. It was found that the forming method with appropriate pulsed punch motion reduces the shear friction coefficient to lower than 0.2. A liquid lubricant was supplied through the internal channel for retracting of punch. Syahrulail et al. [87] investigated palm oil as a lubricant oil for the cold forward extrusion process. The study was performed to compare the results with paraffinic mineral oil data. The velocities and effective strain were calculated by viscoelasticity method. It was found that palm oil showed good lubrication performance by reducing the friction and extrusion load compared to additive free paraffinic mineral oil.

Hafis et al. [82] investigated the effect of paraffinic mineral oil as a lubricant for the cold forward extrusion process. It was found that at the friction factor 0.09, it is the most suitable lubricant for reducing the extrusion load. It was noticed that the contact pressure on taper dies surface is reduced by using paraffinic mineral oil as a lubricant. It was suggested that extrusion load can be reduced if a correct quantity of lubricant is taken. Caminaga et al. [88] investigated the effect of various lubricants. The lubricants tested were mineral oil, semi-synthetic oil, powder soap and wheat flour which are less pollutant than zinc phosphate or MoS_2. It was found that for single stage extrusion wheat flour can acted as a best lubricant and mineral oil would be a better lubricant for two stage extrusion. Bay et al. [89] and Schrader et al. [90] adopted simulative based tribological

analysis for cold forging process and compared the same with experimental results. The test was performed to establish the friction stress for aluminium and stainless steel with different lubricants.

2.3 Research Gaps Identified from the Literature Review

On the basis of literature review, following research gaps have been identified:

- It is observed from the exhaustive literature review that most of the studies have targeted the bulk metal forming through, a single route process such as forward, backward, and/or lateral extrusion techniques to manufacture a component. Small amount of works have been reported regarding CEF and CE processes and particularly no report was found on manufacture of an industrial component, a collet chuck holder.
- From literature review, it was observed that very less works have been reported on combined extrusion-forging and combined extrusion processes. Most of the works were limited to experimental analysis only. Hence, a deep assessment for improvement of mechanical and metallurgical properties of components manufactured through CEF and CE processes is required.
- In the available literature, analytical analysis has been investigated using single route process (forward/backward extrusion) by various researchers. It is pertinent to mention that upper bound elemental method predicts appreciable results in comparison with other techniques with less computational cost and time. Hence, the focus on upper bound technique for predicting the forming load is needed for a complex component.
- Very few analyses are reported to date based on effect of lubricants or combination of different lubricants on CEF and CE processes. Under the influence of tribological conditions the mechanical and metallurgical properties of a component alter during CEF and CE processes, which has not been emphasized in past research work.
- Very less investigation on metallurgical parameters such as hardness, grain orientation and residual stress have been reported on CEF and CE processes.
- The impact of process parameters on forming load, metal flow pattern and its validation through optical/electron microscopy for CEF and CE processes has not been found in many reported investigations.
- Not much literature is available on numerical analyses on CEF and CE processes.

2.4 Novelty of the Present Investigations and Methodology

The identified research gaps have been filled by the present investigation and the novelty of the research objectives can be summarized as follow:

- The present work deals with a novel approach for manufacturing of various collet chuck holders by CEF and CE process (which are conventionally manufactured through casting and machining) under various tribological conditions with varying ram velocities. Further, to analyse the process experimentally and validate the same with analytical and numerical results.
- To propose suitable kinematically velocity fields for the application of upper bound elemental technique to predict the forming load at different stages of extrusion process for manufacturing the components. The analysis is performed under the influence of different friction factors and at varying rates of ram displacements.
- An experimental set-up was designed fabricated, performed tests were performed with different lubricants and different rates of ram velocities.
- Numerical analyses were performed to predict the results with similar conditions of experimental analysis.
- The manufactured components were characterized metallurgical (Optical microscopy, residual stress) and mechanical (Hardness). To test the influence of various parameters.
- The analytical, numerical, experimental and metallurgical results are compared to substantiate the suitability of the proposed CEF and CE process to manufacture the collect chuck holder.

The overall methodology to be followed for this research work is shown in form of flow chart in Figure 2.1.

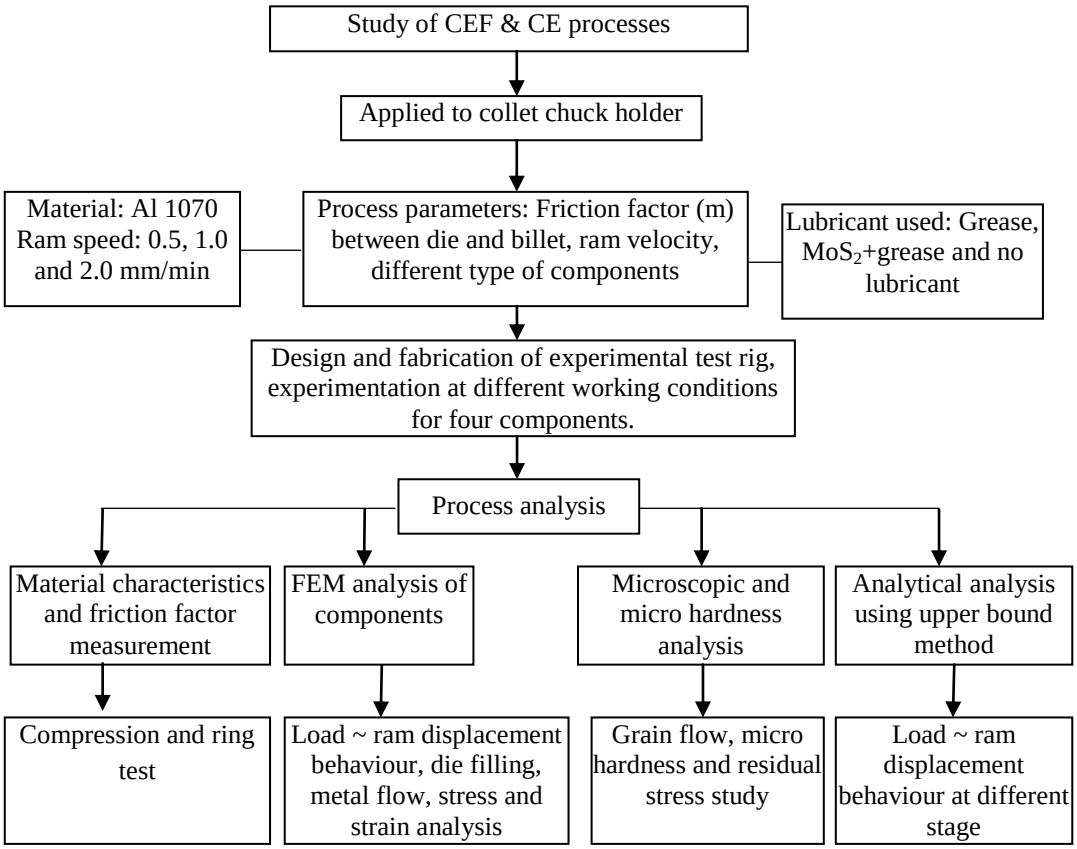

Figure 2.1: Methodology of the present investigation

2.5 Summary

The chapter present's a critically review of various developments took place during the years in metal forming. The literature presented on extrusion and forging processes by different researchers were analysed, and the research voids are identified. The chapter consists of four sub-sections summarizing experimental, analytical, numerical, and tribological works.

- The collected work related to experimental analysis describes various bulk metal forming techniques such as forging, extrusion, and combined routes to obtain various components and how different parameters influences the process.
- The analytical study explains about, the application of different techniques such as upper bound method; slip line field analysis, slab method and SERR (Spatial elemental rigid region) techniques. This section is primarily focused on the analysis performed by different researchers to predict the forming load.

- The numerical analysis section describes the progressive application of numerical methods, mostly FEM, to simulate the different bulk metal forming processes.
- The tribology section describes various lubricants employed in the metal forming processes.
- Research gaps are identified; novelty of the present work with methodology to be adopted is depicted.

In the next chapter, different analytical methods including upper bound technique which can be utilised to predict the load requirements to manufacture four type of collet chuck holders is described.

Chapter 3

Solutions to Metal Forming Problems

3.1 Introduction

It is very difficult to analyse the metal forming processes to find the actual stress-strain field in practical conditions because of complexity in the deformation mechanics. When the influence of friction and other metallurgical factors are considered, it becomes even more complicated. All analytical techniques applied to solve metal deformation problems are based on simplified assumptions with regard to material behaviour's and boundary conditions [91]. Metallurgical issues, for example, grain size and shape, internal flaws like dislocations, non-homogeneities in structure, etc. are usually ignored in most of conventional means of solutions.

In most of the cases, the influences of temperature and strain rate are ignored because these cannot be effectively taken into consideration in plasticity rules with the present state of understanding. For a symmetrical geometry and homogeneous deformation, the mathematical analysis is also tedious with all these simplified assumptions. Metal forming problems in general, combined extrusion-forging of a collet chuck holder in particular, involves different frictional conditions, non-homogeneous deformation, anisotropy of material, strain hardening, etc. In addition, some solutions will give average stresses and strains whereas others give local distributions. Although, simplified assumptions will decrease the efficiency of the obtained results for a real situation, however, of requirement some approximation to be made for estimation of load required in tooling design. There are a number of approximate methods (graphical, analytical and/or numerical) are proposed to analyse the metal forming problems [92].

3.2 Solution of a Plastic Deformation Problem

The theory of plasticity is the formulation of the mathematical relationship of stress and strain in plastically deforming solid (metals). The governing equations for the solution of the mechanics of plastic deformation of rigid-plastic materials must satisfy equilibrium equations, stress-strain relations, yield criterion, compatibility equations, and boundary

condition on stress, and boundary condition on velocity and volume constancy. As the strain involved in plastic deformation process is very large, it is usually possible to neglect elastic strain and consider only the plastic strain (rigid-plastic region). The strain hardening is also neglected to formulate the analysis simpler. Thus, a solution should satisfy the following conditions:

(a) The static equilibrium equations:

$$\frac{\sigma_{ij}}{x_j} + X_i = 0 \qquad (3.1)$$

Where σ_{ij} is the stress tensor and X_i is the body force per unit volume. In the absence of body forces, there are six unknown stress components in these three equilibrium conditions.

(b) The instantaneous yield condition:

One of the simplest is the von Mises yield condition, which gives

$$\sigma'_{ij}\ \sigma'_{ij} = 2k^2 \qquad (3.2)$$

Where σ'_{ij} = deviatoric stress tensor and k = the yield stress in shear.

(c) The six plasticity equations:

Most commonly used are the Prandtl-Reuss equations, which give

$$d\varepsilon'_{ij} = \frac{3}{2}\sigma'_{ij}\frac{d\bar{\varepsilon}^P}{\bar{\sigma}} + \frac{d\sigma'_{ij}}{2G} \qquad (3.3)$$

Where ε'_{ij} is the deviatoric strain tensor, $\bar{\sigma}$ and $\bar{\varepsilon}$ are the effective stress and strain respectively and G is the modulus of rigidity. Strain components are related to the displacement components by $\varepsilon_{ij} = \frac{1}{2}\left(u_{i,j} + u_{j,i}\right)$ (3.4)

and we know that $\varepsilon_{ij} = \varepsilon_{ji}$. The six equations of plasticity can be written in terms of displacement (u, v, w) and the stress components.

(d) The volume constancy condition:

It gives a relation among the normal strains, ε_{ii}. It is taken care by the plasticity equations.

Thus, we have ten unknowns, which include six stress values, three displacement components and one yield stress. Hence, theoretically, exact solution is possible. However, as discussed earlier, at present there is no general procedure to obtain such a solution. As a result, several approximate analytical and numerical techniques are proposed by different researchers. Some of the commonly used ones are:

i. Uniform energy method

Siebel [93] proposed the ideal work or uniform energy method of solution for metal forming processes. It uses the principle of work or energy balance. External work/energy is equated with work/energy consumed for plastic work/deformation. Process is assumed to be ideal, i.e., all work/energy supplied is completely utilised for plastic work only. Effect of friction and non-homogeneous deformation are ignored. Therefore, we estimate the minimum amount of work required and can also estimate the minimum force required. This approach assumes that the change in geometry/plastic deformation in a process is carried out in the most efficient way possible. An ideal/hypothetical process is assumed which produces the desired shape change by homogeneous deformation, i.e., forging by compression, wire drawing by uni-axial tension, etc.

ii. Slab or Stress equilibrium method

It is also called free body-equilibrium approach, makes a force balance on a slab of metal of differential thickness in the deformation zone. This produces a differential equation, where variations are considered in one direction only. Using relevant boundary conditions, an integration of this equation then provide a solution.

The major assumptions considered are: i) The direction of the applied load and planes perpendicular to this direction define principal directions, and principal stresses do not vary on these planes, ii) Although effects of surface friction are included in the force balance, these do not influence the internal distortion of the metal or the orientation of principal directions, and iii) Plane sections remain plane, thus the deformation is homogeneous in regard to the deformation of induced strain.

iii. Slip-line field theory [92]

In most of the metal deformation processes, the material undergoes a large plastic strains. The magnitude of elastic strains is very small in comparison to plastic strains, can safely be ignored. In that situation, the metal will behave like a rigid-plastic material. Non-homogeneous plane strain deformation of a rigid-perfectly plastic material can be analysed by slip-line field theory. We know that the equilibrium equations of plane strain deformation are hyperbolic and the characteristics arc lines of maximum shear stress called slip-lines [94]. Different graphical and mathematical methods are available for the construction of slip line nets for various boundary-value problems. Hencky [95] proposed

a set of relationships to find out the stress state of a point along the slip line from knowledge of the stress condition at other points. Hilda [96] proposed a similar set of relations to determine the velocity distribution for the slip-line field.

Slip line theory has been used extensively for plane strain deformation [94]. The analysis is generally limited to the behavior of a rigid plastic, non-work hardening material when temperature and strain rate effects are neglected. Oxley and Palmer [97] have attempted to include work-hardening of material in slip line field theory but still no general procedures have been developed to solve problems of forming strain hardening materials. Hill [98] showed that beside idealized assumptions made for the work material; many times slip line solutions provide more than one answer for a particular set of boundary conditions. In addition, most slip line solutions are incomplete, i.e., while the rate of plastic work may have been determined to be positive throughout the deforming regions, the stress state in the assumed rigid regions has not been examined [99]. Attempts by Charles [100] have been made to solve axisymmetric problems by assuming an artificial yield condition which makes the equations analogous to the plane strain equations. Shield [101] has shown, however, that when the Tresca yield criterion and associated flow rule are employed, the governing equations are kinematically or statically determinate in character. The stress and velocity fields are then hyperbolic with identical families of characteristics. The equations along slip lines are however more difficult to handle compared to those for plane strain and are generally employed in their finite difference form. Except for some simple problems, slip line theory has not been applied successfully to solution of axisymmetric problems.

iv. Visio plasticity method

This technique has been developed by Thomsen and co-workers [102, 103]. In visio plasticity technique the distortion of grids marked on a plane of symmetry is analysed by means of the differential equations satisfying plastic flow of materials. The velocity components, strain rate and stress distribution are calculated from the experimentally determined flow lines by the use of a computer technique [104]. This method provides all the necessary information about the mechanics of the process and can be applied to both plane strain and axisymmetric metal forming problems. Still, the major drawback of this technique is that an experiment must be carried out first before a solution can be found out.

v. Finite element method

With the fast growth of digital computers and enhancement of their speeds and memory it is now possible to analyse practical metal forming problems using finite element method. The formulation of finite element method for metal forming processes has been performed by many researchers, and results have been reported for numerous engineering problems [99, 105]. In many forming problems, the geometrical configuration of the deforming body changes continuously during the process and these changes in shape can be determined only by following the path of deformation. Where further deformation maintains the original geometry, slip-line field theory can be used to provide solution to plane strain deformation. Where the original geometry is not maintained, a step by step solution may be required for problems involving large plastic deformations. The finite element method, which also provides only an approximate solution, can successfully be applied to such problems.

vi. Upper bound method

An upper bound solution will give a load prediction that is greater than or equal to the exact load cause a body to experience full plastic deformation. The upper bound is also associated with the principle of maximum work, but in the point of view of strain. It states that among all kinematically admissible velocity fields the actual one minimize the deformation load. A kinematically admissible velocity should satisfy the continuity equation, velocity boundary condition and volume constancy condition. In metal forming operations, it is of greater interest to predict a force that will cause the body to deform plastically to produce the desired shape change. Upper bound analysis focus upon satisfying a yield criterion and assuring the shape changes are geometrically self-consistent.

Attention has been consolidated on obtaining upper bounds to the yield point load, since, in metal forming processes, over-estimate constitutes a safe load. This technique has played a dominant role in the analysis of three-dimensional metal deformation process. Because it gives a complete solution to the problem consists of an equilibrium stress field and the associated velocity field satisfying the deformation occurs even with the rigid-plastic assumption and does not violate the yield criterion in the rigid region. Besides, other available analytical techniques such as Hill's [94] general method is usually not suitable to deal with problems involving complex geometries.

The upper bound solution is constructed on a kinematically admissible velocity field. A velocity field satisfies the compatibility, flow rule and the velocity boundary conditions both in the rigid as well as the plastic zones is known as kinematically admissible velocity field. When the admissible velocity field is determined, upper bound to the deformation load is estimated from virtual work principle by equating the rate of external work done to the rate of energy dissipated.

For a continuum deforming plastically in contact with a die, the rate of energy dissipated, J, is given by the relation

$$J = J_1 + J_2 + J_3 \tag{3.5}$$

where,

J_1 = internal power dissipated due to plastic deformation,

J_2 = power for shear deformation against the velocity discontinuities, and

J_3 = frictional power dissipated at the tool/work interface.

For a material obeying Levy-Misses flow rule, the internal power J_1 is given by

$$J_1 = \frac{2\sigma_0}{\sqrt{3}} \int_v \sqrt{\tfrac{1}{2}\dot{\varepsilon}_{ij}\dot{\varepsilon}_{ij}}\, dv \tag{3.6}$$

Where,

σ_0= yield stress in uniaxial tension, and

ε_{ij}= strain rate tensor

Evidently, the internal power is computed by integrating Von-Misses work equation [106] over the total volume V_0.

The power of shear deformation J_2, along the velocity discontinuity surface S_i in the deformation zone is given by

$$J_2 = \frac{\sigma_0}{\sqrt{3}} \int_{Si} \left|\Delta V\right|_{Si} dS_i \tag{3.7}$$

Finally, the friction power J_3, dissipated at the tool/work piece interface is determined from the relation,

$$J_3 = \frac{m\sigma_0}{\sqrt{3}} \int_{S_{D_i}} \left|\Delta V\right|_{S_{D_i} i} dS_{D_i} \tag{3.8}$$

Where, m is the friction factor and $|\Delta V|_{Si}$ and $|\Delta V|_{S_{D_i}}$ are the magnitude of velocity discontinuity at the surfaces S_i and S_{D_i} respectively.

The power *J*, calculated from equation (3.5), will be exact when the kinematically admissible velocity field postulated for the forming process under consideration is the actual one. But, if it is different from the actual, equation (3.5) yields an upper bound to the power necessary for the forming operation in question. This is precisely the upper bound method as suggested by Hill [94] for a rigid-perfectly plastic material.

The present chapter is devoted to a brief discussion of the various techniques normally employed to derive kinematically admissible velocity fields in case of three-dimensional metal deformation problems. While such techniques for plane-strain problems are well established [94, 107–109], similar procedures for three-dimensional problems are relatively recent. The following section presents a brief review of the methods normally employed to construct admissible velocity fields for the three-dimensional problems. A generalized procedure is presented to construct the velocity field when the deformation zone is subdivided into rigid tetrahedral blocks. A two-dimensional deformation problem where the deformation zone consists of triangular rigid regions is solved applying the proposed procedure.

3.3 Techniques for Deriving the Kinematically Admissible Velocity Fields in 3-D Metal Deformation Problems

Numbers of techniques have been reported to find out kinematically admissible velocity fields for three-dimensional metal forming problems. These are,

1. The Dual stream Function Method,
2. The Conformal Transformation Technique,
3. The Generalized Velocity Field Technique, and
4. The SERR Technique.

The first three techniques mentioned above lead to continuous velocity fields in the deformation region, where the velocity at any point is described by a continuous function of the space coordinates, whereas, the last method leads to a discontinuous velocity field.

The following sections outline the salient features of these techniques and their limitations.

3.3.1 Dual stream function method

For ideal fluid flow in three dimensions, Yih [110] suggested the use of two stream functions in place of one as in case of two-dimensional flow. Each stream function represents a class of surfaces called stream surfaces. The line of intersection of two stream surfaces, one taken from each class, is the three-dimensional stream line. Nagpal [92] used these dual stream functions to determine kinematically admissible velocity fields for different three-dimensional plastic flow problems.

Let $\Psi_1(x, y, z)$ and $\Psi_2(x, y, z)$ be two continuous functions. These two can be treated as a pair of dual stream functions if they satisfy the boundary conditions on velocity. The three velocity components are then given as

$$V_x = \left(\frac{\partial \Psi_2}{\partial y}\right)\left(\frac{\partial \Psi_1}{\partial z}\right) - \left(\frac{\partial \Psi_1}{\partial y}\right)\left(\frac{\partial \Psi_2}{\partial z}\right) \tag{3.09}$$

$$V_y = \left(\frac{\partial \Psi_2}{\partial z}\right)\left(\frac{\partial \Psi_1}{\partial x}\right) - \left(\frac{\partial \Psi_1}{\partial z}\right)\left(\frac{\partial \Psi_2}{\partial x}\right) \tag{3.10}$$

$$V_z = \left(\frac{\partial \Psi_2}{\partial x}\right)\left(\frac{\partial \Psi_1}{\partial y}\right) - \left(\frac{\partial \Psi_1}{\partial x}\right)\left(\frac{\partial \Psi_2}{\partial y}\right) \tag{3.11}$$

When the velocity field is generated through equations (3.09-3.11), becomes kinematically admissible since the continuity condition is implicitly satisfied. The only limitation of this procedure is that it may be extremely difficult to find dual stream functions when the section shape is complex or when it involves re-entrant corners.

3.3.2 Conformal transformation technique

In ideal fluid flow problem in three dimensions, the equation of a stream line is given by

$$\frac{dx}{V_x} = \frac{dy}{V_y} = \frac{dz}{V_z} \tag{3.12}$$

By finding a transformation function that transforms an intermediate section in the deformation zone along the axis into a unit square (or circle), it can be stated as

$$\frac{dx}{F(x, y, z)} = \frac{dy}{G(x, y, z)} = \frac{dz}{1} \tag{3.13}$$

Functions F and G depend upon the parameters of the section geometry which are functions of x, y and z. Comparing equations (3.12) and (3.13) we get,

$$\frac{V_x}{F(x,y,z)} = \frac{V_y}{G(x,y,z)} = \frac{V_z}{1} \tag{3.14}$$

The axial velocity component V_z is found by applying the continuity condition (or volume constancy condition) to the deformation zone. Thus,

$$V_x = \frac{A_b V_b}{A(z)} \tag{3.15}$$

Where,

A_b , V_b = billet cross-section area and billet velocity respectively, and

$A(z)$ = cross-sectional area of the die cavity at any point on z-axis.

Hence, velocity components V_x and V_y can be calculated using equation (3.15).

The present method is similar to the dual steam function method (section 3.3.1) in the sense that in either case the velocity at any point in the deformation zone is calculated from the corresponding equation to the stream line through that point. But this method is more versatile and can deals with problems involving relatively complex geometries for which dual stream functions may be very difficult to guess. With all its advantages, however, its application is limited to only such sections where the product shape is similar to that of billet. Hence, it is more suitable for polygonal sections with axial symmetry (sections that can be inscribed in a circle) but may lead to considerable difficulties when dealing with sections with re-entrant corners.

3.3.3 Generalized velocity field technique

The conformal mapping technique discussed in the preceding section suffers from three basic limitations. Firstly, for a mapping function to exist, the sectional symmetry must be maintained throughout the deforming region. Further, the surfaces of velocity discontinuity at entry and exit must be assumed planar and the velocity across any intermediate section in the deforming zone must be assumed constant so that it can be calculated from the continuity condition. Hence, the conformal mapping technique can be applied only to limited problems.

When the billet and the product shapes are dissimilar, section symmetry does not exist in the deforming region. Such a situation is encountered when a polygonal shape is extruded from a round billet. To deal with such problems, Yang et al. [67] have recently proposed a method in which the velocity at any point in the deformation zone is expressed as a general function of the space coordinates. The proposed method has none of the limitations

of the conformal mapping technique and has been used to analyse extrusion of clover and regular polygonal sections from round billets. The method is also suitable for predicting intermediate shapes of the die profile when extrusion is carried out with the help of converging dies. However, this method is tedious and involves considerable amount of computation for prediction of upper bound load.

3.3.4 The SERR technique

Gatto and Giardia [111] were the first team to propose a three dimensional kinematic model by limit analysis for plastic deformation which was denoted by SERR (Spatial Elemental Rigid Region). In this analysis, the volume of the solid was thought of as made up of rigid polyhedral with the plastic deformation localized on the faces of the same spatial figure, but which are allowed to glide over another whilst maintain contact. This scheme is generalized of the model used in the limit analysis of plain plastic deformation. They analyzed the characteristics of some spatial figure, which were considered as particularly useful in partitioning the space in the limit analysis of certain three-dimensional plastic deformation.

3.4 The Continuity Condition of a Discontinuous Velocity Field

As described in the previous section, in the SERR technique, the deformation zone is envisaged to consist of tetrahedral rigid blocks and each block separated from other by planes of velocity discontinuity. Each rigid block has its own internal velocity vector consistent with the bounding conditions. If there are N rigid blocks, then the number of unknown internal velocity vectors is also N and there by 3N spatial velocity components. The velocity at entry to the deformation zone (the billet velocity) is normally known. The exit velocity (product velocity) is assumed to unidirectional (coincide with extrusion axis, i.e., z-axis of the proposed coordinate system) and has a single component. Therefore, the total number of unknown velocity components in the global level is 3N+1. The unknown velocity components can be determined if an equal number of equations is generated. This is done by applying the mass continuity condition to the bounding faces of all the tetrahedral rigid blocks taken together. The set of velocity equations so generated becomes consistent and can be determined only if the SERR blocks are tetrahedral in shape, where the number of triangular bounding faces is 3N+1.

To illustrate the application of the above principles, let the equation of the i[th] bounding face in the assembly of tetrahedrons be

$$\phi(x, y, z) \equiv a_{i1}x + a_{i2}y + a_{i3}z + 1 = 0 \tag{3.16}$$

The coefficients, a_{i1}, a_{2i} and a_{3i} can be determined by specifying the coordinates of the three vertices of the concerned triangular face. Then the unit normal vector to this face is given by the relation

$$\hat{n} = \frac{\nabla\phi}{|\nabla\phi|} \tag{3.17}$$

Figure 3.1 shows a surface separating two spatial regions with $\vec{V}_1$ and $\vec{V}_2$ as the velocity vectors on both sides. The components of these two vectors normal to the separating surface ϕ are given by the following equations:

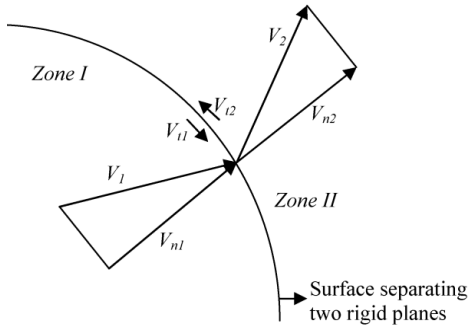

Figure 3.1: A general surface separating two rigid regions

$$V_{n1} = \hat{n}\vec{V}_1 = \frac{\Delta\phi}{|\Delta\phi|}.\vec{V}_1 \tag{3.18}$$

$$V_{n2} = \hat{n}\vec{V}_2 = \frac{\Delta\phi}{|\Delta\phi|}.\vec{V}_2 \tag{3.19}$$

If A and ρ denote the area of the surface segment and the material density respectively, then $A\rho V_{n1}$ and $A\rho V_{n2}$ are the mass flow rates across the surface segment taken from both sides. Applying the mass continuity condition and equating V_{n1} and V_{n2} gives

$$\Delta\phi\vec{V}_1 = \Delta\phi\vec{V}_2 \tag{3.20}$$

It may be noted that the regions on both sides of the surface ϕ are rigid if $\vec{V}_1$ and $\vec{V}_2$ are constant vectors, i.e., when the equation (3.20) is linear. The linearity of equation (3.20) is

assured when the surface ϕ is a plane. Thus the bounding faces of the spatial elementary rigid regions can only be planar. Some of these bounding faces may lie on the die surface (or, the dead metal surface in case of square die), or on the planes of symmetry. Since no material flow occurs across such faces, equation (3.20) takes the following form:

$$\Delta\phi\vec{V}_1 = 0 \tag{3.21}$$

The equation of each of the triangular faces can be determined when the coordinates of the three vertices are specified. Then the velocity equations can be formed by applying the mass continuity condition either in the form of equation (3.20) or (3.21) as applicable. The velocity of material in the zones I and II are V_1 and V_2 respectively are not identical. The components of velocity in the normal and tangential direction of the surface are, V_{n1}, V_{n2} and V_{t1}, V_{t2}. The normal velocity V_{n1} should be equal to V_{n2} for the continuity of the material. The tangential velocity V_{t1} and V_{t2} need not be equal. The difference is called the velocity discontinuity ΔV and is given as follows:

$$\Delta V = V_{t1} - V_{t2} \tag{3.22}$$

Such equations are formulated for each of faces bounding the rigid regions to give a determinate set of equations. This set of equations, when solved, generates the velocity components in the rigid regions constituting the deformation zone. For a plane strain problem the above solution is conveniently carried out graphically by the hodograph method [108-110]. For a three-dimensional problem involving complex geometry, however, such a method will be extremely tedious and a digital computer has to be used to generate the velocity vectors in the deformation zone. The basic advantage in formulating the equations (3.20) and (3.21) based on continuity condition is that the solution to the velocity equations can be carried out conveniently by numerical computation.

3.5 Solution of a Plane Strain Problem

The method of solution elucidated in the previous section is illustrated by taking an example of a plane strain extrusion process. The geometry of the process is shown in Figure 3.2 for a rough square/flat die. Dead metal zones ABC and DEF are formed on both sides of the extrusion axis. Only one half of the deformation zone, consisting of the triangle ABO, is considered for this analysis. Thus, this triangle is a single planar elementary rigid region is bounded by lines AB, BO and OA which are also lines of velocity discontinuity. Since the

extrusion axis is presumed to coincide with x-direction, the billet and product velocity vectors have only one component each. It may be noted that **a** and **W** are known parameters, being the half widths of the product and the billet respectively. **L**, the distance of the floating point O from the midpoint of the die orifice and **H**, the overall length of the deformation zone along the extrusion axis are two unknowns. These two variables are to be selected such that the power of deformation becomes minimum i.e., L and H are the variables with respect to which deforming power is minimized.

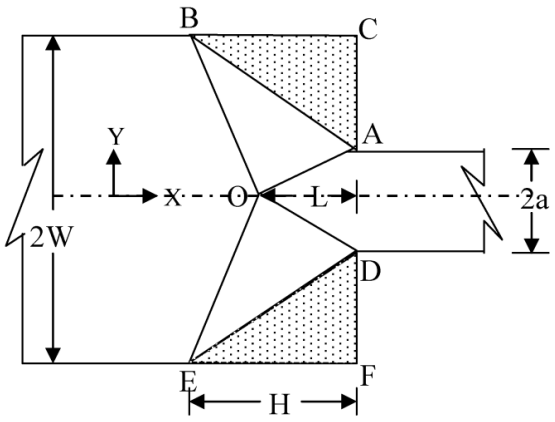

Figure 3.2: Plane strain extrusion problem

In terms of the coordinates of the vertices, the equations of the three bounding lines are given by

$$\text{Line AB: } \frac{W-a}{H}x + y - a = 0 \tag{3.23}$$

$$\text{Line BO: } \frac{W}{H-L}x + y - \frac{W.L}{H-L} = 0 \tag{3.24}$$

$$\text{Line OA: } \frac{a}{L}x + y - a = 0 \tag{3.25}$$

When the billet velocity V_b is known, there are three unknown velocity components, i.e., V_p, the product velocity, and V_x and V_y the x- and y-components of the velocity vector in the elementary rigid region.

The line AB (Figure) is the limiting line for the dead metal zone. Material enters the deformation zone across line BO and the product leaves the deformation zone through line AB. Table 3.1 describes these lines and the velocity vectors corresponding to both sides of each line.

Table 3.1: Summary of discontinuity lines and velocity vectors on their sides

Lines and their equations	Side 1	Velocity vector on side 1	Side 2	Velocity vector on side 2
AB = (W-a)x/L +y-a=0	Deformation zone	$\hat{i}\,V_x + \hat{j}\,V_y$	Dead metal zone	0
BO =Wx/(H-L)+y+ WL/(H-L)=0	Deformation zone	$\hat{i}\,V_x + \hat{j}\,V_y$	Billet	$\hat{i}\,V_b$
OA = ax/L +y-a=0	Deformation zone	$\hat{i}\,V_x + \hat{j}\,V_y$	Product	$\hat{i}\,V_p$

Employing the mass continuity condition (equations 3.20 and 3.21 appropriately), velocity equations are given by

$$\frac{W - a}{H} V_x + V_y = 0 \tag{3.26}$$

$$\frac{W}{H - L} V_x + V_y = \frac{W}{H - L} V_b \tag{3.27}$$

$$\frac{-a}{L} V_x + V_y = \frac{a}{L} V_p \tag{3.28}$$

On solving this set of linear equations the velocity vectors obtained are

$$V_x = \frac{HWV_b}{Ha + LW - aL} \tag{3.29}$$

$$V_y = \frac{-(W - a)WV_b}{Ha + LW - aL} \tag{3.30}$$

$$V_p = \frac{WV_b}{a} \tag{3.31}$$

Since the elementary region is rigid, the strain rate tensor in this region is zero. Therefore the power for internal deformation J_1, is zero. Further, the deformation zone is separated from the die surface by the dead metal zone and, as such, there is no relative motion between the two. Therefore, there is no dissipation of power due to the friction at the die faces ($J_3 = 0$). Thus the power consumed for deformation is dissipated only along the lines of velocity discontinuity. Hence in this case, equation (3.5) reduces to

$$J = J_2 \tag{3.32}$$

In the present analysis, all the lines of velocity discontinuity separate the rigid regions. Hence the absolute values of the velocity discontinuities at each line are constant. If S_{AB}, S_{BO} and S_{OA} denote the lengths of the line segments AB, BO and OA respectively and

$|\Delta V|_{AB}$, $|\Delta V|_{BO}$ and $|\Delta V|_{OA}$ represents the corresponding absolute values of the velocity discontinuities, then total deformation power can be expressed as

$$J = \frac{\sigma_0}{\sqrt{3}}\left[|\Delta V|_{AB} S_{AB} + |\Delta V|_{BO} S_{BO} + |\Delta V|_{OA} S_{OA}\right] \tag{3.33}$$

Table 3.2 describes the absolute values of the velocity discontinuities across the lines. The lengths of the corresponding line segments, calculated using the coordinates of the points A, B and O, are also mentioned. The upper bound to the deforming power can be calculated from equation (3.33) using the values of velocity discontinuities and lengths of the line segments.

The upper bound so obtained can be optimized with respect to the parameters H and L and the minimum upper bound $J_{\min}$, to the deforming power can be obtained corresponding to this velocity field. The average extrusion pressure, non-dimensionalized by σ_o, can then be calculated from the equation

$$\frac{P_{av}}{\sigma_o} = \frac{J_{\min}}{WV_b\sigma_o} \tag{3.34}$$

It may be noted here that the solution is similar to that presented by Johnson [112]–[114] using the hodograph method. This solution is given here only as a demonstration of the PERR technique which is the two-dimensional representation of the reformulated SERR technique.

Table 3.2: Summary of velocity discontinuities across the lines

Line	Velocity Discontinuity	Length
AB	$\sqrt{\left(\frac{WHV_b}{Ha+LW-aL}\right)^2+\left(\frac{W(W-a)V_b}{Ha+LW-aL}\right)^2}$	$\sqrt{H^2+(W-a)^2}$
BO	$\sqrt{\left(\frac{WHV_b}{Ha+LW-aL}-V_b\right)^2+\left(-\frac{W(W-a)V_b}{Ha+LW-aL}\right)^2}$	$\sqrt{(H-L)^2+W^2}$
OA	$\sqrt{\left(\frac{WHV_b}{Ha+LW-aL}-\frac{W}{a}V_b\right)^2+\left(\frac{W(W-a)V_b}{Ha+LW-aL}\right)^2}$	$\sqrt{(a^2+L^2)}$

3.6 Closure

For the present investigation the current chapter deals with the brief description of the different methods used for metal forming problems and explains the significance of upper bound theorem with a 2D application as an illustration. The kinematic admissible velocity field for a 3D configuration is a major part of an upper bound concept. A number of concepts have been investigated to derive a kinematically admissible velocity field for analysis. Dual stream function, conformal transformation technique and general velocity technique are some of them. These velocity fields are continuous in the sense that the velocities are expressed as a continuous function in the plastic flow zones.

In the next chapter, detail discussion on upper bound technique with proposed kinematically admissible velocity fields is described, applied to study the combined extrusion-forging process for various types of collet chuck holders.

Chapter 4

Analytical Analysis

4.1 Introduction

Upper bound technique, has received broad attention, to analyse the metal forming problems by many investigators. The upper bound method is characterized by its less computational time and computer memory requirement and reasonable accuracy among the widely known methods. Basily and Sansome [115] proposed an approximate solution to the metal forming problem using a kinematically admissible velocity field when a square sectioned billet extruded to triangular sectioned product. Juneja and Prakash [116] found an outcome by working on extrusion with polygonal section using identically shaped billets by conventional spherical velocity. The major constraints of the above technique are that it cannot be used for combined process or irregular shaped billets. Nagpal and Altan [117] (using the concept of dual stream function) have proposed common analytical techniques for deriving kinematically admissible velocity fields for the above class of problems, and by Yang and Lee [118] (using conformal mapping technique). Later it was found that both these methods have constraints which states that only billets and the product area of similar shape so that section similarity is maintained throughout the deforming region. Sahoo et al. [70], [74], [119], [120] have investigated to obtain triangular section from round bars through extrusion process by linearly converging dies. From the literature review it was found, that single process and simple geometries were applied for maximum number of cases.

One of the major objectives of the present investigation is to manufacture the collet chuck holder by different ways using the metal forming route of combined extrusion (CE) and combined extrusion – forging processes. Otherwise, casting and/or machining is/are the method(s) followed by the industries now. In the current chapter a mathematical model is considered using the upper bound method to investigate the load requirement and effect of process parameters. Optimized kinematically admissible velocity fields are proposed for different product shapes and for different stages to obtain better deformation characteristics as per the components geometries. The effects of punch displacement, friction conditions are discussed in relation to punch loads

.

4.2 Modelling of the Process

Upper bound theorem states that depending on the energy balance, such that the internal rate of dissipation of energy must be less than or equal to the rate at which external forces do work. The technique assumes a kinematically admissible velocity field and states that the actual one reduces the upper bound load for deformation among all velocity fields. It was found that upper bound elemental method was practically suitable method for simulating the metal flow, punch load and power requirements. In order to avoid difficulties in the calculations, the following assumptions are taken into consideration.

1. Punch and container are considered as a rigid-body along with the billet material is assumed as isotropic, incompressible, rigid-plastic and obeys von-misses flow rule.
2. The coefficient of friction between die-billet contact surfaces is considered to be constant.
3. Elastic deformation is neglected.
4. The inertia force of the deforming component is neglected.
5. The centroid of the die aperture lies on the billet axis to avoid eccentric effect.
6. It is assumed that metal cannot cross or shear along the plane of symmetry.

The upper bound formulation for total rate of energy dissipation during the deformation is:

$$\dot{W} = \frac{2\sigma_0}{\sqrt{3}} \int_V \sqrt{\dot{\varepsilon}_{ij}\dot{\varepsilon}_{ij}\,dv} + \frac{\sigma_0}{\sqrt{3}} \int_S |\Delta V| ds + \frac{m\sigma_0}{\sqrt{3}} \int_{F_A} |\Delta V| ds \qquad (4.1)$$

The first right hand side term of Eq (4.1) represents internal power dissipated over the volume v, the second term represents shear losses and the third term represents frictional losses on the tool-billet interface.

σ_0 = Flow stress of billet.

$\dot{\varepsilon}_{ij}$ = The derived strain rate tensor.

$|\Delta V|$ = Velocities discontinuity over the shear surfaces.

m = Friction factor.

Four components manufactured by different routes are considered for the present analysis.

1. Product 1: single collar collet chuck holder (SCCCH) by CEF process.
2. Product 2: Double collar collet chuck holder (DCCCH) by CEF Process.
3. Product 3: DCCCH by CE Process.

4. Product 4: SCCCH by Multi-stage extrusion/forging process.

Three ram velocities (0.5 mm/min, 1.0 mm/min and 2.0 mm/min) and three friction conditions, i.e., m= 0.13 (40% grease with 50% MoS_2), m=0.19 (100% grease), and m= 0.38 (without lubrication) are considered to identify their effects.

4.3 Analysis of Single Collet Chuck Holder by CEF Process

The total process of manufacturing the single collar collet chuck holder by combined extrusion-forging process is analysed in four stages. Each stage is further subdivided into different zones. Figure 4.1 (detail dimensions are provided in Figure 5.5) represents the single collar collet chuck holder under consideration. Figure 4.2 represents different zones considered for stage I of the axisymmetric component. A kinematically admissible velocity field for each zone is assumed. For a unit downward velocity of the moving punch the velocity components for each of the individual zones may be determined using the volume constancy equation and boundary conditions of velocity. The cylindrical coordinate system (r, θ, z) is chosen and fixed at the centre point of the bottom surface of the billet. In the present analysis, the initial diameter of the cylindrical billet is assumed to be equal to the container diameter.

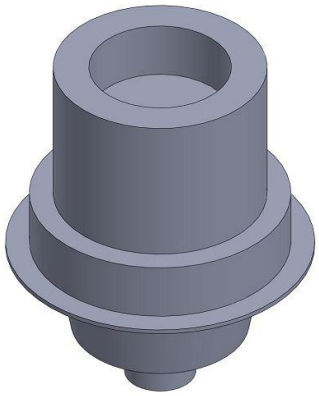

Figure 4.1: Single collar collet chuck holder

From experimental observations, the whole process is reasonably thought of consists of four stages, namely,

a) Stage I: Backward extrusion is completed (after 6.01 mm ram displacement).
b) Stage II: Lateral and forward extrusion starts (after 11.4 mm ram displacement).
c) Stage III: Corners filling takes place (after 15.8 mm ram displacement).
d) Stage IV: Flash is formed (after 18.9 mm ram displacement).

4.3.1 Kinematically admissible velocity fields for Stage I

The stage I is subdivided into five zones in the half longitudinal cross section as represented in Figure 4.2. It is assumed that punch is moving downward with a velocity of u_0 and all the axial velocities are assumed to be linear. No metal can cross or shear along a plane of symmetry.

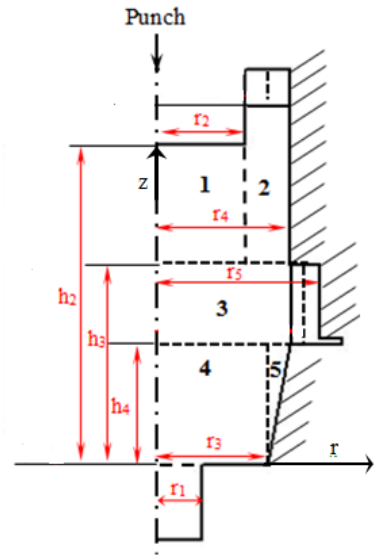

Figure 4.2: Different zones in stage I of SCCH

Zone 1:

In this zone material flow is in both radial and axially directions when punch move downward with a velocity of u_0. The axial velocity component u_z, for zone 1 is subjected to following boundary conditions:

$u_z = 0$ at z = 0 and $u_z = -u_0$ at z = h_2 (4.2)

As the geometry of the present product is axisymmetric in nature, the tangential velocity components of metal flow in different zones are considered to be vanished, i.e.,

$u_\theta = 0.$ (4.3)

Considering the velocity boundary conditions (Eq. 4.2), the following axial velocity component is considered.

$$u_z = -\frac{u_0}{h_2} z \tag{4.4}$$

The volume constancy equation in the cylindrical coordinate system can be expressed as,

$$\frac{\partial u_r}{\partial r} + \frac{u_r}{r} + \frac{1}{r}\frac{\partial u_\theta}{\partial \theta} + \frac{\partial u_z}{\partial z} = 0 \tag{4.5}$$

Substituting, Eqs. (4.3) and (4.4) in Eq. (4.5), integrating the incompressibility condition and using the boundary conditions for the radial velocity (u_r = 0 at r =0), the final form for, u_r is as follow:

$$u_r = \frac{u_0}{h_2}\frac{r}{2} \tag{4.6}$$

For cylindrical coordinates, strain rates can be derived using the following equations:

$$\dot{\varepsilon}_{rr} = \frac{\partial u_r}{\partial r},\ \dot{\varepsilon}_{\theta\theta} = \frac{1}{r}\left(\frac{\partial u_\theta}{\partial \theta} + u_r\right),\ \dot{\varepsilon}_{zz} = \frac{\partial u_z}{\partial z}$$

$$\dot{\varepsilon}_{r\theta} = \frac{1}{2}\left(\frac{1}{r}\frac{\partial u_r}{\partial \theta} + \frac{\partial u_\theta}{\partial r} - \frac{u_\theta}{r}\right).$$

$$\dot{\varepsilon}_{\theta z} = \frac{1}{2}\left(\frac{\partial u_\theta}{\partial z} + \frac{1}{r}\frac{\partial u_z}{\partial \theta}\right), \tag{4.7}$$

$$\dot{\varepsilon}_{rz} = \frac{1}{2}\left(\frac{\partial u_r}{\partial z} + \frac{\partial u_z}{\partial r}\right).$$

The effective strain rate is given as

$$\dot{\varepsilon} = \sqrt{\frac{2}{3}\left(\dot{\varepsilon}_{rr}^2 + \dot{\varepsilon}_{\theta\theta}^2 + \dot{\varepsilon}_{zz}^2 + 2\dot{\varepsilon}_{r\theta}^2 + 2\dot{\varepsilon}_{\theta z}^2 + 2\dot{\varepsilon}_{rz}^2\right)}$$

The strain rates for the zone 1 are:

$$\varepsilon_{rr} = \frac{u_0}{2h_2},\ \varepsilon_{zz} = -\frac{u_0}{h_2},\ \varepsilon_{\theta\theta} = 0 \tag{4.8}$$

Zone 2:

The zone 2, which is subjected to backward extrusion, subjected to following axial velocity boundary conditions:

$u_z = -\frac{u_0}{h_2}h_3$ at z = h_3 and $u_z = +u_B$ at z = h_2, where u_B is the backward extrusion velocity.

Following axial velocity is assumed for the zone 2:

$$u_z = \frac{1}{h_2 - h_3}\left[\left(u_B + \frac{u_0}{h_2}h_3\right)z - (u_0 + u_B)h_3\right] \tag{4.9}$$

Applying the incompressibility condition and radial velocity boundary conditions (u_r = 0 at r = r_4 and u_r for zone 1 and 2 are equal at r = r_2), we have

$$u_r = \frac{u_0 r_2^2}{2h_2\left(r_4^2 - r_2^2\right)}\left[\frac{r_4^2}{r} - r\right] \tag{4.10}$$

$$u_B = \frac{u_0}{h_2}\left(\frac{h_2 r_2^2 - h_3 r_4^2}{r_4^2 - r_2^2}\right) \tag{4.11}$$

Putting the value of u_B, final axial velocity component will be

$$u_z = \frac{u_0}{h_2\left(r_4^2 - r_2^2\right)}\left[r_2^2 z - h_3 r_4^2\right] \tag{4.12}$$

and because of axisymmetric situation, $u_\theta = 0$

The strain rates for the zone 2 are:

$$\varepsilon_{rr} = \frac{u_0 r_2^2}{2h_2\left(r_4^2 - r_2^2\right)}\left[-\frac{r_4^2}{r^2} - 1\right] \tag{4.13}$$

$$\varepsilon_{zz} = \frac{u_0 r_2^2}{h2\left(r_4^2 - r_2^2\right)}, \varepsilon_{\theta\theta} = 0 \tag{4.14}$$

Zone 3:

Velocity boundary conditions for the zone 3 are:

$u_z = -\frac{u_0}{h_2} h_3$ at z = h_3, $u_z = -\frac{u_0}{h_2} h_4$ at z = h_4, u_r = 0 at r = 0. The following velocity components are assumed, which satisfies volume constancy and velocity boundary conditions.

$$u_z = -\frac{u_0}{h_2} z \tag{4.15}$$

$$u_r = \frac{u_0}{h_2}\frac{r}{2} \tag{4.16}$$

$$u_\theta = 0 \tag{4.17}$$

The strain rates for the zone 3 are:

$$\varepsilon_{rr} = \frac{u_0}{2h}, \varepsilon_{zz} = -\frac{u_0}{h_2}, \varepsilon_{\theta\theta} = 0 \tag{4.18}$$

Zone 4:

Similar to zone 3, following velocity components are assumed, which satisfies volume constancy and velocity boundary conditions.

$$u_z = -\frac{u_0}{h_2} z \tag{4.19}$$

$$u_r = \frac{u_0}{h_2}\frac{r}{2} \tag{4.20}$$

$$u_\theta = 0 \tag{4.21}$$

The strain rates for the zone 4 are:

$$\varepsilon_{rr} = \frac{u_0}{2h},\ \varepsilon_{zz} = -\frac{u_0}{h_2},\ \varepsilon_{\theta\theta} = 0 \tag{4.22}$$

Zone 5:

Similar to zone 4, following velocity components are assumed, which satisfies volume constancy and velocity boundary conditions.

$$u_z = -\frac{u_0}{h_2} z \tag{4.23}$$

$$u_r = \frac{u_0}{h_2}\frac{r}{2} \tag{4.24}$$

$$u_\theta = 0 \tag{4.25}$$

The strain rates for the zone 5 are:

$$\varepsilon_{rr} = \frac{u_0}{2h},\ \varepsilon_{zz} = -\frac{u_0}{h_2},\ \varepsilon_{\theta\theta} = 0 \tag{4.26}$$

4.3.2 Kinematically admissible velocity fields for Stage II

In this stage the following assumptions are taken into consideration and further subdivided into seven zones represented in the Figure 4.3.

- Backward extrusion is completed.
- Lateral and forward extrusion starts.
- Corner filling doesn’t takes place.
- Zone 1 moves as a rigid block.

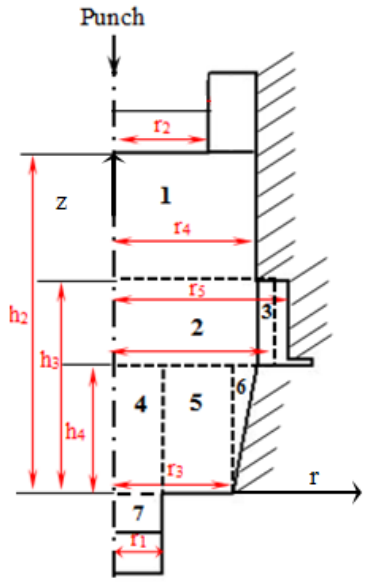

Figure 4.3: Different zones in stage II of SCCH

Following the same procedure applied for stage I, the proposed kinematically velocity fields and strain rates for different zones of stage II are given in Tables 4.1 and 4.2. As the geometry of the present product is axisymmetric in nature, the tangential velocity components of metal flow in different zones are considered to be vanished, i.e., $u_\theta = 0$ at different stages.

Table 4.1: Kinematically admissible velocity fields for stage II

Zone	u_r	u_z
1	0	0
2	$\frac{u_0}{h_3} \times \frac{r}{2}$	$-\frac{u_0}{h_3} \times z$
3	$\frac{u_0}{h_3} \frac{r_4^2}{2r}$	0
4	$\frac{u_0}{2h_3} r\left[1-\frac{r_3^2}{r_1^2}\right]$	$-u_0\left[\frac{r_1^2-r_3^2}{r_1^2 h_3} z+\frac{r_3^2}{r_1^2}\right]$
5	$\frac{u_0}{2h_3}\left[r-\frac{r_3^2}{r}\right]$	$-\frac{u_0}{h_3} z$
6	$\frac{u_0}{h_3}\left[r-\frac{r_3^2}{r}\right]$	$-\frac{u_0}{h_3} z$
7	0	$-u_0 \frac{r_3^2}{r_1^2}$

Table 4.2: Strain rates for stage II

Zone 1	$\varepsilon_{rr}=0,\ \ \varepsilon_{zz}=0,\ \varepsilon_{\theta\theta}=0$
Zone 2	$\varepsilon_{rr}=\frac{u_0}{2h_3},\varepsilon_{zz}=-\frac{u_0}{h_3},\varepsilon_{\theta\theta}=0$
Zone 3	$\varepsilon_{rr}=\frac{u_0 r_4^2}{2h_3}\left[-\frac{1}{r^2}\right]\ \varepsilon_{zz}=0,\ \varepsilon_{\theta\theta}=0$
Zone 4	$\varepsilon_{rr}=\frac{u_0}{2h_3}\left[1-\frac{r_3^2}{r_1^2}\right],\varepsilon_{zz}-u_0\frac{r_1^2-r_3^2}{r_1^2 h_3},\varepsilon_{\theta\theta}=0$
Zone 5	$\varepsilon_{rr}=\frac{u_0}{2h_3}\left[1+\frac{r_3^2}{r_1^2}\right],\ \varepsilon_{zz}=-\frac{u_0}{h_3},\varepsilon_{\theta\theta}=0$
Zone 6	$\varepsilon_{rr}=\frac{u_0}{2h_3}\left[1+\frac{r_3^2}{r_1^2}\right],\ \varepsilon_{zz}=-\frac{u_0}{h_3},\varepsilon_{\theta\theta}=0$
Zone 7	$\varepsilon_{rr}=0,\ \ \varepsilon_{zz}=0,\ \varepsilon_{\theta\theta}=0$

4.3.3 Kinematically admissible velocity fields for Stage III

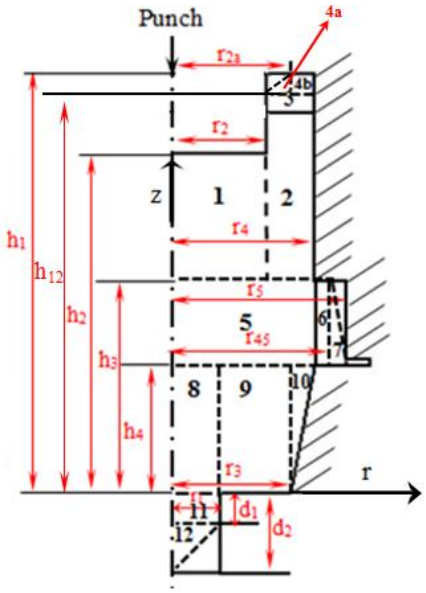

Figure 4.4: Different zones in Stage III of SCCH

Following the same procedure applied for stage I, the proposed kinematically velocity fields and strain rates for different zones of stage III are given in Table 4.3 and 4.4.

Table 4.3: Kinematically admissible velocity fields for stage III

Zone	u_r	u_z
1	$\frac{u_0}{h_2}\times\frac{r}{2}$	$-\frac{u_0}{h_2}\times z$
2	$\frac{u_0}{2h_2}\frac{r_2^2}{\left(r_4^2-r_2^2\right)}\left[\frac{r_4^2}{r}-r\right]$	$\frac{u_0}{h_2\left(r_4^2-r_2^2\right)}\left[r_2^2 z-h_3 r_4^2\right]$
3	0	$\frac{u_0}{h_2\left(r_4^2-r_2^2\right)}\left[r_2^2 h_2-h_3 r_4^2\right]$
4a	$\frac{u_0 r_4^2\left(h_2-h_3\right)}{2h_2\left(h_1-h_{12}\right)\left(r_4^2-r_2^2\right)}\left(r-\frac{r_4^2}{r}\right)$	$\frac{u_0}{h_2\left(h_1-h_{12}\right)\left(r_4^2-r_2^2\right)}\times\left[\begin{array}{l} r_4^2\left(h_3-h_2\right)z+r_2^2 h_2\left(h_1-h_{12}\right)+ \\ r_4^2\left(h_1 h_{12}-h_1 h_3\right)\end{array}\right]$
4b	$\frac{u_0 r_4^2\left(h_2-h_3\right)}{2h_2\left(h_1-h_{12}\right)\left(r_4^2-r_2^2\right)}\left(1-\frac{r_4^2}{r_{2a}^2}\right)\left(\frac{r-r_2}{r_{2a}-r_2}\right)r_{2a}$	$\frac{u_0\left(h_3-h_2\right)r_4^2\left(r_{2a}-\frac{r_4^2}{r_{2a}}\right)\left(\frac{2r-r_2}{r}\right)\left(z-h_{12}\right)}{2h_2\left(h_1-h_{12}\right)\left(r_4^2-r_2^2\right)\left(r_{2a}-r_2\right)}+$ $\frac{u_0}{h_2\left(r_4^2-r_2^2\right)}\left[r_2^2 h_2-r_4^2 h_3\right]$
5	$\frac{u_0}{h_2}\times\frac{r}{2}$	$-\frac{u_0}{h_2}\times z$
6	$\frac{u_0}{h_2}\frac{r_4^2}{2r}$	0
7	$\frac{u_0 r_4^2}{2h_2 r_{45}}\left(\frac{r_5-r}{r_5-r_{45}}\right)$	$\frac{1}{r_5-r_{45}}\left[\frac{u_0 r_4^2}{2h_2 r_{45}}\right]\left(2-\frac{r_5}{r}\right)\left(z-h_4\right)$
8	$\frac{u_0 r}{2h_2}\left(1-\frac{r_3^2}{r_1^2}\right)$	$-u_0\left[\frac{r_1^2-r_3^2}{r_1^2 h_2}z+\frac{r_3^2}{r_1^2}\right]$
9	$\frac{u_0}{2h_2}\left[r-\frac{r_3^2}{r}\right]$	$-\frac{u_0}{h_2}\times z$
10	$\frac{u_0}{2h_2}\left[r-\frac{r_3^2}{r}\right]$	$-\frac{u_0}{h_2}\times z$
11	0	$u_0\frac{r_3^2}{r_1^2}$
12	$\frac{u_0 r_3^2}{r_1^2\left(d_2-d_1\right)}\frac{r}{2}$	$\frac{u_0 r_3^2}{r_1^2}\left[\frac{d_2-z}{d_2-d_1}\right]$

Table 4.4: Strain rates for stage III

Zone 1	$\varepsilon_{rr}=\frac{u_0}{2h_2},\ \varepsilon_{zz}=\frac{u_0}{h_2},\ \varepsilon_{\theta\theta}=0$
Zone 2	$\varepsilon_{rr}=\frac{u_0}{h_2}\frac{r_2^2}{r_4^2-r_2^2}\left[-\frac{r_4^2}{r^2}-1\right],\varepsilon_{zz}=-\frac{u_0}{h_2\left(r_4^2-r_2^2\right)}r_2^2,\varepsilon_{\theta\theta}=0$
Zone 3	$\varepsilon_{rr}=0,\ \varepsilon_{zz}=0,\ \varepsilon_{\theta\theta}=0$
Zone 4a	$\varepsilon_{rr}=\frac{u_0 r_4^2\left(h_2-h_3\right)}{2h_2\left(h_1-h_{12}\right)\left(r_4^2-r_2^2\right)}\left[1+\frac{r_4^2}{r^2}\right]\ \varepsilon_{zz}=\frac{u_0}{h_2\left(h_1-h_{12}\right)\left(r_4^2-r_2^2\right)}\left[r_4^2\left(h_3-h_2\right)\right],$ $\varepsilon_{\theta\theta}=0$
Zone 4b	$\varepsilon_{rr}=\frac{u_0 r_4^2\left(h_2-h_3\right)}{2h_2\left(h_1-h_{12}\right)\left(r_4^2-r_2^2\right)\left(r_{2a}-r_2\right)}\left(r_{2a}-\frac{r_4^2}{r_{2a}}\right),$ $\varepsilon_{zz}=\frac{u_0\left(h_3-h_2\right)r_4^2}{2h_2\left(h_1-h_{12}\right)\left(r_4^2-r_2^2\right)\left(r_{2a}-r_2\right)}\left(r_{2a}-\frac{r_4^2}{r_{2a}}\right)\left(\frac{2r-r_2}{r}\right)$ $\varepsilon_{rz}=\frac{u_0\left(h_3-h_2\right)r_4^2\left(z-h_{12}\right)}{2h_2\left(h_1-h_{12}\right)\left(r_4^2-r_2^2\right)\left(r_{2a}-r_2\right)}\left(r_{2a}-\frac{r_4^2}{r_{2a}}\right)\left(\frac{r_2}{r^2}\right),\varepsilon_{\theta\theta}=0$
Zone 5	$\varepsilon_{rr}=\frac{u_0}{2h_2},\ \varepsilon_{zz}=\frac{u_0}{h_2},\ \varepsilon_{\theta\theta}=0$
Zone 6	$\varepsilon_{rr}=-\frac{u_0}{2h_2}\frac{r_4^2}{r^2}\ \varepsilon_{zz}=0,\ \varepsilon_{\theta\theta}=0$
Zone 7	$\varepsilon_{rr}=-\frac{u_0 r_4^2}{2h_2 r_{45}\left(r_5-r_{45}\right)},\varepsilon_{zz}=-\frac{1}{\left(r_5-r_{45}\right)}\left(\frac{u_0 r_4^2}{2h_2 r_{45}}\right)\left(2-\frac{r_5}{r}\right),$ $\varepsilon_{rz}=\frac{1}{2}\frac{1}{r_5-r_{45}}\frac{u_0 r_4^2}{2h_2 r_{45}}\left(z-h_4\right)\left(\frac{r_5}{r^2}\right),\varepsilon_{\theta\theta}=0$
Zone 8	$\varepsilon_{rr}=\frac{u_0}{2h_2}\left[1-\frac{r_3^2}{r_1^2}\right],\varepsilon_{zz}=-u_0\left[\frac{r_1^2-r_3^2}{r_1^2 h_2}\right],\varepsilon_{\theta\theta}=0$
Zone 9	$\varepsilon_{rr}=\frac{u_0}{2h_2}\left[1+\frac{r_3^2}{r^2}\right],\ \varepsilon_{zz}=-\frac{u_0}{h_2},\varepsilon_{\theta\theta}=0$
Zone 10	$\varepsilon_{rr}=\frac{u_0}{2h_2}\left[1+\frac{r_3^2}{r^2}\right],\varepsilon_{zz}=-\frac{u_0}{h_2},\varepsilon_{\theta\theta}=0$
Zone 11	$\varepsilon_{rr}=0,\ \varepsilon_{zz}=0,\ \varepsilon_{\theta\theta}=0$
Zone 12	$\varepsilon_{rr}=\frac{u_0 r_3^2}{r_1^2\left(d_2-d_1\right)}\frac{1}{2},\varepsilon_{zz}=\frac{u_0 r_3^2}{r_1^2}\left[-\frac{1}{\left(d_2-d_1\right)}\right],\varepsilon_{\theta\theta}=0$

4.3.4 Kinematically admissible velocity fields for Stage IV

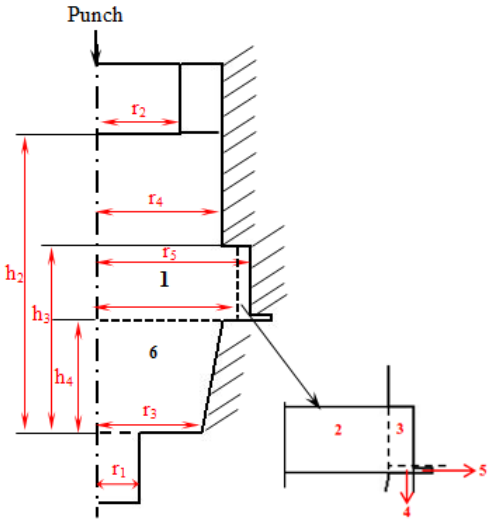

Figure 4.5: Different zones in stage IV of SCCH

Following the same procedure applied for stage I, the proposed kinematically velocity fields and strain rates for different zones of stage IV are given in Table 4.5 and 4.6.

Table 4.5: Kinematically admissible velocity fields for stage IV

Zone	u_r	u_z
0	0	$-u_0$
1	$\frac{u_0}{2(h_3-h_4)}r$	$\frac{u_0}{h_3-h_4}(h_4-z)$
2	$\frac{u_0}{(h_3-h_4)}\frac{r_4^2}{2r}$	0
3	$\frac{u_0}{2(h_3-h_4)}\frac{r_4^2}{(r_5-r_{45})r_{45}}[r_5-r]$	$\frac{1}{r_{45}}\frac{u_0}{2(h_3-h_4)}\frac{r_4^2}{(r_5-r_{45})}\left(2-\frac{r_5}{r}\right)[(z-h_3)]$
4	$\frac{u_0 r_4^2}{2(h_3-h_4)}\left[\frac{1}{r}+\frac{1}{h_f}\frac{1}{r_{45}}\frac{h_3-h_4-h_f}{(r_5-r_{45})}\times\left(r-r_5-\frac{r_{45}^2}{r}+\frac{r_{45}r_5}{r}\right)\right]$	$\frac{1}{h_f}\left[\frac{1}{r_{45}}\frac{u_0}{2(h_2-h_4)}\frac{r_4^2}{r_5-r_{45}}\left(2-\frac{r_5}{r}\right)\times(h_4+h_f-h_3)(z-h_4)\right]$
6	0	0

Table 4.6: Strain rates for stage IV

Zone 0	$\varepsilon_{rr}=0,\ \ \varepsilon_{zz}=0,\ \varepsilon_{\theta\theta}=0$
Zone 1	$\varepsilon_{rr}=\frac{u_0}{2(h_3-h_4)},\varepsilon_{zz}=-\frac{u_0}{h_3-h_4},\varepsilon_{\theta\theta}=0$
Zone 2	$\varepsilon_{rr}=\frac{u_0}{2(h_3-h_4)}\frac{r_4^2}{r^2},\varepsilon_{zz}=0\ ,\ \varepsilon_{\theta\theta}=0$
Zone 3	$\varepsilon_{rr}=-\frac{u_0}{2(h_3-h_4)}\frac{r_4^2}{(r_5-r_{45})r_{45}},\ \varepsilon_{\theta\theta}=0$ $\varepsilon_{zz}=\frac{u_0}{2(h_3-h_4)}\left(\frac{r_4^2}{r_5-r_{45}}\right)\left(2-\frac{r_5}{r}\right)\frac{1}{r_{45}},$ $\varepsilon_{rz}=\frac{1}{2}\frac{u_0}{2(h_3-h_4)}\left(\frac{r_4^2}{r_5-r_{45}}\right)(z-h_3)\left(\frac{r_5}{r}\right)\frac{1}{r_{45}}$
Zone 4	$\varepsilon_{rr}=\frac{u_0r_4^2}{2(h_3-h_4)}\left[-\frac{1}{r^2}+\frac{1}{h_f}\frac{1}{r_{45}}\frac{h_3-h_4-h_f}{(r_5-r_{45})}\left(1+\frac{r_{45}^2}{r^2}-\frac{r_{45}r_5}{r^2}\right)\right],$ $\varepsilon_{zz}=\frac{1}{h_f}\left[\frac{1}{r_{45}}\frac{u_0}{2(h_3-h_4)}\left(\frac{r_4^2}{r_5-r_{45}}\right)(h_4+h_f-h_3)\left(2-\frac{r_5}{r}\right)\right],\varepsilon_{\theta\theta}=0$ $\varepsilon_{rz}=\frac{1}{2}\frac{1}{h_f}\left[\frac{1}{r_{45}}\frac{u_0}{2(h_3-h_4)}\left(\frac{r_4^2}{r_5-r_{45}}\right)(h_4-h_f-h_3)(z-h_4)\left(\frac{r_5}{r^2}\right)\right]$
Zone 5	$\varepsilon_{rr}=-\frac{u_0}{2(h_3-h_4)}\frac{r_4^2}{r^2}\left[1+\frac{1}{h_f}\frac{1}{r_{45}}\frac{(h_3-h_4-h_f)}{(r_5-r_{45})}\left(-r_{45}^2+r_{45}r_5\right)\right],$ $\varepsilon_{zz}=0,\varepsilon_{\theta\theta}=0$
Zone 6	$\varepsilon_{rr}=0,\ \ \varepsilon_{zz}=0,\ \varepsilon_{\theta\theta}=0$

4.4 Analysis of Double Collet Chuck Holder by CEF Process

In this section, the plastic flow of metal to make a double collar collet chuck holder by combined extrusion-forging process is analysed in four stages, namely,

a) Stage I: Backward extrusion is completed (after 8.47 mm ram displacement).
b) Stage II: Lateral and forward extrusion starts (after 16.6 mm ram displacement).
c) Stage III: Corners filling takes place (after 23.4 mm ram displacement).
d) Stage IV: Flash is formed (after 25.3 mm ram displacement).

Each stage is further subdivided into different zones. It is assumed that no metal can cross or shear along a plane of symmetry. Figure 4.6 (detail dimensions are provided in Figure 5.14) represents the double collar collet chuck holder manufactured by CEF process, to be

analysed. The Figures 4.7- 4.10 represents different zones (half sectional view) considered for stages I-IV of the axisymmetric component.

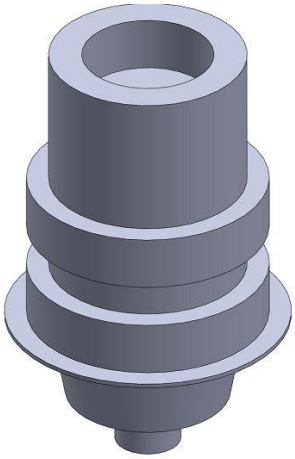

Figure 4.6: Double collar collet chuck holder processed by CEF process

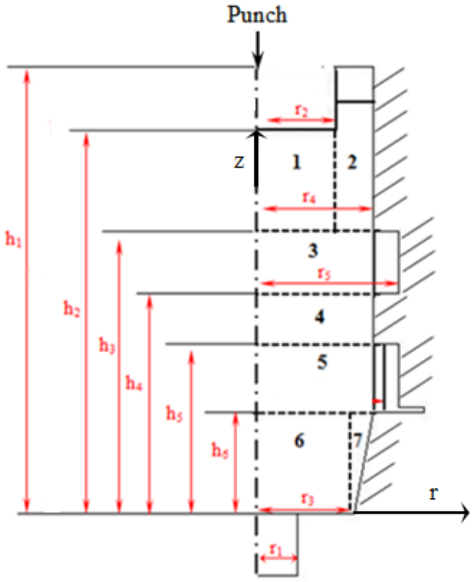

Figure 4.7: Different zones in Stage I of DCCCH

Following the same procedure applied for product I, the proposed kinematically velocity fields for different zones of stage I-IV are given in Tables 4.7 - 4.10 for a DCCCH component. As the geometry of the present product is axisymmetric in nature, the tangential velocity components of metal flow in different zones are considered to be vanished, i.e., $u_\theta = 0$ for all four stages.

Table 4.7: Kinematically admissible velocity fields stage I

Zone	u_r	u_z
1	$\frac{u_0}{h_2}\frac{r}{2}$	$-\frac{u_0}{h_2}z$
2	$\frac{u_0}{2h_2}\frac{r_2^2}{\left(r_4^2-r_2^2\right)}\left[\frac{r_4^2}{r}-r\right]$	$\frac{u_0}{h_2\left(r_4^2-r_2^2\right)}\left[r_2^2 z-h_3 r_4^2\right]$
3	$\frac{u_0}{h_2}\frac{r}{2}$	$-\frac{u_0}{h_2}z$
4	$\frac{u_0}{h_2}\frac{r}{2}$	$-\frac{u_0}{h_2}z$
5	$\frac{u_0}{h_2}\frac{r}{2}$	$-\frac{u_0}{h_2}z$
6	$\frac{u_0}{h_2}\frac{r}{2}$	$-\frac{u_0}{h_2}z$
7	$\frac{u_0}{h_2}\frac{r}{2}$	$-\frac{u_0}{h_2}z$

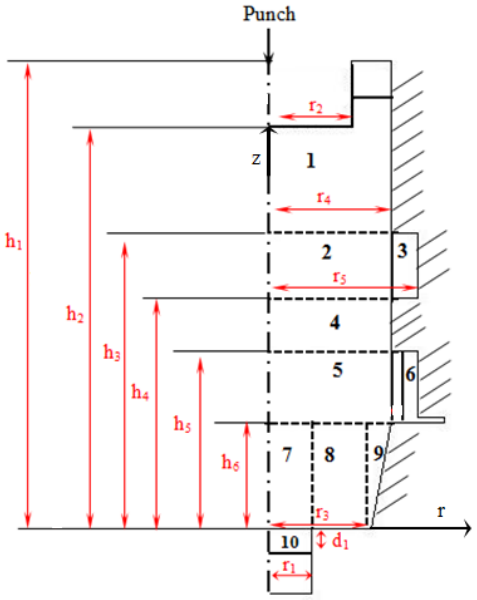

Figure 4.8: Different zones in Stage II of DCCCH

Table 4.8: Kinematically admissible velocity fields stage II

Zone	u_r	u_z
1	0	0
2	$\frac{u_0}{h_3}\times\frac{r}{2}$	$-\frac{u_0}{h_3}\times z$
3	$\frac{u_0}{h_3}\frac{r_4^2}{2r}$	0
4	0	$-\frac{u_0}{h_3}\times z$
5	$\frac{u_0}{h_3}\times\frac{r}{2}$	$-\frac{u_0}{h_3}\times z$
6	$\frac{u_0}{h_3}\times\frac{r_4^2}{2r}$	0
7	$\frac{u_0}{2h_3}r\left[1-\frac{r_3^2}{r_1^2}\right]$	$-u_0\left[\frac{r_1^2-r_3^2}{r_1^2h_3}z+\frac{r_3^2}{r_1^2}\right]$
8	$\frac{u_0}{2h_3}\left[r-\frac{r_3^2}{r}\right]$	$-\frac{u_0}{h_3}z$
9	$\frac{u_0}{h_3}\left[r-\frac{r_3^2}{r}\right]$	$-\frac{u_0}{h_3}z$
10	0	$-u_0\frac{r_3^2}{r_1^2}$

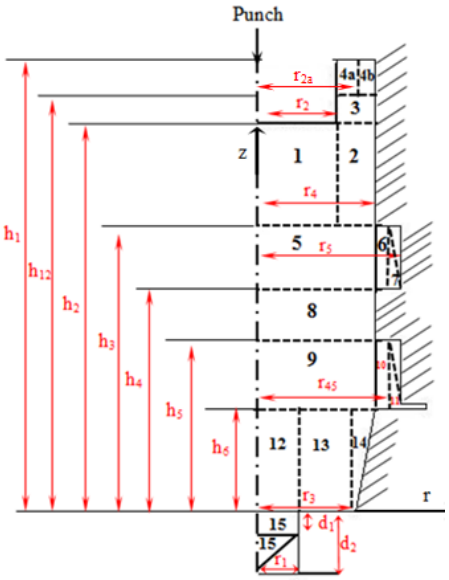

Figure 4.9: Different zones in Stage III of DCCCH

Table 4.9: Kinematically admissible velocity fields for stage III

Zone	u_r	u_z
1	$\frac{u_0}{h_2}\times\frac{r}{2}$	$-\frac{u_0}{h_2}\times z$
2	$\frac{u_0}{2h_2}\frac{r_2^2}{\left(r_4^2-r_2^2\right)}\left[\frac{r_4^2}{r}-r\right]$	$\frac{u_0}{h_2\left(r_4^2-r_2^2\right)}\left[r_2^2 z-h_3 r_4^2\right]$
3	0	$\frac{u_0}{h_2\left(r_4^2-r_2^2\right)}\left[r_2^2 h_2-h_3 r_4^2\right]$
4a	$\frac{u_0 r_4^2\left(h_2-h_3\right)}{2h_2\left(h_1-h_{12}\right)\left(r_4^2-r_2^2\right)}\left(r-\frac{r_4^2}{r}\right)$	$\frac{u_0}{h_2\left(h_1-h_{12}\right)\left(r_4^2-r_2^2\right)}\times\left[\begin{array}{l}r_4^2\left(h_3-h_2\right)z+r_2^2 h_2\left(h_1-h_{12}\right)+\\ r_4^2\left(h_1 h_{12}-h_1 h_3\right)\end{array}\right]$
4b	$\frac{u_0 r_4^2\left(h_2-h_3\right)}{2h_2\left(h_1-h_{12}\right)\left(r_4^2-r_2^2\right)}\left(r-\frac{r_4^2}{r}\right)\left(\frac{r-r_2}{r_{2a}-r_2}\right)r_{2a}$	$\frac{u_0\left(h_3-h_2\right)r_4^2\left(r_{2a}-\frac{r_4^2}{r_{2a}}\right)\left(\frac{2r-r_2}{r}\right)\left(z-h_{12}\right)}{2h_2\left(h_1-h_{12}\right)\left(r_4^2-r_2^2\right)\left(r_{2a}-r_2\right)}+$ $\frac{u_0}{h_2\left(r_4^2-r_2^2\right)}\left[r_2^2 h_2-r_4^2 h_3\right]$
5	$\frac{u_0}{h_2}\times\frac{r}{2}$	$-\frac{u_0}{h_2}\times z$
6	$\frac{u_0}{h_2}\frac{r_4^2}{2r}$	0
7	$\frac{u_0 r_4^2}{2h_2 r_{45}}\left(\frac{r_5-r}{r_5-r_{45}}\right)$	$\frac{1}{r_5-r_{45}}\left[\frac{u_0 r_4^2}{2h_2 r_{45}}\right]\left(2-\frac{r_5}{r}\right)\left(z-h_4\right)$
8	0	$-\frac{u_0}{h_2}\times z$
9	$\frac{u_0}{h_2}\times\frac{r}{2}$	$-\frac{u_0}{h_2}\times z$
10	$\frac{u_0}{h_2}\times\frac{r_4^2}{2r}$	0
11	$\frac{u_0 r_4^2}{2h_2 r_{45}}\left(\frac{r_5-r}{r_5-r_{45}}\right)$	$\frac{1}{r_5-r_{45}}\left[\frac{u_0 r_4^2}{2h_2 r_{45}}\right]\left[2-\frac{r_5}{r}\right]\left[z-h_6\right]$
12	$\frac{u_0 r}{2h_2}\left(1-\frac{r_3^2}{r_1^2}\right)$	$-u_0\left[\frac{r_1^2-r_3^2}{r_1^2 h_2}z+\frac{r_3^2}{r_1^2}\right]$
13	$\frac{u_0}{2h_2}\left[r-\frac{r_3^2}{r}\right]$	$-\frac{u_0}{h_2}\times z$
14	$\frac{u_0}{2h_2}\left[r-\frac{r_3^2}{r}\right]$	$-\frac{u_0}{h_2}\times z$

15	0	$-u_0 \dfrac{r_3^2}{r_1^2}$
16	$\dfrac{u_0 r_3^2}{r_1^2 (d_2 - d_1)} \dfrac{r}{2}$	$\dfrac{u_0 r_3^2}{r_1^2} \left[\dfrac{d_2 - z}{d_2 - d_1} \right]$

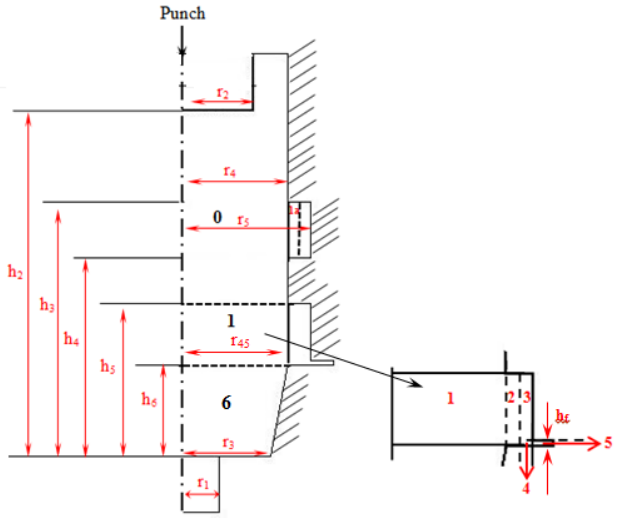

Figure 4.10: Different zones in Stage IV of DCCCH

Table 4.10: Kinematically admissible velocity fields for stage IV

Zone	u_r	u_z
0	0	$-u_0$
1	$\dfrac{u_0}{2(h_5 - h_6)} r$	$\dfrac{u_0}{h_5 - h_6} (h_6 - z)$
1a	0	0
2	$\dfrac{u_0}{(h_5 - h_6)} \dfrac{r_4^2}{2r}$	0
3	$\dfrac{u_0}{2(h_5 - h_6)} \dfrac{r_4^2}{(r_5 - r_{45}) r_{45}} [r_5 - r]$	$\dfrac{1}{r_{45}} \dfrac{u_0}{2(h_5 - h_6)} \dfrac{r_4^2}{(r_5 - r_{45})} \left(2 - \dfrac{r_5}{r} \right) [(z - h_3)]$
4	$\dfrac{u_0 r_4^2}{2(h_5 - h_6)} \left[\dfrac{1}{r} + \dfrac{1}{h_f} \dfrac{1}{r_{45}} \dfrac{h_5 - h_6 - h_f}{(r_5 - r_{45})} \times \left(r - r_5 - \dfrac{r_{45}^2}{r} + \dfrac{r_{45} r_5}{r} \right) \right]$	$\dfrac{1}{h_f} \left[\dfrac{1}{r_{45}} \dfrac{u_0}{2(h_5 - h_6)} \dfrac{r_4^2}{r_5 - r_{45}} \left(2 - \dfrac{r_5}{r} \right) \times (h_6 + h_f - h_5)(z - h_6) \right]$
5	$\dfrac{u_0}{2(h_5 - h_6)} \dfrac{r_4^2}{r} \left[1 + \dfrac{1}{h_f} \dfrac{1}{r_{45}} \dfrac{h_5 - h_6 - h_f}{(r_5 - r_{45})} \left(- r_{45}^2 + r_{45} r_5 \right) \right]$	0
6	0	0

4.5 Analysis of Double Collet Chuck Holder by CE Process

In this section, a double collar collet chuck holder manufactured by combined extrusion process is analysed by in four stages. Each stage is further subdivided into different zones. The Figure 4.11 (detail dimensions are provided in Figure 5.23) represents the double collar collet chuck holder which is to be analysed.

Figure 4.11: Double collar collet chuck holder processed by CE process

The Figures 4.12 - 4.15 represents different zones considered for stages I-IV of the said product. The different stages are:

a) Stage I: Backward extrusion is completed (after 6.71 mm ram displacement).
b) Stage II: Lateral and forward extrusion starts (after 12.8 mm ram displacement).
c) Stage III: Corners filling takes place (after 18.6 mm ram displacement).
d) Stage IV: Forward extrusion takes place (after 21.3 mm ram displacement).

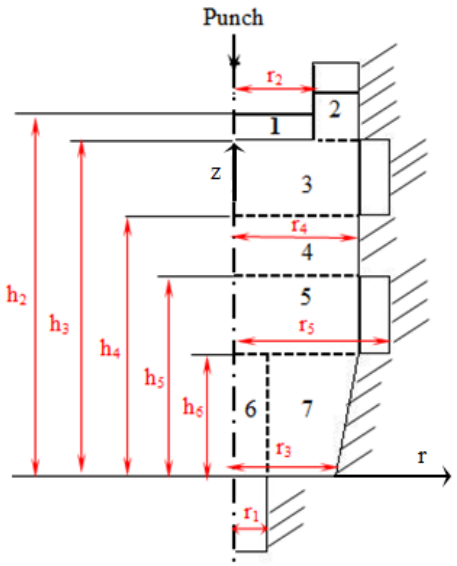

Figure 4.12: Different zones in Stage I of DCCCH

Following the same procedure applied for product I, the proposed kinematically velocity fields for different zones of stage I are given in Tables 4.11 - 4.14 for a DCCCH component by CE process. As the geometry of the present product is axisymmetric in nature, the tangential velocity components of metal flow in different zones are considered to be vanished, i.e., $u_\theta = 0$ for four all stages.

Table 4.11: Kinematically admissible velocity fields for stage I

Zone	u_r	u_z
1	$\frac{u_0}{h_2}\frac{r}{2}$	$-\frac{u_0}{h_2}z$
2	$\frac{u_0}{2h_2}\frac{r_2^2}{\left(r_4^2-r_2^2\right)}\left[\frac{r_4^2}{r}-r\right]$	$\frac{u_0}{h_2\left(r_4^2-r_2^2\right)}\left[r_2^2 z-h_3 r_4^2\right]$
3	$\frac{u_0}{h_2}\frac{r}{2}$	$-\frac{u_0}{h_2}z$
4	$\frac{u_0}{h_2}\frac{r}{2}$	$-\frac{u_0}{h_2}z$
5	$\frac{u_0}{h_2}\frac{r}{2}$	$-\frac{u_0}{h_2}z$
6	$\frac{u_0}{h_2}\frac{r}{2}$	$-\frac{u_0}{h_2}z$
7	$\frac{u_0}{h_2}\frac{r}{2}$	$-\frac{u_0}{h_2}z$

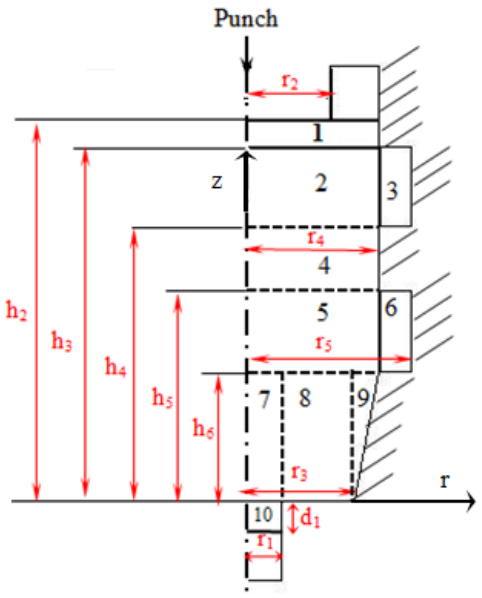

Figure 4.13: Different zones in Stage II of DCCCH

Table 4.12: Kinematically admissible velocity fields for stage II

Zone	u_r	u_z
1	0	$-u_0$
2	$\frac{u_0}{h_3}\times\frac{r}{2}$	$-\frac{u_0}{h_3}\times z$
3	$\frac{u_0}{h_3}\frac{r_4^2}{2r}$	0
4	0	$-\frac{u_0}{h_3}\times z$
5	$\frac{u_0}{h_3}\times\frac{r}{2}$	$-\frac{u_0}{h_3}\times z$
6	$\frac{u_0}{h_3}\times\frac{r_4^2}{2r}$	0
7	$\frac{u_0}{2h_3}r\left[1-\frac{r_3^2}{r_1^2}\right]$	$-u_0\left[\frac{r_1^2-r_3^2}{r_1^2h_3}z+\frac{r_3^2}{r_1^2}\right]$
8	$\frac{u_0}{2h_3}\left[r-\frac{r_3^2}{r}\right]$	$-\frac{u_0}{h_3}z$
9	$\frac{u_0}{h_3}\left[r-\frac{r_3^2}{r}\right]$	$-\frac{u_0}{h_3}z$
10	0	$-u_0\frac{r_3^2}{r_1^2}$

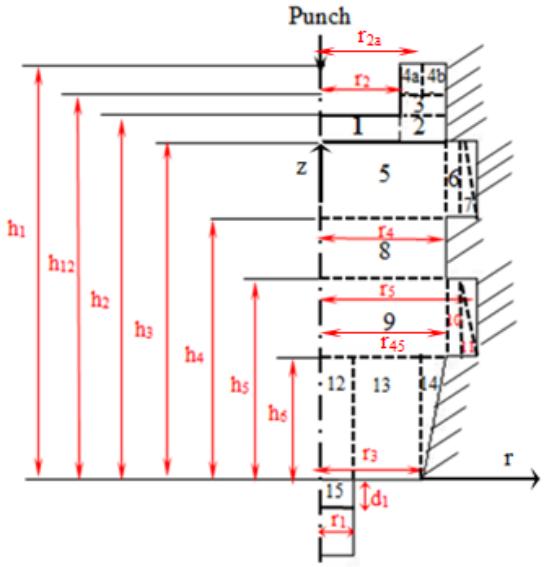

Figure 4.14: Different zones in Stage III of DCCCH

Table 4.13: Kinematically admissible velocity fields for stage III

Zone	u_r	u_z
1	$\frac{u_0}{h_2}\times\frac{r}{2}$	$-\frac{u_0}{h_2}\times z$
2	$\frac{u_0}{2h_2}\frac{r_2^2}{\left(r_4^2-r_2^2\right)}\left[\frac{r_4^2}{r}-r\right]$	$\frac{u_0}{h_2\left(r_4^2-r_2^2\right)}\left[r_2^2 z-h_3 r_4^2\right]$
3	0	$\frac{u_0}{h_2\left(r_4^2-r_2^2\right)}\left[r_2^2 h_2-h_3 r_4^2\right]$
4a	$\frac{u_0 r_4^2\left(h_2-h_3\right)}{2h_2\left(h_1-h_{12}\right)\left(r_4^2-r_2^2\right)}\left(r-\frac{r_4^2}{r}\right)$	$\frac{u_0}{h_2\left(h_1-h_{12}\right)\left(r_4^2-r_2^2\right)}\times\left[\begin{matrix}r_4^2\left(h_3-h_2\right)z+r_2^2 h_2\left(h_1-h_{12}\right)+\\ r_4^2\left(h_1 h_{12}-h_1 h_3\right)\end{matrix}\right]$
4b	$\frac{u_0 r_4^2\left(h_2-h_3\right)}{2h_2\left(h_1-h_{12}\right)\left(r_4^2-r_2^2\right)}\left(1-\frac{r_4^2}{r_{2a}^2}\right)\left(\frac{r-r_2}{r_{2a}-r_2}\right)r_{2a}$	$\frac{u_0\left(h_3-h_2\right)r_4^2\left(r_{2a}-\frac{r_4^2}{r_{2a}}\right)\left(\frac{2r-r_2}{r}\right)\left(z-h_{12}\right)}{2h_2\left(h_1-h_{12}\right)\left(r_4^2-r_2^2\right)\left(r_{2a}-r_2\right)}+\frac{u_0}{h_2\left(r_4^2-r_2^2\right)}\left[r_2^2 h_2-r_4^2 h_3\right]$
5	$\frac{u_0}{h_2}\times\frac{r}{2}$	$-\frac{u_0}{h_2}\times z$
6	$\frac{u_0}{h_2}\frac{r_4^2}{2r}$	0
7	$\frac{u_0 r_4^2}{2h_2 r_{45}}\left(\frac{r_5-r}{r_5-r_{45}}\right)$	$\frac{1}{r_5-r_{45}}\left[\frac{u_0 r_4^2}{2h_2 r_{45}}\right]\left(2-\frac{r_5}{r}\right)\left(z-h_4\right)$
8	0	$-\frac{u_0}{h_2}\times z$
9	$\frac{u_0}{h_2}\times\frac{r}{2}$	$-\frac{u_0}{h_2}\times z$
10	$\frac{u_0}{h_2}\times\frac{r_4^2}{2r}$	0
11	$\frac{u_0 r_4^2}{2h_2 r_{45}}\left(\frac{r_5-r}{r_5-r_{45}}\right)$	$\frac{1}{r_5-r_{45}}\left[\frac{u_0 r_4^2}{2h_2 r_{45}}\right]\left[2-\frac{r_5}{r}\right]\left[z-h_6\right]$
12	$\frac{u_0 r}{2h_2}\left(1-\frac{r_3^2}{r_1^2}\right)$	$-u_0\left[\frac{r_1^2-r_3^2}{r_1^2 h_2}z+\frac{r_3^2}{r_1^2}\right]$
13	$\frac{u_0}{2h_2}\left[r-\frac{r_3^2}{r}\right]$	$-\frac{u_0}{h_2}\times z$
14	$\frac{u_0}{2h_2}\left[r-\frac{r_3^2}{r}\right]$	$-\frac{u_0}{h_2}\times z$
15	0	$-u_0\frac{r_3^2}{r_1^2}$

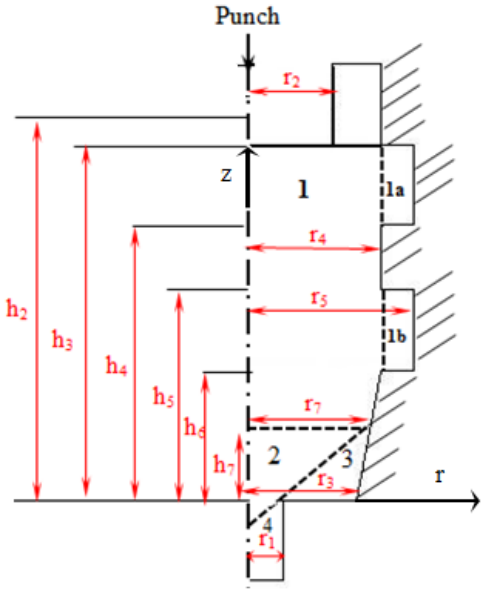

Figure 4.15: Different zones in Stage IV of DCCH

Table 4.14: Kinematically admissible velocity fields for stage IV

Zone	u_r	u_z
1	0	$-u_0$
1a	0	0
1b	0	0
2	$\frac{u_0}{h_7}\left(\frac{r_7^2}{r_1^2}-1\right)\frac{r}{2}$	$\frac{u_0}{h_7}\left[\left(\frac{r_7^2}{r_1^2}-1\right)z-h\frac{r_7^2}{r_1^2}\right]$
3	0	0
4	0	$-u_0\frac{r_7^2}{r_1^2}$

4.6 Analysis of Single Collet Chuck Holder by Multi-stage Extrusion/forging Process

In this section, a single collar collet chuck holder manufactured by multi stage extrusion/forging process is analysed in two stages. The first product is the input specimen/initial shape to get the final shape (Figure 4.16, detail dimensions are provided in Figure 5.32). The Figures 4.17 - 4.18 represent (half sectional view) the different zones considered for stages I & II of this axisymmetric component respectively. For the present analysis each stage is further subdivided into different zones. The different stages are:

a) Stage I: Extrusion/forging to fill the cavity (after 6.0 mm ram displacement).

b) Stage II: Flash formation (after 8.2 mm ram displacement)

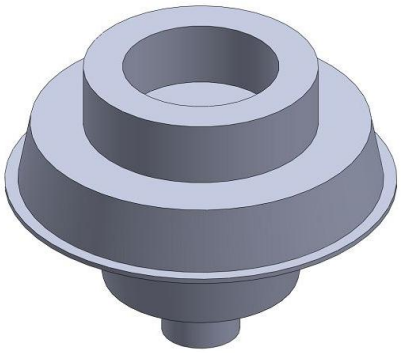

Figure 4.16: Single collar collet chuck holder processed by multi-stage CEF process

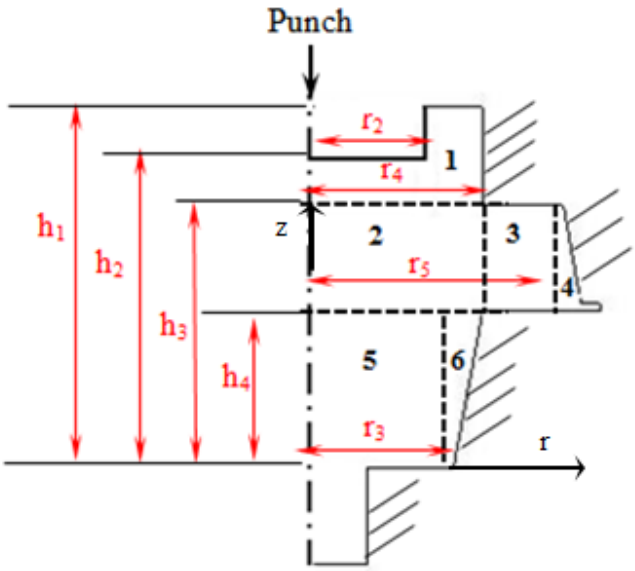

Figure 4.17: Different zones in Stage I of SCCCH

Following the same procedure applied for product I, the proposed kinematically velocity fields for different zones of stage I & II are given in Tables 4.15 - 4.16 respectively. As the geometry of the present product is axisymmetric in nature, the tangential velocity components of metal flow in different zones are considered to be vanished, i.e., $u_\theta = 0$ for all four stages.

Table 4.15: Kinematically admissible velocity fields for stage I

Zone	u_r	u_z
1	0	$-u_0$
2	$\frac{u_0}{h_3} \times \frac{r}{2}$	$-\frac{u_0}{h_3} \times z$
3	$\frac{u_0}{h_3} \frac{r_4^2}{2r}$	0

4	$\frac{u_0 r_4^2}{2h_3 r_5}\left(\frac{r_6 - r}{r_6 - r_5}\right)$	$\frac{1}{r_6 - r_5}\left[\frac{u_0 r_4^2}{2h_3 r_5}\right]\left(2 - \frac{r_6}{r}\right)(z - h_4)$
5	$\frac{u_0}{h_3} \times \frac{r}{2}$	$-\frac{u_0}{h_3} \times z$
6	$\frac{u_0}{h_3} \times \frac{r_4^2}{2r}$	$-\frac{u_0}{h_3} \times z$

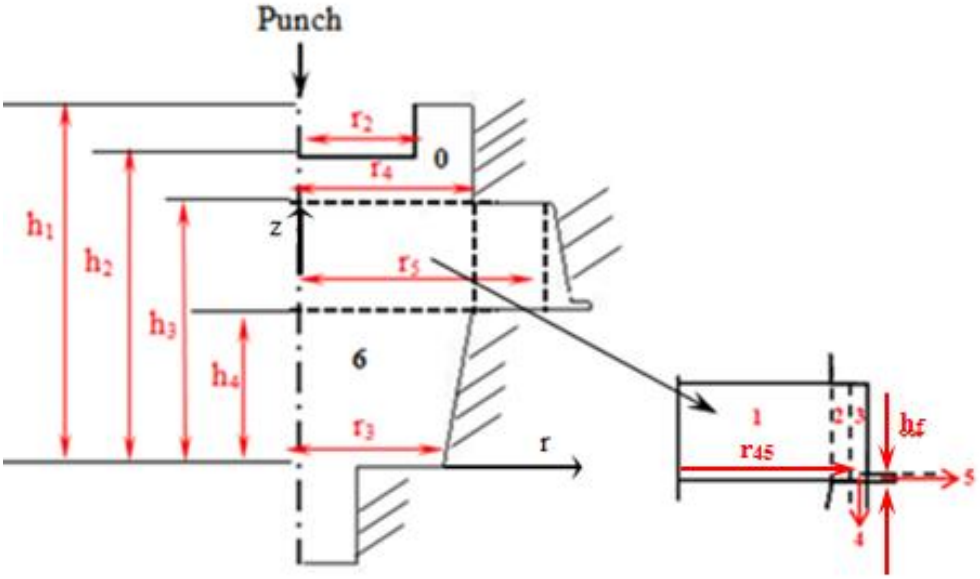

Figure 4.18: Different zones in Stage II of SCCCH

Table 4.16: Kinematically admissible velocity fields for stage II

Zone	u_r	u_z
0	0	$-u_0$
1	$\frac{u_0}{2(h_3 - h_4)} r$	$\frac{u_0}{h_3 - h_4}(h_4 - z)$
2	$\frac{u_0}{(h_3 - h_4)} \frac{r_4^2}{2r}$	0
3	$\frac{u_0}{2(h_3 - h_4)} \frac{r_4^2}{(r_5 - r_{45}) r_{45}} [r_5 - r]$	$\frac{1}{r_{45}} \frac{u_0}{2(h_3 - h_4)} \frac{r_4^2}{(r_5 - r_{45})} \left(2 - \frac{r_5}{r}\right) [(z - h_3)]$
4	$\frac{u_0 r_4^2}{2(h_3 - h_4)} \left[\frac{1}{r} + \frac{1}{h_f} \frac{1}{r_{45}} \frac{h_3 - h_4 - h_f}{(r_5 - r_{45})} \times \left(r - r_5 - \frac{r_{45}^2}{r} + \frac{r_{45} r_5}{r}\right)\right]$	$\frac{1}{h_f}\left[\frac{1}{r_{45}} \frac{u_0}{2(h_3 - h_4)} \frac{r_4^2}{r_5 - r_{45}} \left(2 - \frac{r_5}{r}\right) \times (h_4 + h_f - h_3)(z - h_4)\right]$

5	$\frac{u_0}{2(h_3-h_4)}\frac{r_4^2}{r}\left[1+\frac{1}{h_f}\frac{1}{r_{45}}\frac{h_3-h_4-h_f}{(r_5-r_{45})}\left(-r_{45}^2+r_{45}r_5\right)\right]$	0
6	0	0

4.7 Upper Bound Solution

The total power of deformation can be calculated using the Equation (4.1) on the basis of the above derived velocity fields. The upper bound solution of forming load will be given by:

$$F = \frac{\dot{W}}{u_B} \tag{4.27}$$

Where u_B is the velocity of punch

4.7.1 Internal power, $\dot{W}_P$

It can be calculated using the effective strain rate, $\dot{\varepsilon}$**,** Equation 4.2 and the internal power expression,

$$\dot{W}_{P,i} = \int_V \sigma_{0,i}\dot{\varepsilon}_i dV \tag{4.28}$$

Where, $\sigma_{0,\,i}$ is the yield stress of the material. We know that this value differs/changes at different strain rate value because of work-hardening effect. In order to take the strain hardening into account, $\sigma_{0,i}$ is taken as the mean/average yield stress of the corresponding zone, i, which follow the true stress-strain behaviour $\sigma = K\varepsilon^n$. Where, K is the strength coefficient and n refers to strain hardening exponent. Mean/average yield stress is given by, $\sigma_0 = \frac{K\varepsilon^n}{n+1}$.

(4.29)

i represents zones 1,2,3,……, etc. of each stages of different products.

4.7.2 Shear power, $\dot{W}_S$

The shear power dissipated at the velocity discontinuity surfaces can be obtained using the expression:

$$\dot{W}_{S,i} = \frac{1}{\sqrt{3}} \int_S \sigma_0 |\Delta V_i| dS \tag{4.30}$$

Where *i* represent velocity discontinuity surfaces 1, 2, 3, etc. of each stage of different products. Velocity discontinuity surfaces for different stages of the first products are provided in Tables 4.17 - 4.20 as an illustration. In order to consider the work-hardening effect into account, the yield stress of shear is calculated as a mean value of two connected zones, i.e., shear yield stress at the surface connecting zones 1 and 2 will be,

$$\frac{\sigma_{0,1} + \sigma_{0,2}}{2\sqrt{3}} \text{ [121], [122]} \tag{4.31}$$

Table 4.17: Velocity discontinuity surfaces for stage I of product 1

Surface	**Velocity discontinuity**
Between zone 1-2	$\left\lvert \frac{u_0}{h_2}\left[z + \frac{1}{\left(r_4^2 - r_2^2\right)}\left(r_2^2 z - h_3 r_4^2\right)\right]\right\rvert$
Between zone 2-3	$\left\lvert \frac{u_0}{2h_2} \frac{r_2^2}{r_4^2 - r_2^2}\left(\frac{r_4^2}{r} - r\right)\right\rvert$
Between zone 1-3	0
Between zone 3-4	0
Between zone 3-5	0
Between zone 4-5	0

Table 4.18: Velocity discontinuity surfaces for stage II of product 1

Surface	**Velocity discontinuity**
Between zone 1-2	$\left\lvert \frac{u_0}{h_3}\frac{r}{2}\right\rvert$
Between zone 2-3	$\left\lvert \frac{u_0}{h_3} z\right\rvert$
Between zone 2-4	$\left\lvert \frac{u_0}{2h_3} r\left(\frac{r_3^2}{r_1^2}\right)\right\rvert$
Between zone 2-5	$\left\lvert \frac{u_0}{2h_3}\left(\frac{r_3^2}{r}\right)\right\rvert$
Between zone 2-6	$\left\lvert \frac{u_0}{2h_3}\left(\frac{r_3^2}{r}\right)\right\rvert$
Between zone 4-5	$\left\lvert \frac{r_1^2 - r_3^2}{r_1^2 h_3} z + \frac{r_3^3}{r_1^2} - \frac{z}{h_2}\right\rvert$
Between zone 5-6	0

Table 4.19: Velocity discontinuity surfaces for stage III of product 1

Surface	**Velocity discontinuity**
Between zone 1-2	$\left\lvert \frac{u_0}{h_2}\left(\frac{r_2^2 z - h_3 r_4^2}{r_4^2 - r_2^2} + z \right) \right\rvert$
Between zone 2-3	$\left\lvert \frac{u_0}{2h_2} \frac{r_2^2}{r_4^2 - r_2^2}\left(\frac{r_4^2}{r} - r \right) \right\rvert$
Between zone 3-4a	$\left\lvert \frac{u_0}{2h_2} \frac{r_4^2 (h_2 - h_3)}{(h_1 - h_2)(r_4^2 - r_2^2)}\left(r - \frac{r_4^2}{r} \right) \right\rvert$
Between zone 3-4b	$\left\lvert \frac{u_0}{2h_2} \frac{r_4^2 (h_2 - h_3)}{(h_1 - h_2)(r_4^2 - r_2^2)}\left(r_{2a} - \frac{r_4^2}{r_{2a}} \right) \right\rvert$
Between zone 4a-4b	$\left\lvert \frac{u_0}{h_2(r_4^2 - r_2^2)} \left[\begin{array}{l} \frac{1}{(h_1 - h_{12})} \\ \left\{ \begin{array}{l} r_4^2 (h_3 - h_2) z + r_2^2 h_2 (h_1 - h_{12}) + \\ r_4^2 (h_1 h_{12} - h_1 h_3) \end{array} \right\} - \\ \frac{(h_3 - h_2) r_4^2 (z - h_{12})}{2(h_1 - h_{12})(r_{2a} - r_2)}\left(r_{2a} - \frac{r_4^2}{r_{2a}} \right) \\ \left(\frac{2r_{2a} - r_2}{r_{2a}} \right) + (r_2^2 h_2 - r_4^2 h_3) \end{array} \right] \right\rvert$
Between zone 1-5	0
Between zone 2-5	$\left\lvert \frac{u_0}{2h_2}\left[\frac{r_2^2}{(r_4^2 - r_2^2)}\left(\frac{r_4^2}{r} - r \right) - r \right] \right\rvert$
Between zone 5-6	$\left\lvert \frac{u_0}{h_2} z \right\rvert$
Between zone 5-8	$\left\lvert \frac{u_0 r}{2h_2}\left(\frac{r_3^2}{r_1^2} \right) \right\rvert$
Between zone 5-9	$\left\lvert \frac{u_0 r}{2h_2}\left(\frac{r_3^2}{r} \right) \right\rvert$
Between zone 5-10	$\left\lvert \frac{u_0 r}{2h_2}\left(\frac{r_3^2}{r} \right) \right\rvert$
Between zone 8-11	$\left\lvert \frac{u_0 r}{2h_2}\left(1 - \frac{r_3^2}{r_1^2} \right) \right\rvert$
Between zone 11-12	$\left\lvert \frac{u_0 r_3^2}{r_1^2 (d_2 - d_1)} \frac{r}{2} \right\rvert$

Table 4.20: Velocity discontinuity surfaces for stage IV of product 1

Surface	**Velocity discontinuity**
Between zone 1-2	$\left\lvert -\frac{u_0}{(h_3-h_4)} \right\rvert$
Between zone 2-3	$\left\lvert \frac{1}{r_{45}} \frac{u_0}{2(h_3-h_4)} \frac{r_4^2}{r_5-r_{45}} \left(2-\frac{r_5}{r_{45}}\right)(z-h_3) \right\rvert$
Between zone 2-4	$\left\lvert \frac{1}{h_f} \frac{1}{r_{45}} \left[\frac{u_0}{2(h_3-h_4)} \frac{r_4^2}{r_5-r_{45}} \left(2-\frac{r_5}{r_{45}}\right) (h_4+h_f-h_3)(z-h_3) \right] \right\rvert$
Between zone 4-5	$\left\lvert \frac{1}{h_f} \frac{1}{r_{45}} \left[\frac{u_0}{2(h_3-h_4)} \frac{r_4^2}{r_5-r_{45}} (h_4+h_f-h_3)(z-h_3) \right] \right\rvert$
Between zone 0-1	$\left\lvert \frac{u_0}{2(h_3-h_4)} r \right\rvert$
Between zone 1-6	$\left\lvert \frac{u_0}{2(h_3-h_4)} r \right\rvert$
Between zone 3-4	$\left\lvert \frac{u_0 r_4^2}{2(h_3-h_4)} \left[\frac{1}{r} + \frac{1}{h_f} \frac{1}{r_{45}} \frac{h_3-h_4-h_f}{r_5-r_{45}} \left(r-r_5-\frac{r_{45}^2}{r}+\frac{r_{45}r_5}{r} \right) - \frac{r_5-r}{r_{45}(r_5-r_{45})} \right] \right\rvert$

Similarly, for the second, third and fourth products, related velocity discontinuity equations are derived and applied to upper bound solutions.

4.7.3 Frictional power, $\dot{W}_f$

The frictional power dissipated at the punch and die/material interfaces can be obtained using the expression:

$$\dot{W}_{f,i} = \frac{m}{\sqrt{3}} \int_{A_f} \sigma_0 |\Delta V_i| dA_f \tag{4.32}$$

Where *i* represent velocity at frictional interfaces 1, 2, 3… etc. of each stages of different products. Shear yield strength at friction interface is taken as $\frac{\sigma_{0,i}}{\sqrt{3}}$ to take care of strain-hardening effect. As an illustration, relative velocity at frictional interfaces for different stages for SCCCH are provided in Tables 4.21 - 4.24

Table 4.21: Frictional surfaces for stage I of product 1

Surface	**Relative velocity at frictional interface**
Zone 1 & punch bottom surface	$\left\lvert \frac{u_0}{h_2} - \frac{r}{2} \right\rvert$
zone 2 & side wall	$\left\lvert \frac{u_0}{h_2\left(r_4^2 - r_2^2\right)} \left[r_2^2 z - h_3 r_4^2 \right] \right\rvert$
Zone 4 & die bottom wall	$\left\lvert \frac{u_0}{h_2} - \frac{r}{2} \right\rvert$
Zone 5 & die side wall	$\left\lvert \left(-\frac{u_0}{h_2} z \right) \sin\theta + \left(\frac{u_0}{h_2} \frac{r}{2} \right) \cos\theta \right\rvert$
Zone 5 & die bottom surface	$\left\lvert \frac{u_0}{h_2} - \frac{r}{2} \right\rvert$

Table 4.22: Frictional surfaces for stage II of product 1

Surface	**Relative velocity at frictional interface**
Zone 1 & punch bottom surface	$\lvert -u_0 \rvert$
Zone 1 & side wall	0
Zone 3 & Upper die surface	$\left\lvert \frac{u_0}{h_3} \frac{r_4^2}{2r} \right\rvert$
Zone 3 & lower die surface	$\left\lvert \frac{u_0}{h_3} \frac{r_4^2}{2r} \right\rvert$
Zone 5 & lower die surface	$\left\lvert \frac{u_0}{2h_3} \left[r - \frac{r_3^2}{r} \right] \right\rvert$
Zone 6 & die side wall	$\left\lvert \left(-\frac{u_0}{h_3} z \right) \sin\theta + \frac{u_0}{2h_3} \left(r - \frac{r_3^2}{r} \right) \cos\theta \right\rvert$
Zone 7 & die side wall	$\left\lvert u_0 \frac{r_3^2}{r_1^2} \right\rvert$
Zone 1 & die side wall	$\lvert u_0 \rvert$
Zone 1 & side of punch	$\lvert u_0 \rvert$
Zone 1 & punch bottom surface	$\left\lvert \frac{u_0}{h_2} - \frac{r}{2} \right\rvert$

Table 4.23: Frictional surfaces for stage III of product 1

Surface	**Relative velocity at frictional interface**
Zone 1 & punch bottom surface	$\left\lvert \frac{u_0}{h_2} \frac{r}{2} \right\rvert$
Zone 2 & die side wall	$\left\lvert \frac{u_0}{h_2\left(r_4^2 - r_2^2\right)} \left(r_2^2 z - h_3 r_4^2\right) \right\rvert$
Zone 3 & die side wall	$\left\lvert \frac{u_0}{h_2\left(r_4^2 - r_2^2\right)} \left(r_2^2 h_2 - h_3 r_4^2\right) \right\rvert$
Zone 3 & punch side wall	$\left\lvert \frac{u_0}{h_2\left(r_4^2 - r_2^2\right)} \left(r_2^2 h_2 - h_3 r_4^2\right) \right\rvert$
Zone 4a & side wall	$\left\lvert \frac{u_0}{h_2\left(h_1 - h_{12}\right)\left(r_4^2 - r_2^2\right)} \left[\begin{matrix} r_4^2\left(h_3 - h_2\right)z + r_2^2 h_2 \\ \left(h_1 - h_{12} + r_4^2\left(h_2 h_{12} - h_1 h_3\right)\right) \end{matrix} \right] \right\rvert$
Zone 6 & upper die surface	$\left\lvert \frac{u_0}{h_2} \frac{r_4^2}{2r} \right\rvert$
Zone 6 & lower die surface	$\left\lvert \frac{u_0}{h_2} \frac{r_4^2}{2r} \right\rvert$
Zone 7 & lower die surface	$\left\lvert \frac{u_0 r_4^2}{2h_2 r_{45}} \frac{\left(r_5 - r\right)}{r_5 - r_{45}} \right\rvert$
Zone 9 & lower die surface	$\left\lvert \frac{u_0}{2h_2} \left(r - \frac{r_3^2}{r} \right) \right\rvert$
Zone 11 & side die wall	$\left\lvert u_0 \frac{r_3^2}{r_1^2} \right\rvert$
Zone 10 & side inclined wall	$\left\lvert \left(-\frac{u_0}{h_2} z \right) \sin\theta + \frac{u_0}{2h_2} \left(r - \frac{r_3^2}{r} \right) \cos\theta \right\rvert$

Table 4.24: Frictional surfaces for stage IV of product 1

Surface	**Relative velocity at frictional interface**
one 1 & side wall	$\left\lvert -\frac{u_0}{h_3 - h_4} z \right\rvert$
Zone 2 & upper die surface	$\left\lvert \frac{u_0}{h_3 - h_4} \frac{r_4^2}{2r} \right\rvert$
Zone 2 & lower die surface	$\left\lvert \frac{u_0}{h_3 - h_4} \frac{r_4^2}{2r} \right\rvert$
Zone 3 & upper die surface	$\left\lvert \frac{u_0}{2\left(h_3 - h_4\right)} \frac{r_4^2}{\left(r_5 - r_{45}\right)} \frac{\left(r_5 - r\right)}{r_{45}} \right\rvert$

Zone 3 & side wall	$\left\lvert \frac{1}{r_{45}} \frac{u_0}{2(h_3-h_4)} \frac{r_4^2}{(r_5-r_{45})} (z-h_3) \right\rvert$
Zone 4 & lower die surface	$\lvert \Delta V \rvert = \left\lvert \frac{u_0 r_4^2}{2(h_3-h_4)} \left[\frac{1}{r} + \frac{1}{h_f} \frac{1}{r_{45}} \frac{h_3-h_4-h_f}{(r_5-r_{45})} \left(r - r_5 - \frac{r_{45}^2}{r} + \frac{r_{45} r_5}{r} \right) \right] \right\rvert$
Zone 5 & upper, lower die surface	$2 \times \left\lvert \frac{u_0 r_4^2}{2(h_3-h_4)} \frac{r_4^2}{r} \left[1 + \frac{1}{h_f} \frac{1}{r_{45}} \frac{h_3-h_4-h_f}{(r_5-r_{45})} \left(r_{45}^2 + r_{45} r_5 \right) \right] \right\rvert$
Zone 0 & side die wall	$\lvert u_0 \rvert$
Zone 0 & punch bottom surface	0
Zone 0 & punch side wall	$\lvert u_0 \rvert$

Similarly, for the second, third and fourth products, equations associated with relative velocities at frictional interfaces are derived and applied to upper bound solutions.

4.8 Results and Discussion

4.8.1 CEF process for single collar collet chuck holder

Case I: m = 0.13 (60:40 MoS_2 + Grease)

Upper bound analysis is carried out to find the forming load for single collar collet chuck holder using proposed kinematically admissible velocity fields at three ram displacements, i.e., 0.5 mm/min, 1.0 mm/min and 2.0 mm/min for four stages. In stage I backward extrusion is completed, in stage II collar and end stud are formed by lateral and forward extrusions, in stage III die corners are filled and in stage IV flash is formed to complete the process. The maximum upper bound loads obtained for the component to process are 175.4 kN, 191.2 kN and 203.5 kN at ram velocities of 0.5 mm/min, 1.0 mm/min and 2.0 mm/min respectively (shown in Figure 4.19) for m = 0.13 at end of the process for this stage.

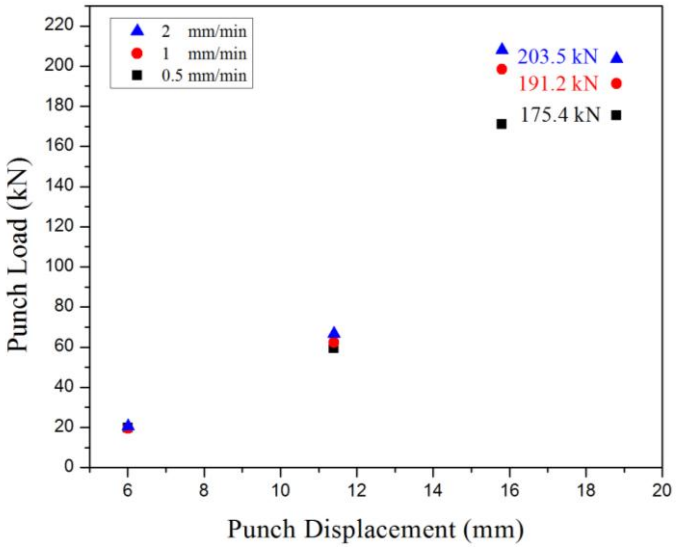

Figure 4.19: Variation of punch load with ram displacement at m = 0.13

Case II: m = 0.19 (100 % Grease)

Similarly, upper bound loads are predicted at three ram speeds, i.e., 0.5 mm/min, 1.0 mm/min and 2.0 mm/min under full grease lubrication condition (m = 0.19). The maximum forming loads obtained for the component at the end of the process are 184.8 kN, 201.3 kN and 214.6 kN respectively (Figure 4.20) for these three ram speeds. It is found that the maximum load increases with ram velocity because of increase in flow stress (due to work hardening effect).

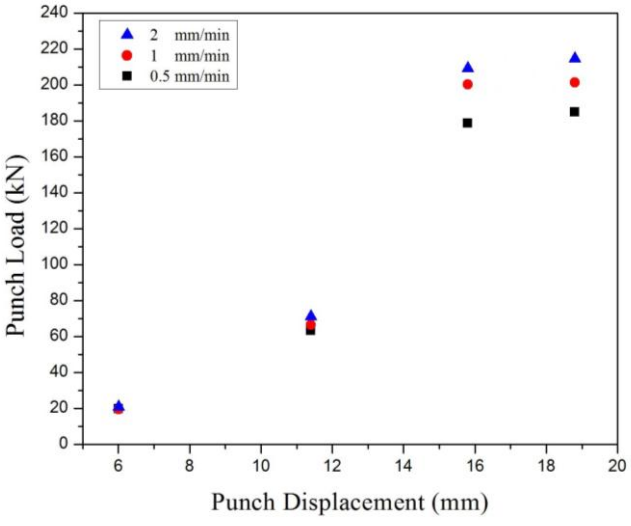

Figure 4.20: Variation of punch load with ram displacement at m = 0.19

Case III: m = 0.38 (*Unlubricated conditions)*

Similarly, analysis are carried out to predict the upper bound load for the same single collar collet chuck holder manufactured by combined extrusion forging process at three ram displacements, i.e., 0.5 mm/min, 1.0 mm/min and 2.0 mm/min under no lubrication condition (friction factor, m = 0.38). The maximum forming loads obtained for the component to manufacture are 217.9 kN, 236.5 kN and 252.7 kN respectively (Figure 4.21) at the end of the process. It is also observed that the maximum load increases with ram velocity because of work hardening effect and values are more in comparison with lower friction (due to more energy loss in frictional surfaces).

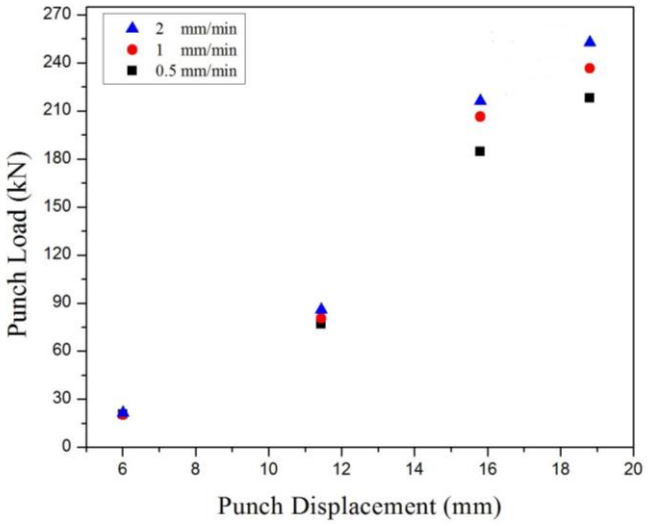

Figure 4.21: Variation of punch load with ram displacement at m = 0.38

4.8.2 CEF process for double collar collet chuck holder

Case I: (60:40 Mos2 + Grease) at different ram velocities

Upper bound analyses are carried out to manufacture the double collar collet chuck holder using combined extrusion forging process at three ram displacements, i.e., 0.5 mm/min, 1.0 mm/min and 2.0 mm/min. All stages are similar to the first product, but in the second stage, two collars are made instead of one. The maximum forming loads obtained for the component to manufacture are 164.6 kN, 182.6 kN and 188.0 kN for ram speeds of 0.5 mm/min, 1.0 mm/min and 2.0 mm/min respectively (shown in Figure 4.22).

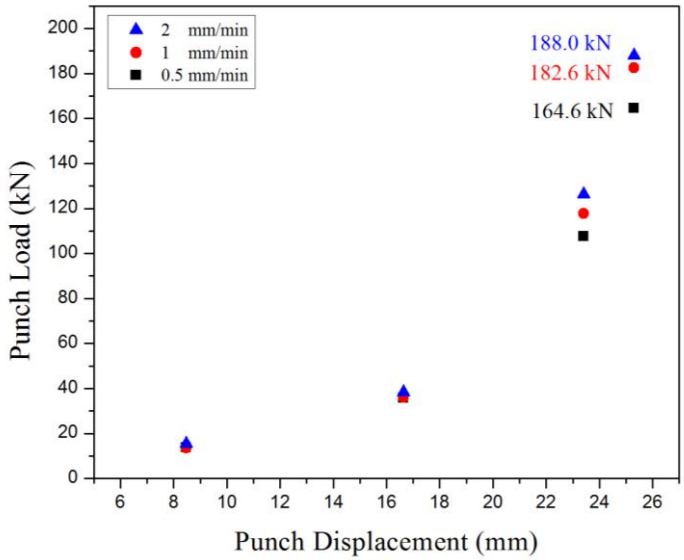

Figure 4.22: Variation of punch load with ram displacement at m = 0.13

Case II: (100 % Grease) at different ram velocities

Similarly, upper bound analysis are carried out to process the same double collar collet chuck holder using combined extrusion forging process at three ram speeds, i.e., 0.5 mm/min, 1.0 mm/min and 2.0 mm/min under full grease lubrication condition. The maximum forming loads obtained at end of the process for the component to manufacture are 170.2, 188.6 and 194.1 kN for ram speeds of 0.5 mm/min, 1.0 mm/min and 2.0 mm/min respectively (Figure 4.23).

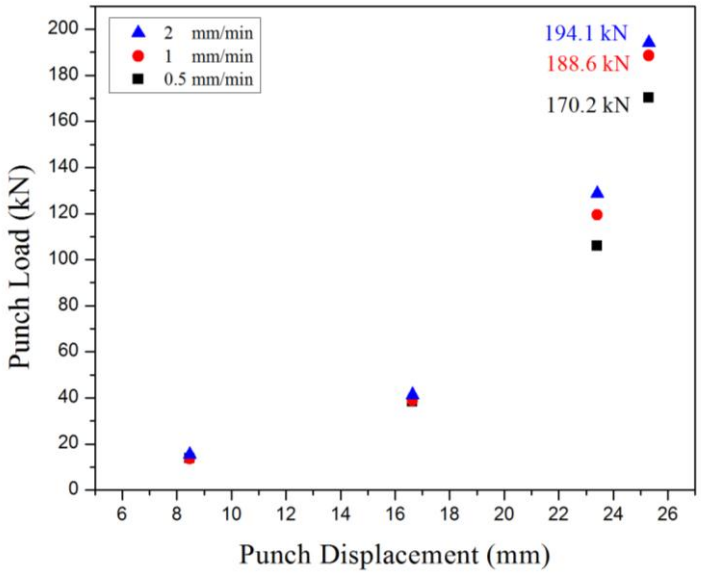

Figure 4.23: Variation of punch load with ram displacement at m = 0.19

Case III: ***Unlubricated conditions at different ram velocities***

The maximum forming loads obtained for the component to manufacture are 188.4, 207.9 and 215.2 kN for ram speeds of 0.5 mm/min, 1.0 mm/min and 2.0 mm/min respectively (Figure 4.24). It is observed that the maximum load increases with ram velocity because of work hardening effect and also increase with friction (due to more energy loss in frictional surfaces).

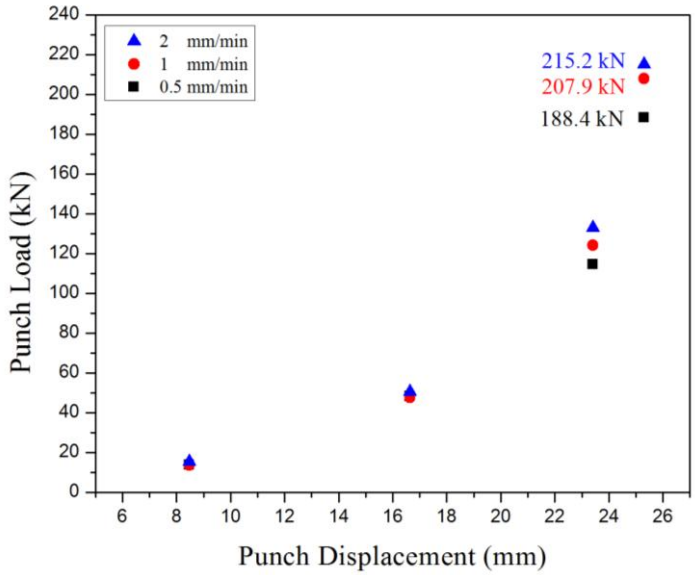

Figure 4.24: Variation of punch load with ram displacement at m = 0.38

4.8.3 CE process for double collar collet chuck holder

Figures 4.25 - 4.27 show the upper bound loads at the end of different stages for different with ram velocities (0.5 mm/min, 1.0 mm/min and 2.0 mm/min) at frictional conditions, ,m = 0.13, 0.19 and 0.38 respectively. Initial three stages are similar to the second product and in the fourth stage forward extrusion takes place instead of flashing. It is observed that the maximum load increases with ram velocity because of work hardening effect and also increases with friction (due to more energy loss in frictional surfaces).

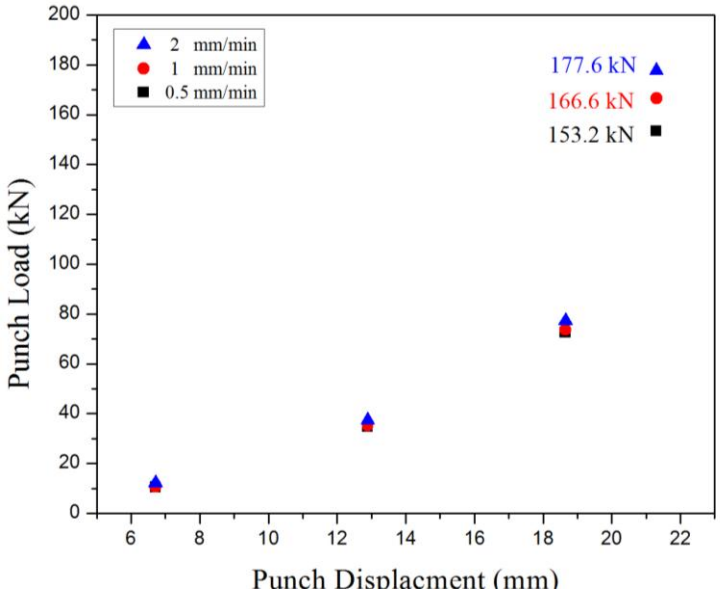

Figure 4.25: Variation of punch load with ram displacement at m = 0.13

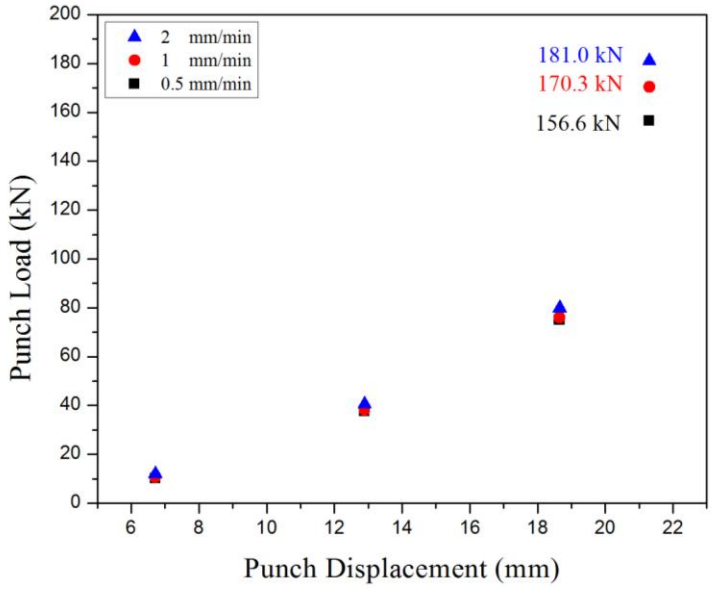

Figure 4.26: Variation of punch load with ram displacement at m = 0.19

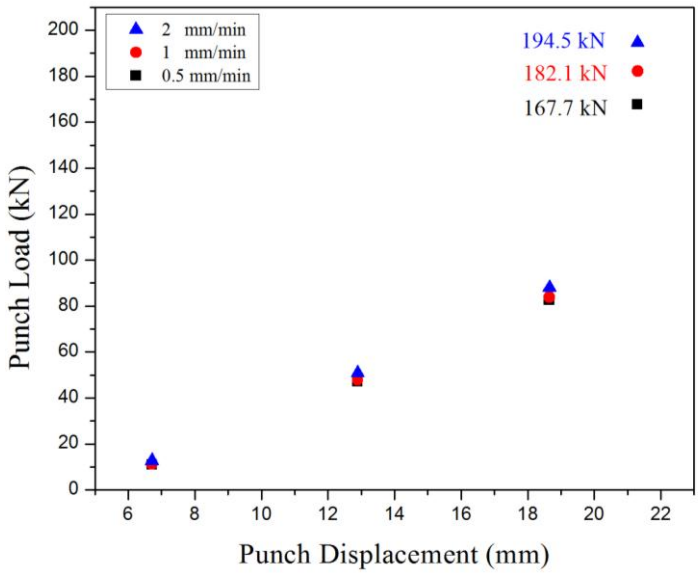

Figure 4.27: Variation of punch load with ram displacement at m = 0.38

4.8.4 Multi-stage extrusion/forging process for single collar collet chuck holder

The present analytical analysis is an approach of multistage extrusion/forging to process a single collar collet chuck holder. The concept deals with the use of multi-stage combined extrusion-forging technique for processing a component without defects. The first product (single collar collet chuck holder) is the input specimen for the present analysis to get the final product. In the present study we have considered grease (m = 0.19) as lubricant with a ram displacement of 1 mm/min.

As an illustration, Figure 4.28 shows the loads at the end of stage I and stage II when ram moves at 1.0 mm/min and with frictional condition of m = 0.19. It is evident that punch load increases with ram displacement and reaches maximum value during flashing.

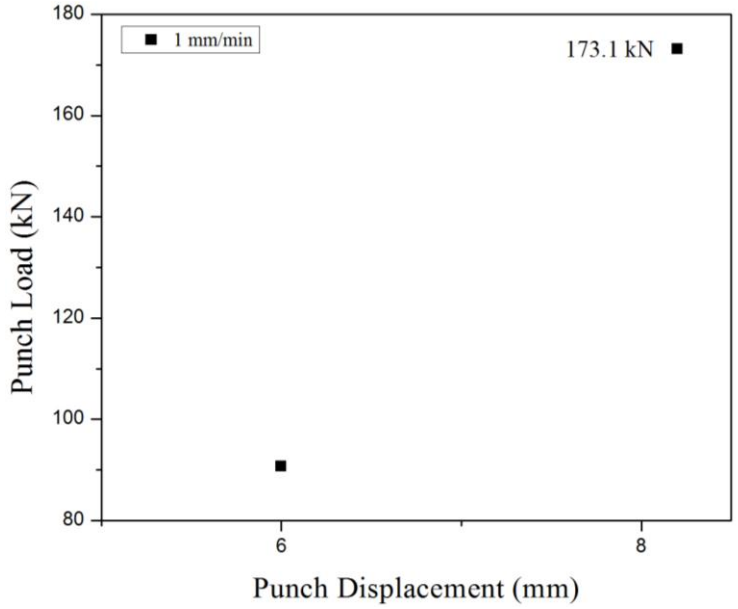

Figure 4.28: Variation of punch load with ram displacement

4.9 Conclusions

In the present research work, philosophy of upper bound method is applied to perform a mathematical analysis to find the forming load for manufacturing different types of collet chuck holders using CEF and CE processes. The following observations have been made based on the obtained results:

- The complete process to get the first three components are assumed to compose of four stages and fourth component of two stages with regard to forward/backward extrusion, forging, die corner filling, and flash formation.
- Kinematically admissible velocity fields for four different types of collet chuck holders is proposed under varying frictional conditions and ram velocities for different zones of all stages.
- The minimum (175.4 kN) and maximum (252.7 kN) upper bound load for SCCCH manufactured by CEF process obtained at m = 0.13 with 0.5 mm/min ram velocity and m = 0.38 at 2 mm/min ram velocity respectively at end of the process.
- Similarly for DCCCH manufactured by CEF method, the maximum forming load (215.2 kN) was obtained at 0.38 frictional conditions at 0.2 mm/min ram velocity. The minimum forming load (164.6 kN) was obtained at 0.13 frictional condition with 0.5 mm/min ram velocity at end of the process.

- The third product DCCCH processed by CE method, the maximum forming load (194.0 kN) was obtained at m = 0.38 at 0.2 mm/min ram velocity. The minimum forming load (153.2 kN) was noticed to be same at m = 0.13 and 0.19 with 0.5 mm/min ram velocity at end of the process.
- For multi stage process, maximum (173.1 kN) upper bound load at m = 0.19 with 1.0 mm/min ram velocity was obtained at end of the process.
- It is seen that the proposed kinematically admissible velocity fields for different products adequately address the die filling and flow pattern of the metal at different punch position and satisfactorily predict the load requirements taking care of work hardening, friction effects and redundant work.

The obtained analytical results have been considered to compare with that obtained from FEM and experimental results in an elaborated manner in the next chapters.

Chapter 5

Numerical Analysis

5.1 Introduction

During the early periods of forming process analysis and die design, researchers depend on extensive experiments which are costly and time consuming. To overcome the above problem and to cut down the analysis time different numerical methods have been proposed to reduce the material cost and dependency on tedious experiments. The application of numerical technique to metal forming problems has been growing rapidly, as a result of significant development attained in computer hardware and software. Among different numerical techniques, finite element method (FEM) has been demonstrated to be the most excellent way for analysing metal forming problems. Normally, any physical system can be illustrated in the form of partial differential equations utilizing the understanding of mathematical formulations and engineering sciences. In particular, metal forming problems can be mathematically simulated by applying the theory of elasticity and plasticity, solving a set of second order partial differential equations. Finite element has turn out to be the most accepted technique for solving such equations. FEM has been effectively applied to the solution of steady state and transient problems and non-linear situations of one-, two-, and three dimensional geometrical forms and different material behaviours. The finite element discretization process, like the finite difference process, transforms partial differential equations into algebraic equations.

The simulation of aluminium extrusion/forging process is carried out by different researchers using different finite element software. A lot of numerical analysis in the past few years suggests that experimental analysis should be performed to validate the FEM results obtained for different influencing parameters such as strain rate, stress, temperature and velocity of metal flow; the article by Zhao et al. [29] signifies the same. Shatermashhadi et al. [51] provided a brief idea on the experimental and FEM analysis of the combined process of hydrostatic and backward extrusion. Gusel et al. [123] calculated the strain, strain rate and stress distribution by the use of grid lines experimentally and numerically for copper alloy at the various coefficients of friction.

Farhoumand and Ebrahimi [4] used finite element analysis to find the friction at the walls of the die and billet and at die corner. Li et al. [28] investigated a numerical analysis on thin and sharp complex components with light metals. Paltasingh et al. [124] conducted experiments and numerically analyse the spur gears with contour surfaces. In this context Potnuru et al. [125] predicted numerically the metal flow patterns and forming load for a socket wrench. Bingol et al. [126] suggests numerical modelling software's are taking a leading part in the present scenario for predicting the extrusion load which inturn reduces the material wastage and time for the industries. They have performed numerous analysis numerically by finite element method (FEM) and applied Artificial Neural Networks (ANN) for a gear like profile and validated the same with experimental observations. There are various metal forming analysis software that can realistically simulate material forming processes. Among them, DEFORM®-3D is one, which is popular among the researchers and industries.

5.2 Modelling of the System

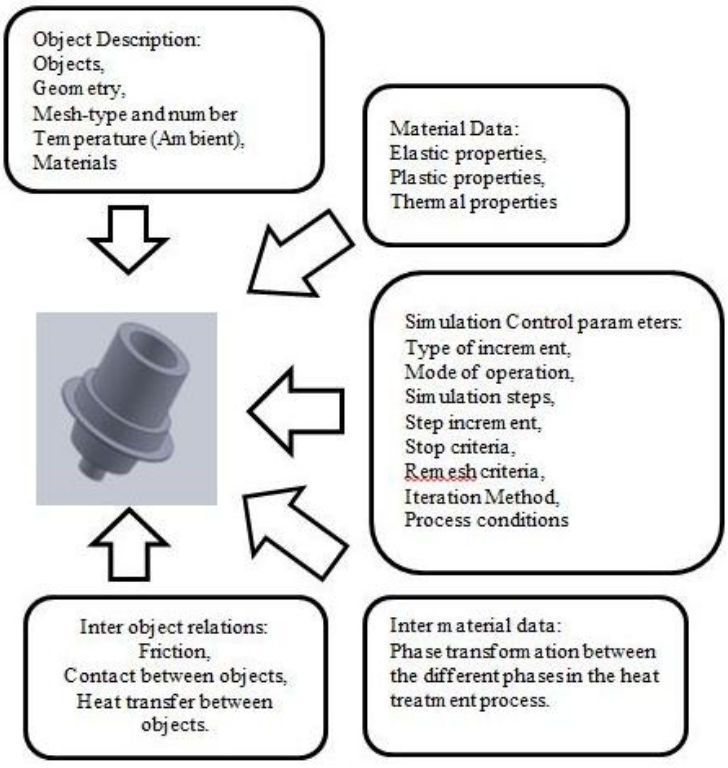

Figure 5.1: Major input parameters for FEM simulation for CEF and CE of collet chuck holders

Figure 5.1 represents the major input parameters which are in application in the present simulation process. The software consists of three key features:

1. Pre-processor:

The objective of this module is to feed the input data required to perform numerical analysis. The models of deformable workpiece and the dies required for the operation are imported.

2. Simulation

The Finite element analysis performs the simulation according to the given input data.

3. Post-processor

The data obtained from the simulation analysis is viewed in a graphical user interface. The graphical representation gives us the geometry data such as effective stress, effective strain, temperature, mean stress, total velocity of the product at various sections. In the post processor section the data can be extracted for further comparison and other application obtained from the numerical analysis.

5.2.1 Interface formulation

In the interface formulation, an interaction between the work piece and dies during metal forming operations is incorporated. The contact conditions can be mathematically described by:

$$[v] \cdot n = 0, \quad [t] = 0 \tag{5.1}$$

Where, v and t are the velocity and traction vector, respectively, n is a unit normal to the contact surface and equation (5.1) indicates the discontinuity amount across the contact boundary. Moreover, the traction in the tangential direction should satisfy the frictional law. The interface formulation between the work piece and rigid dies is relatively simple. In order to simulate more complicated forming operations, such as canned extrusion, pack rolling, and hot isostatic pressing, the interface formulation should be capable of handling the contact conditions between the deforming bodies. The interface conditions given in equation (5.1) can be expressed in variational form as

$$\int_S K_i \Delta v_n \delta \Delta v_n \mathrm{d}S + \int_S t_s \delta \Delta v_s \mathrm{d}S = 0 \tag{5.2}$$

Where, Δv_n is a penetrating velocity in the normal direction, Δv_s sliding velocity in the tangential direction, and t_s traction, representing the frictional stress. Here K_i is a large positive constant to penalize the penetration.

5.2.2 Simulation control

The SI unit convention with the langrangian incremental type followed by a deformation mode is opted for the simulation. The mechanical, thermal or phase transformations simulates the deformation in the workpiece. Here the top die is the primary die; the primary die is priory defined with initiate or abort the simulation. Aborting the operation is performed when the specified distance is reached by the primary die. Aborting distance are in combination with the reference points. The step size is the crucial for the simulation to perform the operation. The step size can be controlled by two ways either by die displacement or by time increment. The present simulation analysis is performed by controlling the time increment. During the simulation severe plastic deformation takes of the workpiece (Slave). This Severe plastic deformation causes the workpiece to distort which can be used further (negative Jacobean). The operation to be performing remeshing after the mesh is distorted. The process of remeshing is substituting the distorted mesh with a new mesh along with interpolating the field variables (strain, velocity, damage, and temperature, etc.) from old mesh to new mesh. The object remeshing is performed to a slave (billet). The remeshing depends on the interference between the primary die and the billet. The depth of interference is the depth an element edge of the slave object crosses the surface of a master object.

5.2.3 Simulation modelling

In finite element modelling (FEM), combined extrusion-forging and combined extrusion process technique is used to produce different types of collet chuck holders, at varying rate of ram displacements. The Non-linear-equations are solved with the help of direct iteration method and the Newton-Raphson method. Flow behaviour was studied with, a modified Lagrangian method for the finite element code. The initial estimate of the Conjugate Gradient method, the direct iteration method is employed in the solution procedure, which is further used to find the velocity error and force error, obtained as 0.005 and 0.05 respectively. It has assumed that the billet was rigid plastic and the die, container, and flow guide is indeed rigid during the simulation process. The four-noded tetrahedron elements have been employed. In this finite element simulation, an isothermal process was adopted.

5.2.4 Formulation

Rigid-plastic material formulation

The material taken is rigid-plastic material for the current cold forming analysis. The analysis is based on CEF and CE process. The following are the governing equations which satisfies the combined extrusion/forging process:

Equilibrium Equations are:

$$\sigma_{ij,j} = 0 \tag{5.3}$$

Compatibility condition:

$$\dot{\varepsilon}_{ij} = \frac{1}{2}\left(u_{i,j} + u_{j,i}\right) \tag{5.4}$$

Incompressibility condition:

$$\dot{\bar{\varepsilon}}_v = u_{i,i} = 0 \tag{5.5}$$

Constitutive equations:

$$\sigma_{ij}^{'} = \frac{2\bar{\sigma}}{3\dot{\bar{\varepsilon}}}\varepsilon_{ij}, \quad \bar{\sigma} = \sqrt{\frac{3}{2}\left(\sigma'_{ij}\sigma'_{ij}\right)}, \quad \dot{\bar{\varepsilon}} = \sqrt{\frac{2}{3}\left(\dot{\varepsilon}_{ij}\dot{\varepsilon}_{ij}\right)} \tag{5.6}$$

Boundary conditions:

$$\sigma_{ij}n_i = F_j \text{ on } S_F, \; u_i = U_i \text{ on } S_U \tag{5.7}$$

Here σ_{ij} = Stress

$\dot{\varepsilon}_{ij}$ = Strain velocity

$\bar{\sigma}$ = Effective stress

$\dot{\bar{\varepsilon}}$ = Effective strain velocity

F_j = Force on the boundary surface of S_F

U_i = Deformation velocity on the boundary surface of S_U

To determine the weak form for rigid-plastic FEM the variational method can be applied to the equations (5.3-5.7)

$$\int\left(\frac{2\bar{\sigma}}{3\dot{\bar{\varepsilon}}}\right)\dot{\varepsilon}_{ij}\delta\dot{\varepsilon}_{ij}dV + \int K\dot{\varepsilon}_{kk}\delta\dot{\varepsilon}_{ii}dV - \int_{SF} F_i\delta u_i dS = 0 \tag{5.8}$$

V, S = Volume & surface area of the material

K = Penalty Constant,

Using the FEM discretization procedure the variational function can be converted to non-linear algebraic equation. In an isotropic rigid-plastic material model flow stress is a function

of effective stress, strain rate and temperature which can be solved by the Newton-Raphson method

$$\bar{\sigma} = \bar{\sigma}\left(\bar{\varepsilon}, \dot{\bar{\varepsilon}}, T\right) \tag{5.9}$$

A shear type friction is assumed between the billet and the tool, the friction factor m ($0 \leq m \leq 1$) is represented by

$$m = \sqrt{3}\frac{\tau}{\bar{\sigma}} \tag{5.10}$$

τ = Frictional shear stress

The values of constant interface friction factor *m* for the applied lubricating situations have been decided by carrying out ring tests and the results are mentioned in section 6.7 afterward in Chapter 6. In the present formulation frictional force has been applied as a surface force at the die-billet contact surfaces.

5.2.5 Simulation for the present problem

In the present CEF and CE processes a cylindrical billet made of Aluminium Al-1070 (chemical composition shown in Table 5.1) is forced by the punch, against the bottom die, which is stationary. Followed by extrusions in the various directions and filling in the radial orientation of the die cavity. The die-punch set-up and the final product (right side) of the process is shown in Figure 5.2. At most of the locations, the direction of metal flow is perpendicular to the direction of punch movement. The present study is aimed at manufacturing the collet chuck holders through CEF and CE processes. Die punch setup for combined process in simulation modelling to produce the collet chuck holder is shown in Figure 5.2. It is assumed that top die (Punch); the bottom die (container) and flow guide is rigid during the simulation processes that are shown in Figure 5.3. The billet is assumed as plastic as it is subjected to deformation as shown in Figure 5.3.

Table 5.1: Composition of specimen (Aluminum 1070)

Al	Si	Mn	Zn	Cu	V	Ti	Fe	Ga
99.727%	0.07%	0.002%	0.003%	0.001%	0.01%	0.007%	0.18%	0.01

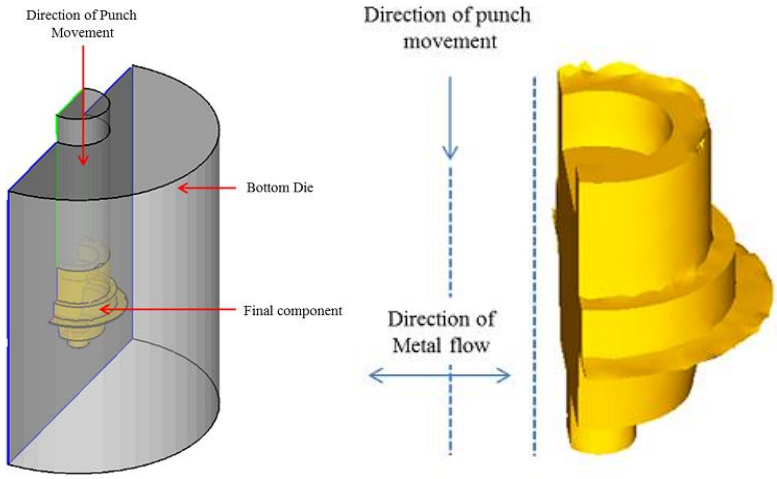

(a) Final position of billet (b) Final Shape of the product

Figure 5.2: Schematic view of combined extrusion-forging process

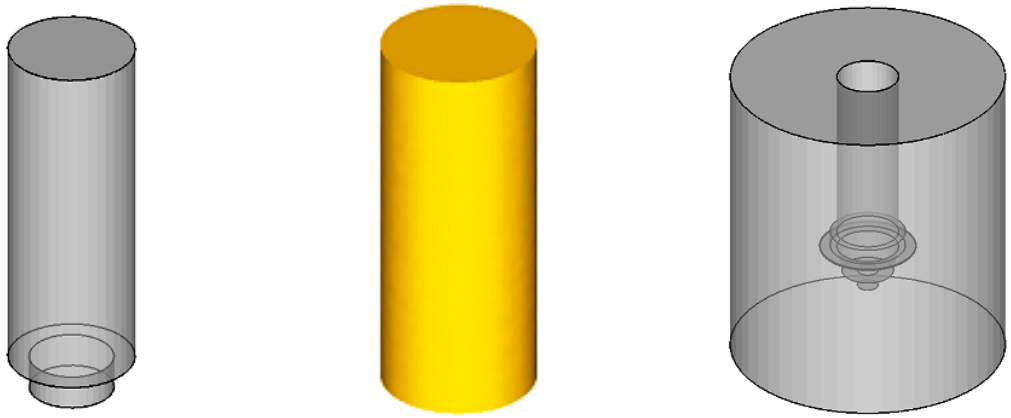

(a)Punch with punch head (b) Billet (c) Bottom die

5.3: Input parts required for the simulation process

A defined friction factor for the billet, die, container and flow guide interfaces has been set for the cold forming condition. The four-node tetrahedron elements have employed. A mesh independence test was performed (to use DEFORM 3D® for the subsequent analyses) to get the desired and accurate punch loads at various frictional conditions (friction factor of 0.13, 0.19 and 0.38) which is calibrated at different ranges of elements as shown in the Figure 5.4 (at ram velocity of 1.0 mm/min for first product as an illustration). The workpiece is modelled using approximately 20000 meshing elements and 3479 nodes for the billet without hampering the accuracy of the final results. Similar grid independence test were conducted at different ram velocities which has negligible effect. The temperature of all the objects is set to 30ºC. The process parameters assumed for the current analysis is shown in Table 5.2. The physical properties such as elastic modulus,

density and Poisson's ratio data were procured from the manufactured of the ingot (Al 1070). The flow stress is obtained from the experimental results during compression test.

For the present finite element analysis, isothermal condition is assumed. Direct iteration method and Newton-Raphson methods have been adopted for solving the non-linear equations. A good initial guess has generated for the Newton-Raphson method using the direct iteration method, for the speedy final convergence. When the plastic deformation reaches the steady state, the simulation is stopped.

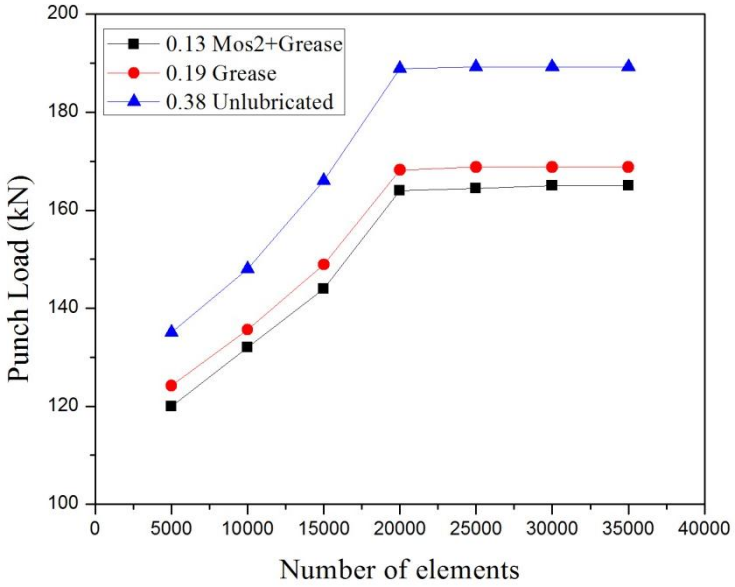

Figure 5.4: Grid independence test result

Table 5.2: Process parameters used in the simulation

Billet length	37, 42, 54 and 31mm
Billet diameter	15 mm
Billet temperature	Ambient (30^0C)
Punch Speeds	0.5, 1 and 2 mm/min
Friction factor	0.13, 0.19 and 0.38
Flow stress	132 MPa
No. of mesh element	20000
Average strain rate	1/s
Limiting strain rate	0.01/s
Poisson's ratio	0.333
Density	2.70×10^3kg/m^3
Elastic modulus	70.0GPa

The assumptions made in the simulation process are as follows:

(1) The material of die has taken as rigid

(2) Aluminium 1070 is taken as the billet in the simulation process and modelled using von Mises yield criterion for a isotropic rigid plastic material.

(3) The friction factor for the interface workpiece/die is considered as constant, which has found from ring test experimentally.

(4) The flow stress governing equations at different ram velocities are taken from equations 6.1 - 6.3 (obtained from experiments, described in section 6.6).

(4) The billet axis has incorporated with the centroid of the die orifice.

(5) Global re-meshing criterion and logarithmic interpolation.

For the present investigation two types of collet chuck holders manufactured by different ways are considered for the analysis. These are:

i) CEF process for single collar collet chuck holder.

ii) CEF process for double collar collet chuck holder.

iii) CE process for Double collar collet chuck holder.

iv) Multistage process for single collar collet chuck holder.

The previous literature studies showed that friction is a very important phenomenon which affects the forming load externally and grain structure internally. After extensive research on lubrication conditions, it was decided to conduct simulations with two different lubricants and also at unlubricated conditions. The lubrication conditions considered are:

i. Coefficient of friction (m = 0.13) which is a mixture of Molybdenum disulphide and Grease (60:40),

ii. Coefficient of friction (m = 0.19) which is obtained by 100% grease, and

iii. Coefficient of friction (m = 0.38) which is performed by the unlubricated condition.

For every friction condition three ram velocities are considered, these are:

i. 0.5 mm/min,

ii. 1.0 mm/min, and

iii. 2 mm/min.

5.3 Results and Discussions of the Simulations

5.3.1 CEF process for Single collar collet chuck holder

Using the methods outlined in section 5.2 numerical analysis is carried out to get the final product from the initial cylindrical billet of 15 mm diameter and 37 mm in length. Figure 5.5 shows the detail dimensions of the final product obtained by compressing the round billet inside a rigid container with required cavity by a rigid punch to demonstrate the process of combined extrusion/forging. The dies and punch plate used for simulation was same as that of experimental sets.

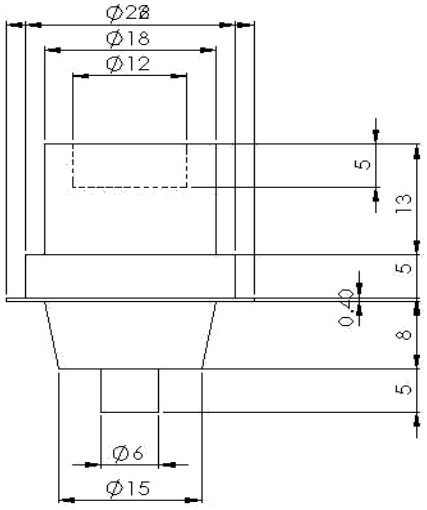

Figure 5.5: Single collar collet chuck holder

5.3.1.1 Extrusion/forging Load at different frictions and ram velocities

Figures 5.6 - 5.8 gives comparison of punch load with punch movement for different velocities using lubricant MoS_2 + grease (60:40) with friction factor 0.13, 100% grease and no lubrication respectively. The maximum extrusion/forging loads at flashing are provided in Table 5.3. The ram displacement behaviours show that the total process can be assumed to consist of four stages:

(i) Initial stage, the load gradually increases backward extrusion takes place,

(ii) second stage, forward and lateral extrusion takes place,

(iii) combined stage, both extrusion and forging takes place for corner filling,

(iv) the unsteady state stage, steep rise in load to form flash. As the metal flow are hindered, redundant work increases, subsequently the load increases unsteadily.

It is evident from the Table 5.3 that with increase of friction the load increases and also with ram velocity load requirements increases because of work hardening.

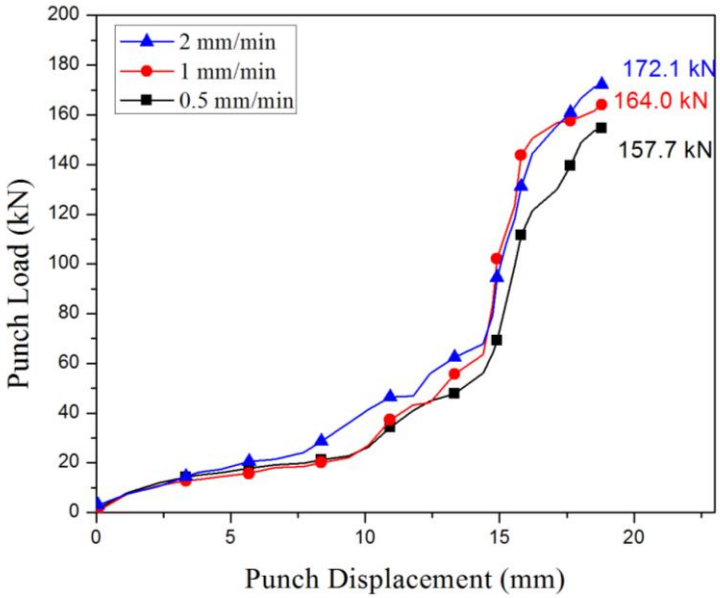

Figure 5.6: Variation of punch load with punch travel at friction factor of 0.13

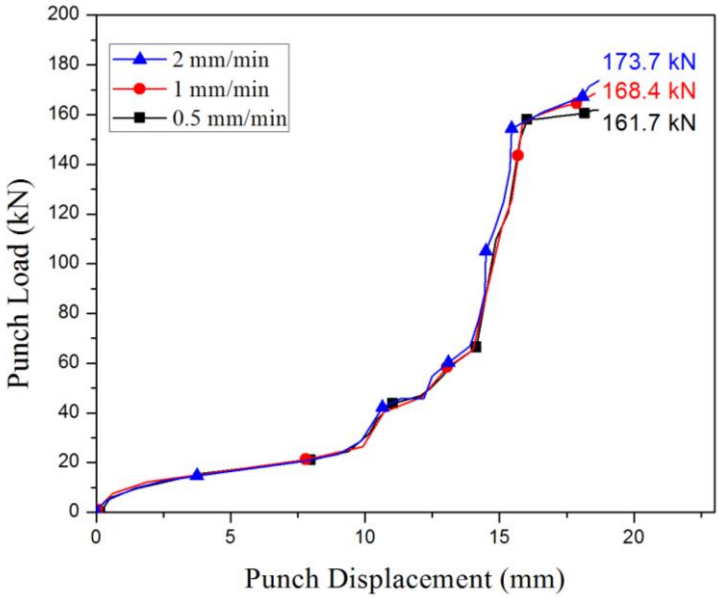

Figure 5.7: Variation of punch load with punch travel at friction factor of 0.19

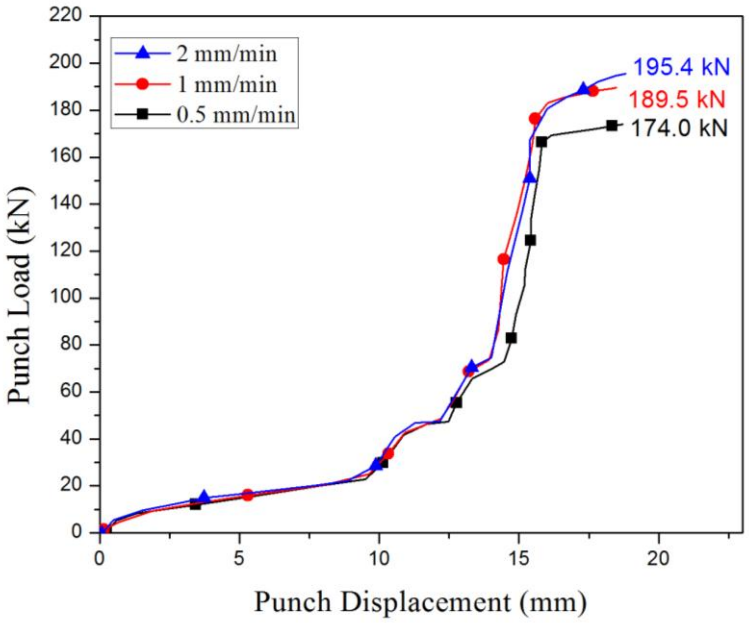

Figure 5.8: Variation of punch load with punch travel at friction factor of 0.38

Table 5.3: Forming load at different ram velocities and friction conditions

Sl. No.	Friction factor	Ram velocity, mm/min	Peak load at flashing, kN
1	0.13	0.5	157.70
2		1.0	164.00
3		2.0	172.10
4	0.19	0.5	161.70
5		1.0	168.40
6		2.0	173.70
7	0.38	0.5	174.00
8		1.0	189.50
9		2.0	195.4

5.3.1.2 Die filling

Figure 5.9 shows the progressive change in shape of extrusion-forged product at different punch movements when the friction factor is 0.13 and the ram speed is 0.5 mm/min (as an illustration). The die filling process substantiate that the total process can be thought of four stages as explained earlier, i.e., initial compression/coining stage backward extrusion takes place during (0 - 10.0 mm of ram movement), in second stage during (10.0 - 16.0 mm ram) travel lateral extrusion takes place to form collar, during third stage (16.0 - 18.0 mm ram travel) corner filling and forward extrusion takes place, and in last stage (18.0 - 18.3 mm ram travel) flash is formed to complete the process. It also explains that combined extrusion forging processes takes place simultaneously till the die cavity is completely filled, after which flash is started to form.

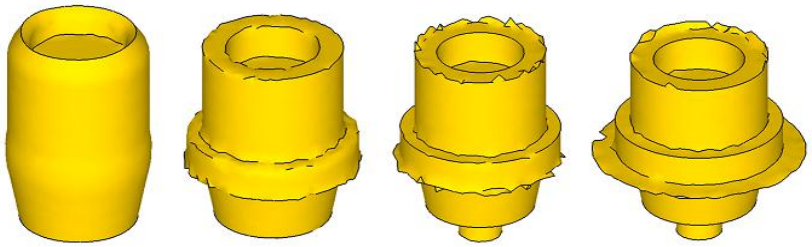

(a) Stage I **(b) Stage II** **(c) Stage III** **(d) Stage IV**

Figure 5.9: Die filling at different punch movement with 0.13 friction factor at 0.5 mm/min ram velocity

5.3.1.3 Metal flow pattern

Figures 5.10(a-c) show the contour of displacements in both the horizontal and axial direction after 10.0 mm, 16.0 mm, 18.0 mm and 18.3 mm ram displacements respectively at 0.5 mm/min ram velocity with varying frictional conditions. Similarly, Figures 5.11(a-c) shows the contour of displacements in both the horizontal and axial direction after 10.0 mm, 16.0 mm, 18.0 mm and 18.3 mm ram displacements respectively with varying ram velocities at 0.13 frictional condition. The degree of distortion of gridlines at different stages confirms the load~ram displacement behaviour. Severe grid distortion at flashing stage validates the maximum load due to maximum redundant work. It is also seen that the whole billet, rather than part close to punch, is deforming simultaneously in different directions. Also, there is a non-uniform grid distortion due to friction at die-billet interface.

Figure 5.10(c) shows the flow pattern at higher friction, giving more non-uniform grid distortion at die-billet interface. Figure 5.11(c) illustrates the flow pattern at higher ram velocity friction, indicating additional grid deformity, increasing work hardening.

a)

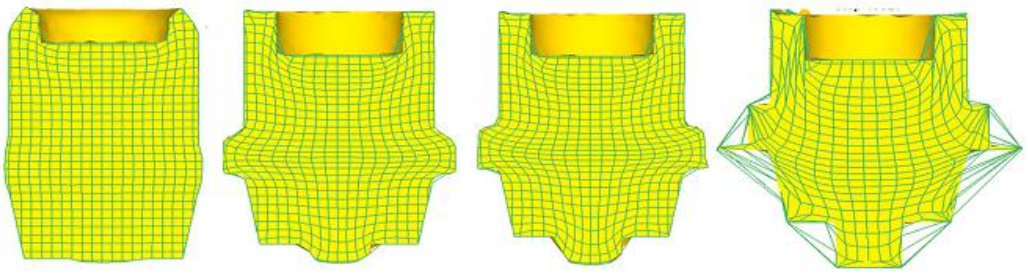

Component with 0.13 friction factor at 0.5 mm/min ram velocity

b)

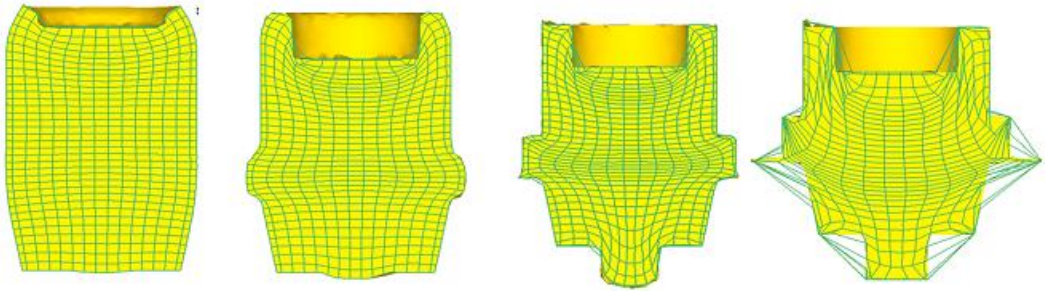

Component with 0.19 friction factor at 0.5 mm/min ram velocity

c)

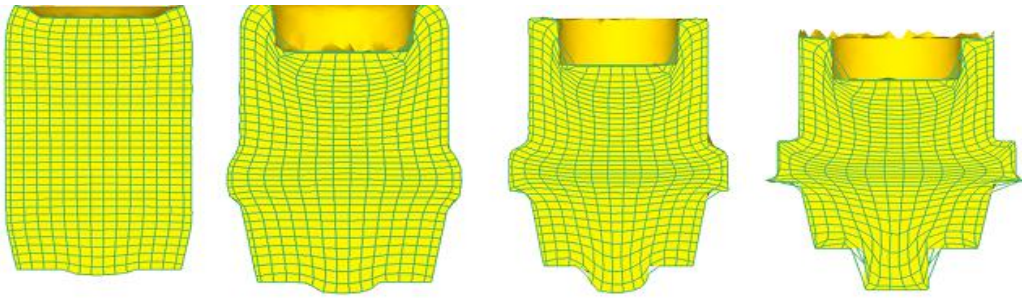

Component with 0.38 friction factor at 0.5 mm/min ram velocity

Stage I **Stage II** **Stage III** **Stage IV**

Figure 5.10: Flow pattern of SCCH with varying frictional condition with ram velocity 0.5 mm/min

a)

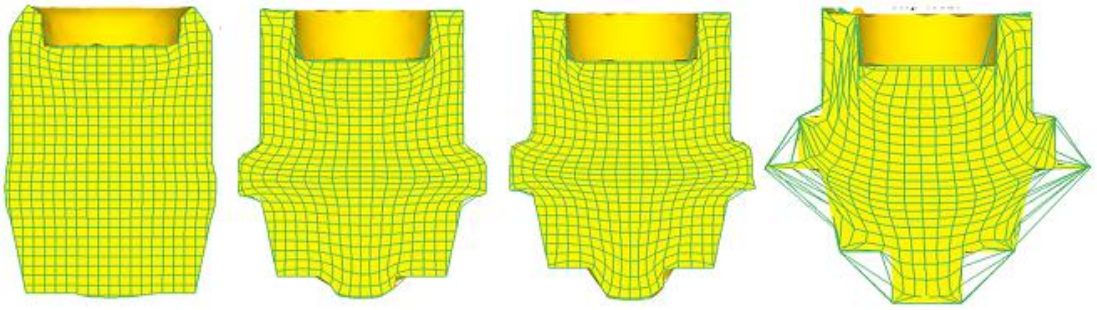

Component with 0.5 mm/min ram velocity at 0.13 friction factor

b)

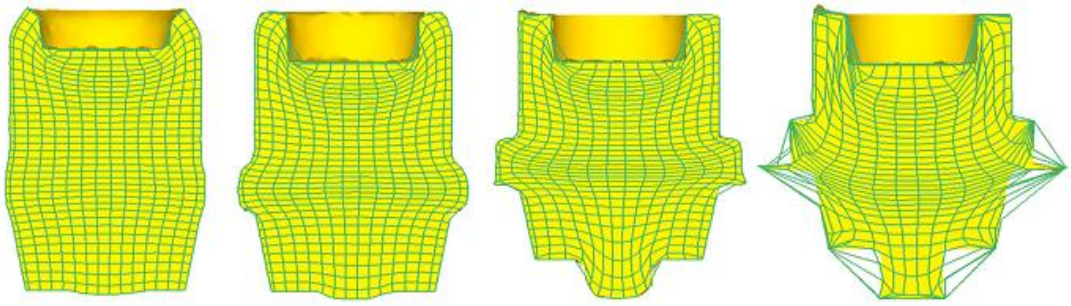

Component with 1 mm/min ram velocity at 0.13 friction factor

c)

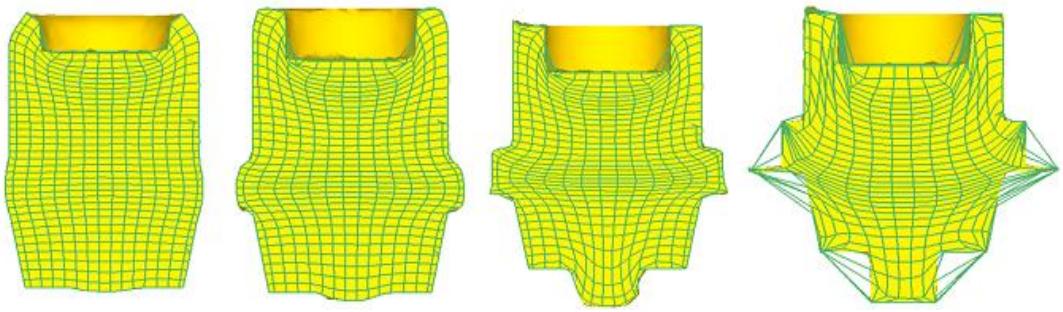

Component with 2 mm/min ram velocity at 0.13 friction factor

Stage I **Stage II** **Stage III** **Stage IV**

Figure 5.11: Flow pattern of SCCH with varying ram velocities at 0.13 frictional condition

5.3.1.4 Stress, strain and velocity pattern

Effective strain, effective stress and total velocity distributions of cross-sections for a billet at the end of CEF process for single collar collet chuck holder under the influence of different friction conditions (0.13, 0.19 and 0.38) at 0.5 mm/min punch velocity is shown in Figures 5.12(a-c) respectively. It can be seen that the effective strain is non-uniform. As the die geometries are same the effective strain distribution for Al 1070 are found to be same at 0.13, 0.38 and varying at 0.19 frictional conditions as shown in Figure 5.12(b). Maximum effective strain is found near the edges of punch and at the middle collar portion, where SVP (severe

plastic deformation) takes place. The increase in effective strain at the middle portion is due to the shear formation which takes place for the formation of collar rings, where the grains tends to change its metal flow direction. The effective stress distribution for the deformed billet is non-uniform and varies with different frictional conditions. It is found that the maximum effective stress is found at the optimum frictional case 0.19 as shown in Figure 5.12(b). The maximum effective stress is found at the edges of the punch and at the middle portion. The maximum values of effective stress are 115, 140 and 184 MPa for frictional condition 0.13, 0.19 and 0.38 respectively at 0.5 mm/min punch velocity. As the die geometries are same a notable variation has not been found in the total velocity for the considered condition as shown in Figures 5.12(a-c).

Effective strain, effective stress and total velocity distributions of cross-sections for a billet at the end of CEF process for single collar collet chuck holder under the influence of different punch velocities (0.5, 1 and 2 mm/min) at 0.13frictional condition is shown in Figures 5.13(a-c). The billet was processed under the influence of different punch velocities (0.5, 1 and 2 mm/min) at 0.13 frictional condition. It can be seen that the effective strain is non-uniform. As the die geometries are same the effective strain distribution for Al 1070 are found to be same at 0.5, 2 mm/min punch velocities and varying at 1 mm/min punch velocity as shown in Figure 5.13(b). Maximum effective strain is found near the edges of punch and at the middle portion, where SVP (severe plastic deformation) takes place. The increase in effective strain at the middle portion is due to the shear formation which takes place for the formation of collar rings, where the grains tends to change its metal flow direction. The effective stress distribution for the deformed billet is non-uniform and varies with different punch velocities. It is observed that the maximum effective stress increases with increase in punch velocity as shown in Figure 5.13(b). The maximum effective stress is found at the edges of the punch and at the middle portion, where the collar ring formation takes place. The maximum values of effective stress are 109, 115 and 168 MPa for punch velocities (0.5, 1 and 2 mm/min respectively) at 0.13 frictional condition. As the die geometries are same a notable variation was not found in the total velocity for the considered condition as shown in Figures 5.13(a-c).

a)

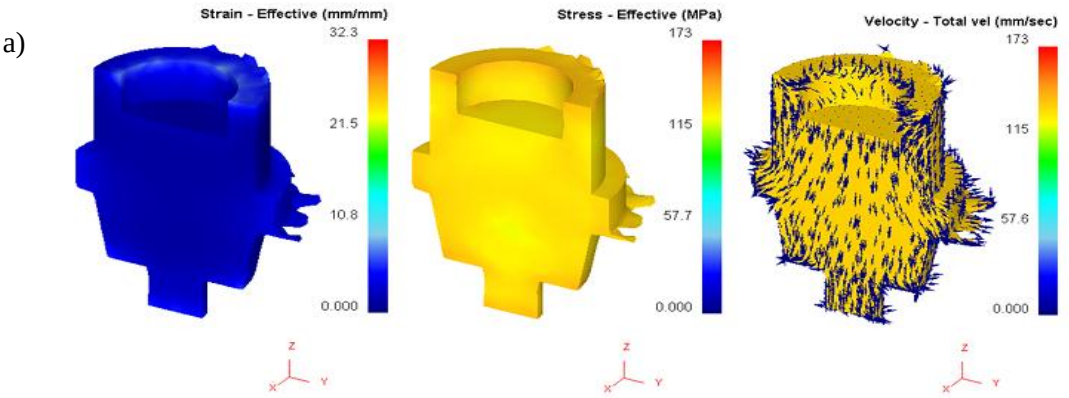

Component with 0.13 friction factor at 0.5 mm/min ram velocity

b)

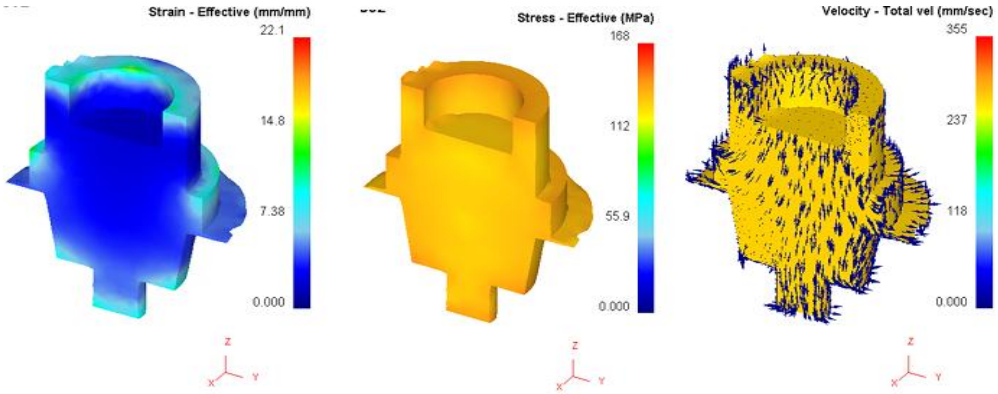

Component with 0.19 friction factor at 0.5 mm/min ram velocity

c)

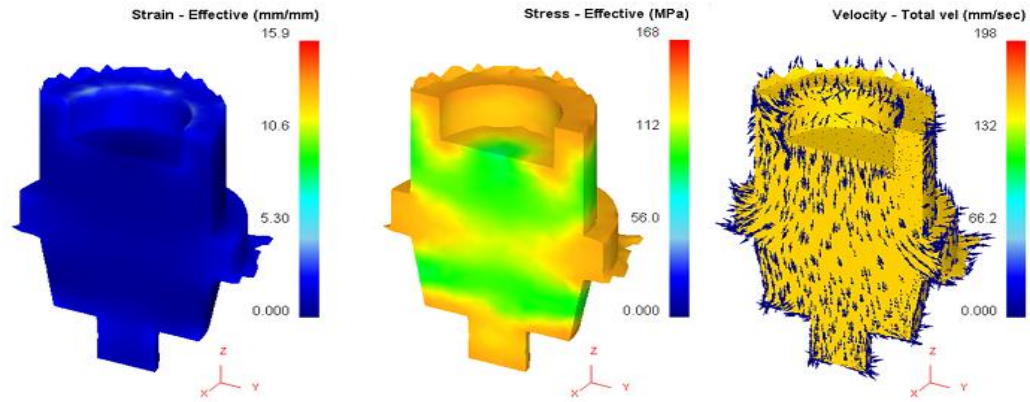

Component with 0.38 friction factor at 0.5 mm/min ram velocity

Effective strain **Effective stress** **Total Velocity**

Figure 5.12: Effective strain, effective stress and total velocity with varying friction factor at 0.5mm/min punch movement

a)

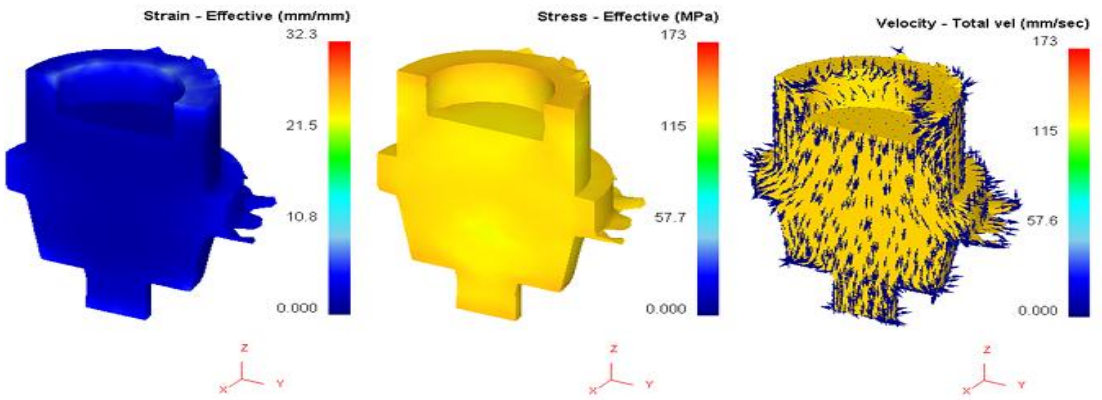

Component with 0.5 mm/min ram velocity at 0.13 friction factor

b)

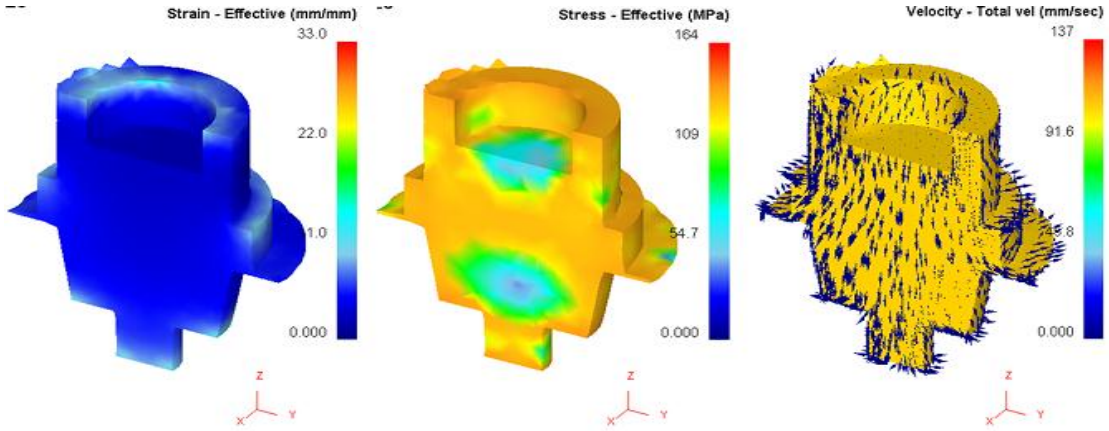

Component with 1 mm/min ram velocity at 0.13 friction factor

c)

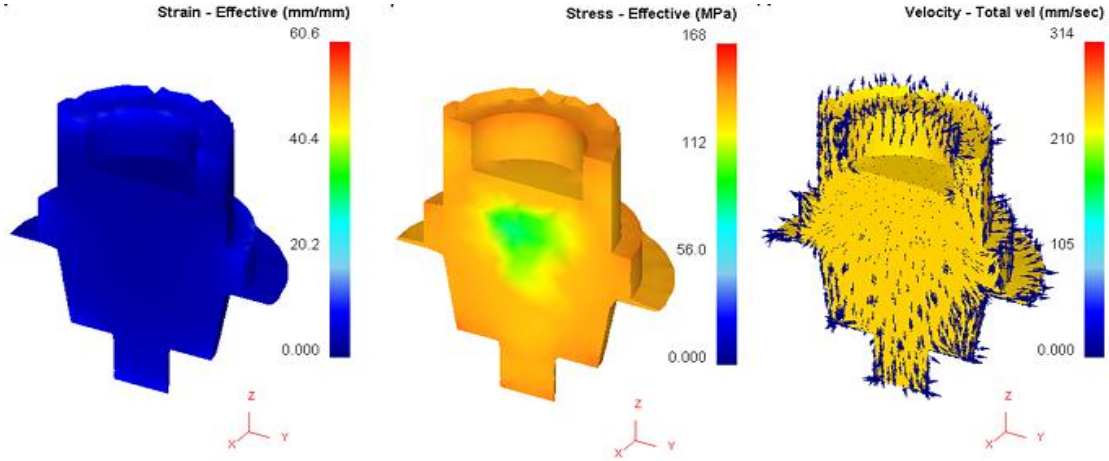

Component with 2 mm/min ram velocity at 0.13 friction factor

Effective strain **Effective stress** **Total Velocity**

Figure 5.13: Effective strain, effective stress and total velocity with 0.13 friction factor at varying punch movements

5.3.2 CEF process for double collar collet chuck holder

Using the methods outlined in section 5.2 numerical analysis of the process is carried out to get the final product from the initial cylindrical billet of 15 mm diameter and 53.3 mm in length. Figure 5.14 shows the detail dimensions of the final product obtained by compressing the round billet inside a rigid container with required cavity by a rigid punch to demonstrate the process of combined extrusion/forging. The dies and punch plate used for simulation was same as that of experimental sets.

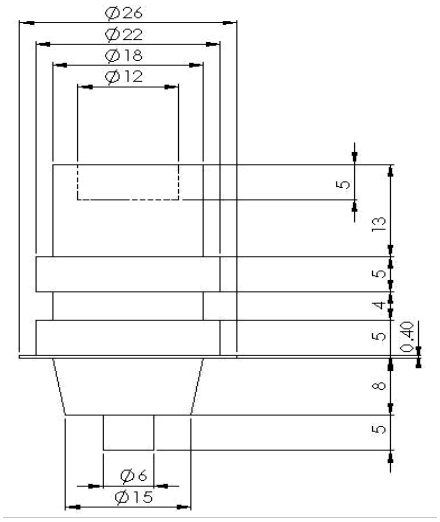

Figure 5.14: Double collar collet chuck holder

5.3.1.1 Extrusion/forging Load at different frictions and ram velocities

Figures 5.15-5.17 gives comparison of punch load with punch movement for different velocities using lubricant MoS_2 + grease (60:40) with friction factor 0.13, 100% grease and no lubrication respectively. The maximum extrusion/forging loads at flashing are provided in Table 5.3. The ram displacement behaviours show that the total process can be assumed to consist of four stages:

(i) Initial stage, the load gradually increases backward extrusion takes place,

(ii) second stage, forward and lateral extrusion takes place,

(iii) combined stage, both extrusion and forging takes place for corner filling,

(iv) the unsteady state stage, with a steep rise in load to form flash. As the metal flow are hindered, redundant work increases, subsequently the load increases unsteadily.

It is evident from the Table 5.4 that with increase of friction the load increases and also with ram velocity load requirements increases because of work hardening.

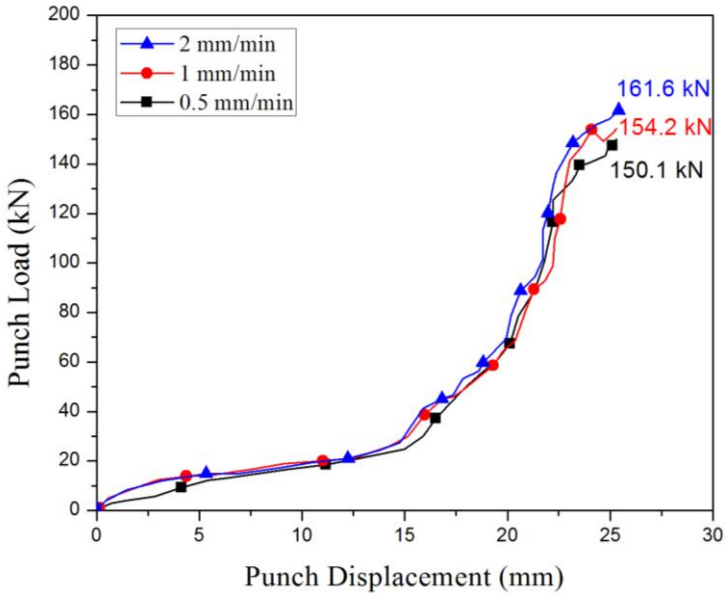

Figure 5.15: Variation of punch load with punch travel at friction factor of 0.13

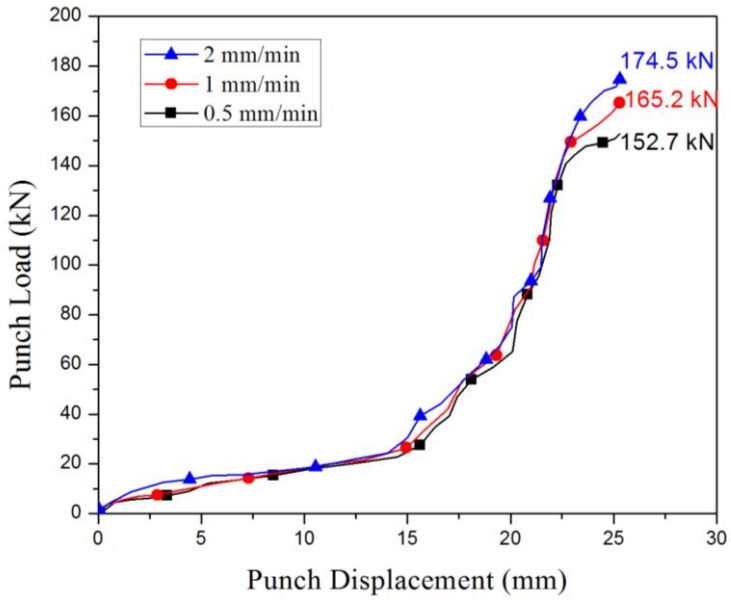

Figure 5.16: Variation of punch load with punch travel at friction factor of 0.19

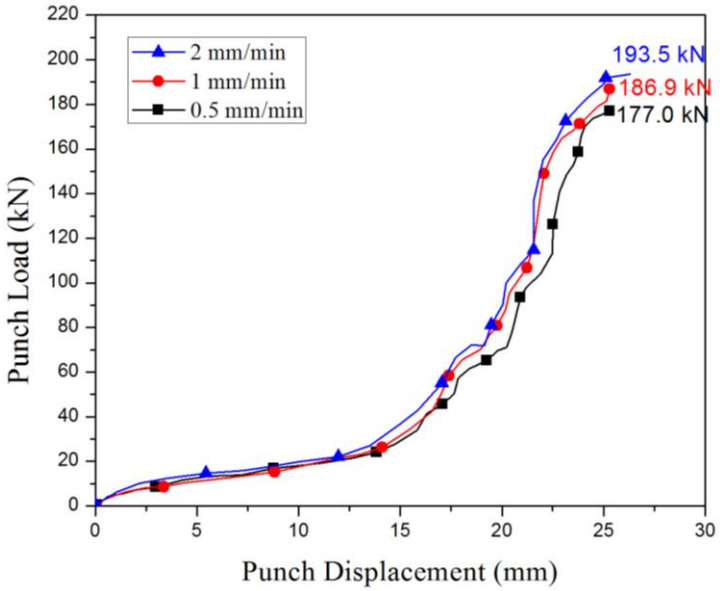

Figure 5.17: Variation of punch load with punch travel at friction factor of 0.38

Table 5.4: Forming load at different ram velocities and friction conditions

Sl. No.	Friction factor	Ram velocity, mm/min	Peak load at flashing, kN
1	0.13	0.5	150.1
2		1.0	154.2
3		2.0	161.6
4	0.19	0.5	152.7
5		1.0	165.2
6		2.0	174.5
7	0.38	0.5	177.0
8		1.0	186.9
9		2.0	193.5

5.3.2.2 Die filling

Figure 5.18 shows the progressive change in shape of extrusion-forged product at different punch movements when the friction factor is 0.19 and the ram speed is 1.0 mm/min. The die filling process substantiate that the total process can be thought of four stages as explained earlier, i.e., initial compression/coining stage backward extrusion takes place during 0-14.0 mm of ram movement, in the second stage during 14.0 - 23.0 mm ram travel lateral extrusion takes place to form collar, during third stage (23.0 - 24.5 mm ram travel) corner filling and forward extrusion takes place, and in last stage (24.5 - 25.3 mm ram travel) flash is formed to complete the process. . It also explains that combined extrusion forging processes takes place simultaneously till the die cavity is completely filled, after which flash is started to form.

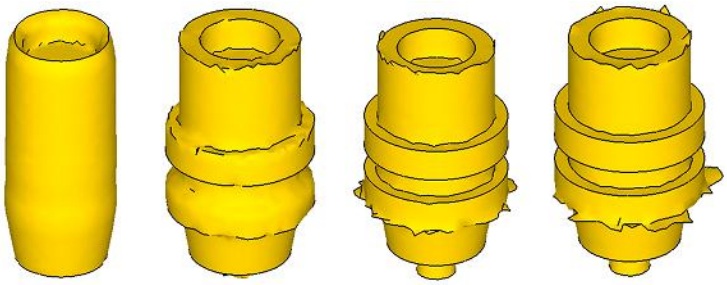

(a) Stage I **(b) Stage II** **(c) Stage III** **(d) Stage IV**

Figure 5.18: Die filling at different punch movement

5.3.2.3 Metal flow pattern

Figures 5.19(a-c) show the contour of displacements in both the horizontal and axial direction after 14.0 mm, 23.0 mm, 24.0 mm and 24.5 mm ram displacements respectively at 1 mm/min ram velocity with varying frictional conditions. Similarly, Figures 5.20(a-c) show the contour of displacements in both the horizontal and axial direction after 10.0 mm, 16.0 mm, 18.0 mm and 18.3 mm ram displacements respectively with varying ram velocities at 0.19 frictional condition. The degree of distorted gridlines at different stages confirms the load~ram displacement behaviour. Severe grid distortion at flashing stage validates the maximum load at this stage due to maximum redundant work. It is also seen that the whole billet, rather than part close to punch, is deforming simultaneously in different directions. It is also observed that, there is a non-uniform grid distortion due to friction at die-billet interface.

Figures 5.19(c) show the flow pattern at higher friction, giving more non-uniform grid distortion at die-billet interface. Figure 5.20(c) illustrates the flow pattern at higher ram velocity friction, indicating additional grid deformity, increasing work hardening.

a)

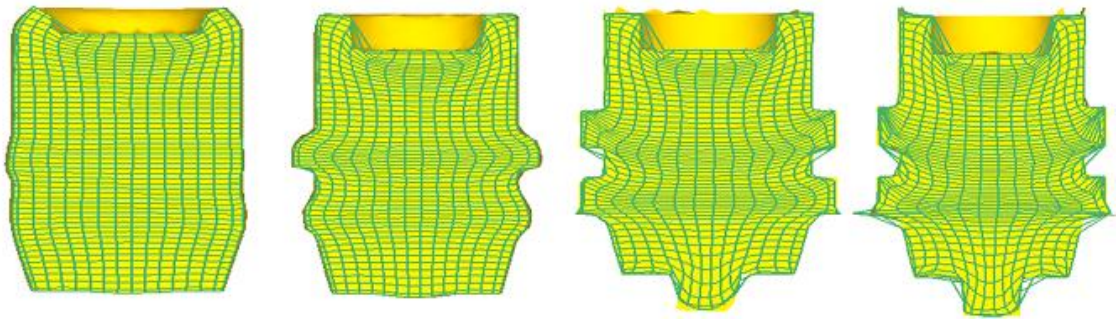

Component with 0.13 friction factor at 1 mm/min ram velocity

b)

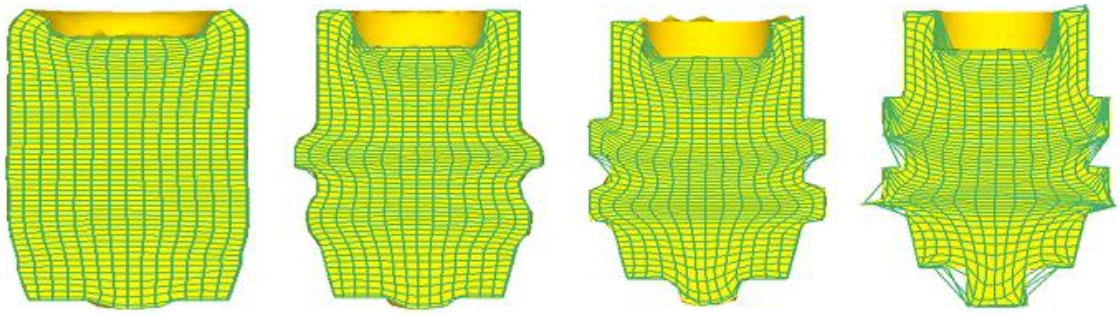

Component with 0.19 friction factor at 1 mm/min ram velocity

c)

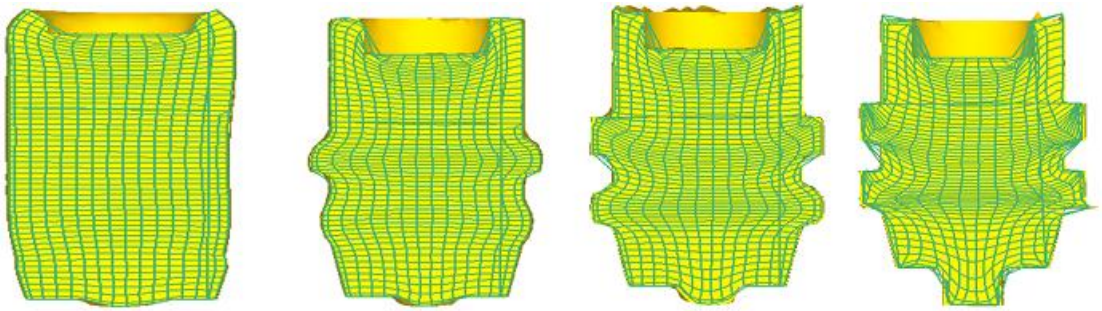

Component with 0.38 friction factor at 1 mm/min ram velocity

Stage I **Stage II** **Stage III** **Stage IV**

Figure 5.19: Flow pattern of DCCH with varying frictional condition with ram velocity 1 mm/min

a)

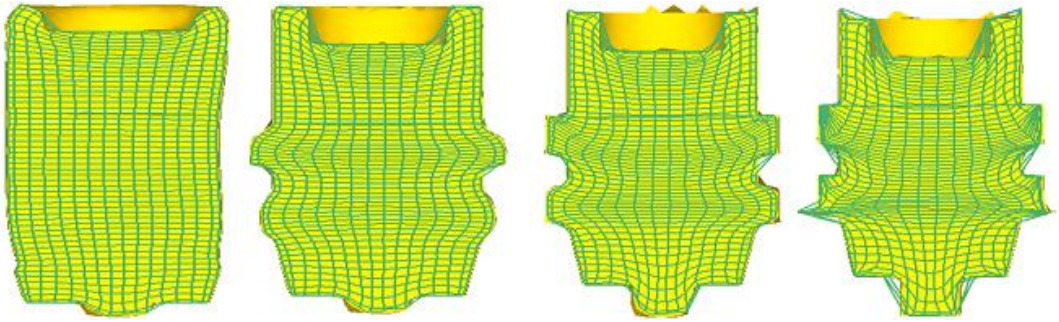

Component with 0.5 mm/min ram velocity at 0.19 friction factor

b)

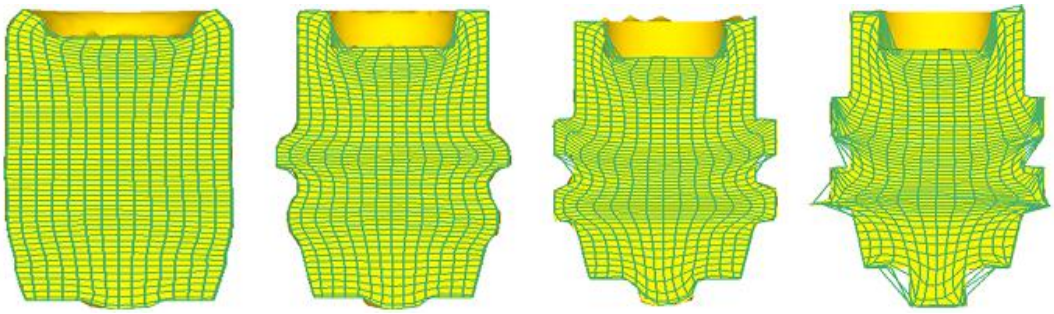

Component with 1 mm/min ram velocity at 0.19 friction factor

c)

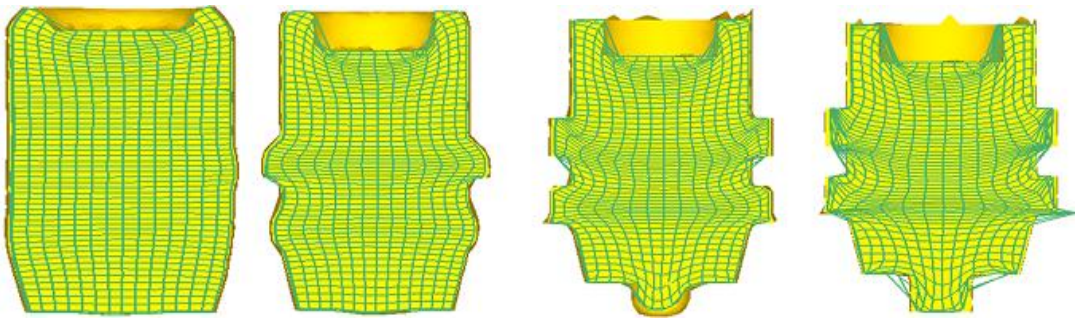

Component with 2 mm/min ram velocity at 0.19 friction factor

Stage I **Stage II** **Stage III** **Stage IV**

Figure 5.20: Flow pattern of DCCH with varying ram velocities at 0.19 frictional condition

5.3.2.4 Stress, strain and velocity pattern

Effective strain, effective stress and total velocity distributions of cross-sections for a DCCCH component/billet is shown at the end of the CEF process. The component was obtained under the influence of different friction conditions (0.13, 0.19 and 0.38) at 1 mm/min punch velocity is shown in Figures 5.21(a-c). It can be seen that the effective strain is non-uniform. As the die geometries are same the effective strain distribution for Al 1070 are found to be same at 0.13, 0.19 and varying at 0.38 frictional conditions as shown in Figure 5.21(c). Maximum effective strain is found near the edges of punch and at the two

collars portion, where SVP (severe plastic deformation) takes place. The increase in effective strain at the middle portion is due to the shear formation which takes place for the formation of collar rings, where the grains tends to change its metal flow direction. The effective stress distribution for the deformed billet is non-uniform and varies with different frictional conditions. It is found that the maximum effective stress is found at the optimum frictional case 0.38 as shown in Figure 5.21(c). The maximum effective stress is found at the edges of the punch and at the middle portion. The maximum values of effective stress are 83.2, 112 and 187.5 MPa for frictional condition 0.13, 0.19 and 0.38 respectively at 1 mm/min punch velocity. As the die geometries are same a notable variation was not found in the total velocity for the considered condition as shown in Figures 5.21(a-c).

Effective strain, effective stress and total velocity distributions of cross-sections for a billet at the end of CEF process for obtaining a double collar collet chuck holder under the influence of different punch velocities (0.5, 1 and 2 mm/min) at 0.19 frictional condition is shown in Figures 5.22(a-c). It can be seen that the effective strain is non-uniform. As the die geometries are similar, the effective strain distribution for Al 1070 are found to be same at 0.5, 1 mm/min punch velocities and varying at 2 mm/min punch velocity as shown in Figure 5.22(c). Maximum effective strain is found near the edges of punch and at the middle portion, where SVP (severe plastic deformation) takes place. The increase in effective strain at the middle portion is due to the shear formation which takes place for the formation of collar rings, where the grains tends to change its metal flow direction. The effective stress distribution for the deformed billet is non-uniform and varies with different punch velocities. It is observed that the maximum effective stress increases with increase in punch velocity as shown in Figure 5.22(c). The maximum effective stress is found at the edges of the punch and at the middle portion, where the collar ring formation takes place. The maximum values of effective stress are 131, 135 and 139 MPa for punch velocities (0.5, 1 and 2 mm/min respectively) at 0.19 frictional condition. As the die geometries are same a notable variation was not found in the total velocity for the considered condition as shown in Figures 5.22(a-c).

a)

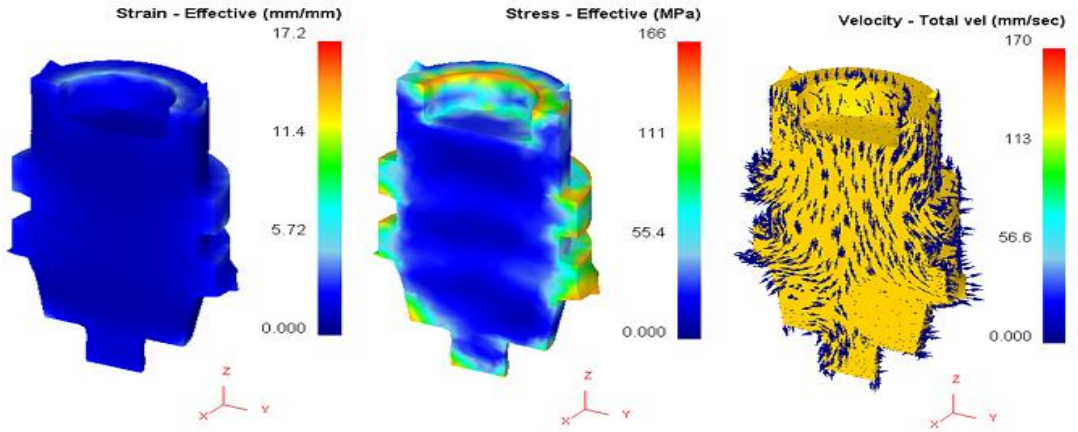

Component with 0.13 friction factor at 1 mm/min ram velocity

b)

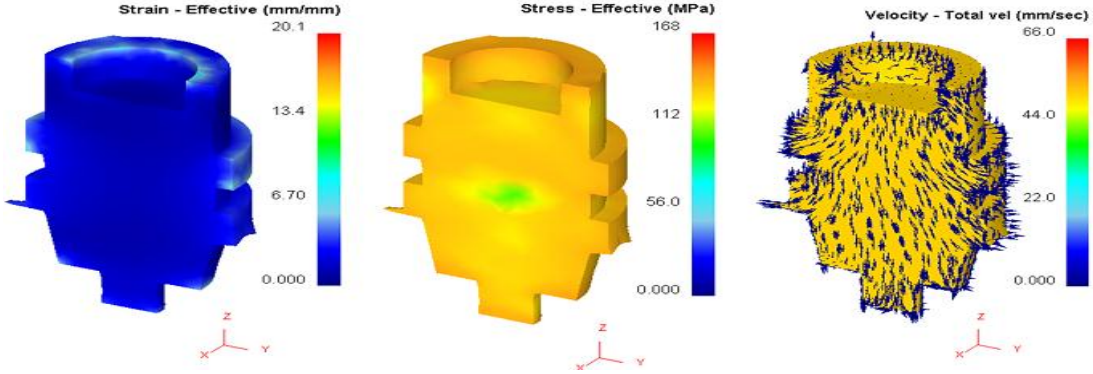

Component with 0.19 friction factor at 1 mm/min ram velocity

c)

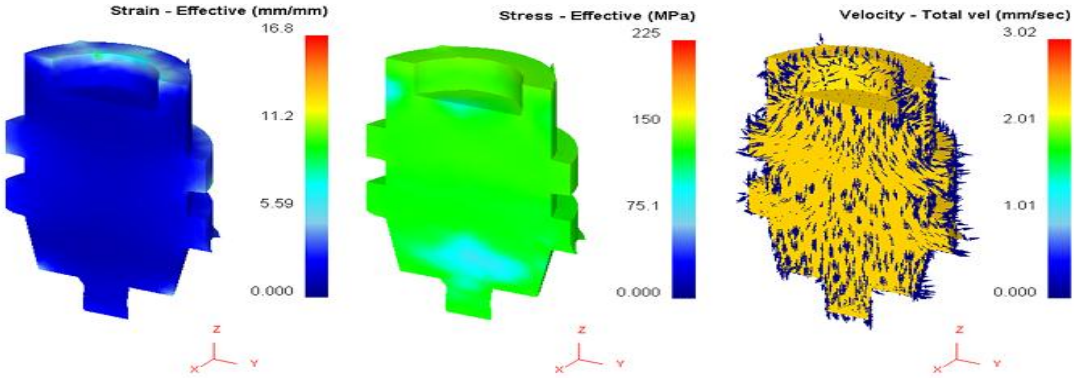

Component with 0.38 friction factor at 1 mm/min ram velocity

Effective strain **Effective stress** **Total velocity**

Figure 5.21: Effective strain, effective stress and total velocity of DCCH with varying frictional condition with ram velocity 1 mm/min

a)

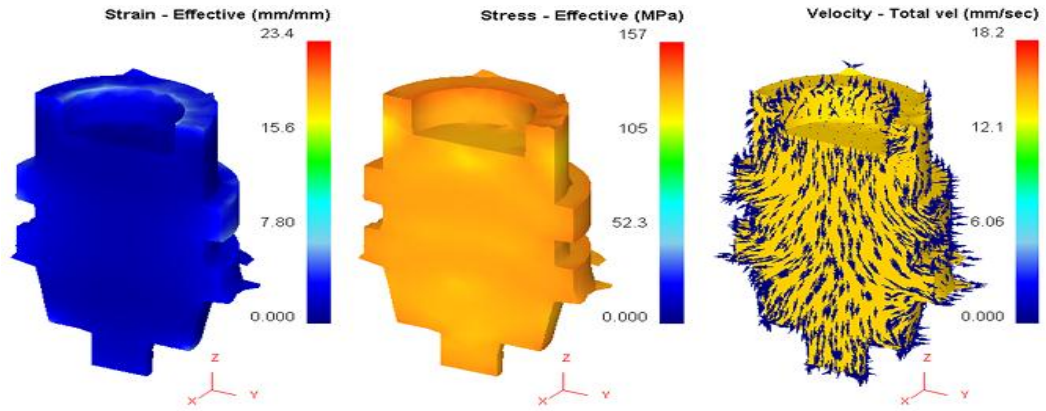

Component with 0.5 mm/min ram velocity at 0.19 friction factor

b)

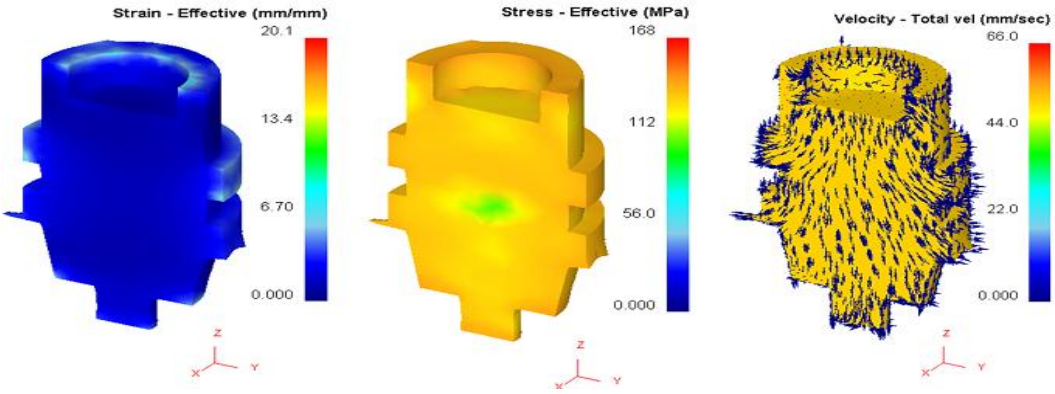

Component with 1 mm/min ram velocity at 0.19 friction factor

c)

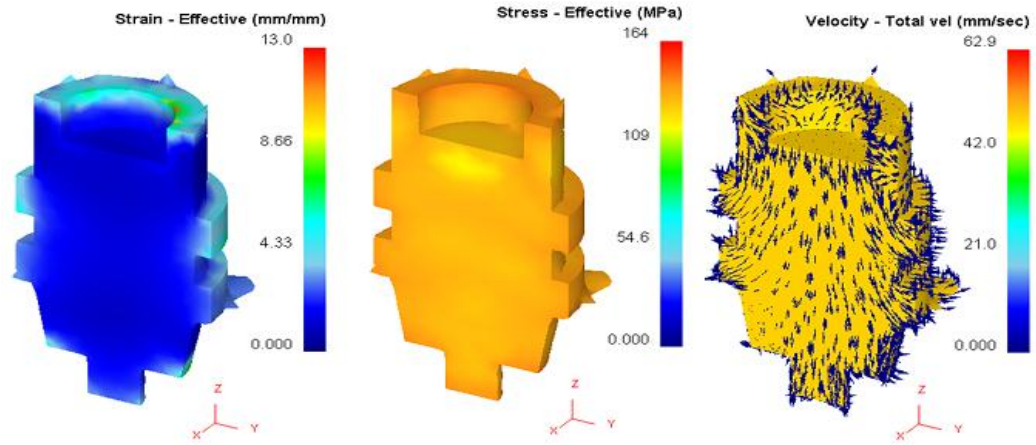

Component with 2 mm/min ram velocity at 0.19 friction factor

Effective strain **Effective stress** **Total velocity**

Figure 5.22: Effective strain, effective stress and total velocity of DCCH with varying ram velocities at 0.19 frictional conditions

5.3.3 CE process for Double collar collet chuck holder

Using the methods outlined in section 5.2 numerical analysis of the process is carried out to get the final product from the initial cylindrical billet of 15 mm diameter and 41.77mm in length. Figure 5.23 shows the detail dimensions of the final product obtained by compressing the round billet inside a rigid container with required cavity by a rigid punch to demonstrate the process of combined extrusion/forging. The dies and punch plate used for simulation was same as that of experimental sets. Flash provision is not engraved on the die as the end part is kept open for direct extrusion.

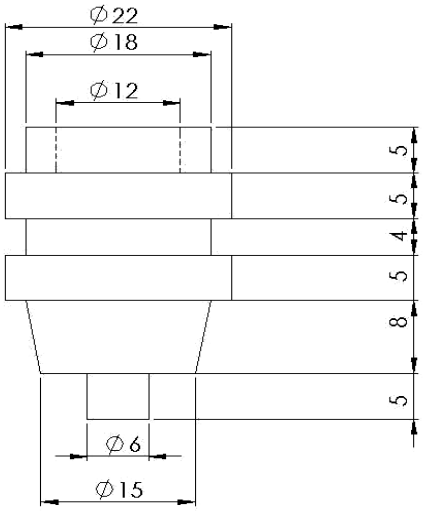

Figure 5.23: Double collar collet chuck holder

5.3.3.1 Extrusion/forging load at different frictions and ram velocities

Figures 5.24 - 5.26 gives comparison of punch load with punch movement for different velocities using lubricant MoS_2 + grease (60:40) with friction factor 0.13, 100% grease and no lubrication respectively. The maximum extrusion/forging loads at flashing are provided in Table 5.3. The ram displacement behaviours show that the total process can be assumed to consist of four stages:

(i) Initial stage, the load gradually increases backward extrusion takes place,

(ii) second stage, forward and lateral extrusion takes place,

(iii) combined stage, both extrusion and forging takes place for corner filling,

(iv) forward extrusion takes place.

It is evident from Table 5.5 that with increase of friction the load increases and also with ram velocity load requirements increases because of work hardening.

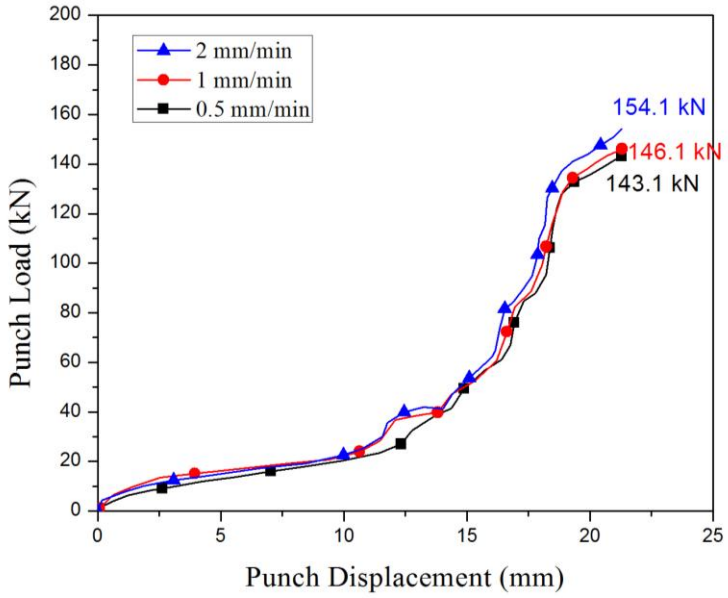

Figure 5.24: Variation of punch load with punch travel at friction factor of 0.13

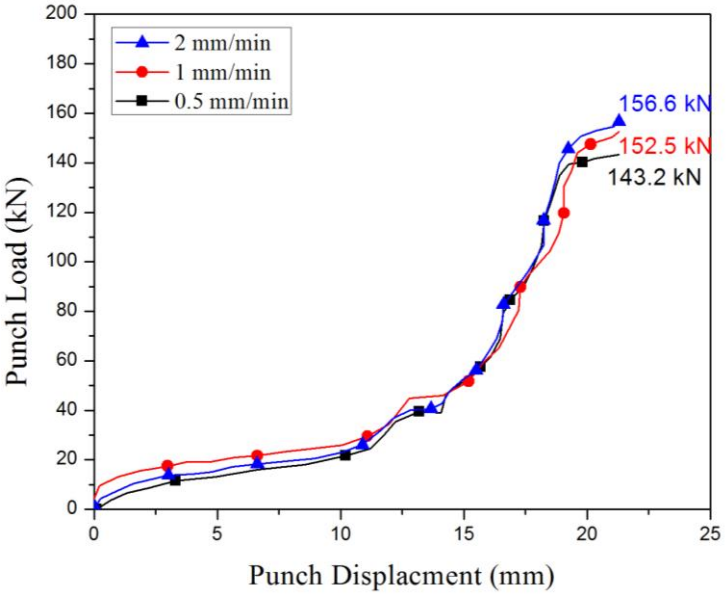

Figure 5.25: Variation of punch load with punch travel at friction factor of 0.19

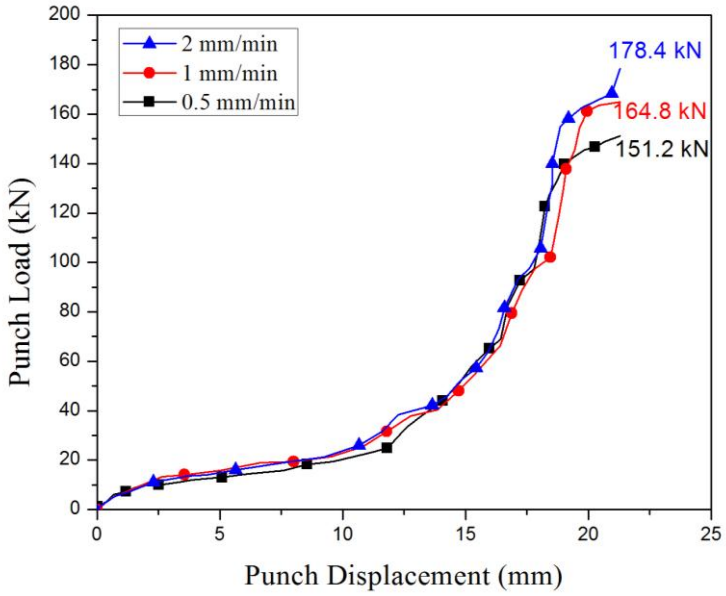

Figure 5.26: Variation of punch load with punch travel at friction factor of 0.38

Table 5.5: Forming load at different ram velocities and friction conditions

Sl. No.	Friction factor	Ram velocity, mm/min	Peak load at flashing, kN
1	0.13	0.5	143.1
2		1.0	146.1
3		2.0	154.6
4	0.19	0.5	143.2
5		1.0	152.5
6		2.0	156.6
7	0.38	0.5	151.2
8		1.0	164.8
9		2.0	178.4

5.3.3.2 Die filling

Figure 5.27 shows the progressive change in shape of extrusion-forged product at different punch movements when the friction factor is 0.38 and the ram speed is 2.0 mm/min. The die filling process substantiate that the total process can be thought of four stages as explained earlier, i.e., initial compression/coining stage backward extrusion takes place during 0-12.0 mm of ram movement, in second stage during 12.0 - 20.0 mm ram travel lateral extrusion takes place to form collar, during third stage (20.0 - 21.0 mm ram travel) corner filling and forward extrusion takes place, and in last stage (21.0 - 21.4 mm ram travel) only direct extrusion takes place to complete the process. It also explains that combined extrusion forging processes takes place simultaneously till the die cavity is completely filled, after which the metal flows outward through the exit present at the bottom die, confirming prior corner filling.

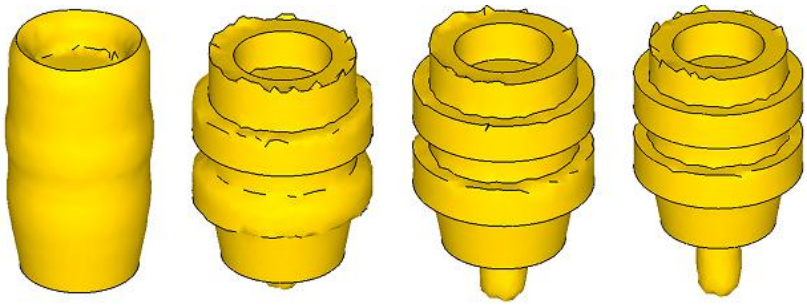

(a) Stage I **(b) Stage II** **(c) Stage III** **(d) Stage IV**

Figure 5.27: Die filling at different punch movement

5.3.3.3 Metal flow pattern

Figures 5.28(a-c) shows the contour of displacements in both the horizontal and axial direction after 12.0 mm, 20.0 mm, 21.0 mm and 21.4 mm ram displacements respectively at 2 mm/min ram velocity with varying frictional conditions. Similarly, Figures 5.29(a-c) shows the contour of displacements in both the horizontal and axial direction after 12.0 mm, 20.0 mm, 21.0 mm and 21.4 mm ram displacements respectively with varying ram velocities at 0.38 frictional condition. The degree of distorted gridlines at different stages confirms the load~ram displacement behaviour. Severe grid distortions were also found during corner filling stage, which increases redundant work. It is also seen that the whole billet, rather than part close to punch, is deforming simultaneously in different directions. It is also observed that, there is a non-uniform grid distortion due to friction at die-billet interface. Figures 5.28(c) shows the flow pattern at higher friction, giving more non-uniform grid distortion at die-billet interface. Figure 5.29(c) illustrates the flow pattern at higher ram velocity friction, indicating additional grid deformity, increasing work hardening.

a)

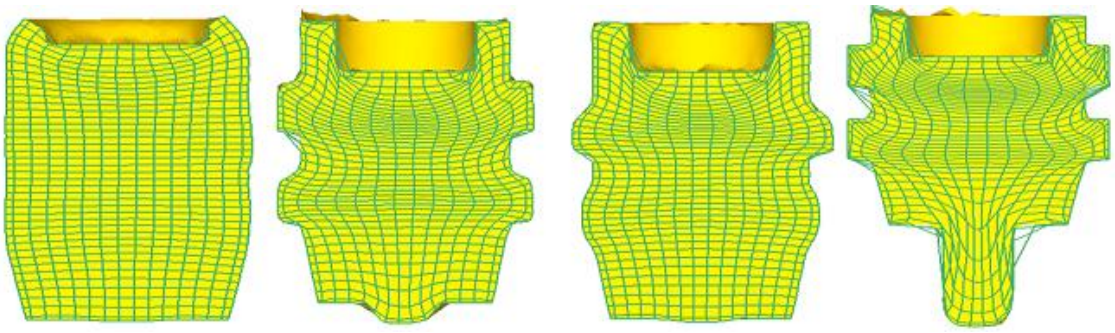

Component with 0.13 friction factor at 2 mm/min ram velocity

b)

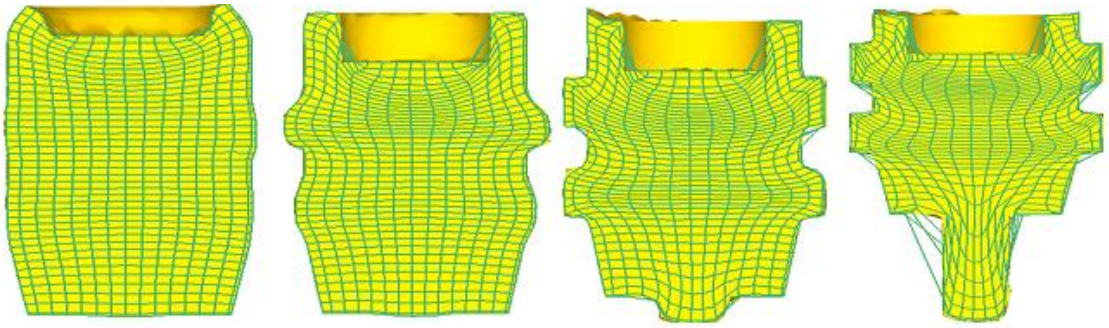

Component with 0.19 friction factor at 2 mm/min ram velocity

c)

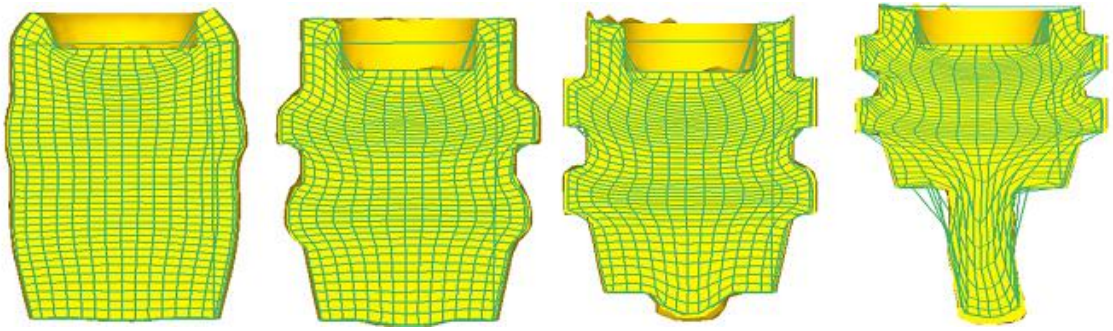

Component with 0.38 friction factor at 2 mm/min ram velocity

Stage I **Stage II** **Stage III** **Stage IV**

Figure 5.28: Flow pattern of DCCH by CE process with varying frictional condition with ram velocity 2 mm/min

a)

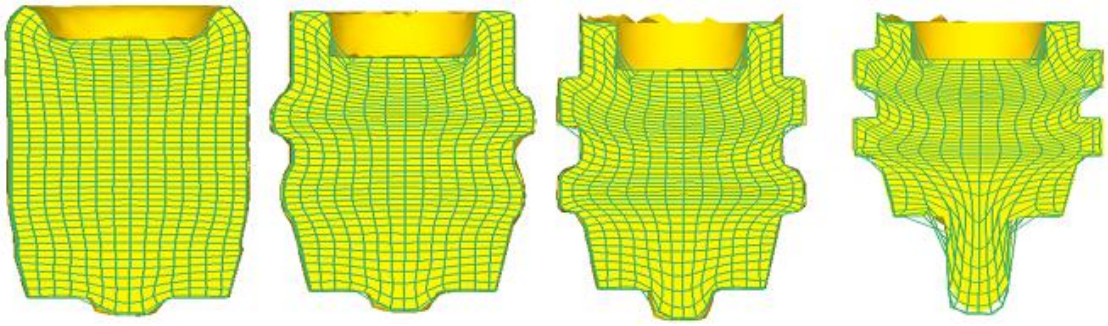

Component with 0.5 mm/min ram velocity at 0.38 friction factor

b)

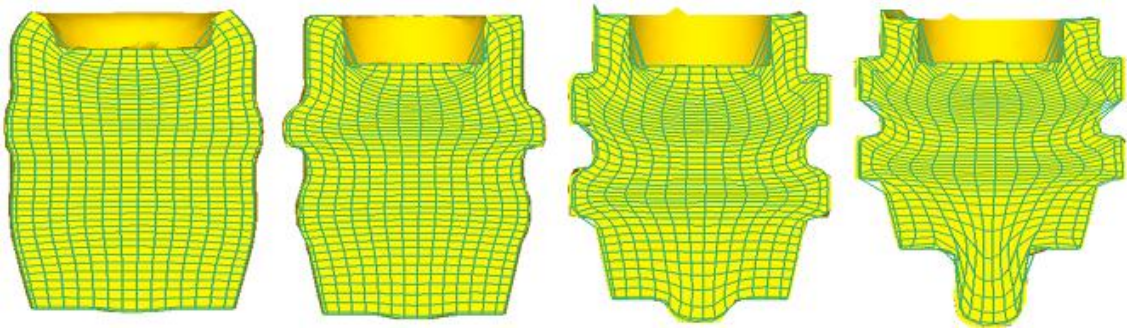

Component with 1 mm/min ram velocity at 0.38 friction factor

c)

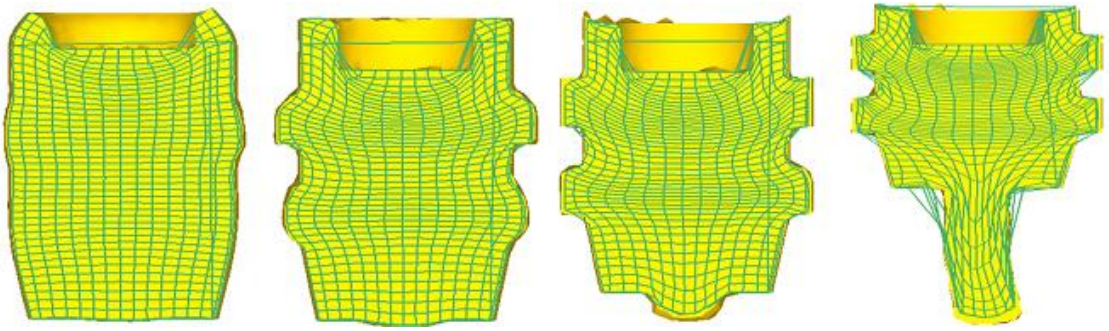

Component with 2 mm/min ram velocity at 0.38 friction factor

Stage I **Stage II** **Stage III** **Stage IV**

Figure 5.29: Flow pattern of DCCH by CE process with varying ram velocities at 0.38 frictional condition

5.3.3.4 Stress, strain and velocity pattern

Effective strain, effective stress and total velocity distributions of cross-sections for a billet at the end of CE process for obtaining a double collar collet chuck holder as shown in Figure 5.30(a-c). The billet was processed under the influence of different friction conditions (0.13, 0.19 and 0.38). It can be seen that the effective strain is non-uniform. As the die geometries are same the effective strain distribution for Al 1070 are found to be same at 0.13, 0.19 and varying at 0.38 frictional conditions as shown in Figure 5.30(c). Maximum effective strain is

found near the edges of punch and at the middle portion, where SVP (severe plastic deformation) takes place. The increase in effective strain at the middle portion is due to the shear formation which takes place for the formation of collar rings, where the grains tends to change its metal flow direction. The effective stress distribution for the deformed billet is non-uniform and varies with different frictional conditions. It is found that the maximum effective stress is found at the higher frictional case 0.38 as shown in Figure 5.30(c). The maximum effective stress is found at the edges of the punch and at the middle portion. The maximum values of effective stress are 109, 140 and 166 MPa for frictional condition 0.13, 0.19 and 0.38 respectively at 2 mm/min punch velocity. As the die geometries are same a notable variation was not found in the total velocity for the considered condition as shown in Figures 5.30(a-c).

Effective strain, effective stress and total velocity distributions of cross-sections of the billet at the end of CE process for double collar collet chuck holder under the influence of different punch velocities (0.5, 1 and 2 mm/min respectively) at 0.38 frictional condition is shown in Figures 5.31(a-c). It can be seen that the effective strain is non-uniform. As the die geometries are same the effective strain distribution for Al 1070 are found to be same at 0.5, 1 mm/min punch velocities and varying at 2 mm/min punch velocity as shown in Figure 5.31(c). Maximum effective strain is found near the edges of punch and at the colar portion, where SVP (severe plastic deformation) takes place. The increase in effective strain at the middle portion is due to the shear formation which takes place for the formation of collar rings, where the grains tends to change its metal flow direction. The effective stress distribution for the deformed billet is non-uniform and varies with different punch velocities. It is observed that the maximum effective stress increases with increase in punch velocity as shown in Figure 5.31(c). The maximum effective stress is found at the edges of the punch and at the middle portion, where the collar ring formation takes place. The maximum values of effective stress are 108, 115 and 140 MPa for punch velocities (0.5, 1 and 2 mm/min respectively) at 0.19 frictional condition. As the die geometries are same a notable variation was not found in the total velocity for the considered condition as shown in Figures 5.31(a-c).

a)

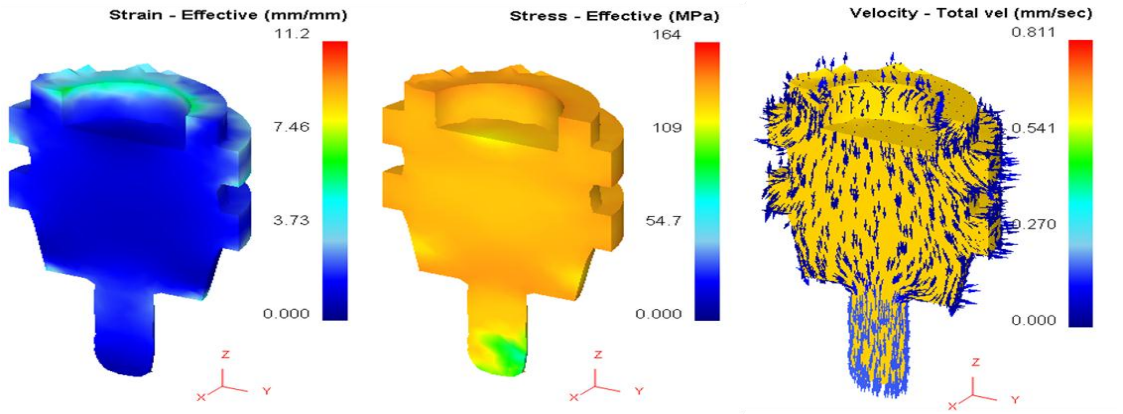

Component with 0.13 friction factor at 2 mm/min ram velocity

b)

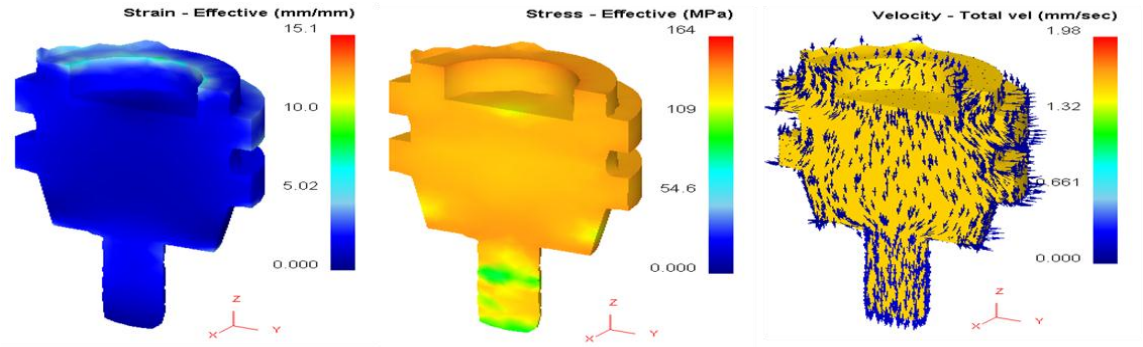

Component with 0.19 friction factor at 2 mm/min ram velocity

c)

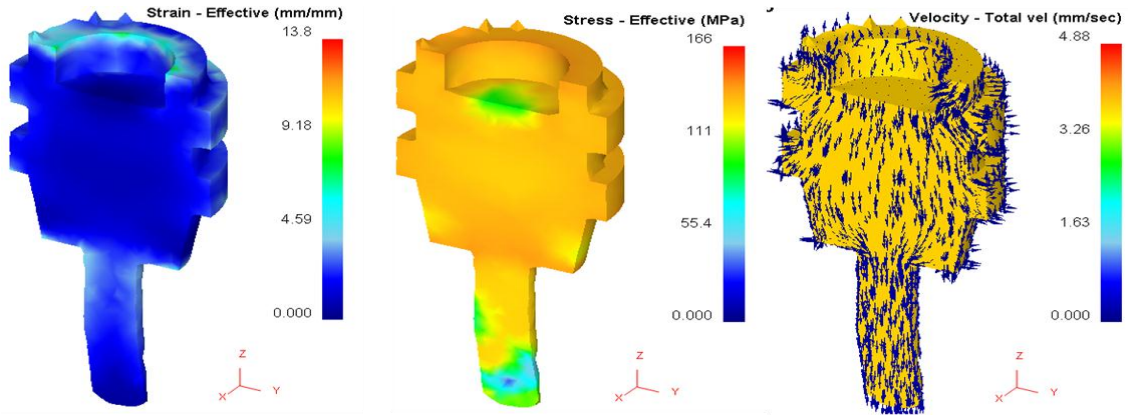

Component with 0.38 friction factor at 2 mm/min ram velocity

Effective strain **Effective stress** **Total velocity**

Figure 5.30: Effective strain, effective stress and total velocity DCCH by CE process with varying frictional condition with ram velocity 2 mm/min

a)

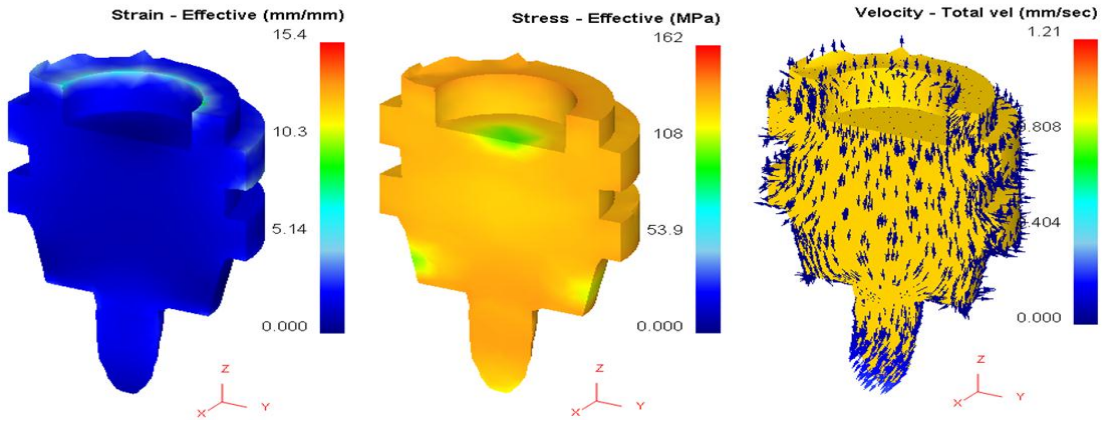

Component with 0.5 mm/min ram velocity at 0.38 friction factor

b)

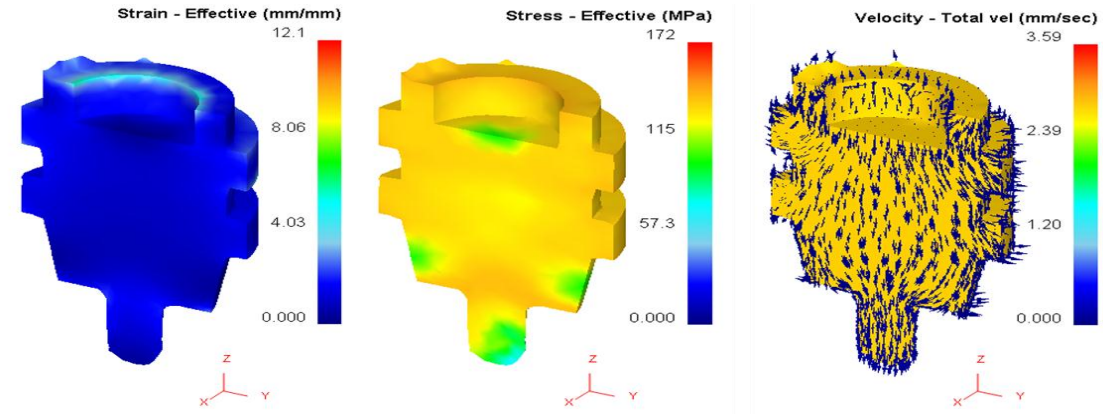

Component with 1 mm/min ram velocity at 0.38 friction factor

c)

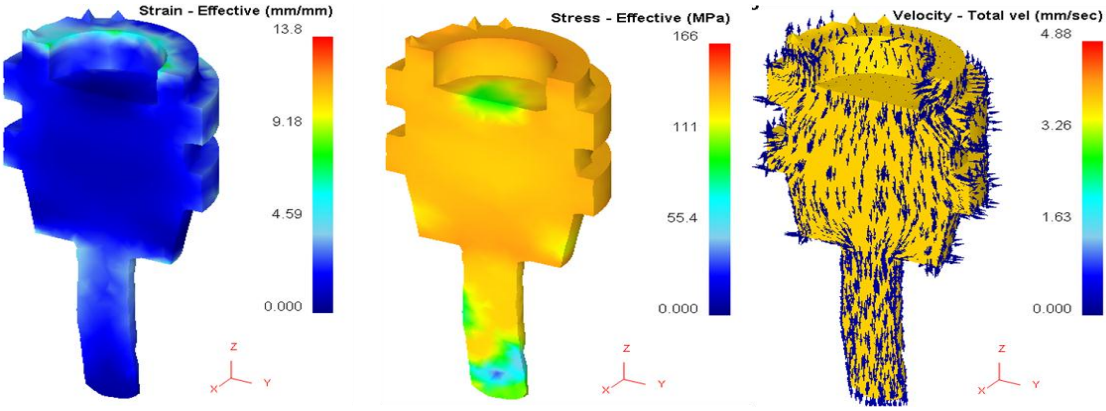

Component with 2 mm/min ram velocity at 0.38 friction factor

Effective strain **Effective stress** **Total velocity**

Figure 5.31: Effective strain, effective stress and total velocity DCCH by CE process with varying ram velocities at 0.38 frictional condition

5.3.4 Multistage extrusion of single collar collet chuck holder

Using the methods outlined in section 5.2 numerical analysis of the process is carried out to get the final product shape from the initial shape of the first product (Figure 5.5, not from cylindrical billet) obtained by CEF process as described in section 5.3.1. Figure 5.32 shows the detail dimensions of the final product obtained by compressing the first product inside a rigid container with required cavity by a rigid punch to demonstrate the multistage process of combined extrusion/forging. The dies and punch plate used for simulation was same as that of experimental sets.

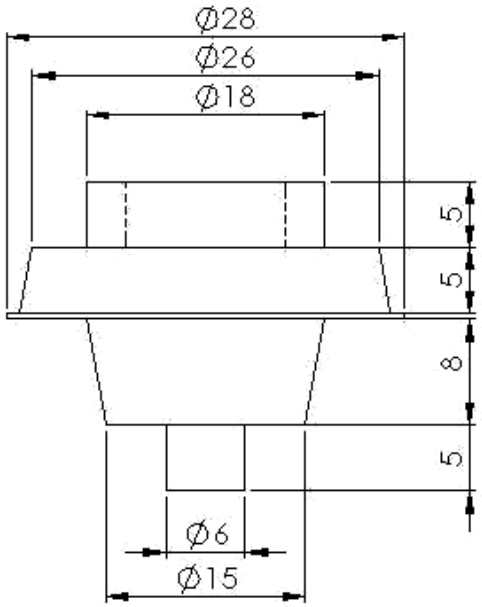

Figure 5.32: Multistage single collar collet chuck holder

5.3.4.1 Extrusion/forging Load

The present experimental analysis is an approach by multistage extrusion process to manufacture a single collar collet chuck holder. The concept deals with the use of multi-stage combined extrusion-forging technique for processing a component without defects. Figure 5.33 gives the load with punch movement at 1 mm/min ram velocity using grease as lubricant (with friction factor 0.19). The maximum extrusion/forging load at flashing is observed.

The ram displacement behaviours show that the total process can be assumed to consist of two stages:

(i) Initial compression stage with cavity filling by forward, bacward and lateral extrusion,

(ii) Second stage, to form flash.

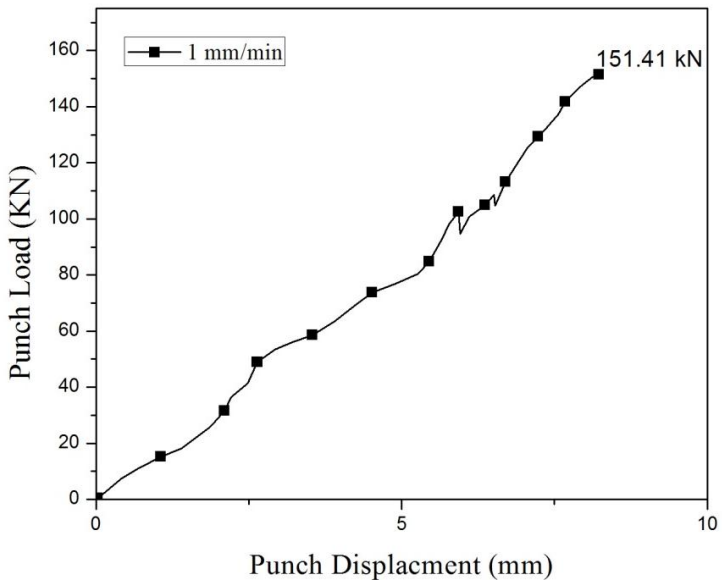

Figure 5.33: Variation of punch load with punch travel at friction factor of 0.13

5.3.4.2 Die filling

Figure 5.34 shows the progressive change in shape of extrusion-forged product at different punch movement when friction factor is 0.19 and ram speed of 1.0 mm/min. The die filling process substantiate that the total process can be thought of consisting of two stages as explained earlier, i.e., initial compression/coining stage with cavity filling by forward, bacward and lateral extrusion, which takes place during 0 - 6.0 mm of ram movement. During 6.0 - 8.2 mm ram travel corner filling with flash is formed to complete the process. It also explains that combined extrusion forging processes takes place simultaneously till the die cavity is completely filled, after which flash is started to form.

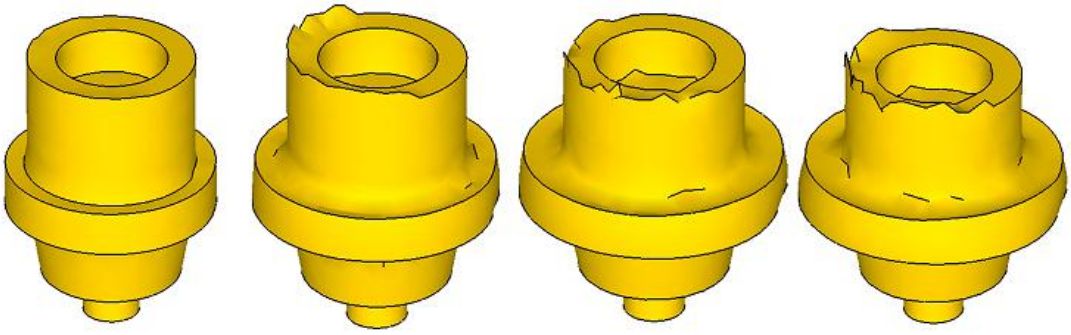

Figure 5.34: Die filling at different punch movement

5.3.4.3 Metal flow pattern

Figure 5.35 shows the contour of displacements in both the horizontal and axial direction after 3.0 mm, 6.0 mm, 8.0 mm and 8.2 mm ram displacements at 1.0 mm/min ram velocity and 0.19 friction factor. The degree of distorted gridlines at different stages confirms the load~ram displacement behaviour. Severe grid distortion at flashing stage validates the maximum load due to maximum redundant work. It is also seen that the whole billet, rather than part close to punch, is deforming simultaneously in different directions. It is observed that, there is a non-uniform grid distortion due to friction at die-billet interface.

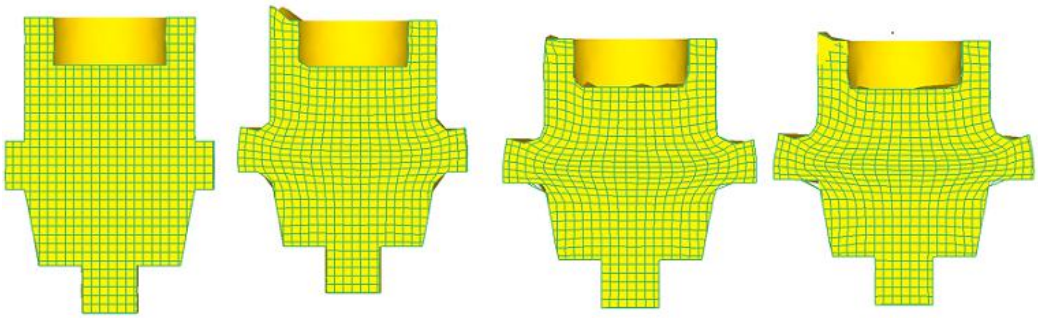

Figure 5.35: Flow pattern at different punch movement

5.3.4.4 Stress, strain and velocity pattern

As an illustration, Figure 5.36 shows the effective stress, effective strain and total velocity distribution and in terms of solid profile for the friction factor of 0.19, at a ram speed of 1 mm/min. From Figure 5.36(a) it is observed that the effective strain is more at upper and at the middle collar portion, In this region, the grains change its flow pattern close to 90 degrees for the formation of the collar that leads to shear of the metal. Further, the metal is also subjected to shear in the middle portion of die filling and the bottom part of forward extrusion where the extruded part is formed due to a decrease in diameter. From the Figure 5.36(b) it can be observed that the effective stress is found to be 111 MPa which is around the flow stress of the material chosen for the complete processing of the component. It is observed that maximum compressive stresses reaches near billet-punch walls (111 - 155 MPa) around the billet-punch interface and minimum compressive stresses can be observed at the middle portion (55 – 111 MPa) is due to maximum load is diverted for the formation of collar rings. Similarly Figure 5.36(c) highlights the total velocity, is found to be more at the edges and at the middle portion, due to the change in the grain flow direction.

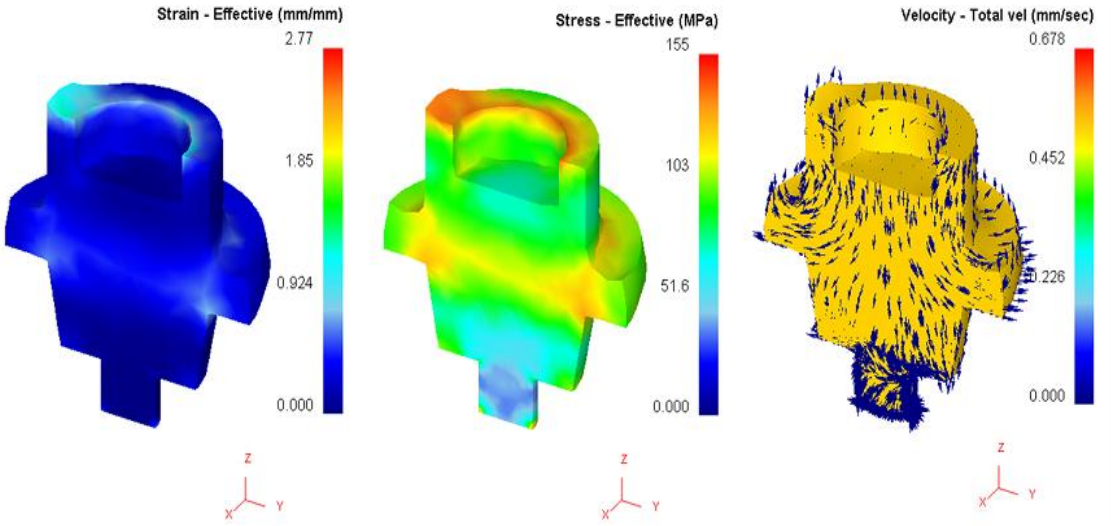

(a) Effective strain (b) Effective stress (c) Total velocity

Figure 5.36: Mean stress, effective strain and velocity at a 0.19 friction factor with 1mm/min punch movement

5.4 Conclusions

Simulations were carried out for the analysis of different types of collet chuck holders by CEF and CE processes. The different stages in the forming of product collet chuck holder by CEF and CE process are explained in detail. Namely (i) Initial compression stage, in which the load gradually increases, forms a small indentation hole by backward extrusion. (ii) Second stage, in which radial extrusion formation of collar ring/rings are formed along with the forward extrusion and forging of the taper part was performed, (iii) combined stage, corner die filling and extrusion of last part was done, (iv) the unsteady state stage, in which there is a steep rise in load. In this stage, flash is formed, as the metal flow has hindered and controlled, the load increases unsteadily. In case of third product metal flows out through the exit extrusion die present at the bottom, hence no flash provision is equipped. The last product is manufactured by multi stage extrusion/forging process in which the first product is the initial input specimen. Hence, the process is thought consists of two stages instead of four that is assumed for previous three products.

The results obtained can be summarized as below:

- In the present chapter the finite element analysis for four types of collet chuck holders were performed by CEF and CE processes.
- Similar conditions of experimental analysis are taken into account for performing the present FEM analysis. Combination of three types of frictional conditions and

three ranges of ram velocities are consider for the analysis to obtain optimum results.

- Among the nine components processed for SCCCH and DCCCH each through CEF process, the lowest forming loads are 157.7 kN and 152.7 kN obtained at 0.13, 0.19 frictional conditions during 0.5 mm/min ram velocity respectively.
- Among the nine components processed for DCCCH by CE process, the lowest forming load is 141.1 kN obtained at 0.13, 0.19 frictional conditions during 0.5 mm/min and 1 mm/min ram velocities.
- The Multistage extrusion for a SCCCH by CEF processes is performed under single frictional condition and rams velocity.
- Different stages of deformation for all the four types of CCH's are performed for clear understating of die filling. Different stages of die filling data are used for further comparison analysis.
- Different stages of metal flow pattern for all the four types of CCH's are obtained for clear understanding of grain flow and shear effected regions.
- The effective stress, strain and total velocity are analysed to get a clear picture of metal flow direction, and stress/strain accumulation points. The data is procured for clear understanding of variation of forming loads at different regions of a component which is processed under different frictional conditions and ram velocities.

Chapter 6

Experimental Analysis

6.1 Introduction

The industrial significance of combined extrusion-forging (CEF) and/or combined extrusion (CE) techniques in particular, metal forming in general, has increased many folds. Many components used by automotive, electrical and aerospace industries prefer to manufacture by these techniques instead of casting and/or machining to get the benefits of metal forming, i.e., low wastage, continuous and multidirectional grain flow direction, better mechanical properties, etc.

Yamin et al. [127] investigated the combined extrusion process to manufacture a cup rod component isothermally taking magnesium alloy (AZ61A) as the product material. They concluded that use of proper lubricant is essential to reduce the forging load. Giardini et al. [128] used an analytical approach to identify the most critical zone in the die to reduce the friction during the forging-extrusion process. Vickery and Monaghan [129 - 130] showed that with proper lubrication friction and subsequently forming load can be reduced, particularly during the steady state process. They also demonstrated the influence of die opening diameter during the process. According to Brayden and Monaghan [131] the neutral radius plays a critical role in extrusion forging process, which influences the metal flow direction, overall volume constancy and load equilibrium conditions. Choi et al. [132] proposed a kinematically admissible velocity field for the forging of a trochoidal gear made of the aluminium alloy. The inward flow of material is illustrated by taking a neutral surface in the forging process using a hollow billet.

Farhoumand and Ebrahimi [4] used the finite element analysis to investigate the effect of friction at the walls of the die-billet and that of die corner radius on the predicted load. Narayanswamy et al. [133] summarized their experimental observations on the extrusion-forging processes in support of barrelling of aluminium alloy with various lubricants. Hwang et al. [134] optimized the forming load and length of travel taking suitable process parameters, like die geometry, friction and deformation zone. Kar et al. [73] investigated the optimal die semi-cone angle for different area reductions under

different friction conditions. It was observed that with the increase of complexity of the die profile the intricacy of its analytical analysis also enhances. Li et al. [28] proposed a numerical technique for the processing of thin and sharp complex components with light metals. Paltasingh et al. [124] conducted experimental and numerical analysis for lateral extrusion of spur gears and Potnuru et al. [125] numerically predicted the metal flow pattern and forming load for a socket wrench with experimental validation.

In the present investigation, experimental studies are carried out with a view to compare the experimental results with those obtained from proposed theoretical ones using upper bound method and finite element analysis. Experiments are performed on an INSTRON®600KN Universal testing machine (maximum capacity of 600 kN) for extrusion-forging of different types of collet chuck holders. Commercially available aluminium Al 1070 is used for above mentioned purpose. An extrusion-forging setup for laboratory experimentation is designed and fabricated. Experiments are performed at different friction and ram velocity conditions with microstructure, micro hardness and load analyses.

6.2 The Test Rig

The block diagram of the experimental setup fabricated for the present analysis is shown in Figure 6.1. The punch die setup for experimentation mainly consists of punch rod, punch head, container, container sleeve, forging-extrusion die-holders, base plate and a series of extrusion-forging dies with different shapes. The container is made up of EN31 steel having a dimensions 140 mm diameter (φ) and 100 mm length with an internal hole with dimensions 50 mm φ and 100 mm length. Using wire EDM the tolerances of $\pm$ 0.01mm have been incorporated for the internal drilling and outer diameter. The cover plate is used to avoid slipping of container sleeve during experiments. The function of container sleeve is to guide the punch rod through the container and prevent bulging of punch rod. The punch head is connected to punch rod using a push-fit arrangement. The base plate and support plates are of EN 8 steel. The details of the components are provided in Table 6.1.

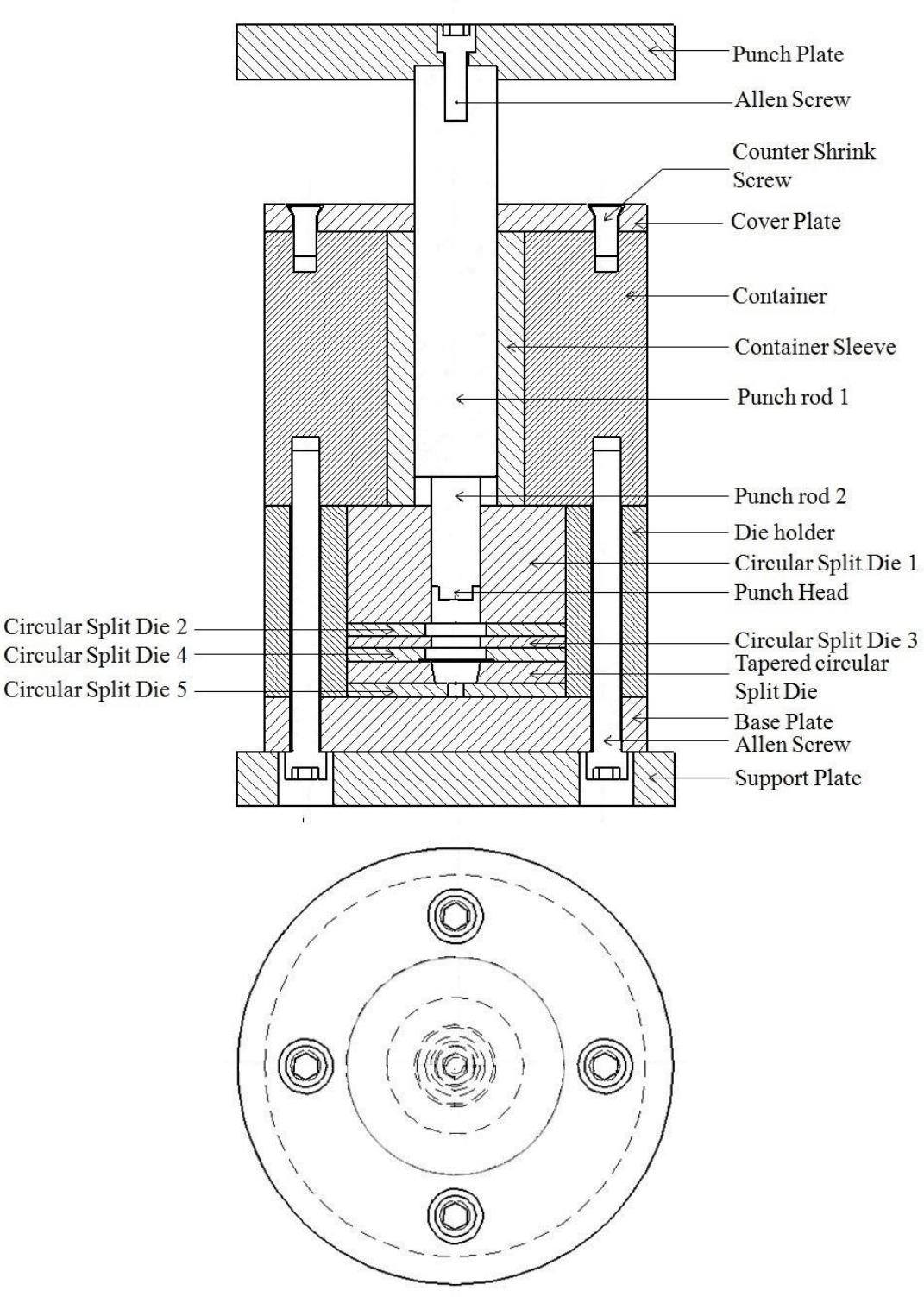

Figure 6.1: Extrusion-forging die set up assembly

Table 6.1: List of components

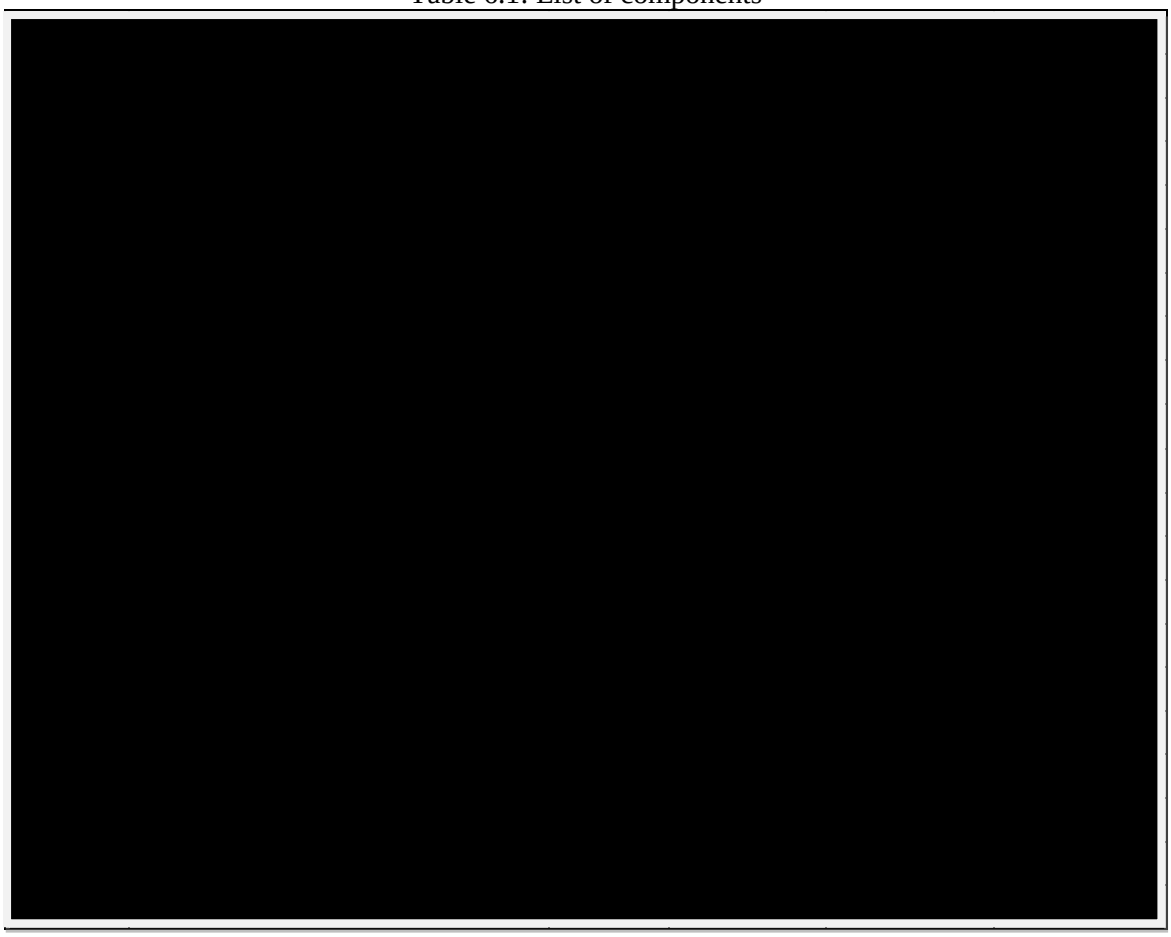

6.3 Dies

Split dies are employed in the current process for easy removal of the product after the extrusion-forging operation is completed. We have designed and assembled die orifices in such a way that centre of gravity lies on the billet axis to avoid eccentricity effect. EN31 hot rolled tool steel of 20 mm thick plates are used to fabricate the dies using wire EDM machine to required dimensions, normalized in reducing atmosphere and oil quenched to improve hardness (up to Rc 60 - 65). As the inner surfaces of dies have importance with regard to friction, required surface roughness is maintained during the finishing operation. To avoid interference with the product the die openings are relieved by close to ten degrees with the die exist for extrusion condition. The details of the circular split dies and other components machined for experimentation are presented in Appendix A (Figures A.1- A.17).

6.4 Specimen

Experiments were performed with commercially available pure Aluminium 1070 (99.70% Pure) as billet material. The composition of Al 1070 is shown in Table 6.2. The billets of required sizes (15 mm in diameter and 32 mm in height, 15mm diameter and 47.8mm in height, 15 mm diameter and 53.30 mm height for different set of experiments) are prepared by casting and followed by turning with kerosene as coolant. These cylindrical billets sizes are decided in such a way that their volume would be accommodated in the combined extrusion and combined extrusion-forging cavities.

Table 6.2: Composition of specimen (Aluminum 1070)

Al	Si	Mn	Zn	Cu	V	Ti	Fe	Other
99.7%	0.2%	0.003%	0.004%	0.004%	0.005%	0.003%	0.2%	0.03

6.5 Experimental Procedure

Initially internal walls of the die sets and die holders were thoroughly cleaned with carbon tetrachloride to remove dirt and oil. Subsequently, lubricant (type depend on friction value required for specific experiments) was smeared properly on the inner sides of the specimen, dies sets and dies holders. Further the split die sets are push fitted into die holders to guard the assembly and tighten by Allen screw. Afterward, the specimen is placed inside the die cavity. Finally, the die assembly is placed on the lower table of the universal testing machine as shown in the Figure 6.2, followed by placing the punch in its position. After the entire setup arrangement is accomplished and rechecked, the machine was started placing the apparatus on the lower table and the experiments were performed. Appropriate movement of the punch is being adjusted and punch load is obtained at every 30 seconds of punch travel. Compression of the billet has been done up to the specified length of travel by the punch. The machine was stopped and the test was terminated at this point. The die punch set is disassembled to push out the product, collet chuck holder, from the split die halves. Experiments are conducted to form the product collet chuck holder using CEF and CE processes at varying coefficient of frictions and rate of punch displacement to find out the forming load, metal flow pattern and check the presence of grain structure.

The different stages in the forming of product collet chuck holder using CEF and CE processes are:

(i) Initial stage, in which the load gradually increases with backward extrusion,

(ii) Second stage, in which forward and lateral extrusion takes place,

(iii) Combined stage, both extrusion and forging takes place for corner filling, and

(iv) The unsteady state stage, with a steep rise in load. In this stage, flash is formed. As the metal flow is hindered, the load increases unsteadily.

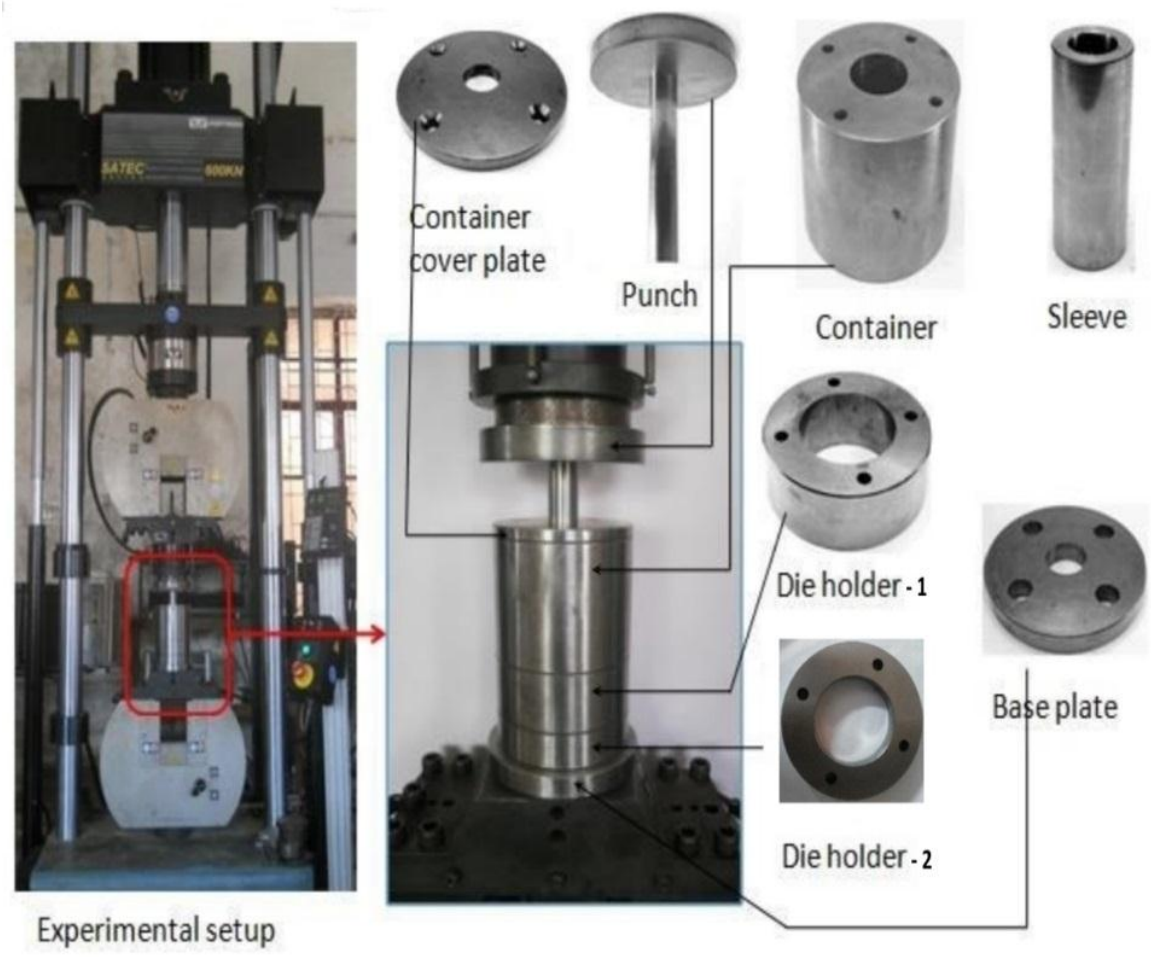

Figure 6.2: Photograph of UTM machine with assembled set-up

6.6 Stress-strain Characteristics of Specimen Al 1070

Billets of dimensions 18 mm in diameter and 37 mm in height were machined with grooves on both ends (grooves were provided for lubrication to minimize bulging effect during compression test) for plotting the stress-strain diagrams. The specimens are also stress relieved by annealing the same in boiling water for two hours. After smearing proper lubricant on both ends of the billet compression tests were performed by UTM

having maximum capacity of 600kN. The compression test set-up along with specimen lubricated in the grooves shown in Figure 6.3. Separate compression tests are carried out with ram displacements of 0.5 mm/min, 1 mm/min and 2 mm/min, which are used for the experimentations applied to CEF/CE processes. The compression load values were recorded for every 1 mm of the displacement of ram. For the present test, the billet was compressed for 5 mm, and then was taken out from the sub-press. The billet was re-machined to its initial diameter of 18 mm followed by providing oil grooves on both ends. Further, similar kind of compression tests were continued till the billet reaches a height of 17 mm from the initial height of 37 mm. The shape of the specimen before and after the final compression test is shown in the Figure 6.4. The stress-strain diagram of billet material Al-1070 at ram displacement of 1 mm/min is shown in Figure 6.5.

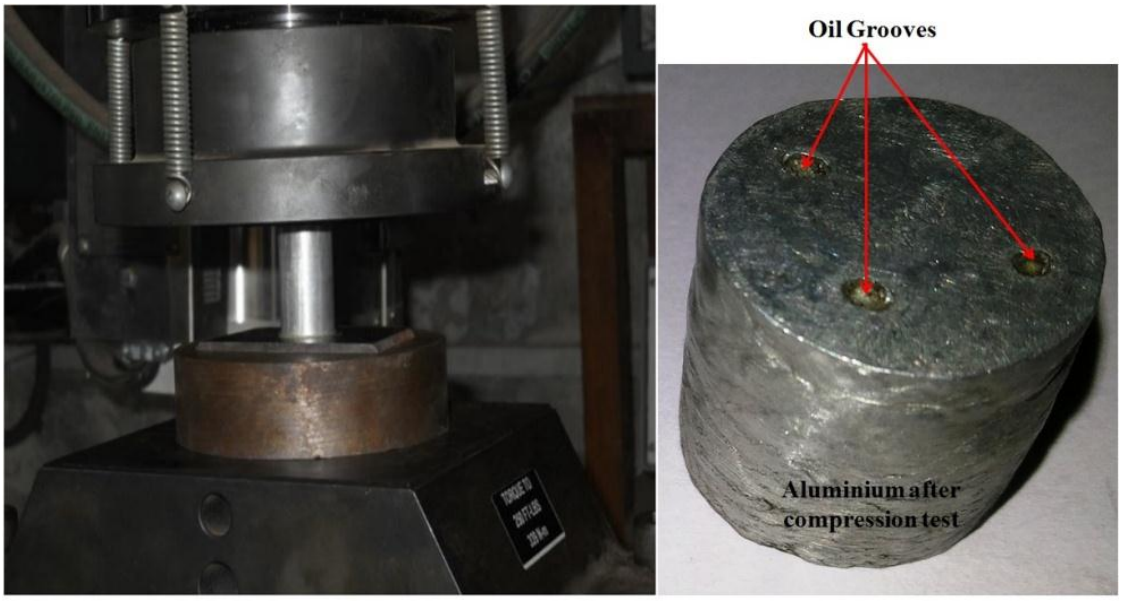

Figure 6.3: Compression test setup with aluminium specimens

Similarly billets are prepared and experiments have been conducted for other ram displacements such as 0.5 mm/min and 2 mm/min. The stress-strain diagram for all the three cases are shown in Figure 6.5. The stress-strain relationship for 1.0 mm/min ram speed obtained by curve fitting to the experimental data for aluminium, using the least square method, is given by the equation:

$$\sigma = 282\varepsilon^{0.495}\text{MPa} \qquad (6.1)$$

Similarly, for ram displacement of 0.5 mm/min. it is,

$$\sigma = 242\varepsilon^{0.454}\text{MPa} \qquad (6.2)$$

and for ram displacement of 2.0 mm/min it is,

$$\sigma = 305\varepsilon^{0.568}\text{MPa} \quad (6.3)$$

with coefficient of correlation r = 0.93.

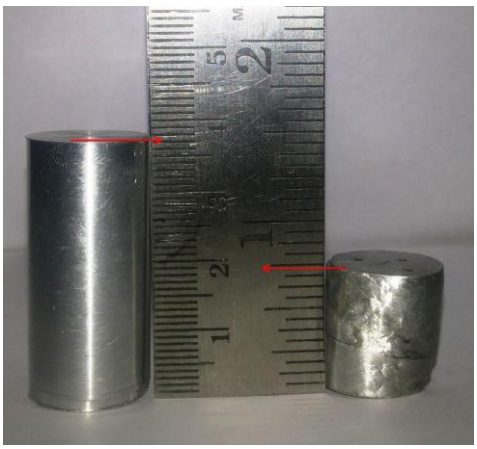

Figure 6.4: Compression test for determination of flow stress

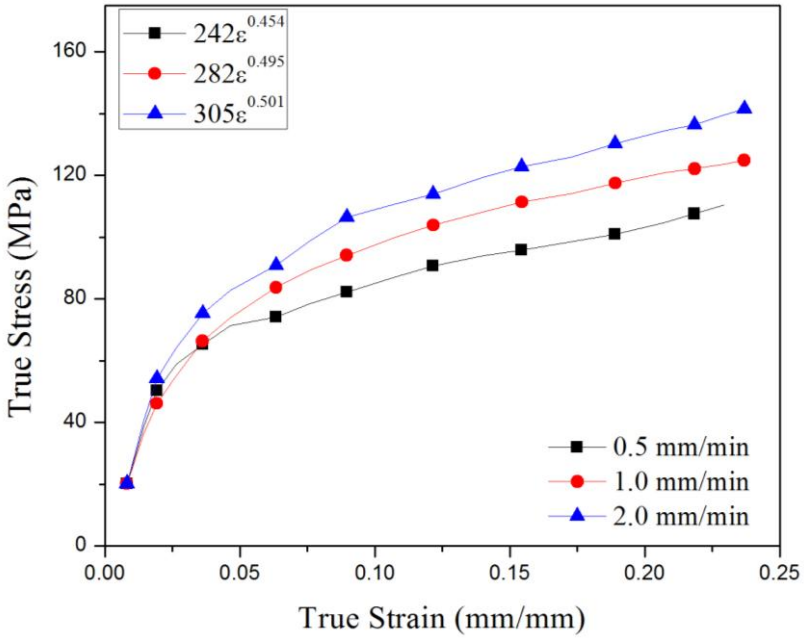

Figure 6.5: Stress-Strain (Flow stress) curves for aluminium specimen

6.7 Ring Test for Determination of Friction Factor

In metal forming process friction plays an important role. The metal flow is caused by the pressure transmitted from the dies to the deforming work piece. Therefore, the friction condition at the material/die interface greatly influences forming load, metal flow pattern and internal microstructure. For our present work, we have carried out experiments under three surface conditions (two lubricated and one un-lubricated condition). The various combinations of lubricated and unlubricated cases are as follows:

1. 100% grease (commercially available SKF® LGMT 3IN1 general purpose grease)
2. MoS_2 + Grease with 60:40 ratio
3. Unlubricated

Ring tests are carried out at ram speed of 1.0 mm/min (assuming no variation of friction value at 0.5 mm/min and 2.0 mm/min ram speed) to find the friction factors at different surface conditions. In this ring test, a flat ring shape specimen having OD: ID: Thickness ratios 6:3:2 is considered. The dimensions of the ring used are 18 : 09 : 06 mm (outside diameter: inside diameter: thickness) shown in Figure 6.6. To estimate accurate friction between die inner surface and the billet material two flat plates having the same surface condition that of internal surface of dies are equipped. The prepared ring specimen was compressed to a fixed percentage of thickness of 1mm and after every compression, internal diameter, outer diameter and thickness is measured for further calculation of friction factor (m) using calibration curves. The flat dies are cleaned using acetone after every 1 mm of compression in order to obtain accurate results. The magnitude of friction factor can be found out by comparing the inner die of compression ring with various available standard theoretical calibration curve shown in Figure 6.7 of friction factor (m). It is found that for the lubricated condition, the friction factor was 0.13 for (MoS_2+Grease) and 0.19 for (Grease). For the unlubricated case the friction factor obtained was 0.38.

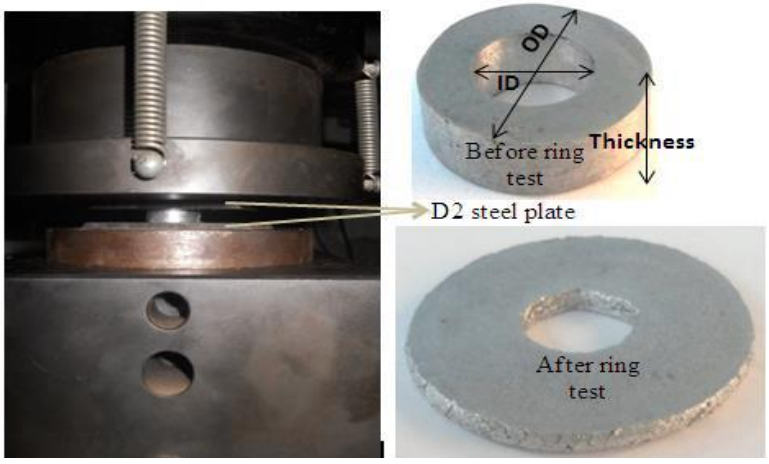

Figure 6.6: Setup for ring test

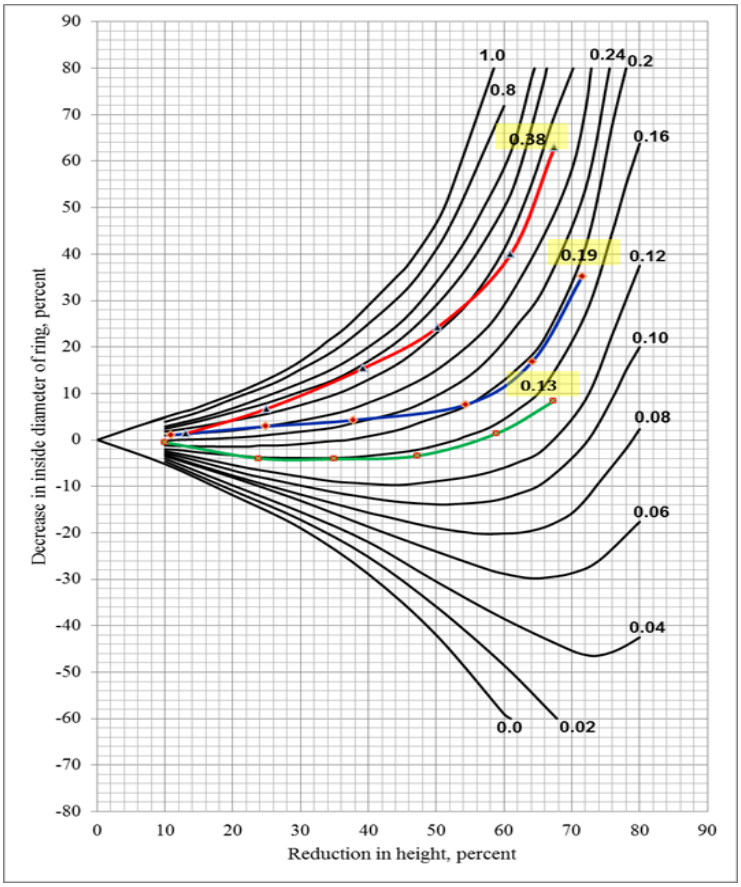

Figure 6.7: Comparing the ring test curves with theoretical standard calibration curve (6:3:2)

6.8 Manufacturing of Collet Chuck Holders

Today's automobile and aero industries have high demands for robust components for sustaining in extreme working conditions. Manufacturing a component with good properties at cheaper price is a tougher job. In the current competitive market trends, we have taken a prototype model to produce it in a cost effective scenario and also taking all the advantages of metal forming process instead of following conventional route of casting and/or machining. The components finalized for the analysis are of four types of collet chuck holders.

1. Product 1: single collar collet chuck holder by CEF process.
2. Product 2: Double collar collet chuck holder by CEF Process.
3. Product 3: Double collar collet chuck holder by CE Process.
4. Product 4: Single collar collet chuck holder by Multi-stage extrusion/forging process.

6.9 Results and Discussions of Experimental Analysis

6.9.1 CEF process for single collar collet chuck holder

It is well known that forming load and its parameters are highly influenced by frictional conditions and ram velocities. In the present study we have considered three types of experimental conditions. The following friction conditions are considered for conducting experiments at varying ram velocities (0.5 mm/min, 1 mm/min and 2 mm/min),

1. Mixture of Molybdenum disulphide and Grease (60:40), friction factor (m = 0.13)
2. 100% grease, friction factor (m = 0.19) and
3. The final is dry condition friction factor (m = 0.38).

For every friction condition three varying rate of ram displacements are considered to get the single collar collet chuck holder as shown in Figure 6.8 (detail dimensions are provided in Figure 5.5). For further validation, microscopic, micro hardness and residual stress analysis were also being performed.

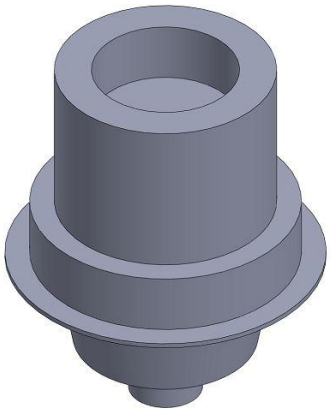

Figure 6.8: Single collar collet chuck holder manufactured by CEF process

6.9.1.1 Lubricated conditions

Case I: (60:40 MoS_2 + Grease) at varying rate of ram displacements

Experiments are carried out to manufacture the single collar collet chuck holder using combined extrusion forging process at three ram displacements, i.e., 0.5 mm/min, 1.0 mm/min and 2.0 mm/min. Initially the punch comes in contact with the billet, backward extrusion takes place. Further in the next stages forward & lateral extrusion and forging takes place to fill the die cavities for manufacturing the final component. The maximum forming loads obtained for the component to manufacture are 148.8 kN, 188.3 kN and 196.2 kN respectively (shown in Figure 6.9).

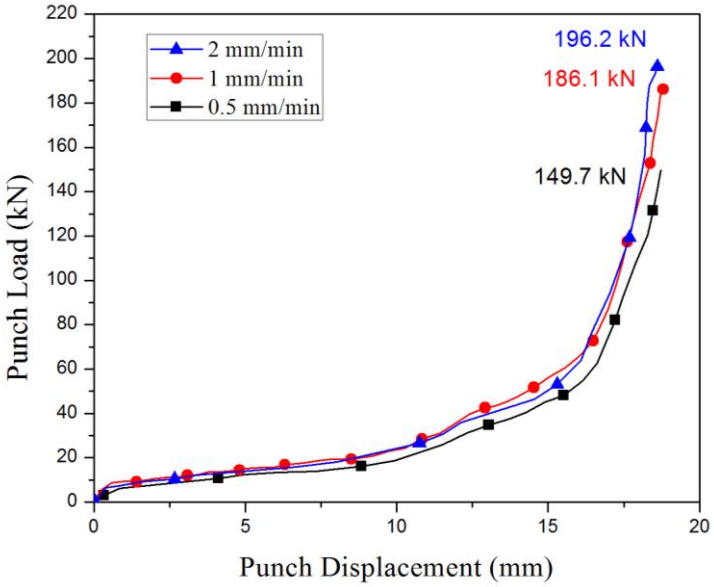

Figure 6.9: Variation of punch load with ram displacement at m = 0.13

Case II: (100 % Grease) at different ram displacement

Similarly, experiments are carried out to manufacture the same single collar collet chuck holder using combined extrusion forging process at three ram displacements, i.e., 0.5 mm/min, 1.0 mm/min and 2.0 mm/min under full grease lubrication condition. Initially the punch comes in contact with the billet, backward extrusion takes place. Further in the next stages forward & lateral extrusion and forging takes place to fill the die cavities for manufacturing the final component. The maximum forming loads obtained for the component to manufacture are 189.4 kN, 194.1 kN and 211.5 kN respectively (shown in Figure 6.10). It is found that the maximum load increases with ram velocity because of work hardening effect.

6.9.1.2 Unlubricated conditions at different ram displacement

Similarly, experiments are carried out to manufacture the same single collar collet chuck holder using combined extrusion forging process at three ram displacements, i.e., 0.5 mm/min, 1.0 mm/min and 2.0 mm/min under no lubrication condition (friction factor m = 0.38). Initially the punch comes in contact with the billet, backward extrusion takes place. Further in the next stages forward & lateral extrusion and forging takes place to fill the die cavities for manufacturing the final component. The maximum forming loads obtained for the component to manufacture are 192.0 kN, 198.0 kN and 219.5 kN respectively (shown in Figure 6.11). It is also observed that the maximum load increases with ram velocity because of work hardening effect and values are more in comparison with lower friction.

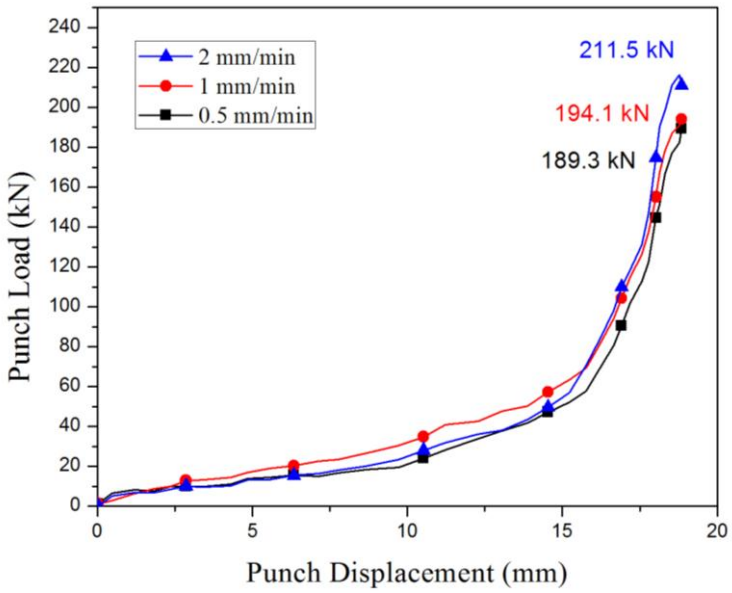

Figure 6.10: Variation of punch load with ram displacement at m = 0.19

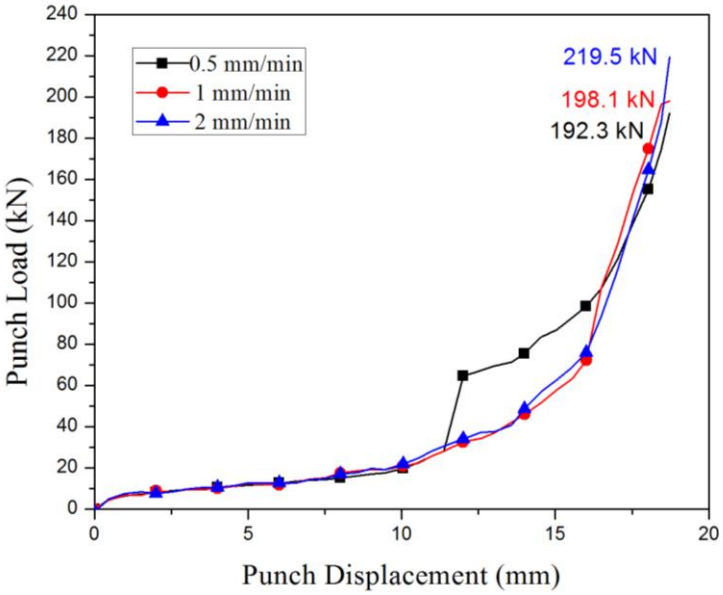

Figure 6.11: Variation of punch load with ram displacement at m = 0.38

6.9.1.3 Punch loads at varying frictional conditions

The Figure 6.12 represents the variation of punch load with rate of ram displacment for single collar collet chuck holder (SCCCH) manufactured by CEF process. It is observed that the minimum load is obtained at 0.5 mm/min ram displacement with 0.13 coeffiecient of friction and it is maximum at 2 mm/min ram displacement with 0.38 coefficient friction. It is also seen that the rate of increase of load requirements when ram speed goes from 0.5 mm/min to 1.0 mm/min is high incomparison to that from 1.0 mm/min to 2.0 mm/min and it is severe at lower friction situation. It appears that because of severe

forming load the chance of breakdown of lubrication layer is higher at lower friction condition when smeared/flooded lubrication is used.

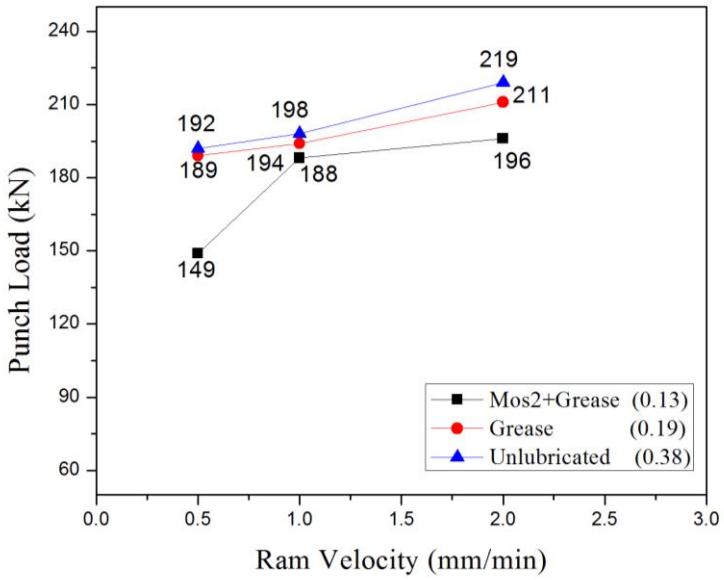

Figure 6.12: Punch load Vs Rate of ram displacement for single collar collet chuck holder

6.9.1.4 Die filling

Figure 6.13 shows the shape of the product at different punch movement, for combined extrusion-forging process, obtained experiments at a ram velocity of 0.5 mm/min and at friction factor of 0.13. It explains that combined extrusion-forging process takes place till the die cavity is completely filled. It was observed that the maximum displacement required for filling the die cavities is 18.8 mm.

(a) Stage I 6.01 mm punch travel	(b) Stage II 11.4 mm punch travel	(c) Stage III 15.8 mm punch travel	(d) Stage IV 18.8 mm punch travel

Figure 6.13 Die filling at different punch movement

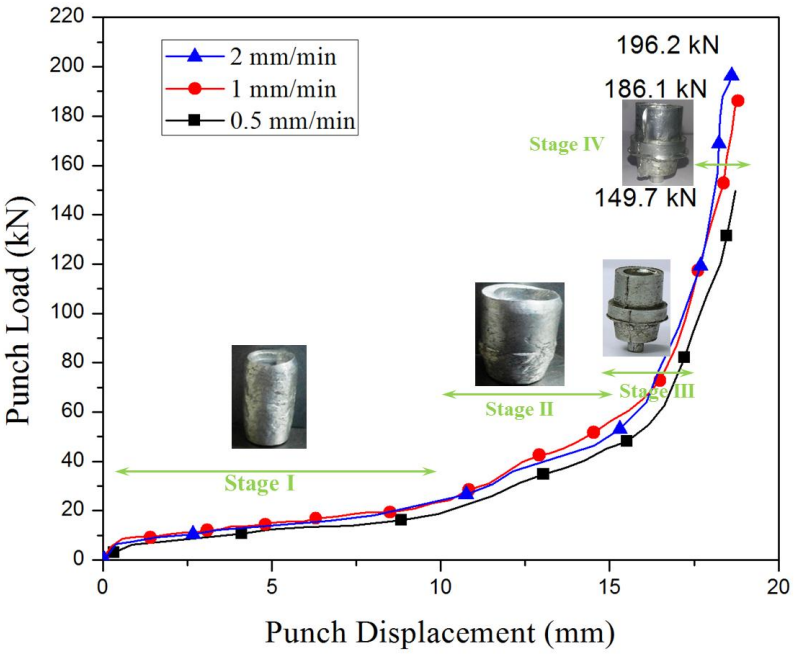

Figure 6.14 Product shape at different punch position

Referring to the Figures 6.13-14, it is seen that the whole process consists of four major stages. It can be explained as follows:

Stage I

In this stage the punch head comes in contact with the billet and applies initial compression. The load gradually increases when the circular punch head penetrates into the billet, this leads to backward extrusion. It can also be named as coining stage, because of the coin shaped indent formed by the punch head on the billet for the backward extrusion. The Figure 6.13(a) represents the stage I process for clear view of the component which has been subjected to CEF process. The displacement takes place in the present stage is 0-6.41 mm.

Stage II

In this stage load increases slowly with respect to punch movement. Forward and lateral extrusions take place simultaneously. Figure 6.13(b) represents the stage II process, which takes place during the 6.41-11.4 mm ram movement.

Stage III

During this stage, 11.4 - 15.8 mm of ram movement, metal flows to fill all the geometrical corner points Figure 6.13(c). As metal flows a longer path, it requires more redundant work, gives a steep rise of load.

Stage IV

The final unsteady stage takes place, between 15.8 - 18.8 mm of ram movement, where metal flow through the constricted passage to form flash. Because of high friction and redundant work, there is a sharp increase in the forming load. The Figure 6.13(d) represents the stage IV for the product manufactured by CEF process. The flash is designed in such a way that the extra metal expel out only when the entire die cavities are filled.

6.9.1.5 Metal flow pattern (Sectional View)

As an illustration, Figure 6.15 shows the photograph of the flow pattern for extrusion-forging process of a single collar collet chuck holder at ram velocity of 0.5 mm/min and friction factor of 0.13 during different punch movement obtained from experiments. The severe grid line distortions at the last two stages confirm the maximum amount of redundant work that is responsible for the steep rise in load.

(a) Stage I 6.01 mm punch travel	(b) Stage II 11.4 mm punch travel	(c) Stage III 15.8 mm punch travel	(d) Stage IV 18.8 mm punch travel

Figure 6.15 Flow pattern at different punch movement

6.9.1.6 Microscopy analysis

Microscopic analysis has been carried out for the manufactured Components to check the grain flow pattern. A Carl Zeiss® made AXIO LAB A1 model optical microscope is used for the present inspection (Figure 6.16).

Figure 6.16: Optical Microscope

To begin with, the half sectioned components (shown in the Figures 6.15(a-d)) have been rough

polished using the belt of coarse grade with 400 grit followed by a fine paper finish with four grades (1/0,2/0,3/0,4/0) of papers. Fine polishing is performed by cloth using alumina powder of 10 microns in size mixed with water. For the final mirror finish the component is polished on velvet cloth using kerosene as medium. Subsequent to mirror finish, the component are etched by the Keller's reagent (95 mL of distilled water, 2.5 mL HNO_3, 1.5 mL HCl, 1.0 mL HF) for 5, 10, 20 seconds for 2 mm/min, 1.0mm/min and 0.5 mm/min ram velocity respectively.

The specimens are analyzed under the microscope at a maginification of 200 and 500 μm to find the grain flow & grain elongation, and shear zones respectively. For the present microscopic analysis five components manufactured at different working conditions are considered (Table 6.3).

Table 6.3: Components considered for microscopic analysis

Component No.	Friction Factor	Ram Displacement (mm/min)
1	0.19	0.5
2	0.19	1.0
3	0.19	2.0
4	0.13	0.5
5	0.38	0.5

Subsequent Figures 6.34-6.38 show the microscopic images procured during the analysis of the above mentioned five components of the CEF of single collar collet chuck holder. Each component is examined at four different locations. The top right location indicate backward extrusion, grain flow is subjected to shear due to the reverse flow for the formation of cup. The centre left and centre points indicate lateral and forward extrusion where the metal is subjected to shear deformation for the formation of the collar ring and flash. With downward movements of the ram hydrostatic compression stress increases at these locations gives rise to severe plastic deformation. The last point indicates the forward extrusion which is due to formation of the stud like element at the bottom representing elongated structure.

To investigate the effect of friction at a particular ram velocity Figures 6.17, 6.20 and 6.21 may be considered (ram speed =0.5 mm/min, friction factors are 0.19, 0.13 and 0.38 respectively). It is observed that no abrupt microstructural change has been observed as the ram displacement and friction condition is low. Figure 6.18 illustrates the

microstructure at five different zones of the sample at ram speed of 1.0 mm/min and m= 0.19. Microstructure of the material show medium sized elongated grains with change of direction (normal to longitudinal axis) and along the shear zones. Similarly, Figure 6.19 illustrates the microstructure at five different zones of the sample at ram speed of 2.0 mm/min and m= 0.19. Microstructure of the material show fine sized elongated grains; it indicates that the material experiences both shear and normal strain to form thin walls of upper cup, collar and bottom stud. As it can be seen the fine grain elongation and high shear is due to the higher ram displacement and medium frictional condition.

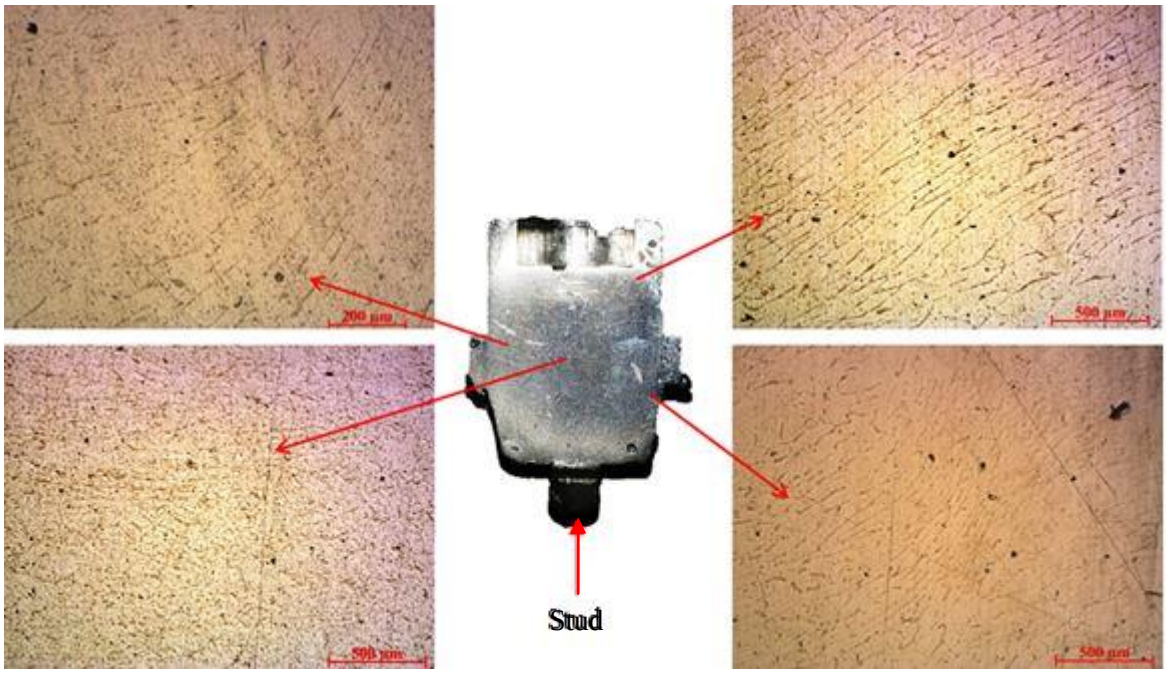

Figure 6.17: Microscopic analyses of CCH with friction factor 0.19 at 0.5 mm/min ram displacement

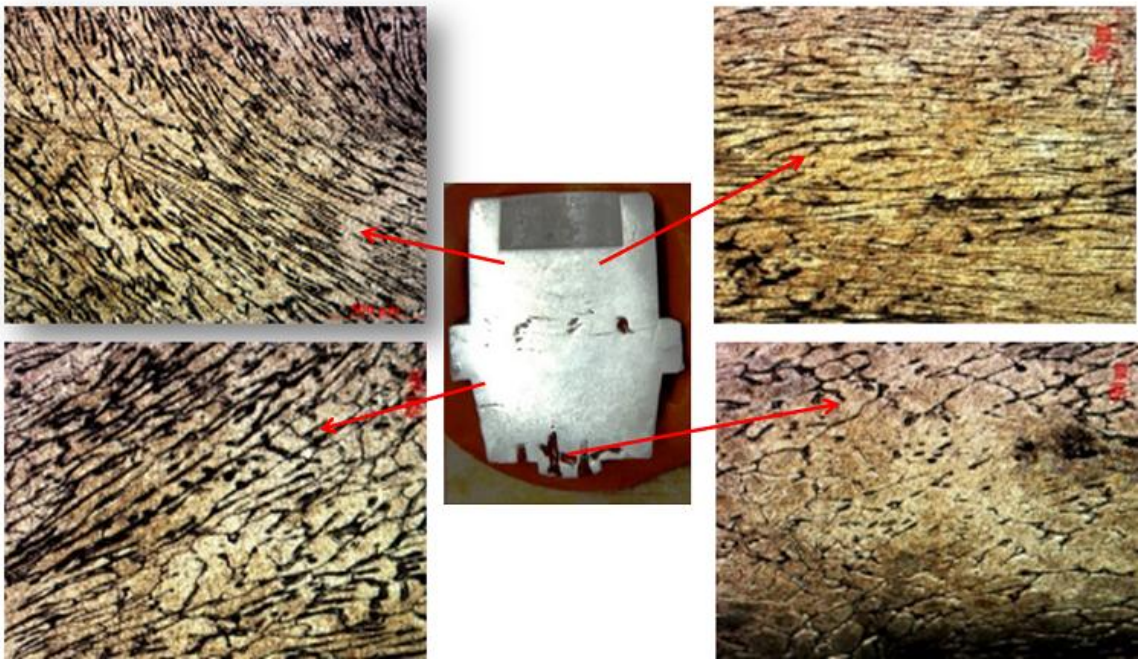

Figure 6.18: Microscopic analyses of CCH with friction factor 0.19 at 1 mm/min ram displacement viewed at 500 µm

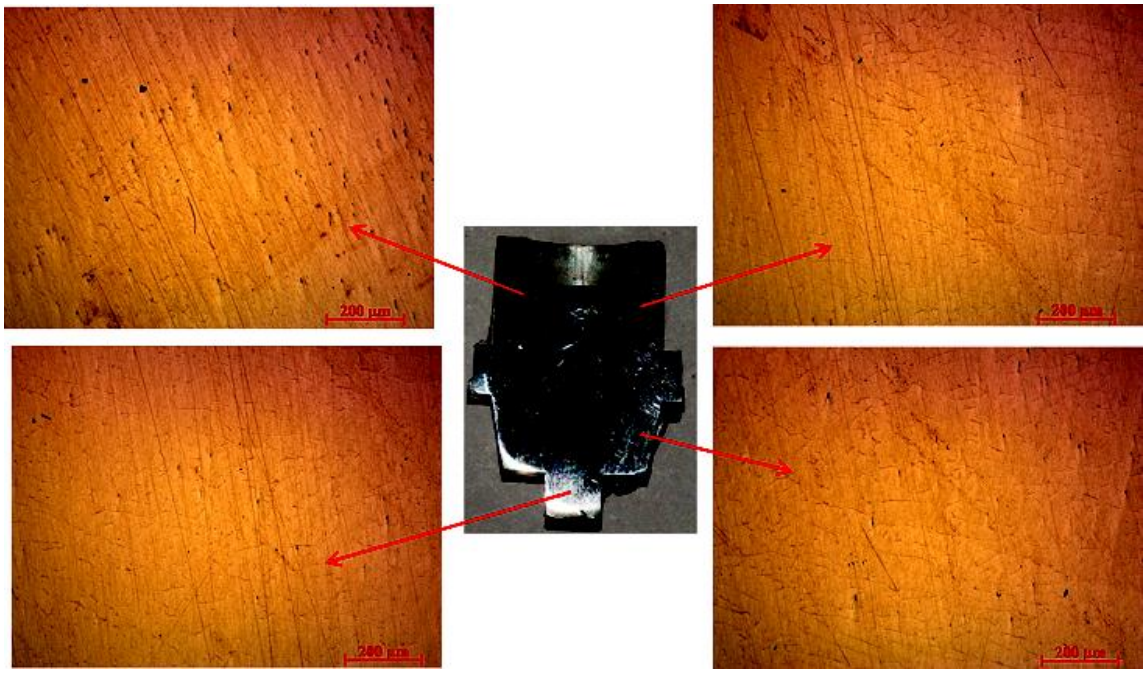

Figure 6.19: Microscopic analyses of CCH with friction factor 0.19 at 2 mm/min ram displacement

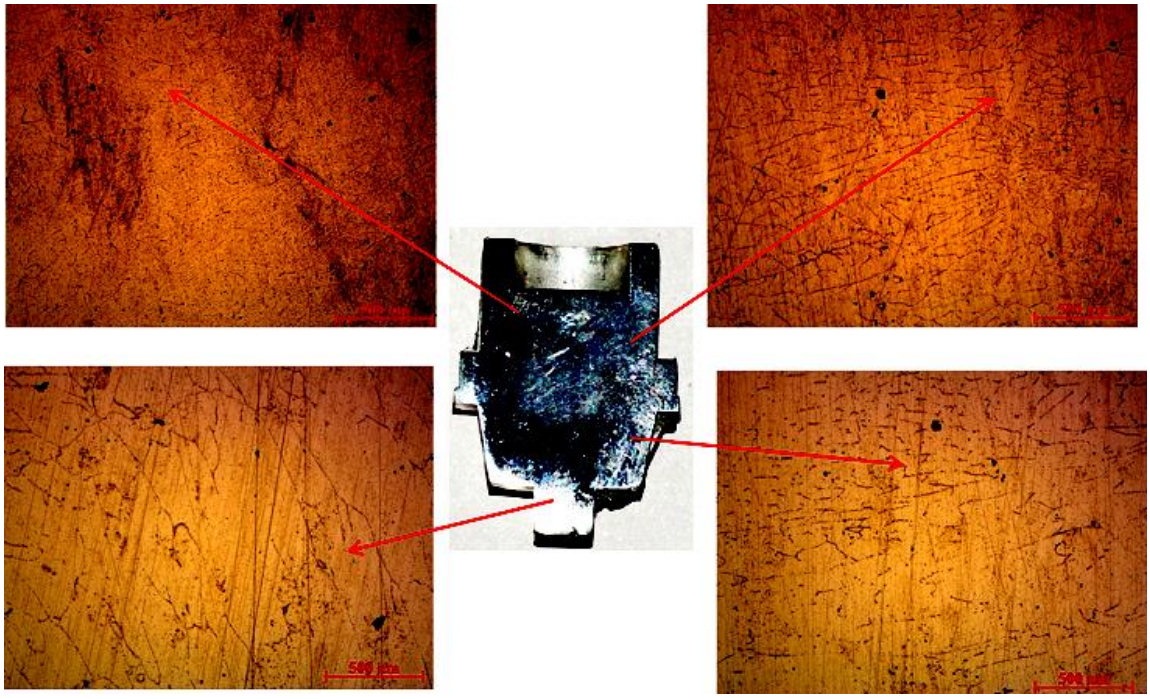

Figure 6.20: Microscopic analyses of CCH with friction factor 0.13 at 0.5 mm/min ram displacement

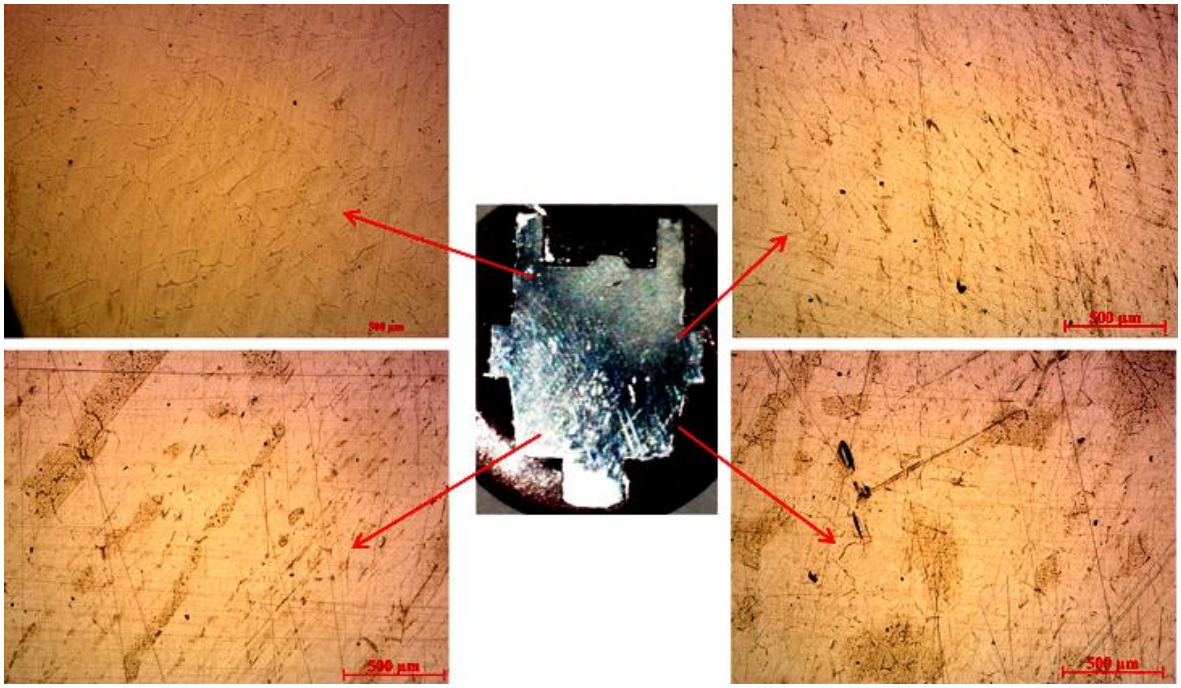

Figure 6.21: Microscopic analyses of CCH with friction factor 0.38 at 0.5 mm/min ram displacement

6.9.1.7 Micro hardness analysis

Micro-hardness of combined extrusion-forged components are taken at different locations using a Leco LM810 modelvicker® hardness tester (Figure 6.22). As the grains dislocate and change its shape there is a high tendency for change in the hardness of the component. We know that hardness is higher for components manufactured under cold conditions in comparsion with hot metal formed components because of strain hardening. The present analysis deals with measuring the hardness of the five components manufactured under the two working conditions considered (mentioned in Table 6.3). The analyses include measurement of hardness at six different locations as shown in Figures 6.23-6.27. The measuring locations P1-P6 are indicated on each component's middle cross sectional plane. An average of three readings is considered at every point, each point has its own industrial significance.

The importance of the six points, where microhardness have been measured are as follows:

P1: Backward extrusion some extent of metal will be subjected to tensile stress.

P2: Backward extrusion with shear as the grain flow changes its direction.

P3: Radial extrusion with shear and metal flow gets hindered by die walls and flash formation

P4: Radial extrusion with shear

P5: forward and radial extrusion is present and metal gets shear

P6: Forward extrusion for formation of pull stud.

Figure 6.22: Vickers Micro-Hardness Tester

As shown in Figures 6.40-6.44, microhardness of the components depends on the position and extrusion conditions. These micro-hardness could be explained by the differences in microstructures. The components shown in Figures 6.23, 6.26 and 6.27 are worked under ram speed of 0.5 mm/min and friction factors of 0.19, 0.13 and 0.38 respectively. The component shown in Figure 6.24 is worked under medium ram displacement and lubrication condtions (ram speed =1.0 mm/min, friction factor 0.19). The componenet shown in Figure 6.25 worked under higher ram displacement and lubrication conditions (ram speed = 2.0 mm/min, friction factor 0.19). It can be observed that the hardness is increased at all points (P1- P6) due to the work hardening effect when compared to the rest. It can also be obsevered the hardness is high at points (P2, P4) for all

components (except first one) due to the presence of shear zones and severe change of grain flow directions.

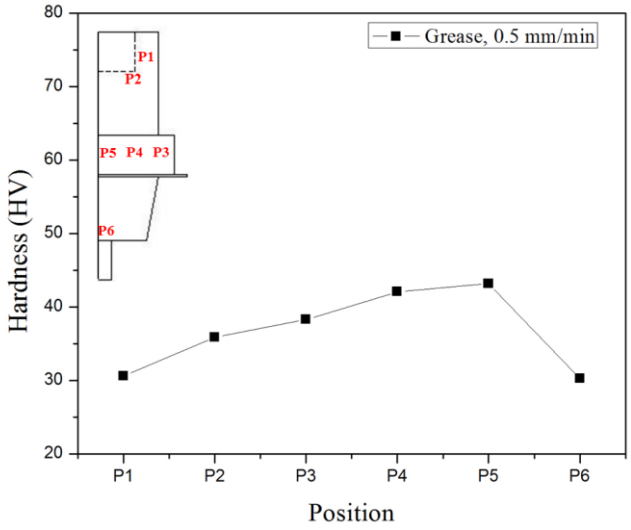

Figure 6.23: Micro hardness analyses of CCH with friction factor 0.19 at 0.5 mm/min ram displacement

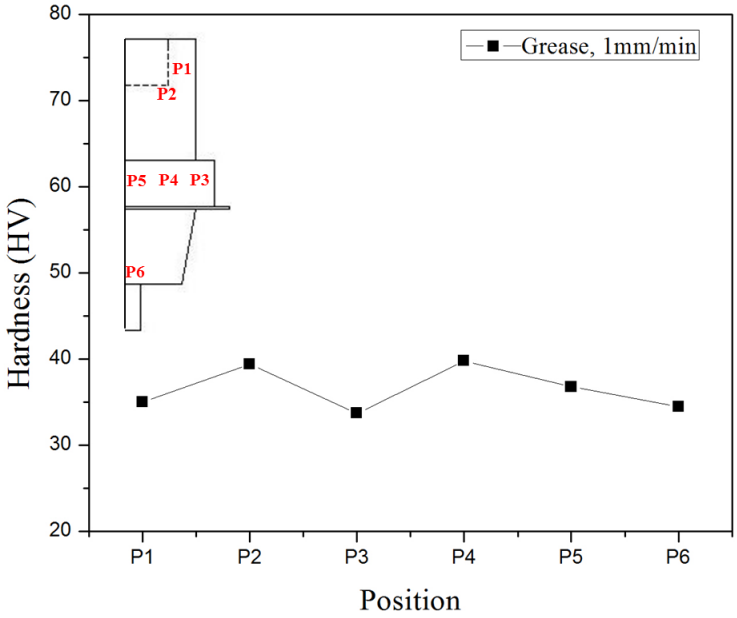

Figure 6.24: Micro hardness analyses of CCH with friction factor 0.19 at 1 mm/min ram displacement

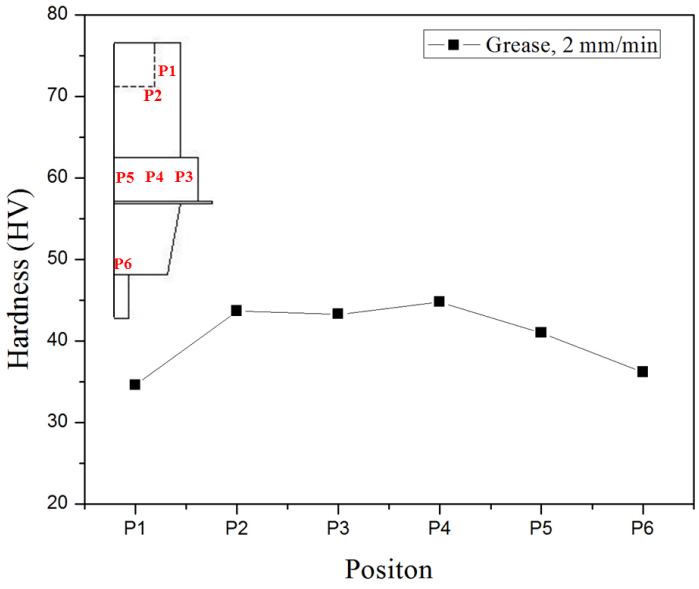

Figure 6.25: Micro hardness analyses of CCH with friction factor 0.19 at 2 mm/min ram displacement

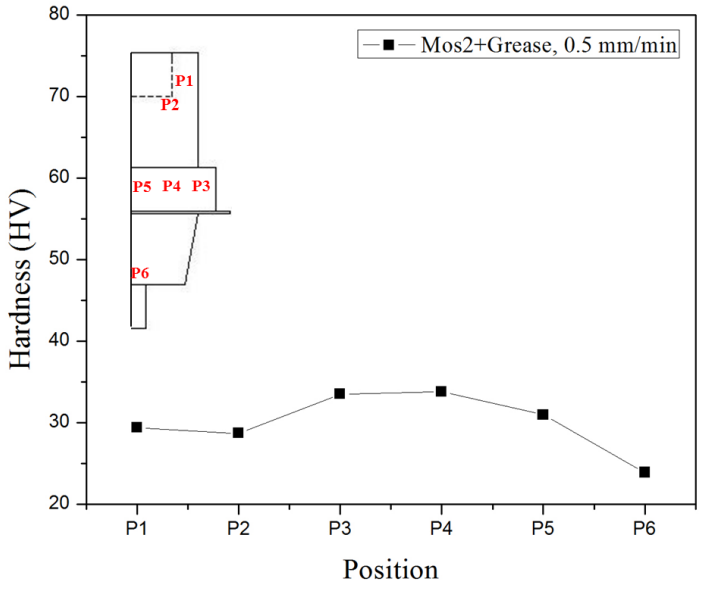

Figure 6.26: Micro hardness analyses of CCH with friction factor 0.13 at 0.5 mm/min ram displacement

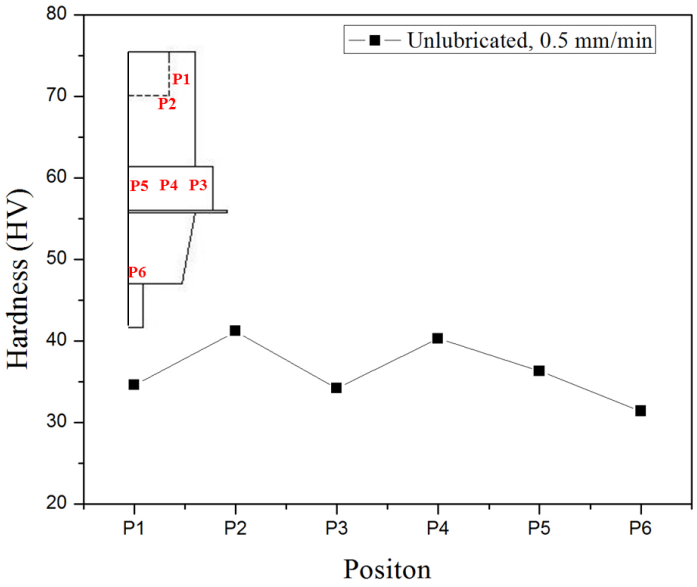

Figure 6.27: Micro hardness analyses of CCH with friction factor 0.38 at 0.5 mm/min ram displacement

6.9.1.8 Residual Stress

In the current research work analysis was performed to find out the amount of residual stress present at various locations for each component. The equipment used for the measurement is shown in the Figure 6.28. Figure 6.29 points out the various positions, where residual stress was calculated (shown in Table 6.4). Each position has its own technical significance. The values obtained are in negative, which indicates that the stresses are compressive in nature.

P1: The metal flows in backward direction, which is further subjected to some amount of shear and tensile force. The metal flowing in reverse direction leads to the maximum residual load which is also supported by cold working. It is expected that due to higher dislocations which enhances to strain hardening is the major phenomena for the maximum compressive stress.

P2: Radial extrusion with shear and metal flow gets hindered by die walls.

P3: Forward and Radial extrusion.

P4: Forward extrusion for formation of pull stud. The stress is high at this region due to the severe strain hardening when passing through constricted passage and grains are also subjected to shear.

Figure 6.28: X-Ray Powder Diffractometer

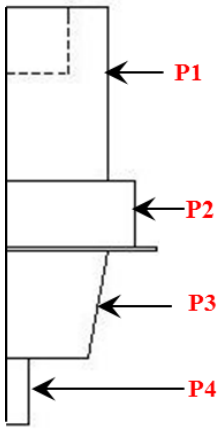

Figure 6.29: Residual stress indicating at various positions for SCCCH

Table 6.4: Residual stress values at various positions of SCCCH

Position	Residual Stress (MPa)
P1	-211.8
P2	-86.6
P3	-89.7
P4	-176.7

6.9.2 CEF Process of double collar collet chuck holder

6.9.2.1 Manufacturing process of double collar collet chuck holder

In the present study we have considered three frictional conditions,

1. Mixture of Molybdenum disulphide and Grease (60:40), friction factor (m = 0.13)
2. 100% grease, friction factor (m = 0.19) and
3. The final is dry condition friction factor (m = 0.38).

For every friction condition three varying rate of ram displacements are considered, these are 0.5 mm/min, 1 mm/min and 2 mm/min to get the double collar collet chuck holder as shown in Figure 6.30 (details dimensions are given in Figure 5.14).

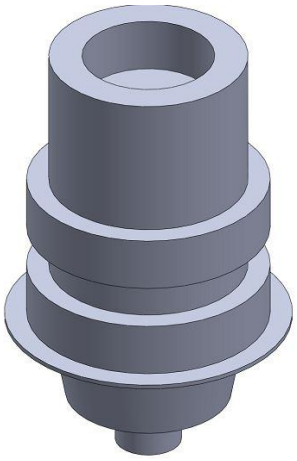

Figure 6.30: Double collar collet chuck holder manufactured by CEF process

6.9.2.2 Lubricated Conditions

Case I: (60:40 Mos2 + Grease) at different ram displacement

Experiments are carried out to manufacture the double collar collet chuck holder using combined extrusion forging process at three ram displacements, i.e., 0.5 mm/min, 1.0 mm/min and 2.0 mm/min. Initially the punch comes in contact with the billet, backward extrusion takes place. Further in the next stages forward & lateral extrusion and forging takes place to fill the die cavities for manufacturing the final component. The maximum forming loads obtained for the component to manufacture are 86.7 kN, 96.9 kN and 99.6 kN respectively (shown in Figure 6.31).

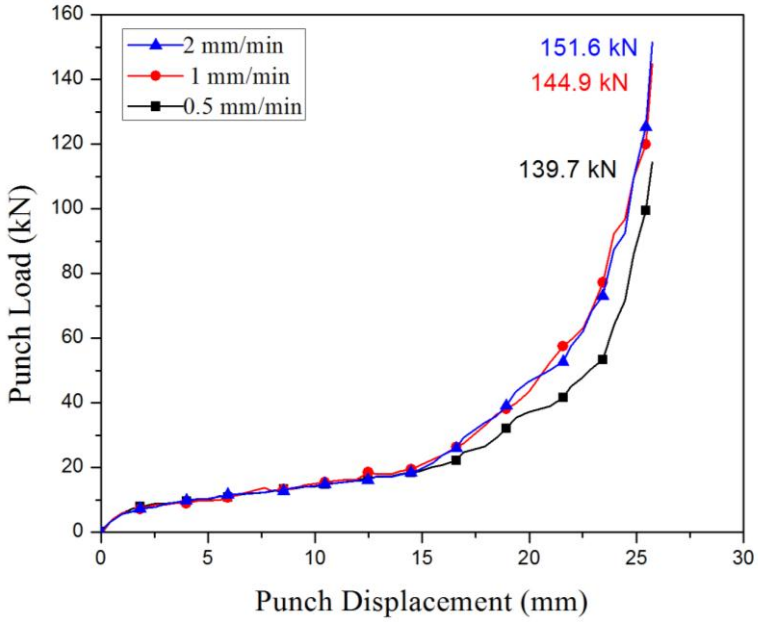

Figure 6.31: Variation of punch load with punch travel at m = 0.13

Case II: (100 % Grease) at different ram displacement

Similarly, experiments are carried out to manufacture the same double collar collet chuck holder using combined extrusion forging process at three ram displacements, i.e., 0.5 mm/min, 1.0 mm/min and 2.0 mm/min under full grease lubrication condition. The maximum forming loads obtained for the component to manufacture are 130.0, 147.9 and 156.3 kN respectively (Figure 6.32). It is found that the maximum load increases with ram velocity because of work hardening effect.

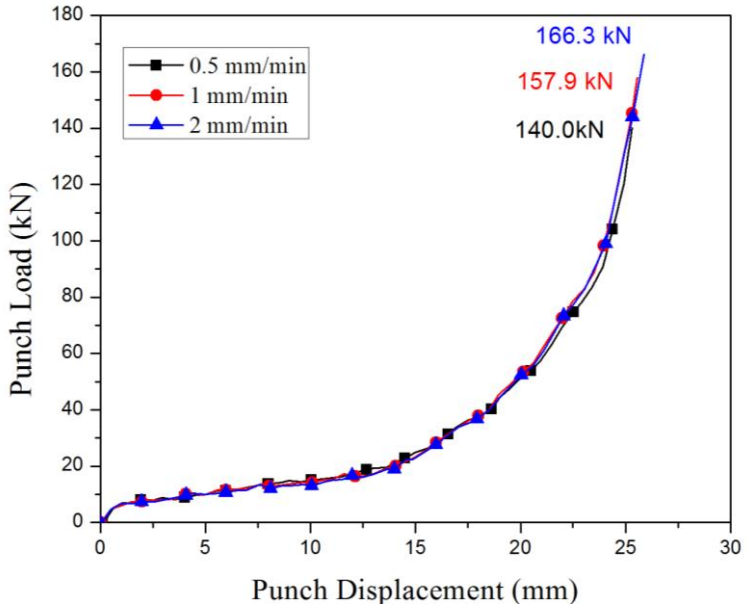

Figure 6.32: Variation of punch load with punch travel at m = 0.19

6.9.2.3 Unlubricated conditions at different ram displacement

The maximum forming loads obtained for the component to manufacture are 150, 188.3 and 199.5 kN respectively (Figure 6.33). It is also observed that the maximum load increases with ram velocity because of work hardening effect and values are more in comparison with lower friction.

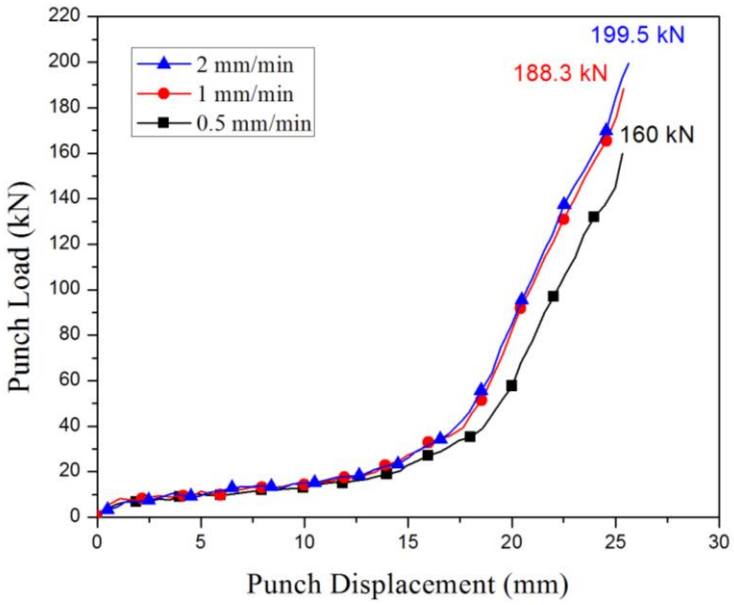

Figure 6.33: Variation of punch load with punch travel at m = 0.38

6.9.2.4 Punch loads at varying frictional conditions

The Figure 6.34 demonstrates for double collar collet chuck holder (DCCCH) by CEF process. It was observed that minimum punch load (86.7 kN) was obtained with 0.13 coefficient of friction at 0.5 mm/min rate of ram displacement. The maximum load (199 kN) was obtained with 0.38 coefficient of friction at 2 mm/min. It ensures the effects of friction and ram speed on work hardening effect.

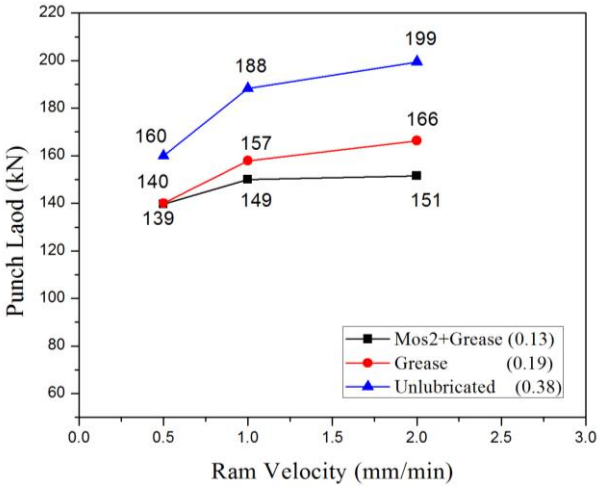

Figure 6.34: Punch load vs rate of ram displacement for double collar collet chuck holder

6.9.2.5 Die filling

Figure 6.35 shows the shape of the product at different punch movement, for combined extrusion-forging process, obtained from experiments at a ram velocity of 1 mm/min and at friction factor of 0.19. It explains that combined extrusion-forging process takes place till the die cavity is completely filled. It was observed that the maximum displacement required for filling the die cavities is 25.3 mm.

(a) Stage I 8.47 mm punch travel | (b) Stage II 16.6 mm punch travel | (c) Stage III 23.4 mm punch travel | (d) Stage IV 25.3 mm punch travel

Figure 6.35: Die filling at different punch movement

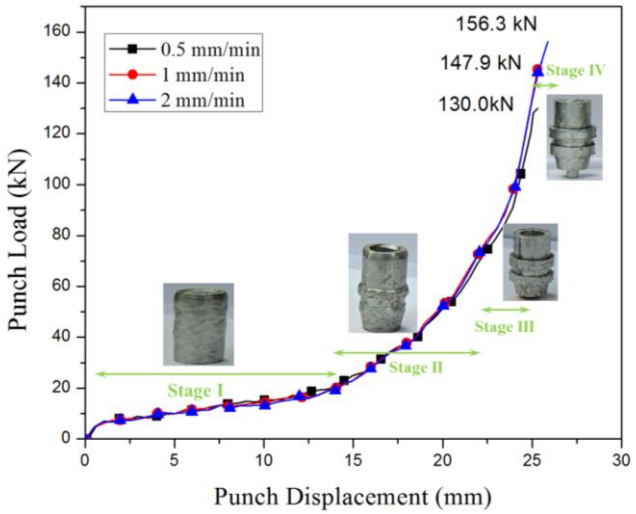

Figure 6.36: Product shape at different punch position

Referring to the Figures 6.35-36, it is seen that the whole process consists of four major stages. It can be explained as follows:

Stage I

In this stage the punch head comes in contact with the billet and applies initial compression. The load gradually increases when the circular punch head penetrates into the billet, this leads to backward extrusion. It can also be named as coining stage, because of the coin shaped indent formed by the punch head on the billet for the backward extrusion. The Figure 6.35(a) represents the stage I process for clear view of the component which has been subjected to CEF process. The displacement takes place in the present stage is 0 - 8.47 mm

Stage II

In this stage load increases slowly with respect to punch movement. Forward and lateral extrusions take place simultaneously. Figure 6.35(b) represents the stage II process, which takes place during the 8.47 - 16.6 mm ram movement.

Stage III

During this stage, 16.6 - 23.4 mm of ram movement, metal flows to fill all the geometrical corner points Figure 6.35(c). As metal flow a longer path, it requires more redundant work, gives a steep rise of load.

Stage IV

The final unsteady stage takes place, between 23.4 - 25.3 mm of ram movement, where the metal flows through the constricted passage to form flash. Because of high friction and

redundant work, there is a sharp increase in the load. The Figure 6.35(d) represents the stage IV for the product manufactured by CEF process. The flash is designed in such a way that the extra metal expels out only when the entire die cavities are filled.

6.9.2.6 Metal flow pattern (Sectional View)

As an illustration, Figure 6.37 shows the photograph of the flow pattern for extrusion-forging process of a double collar collet chuck holder at ram velocity of 1 mm/min and friction factor of 0.19 during different punch movement obtained from experiments. The severe grid line distortions at the last two stages confirm the maximum amount of redundant work that is responsible for the steep rise in load.

(a) Stage I 8.47 mm punch travel | (b) Stage II 16.6 mm punch travel | (c) Stage III 23.4 mm punch travel | (d) Stage IV 25.3 mm punch travel

Figure 6.37: Flow pattern at different punch movement

6.9.2.7 Microscopy analysis of double collar collet chuck holder

Similar to SCCCH, specimens are prepared and microscopic analyses are performed for five components manufactured at different working conditions (Table 6.5).

Table 6.5: Various conditions considered for experimentation of double CCH

Component No.	Friction Factor	Ram Displacement (mm/min)
1	0.13	0.5
2	0.13	1.0
3	0.13	2.0
4	0.19	2.0
5	0.38	2.0

Figures 6.38 illustrates the microstructure at five different zones of the sample at ram speed of 0.5 mm/min and m = 0.13. It is observed that no abrupt microstructural change has been observed at this low ram displacement and friction condition. Similarly Figure 6.39 illustrates the microstructures at ram speed of 1.0 mm/min and m = 0.13, which experiences different type of extrusion/forging processes. Microstructure of the material shows medium sized elongated grains along metal flow direction. Similarly Figures 6.40 - 6.42 illustrates the grain elongations and direction changes at five zones satisfying severity of metal flow and direction change.

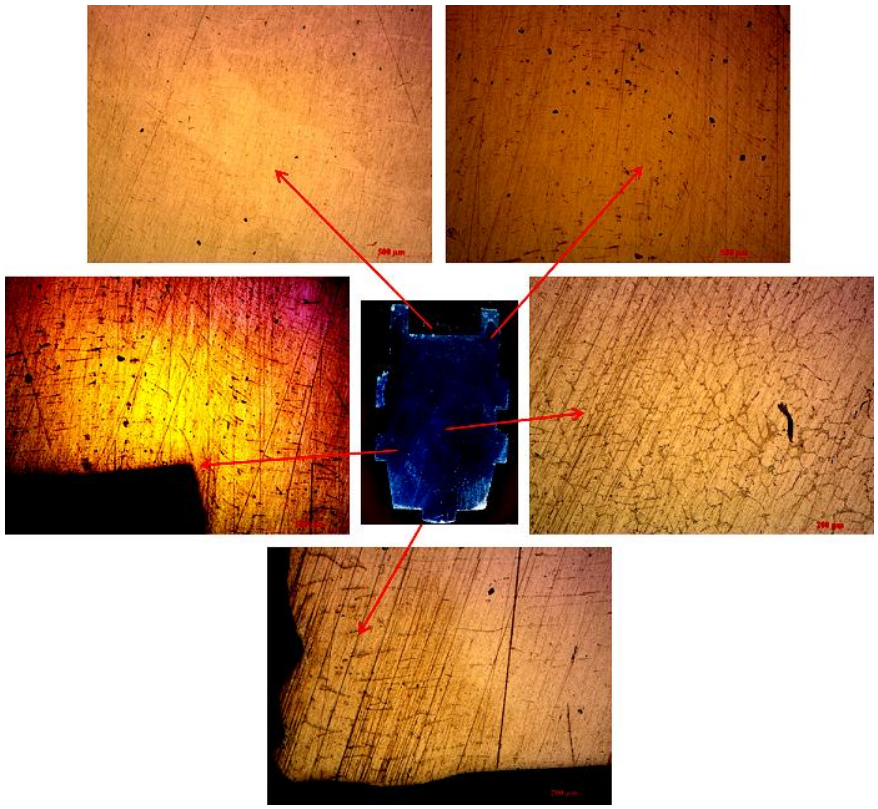

Figure 6.38: Microscopic analyses of double collar CCH with friction factor 0.13 at 0.5 mm/min ram displacement

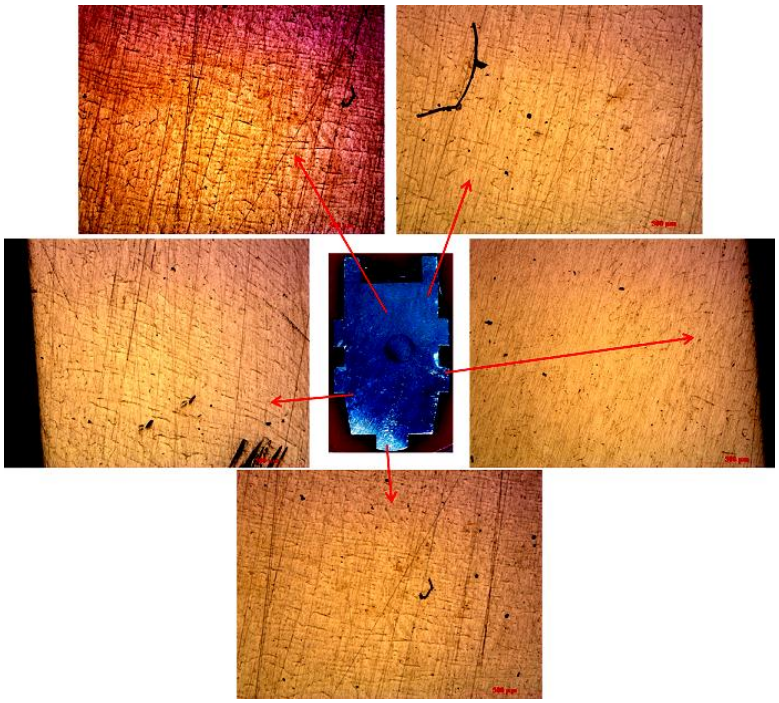

Figure 6.39: Microscopic analyses of double collar CCH with friction factor 0.13 at 1 mm/min ram displacement

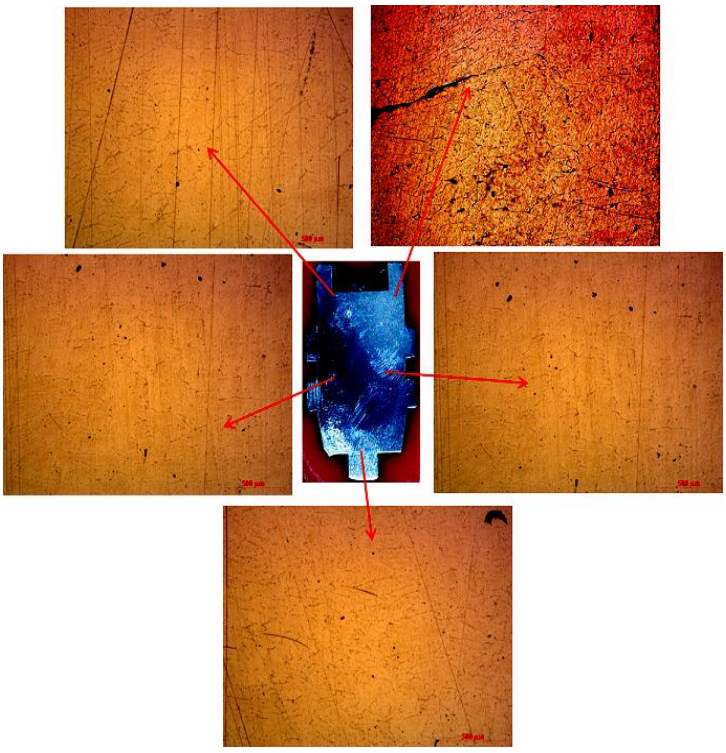

Figure 6.40: Microscopic analyses of double collar CCH with friction factor 0.13 at 2 mm/min ram displacement

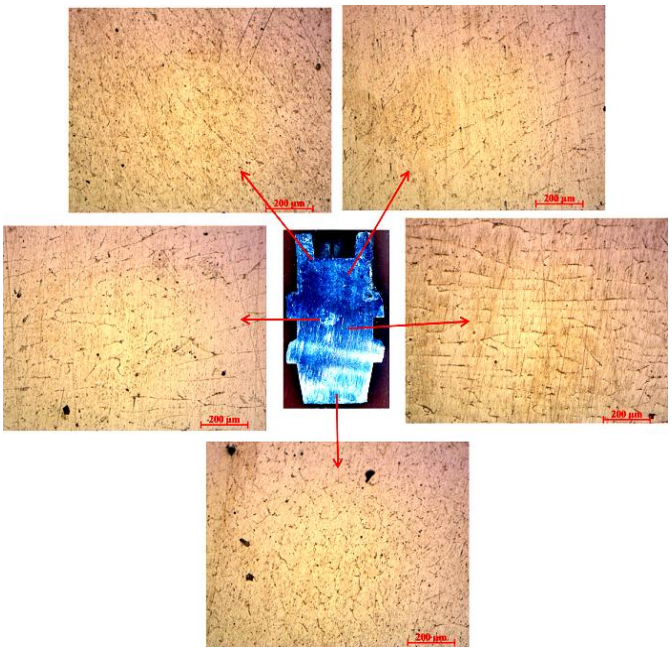

Figure 6.41: Microscopic analyses of double collar CCH with friction factor 0.19 at 2 mm/min ram displacement

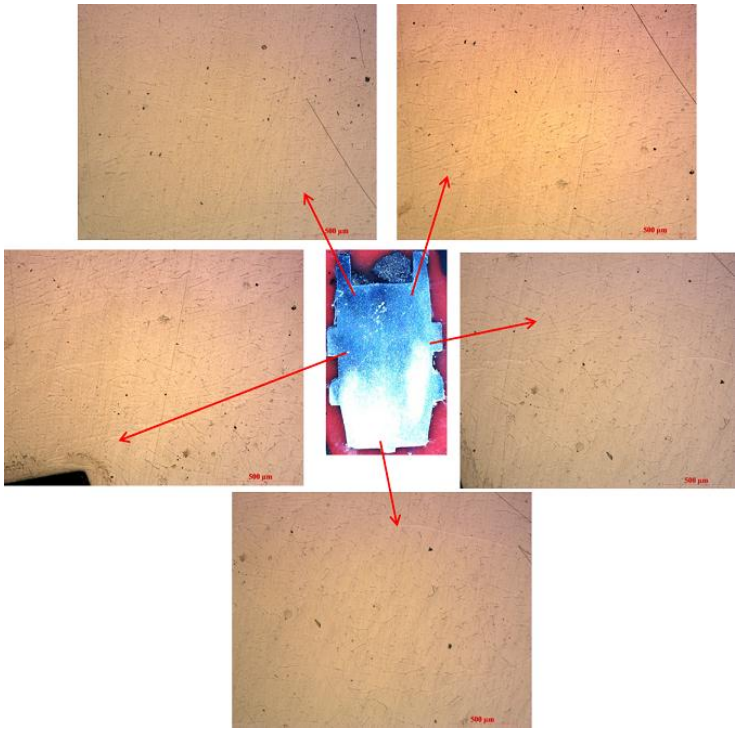

Figure 6.42: Microscopic analyses of double collar CCH with friction factor 0.38 at 2 mm/min ram displacement

6.9.2.7 Micro hardness analysis of double collar collet chuck holder

It is evident that as the grains dislocate and change its shape, there is a high tendency for change in the hardness of the component. The present analysis deals with measuring the

hardness of the five components manufactured under the two working conditions (mentioned in Table 6.3) are considered. As shown in Figures 6.43-6.47, microhardness of the components depends on the position and metal flow conditions as explained in section 6.9.1.7. It is also obsevered that hardness is high at points P2, P4 for higher friction and at P5 for low friction condition due to the variation of severity in change of grain flow directions.

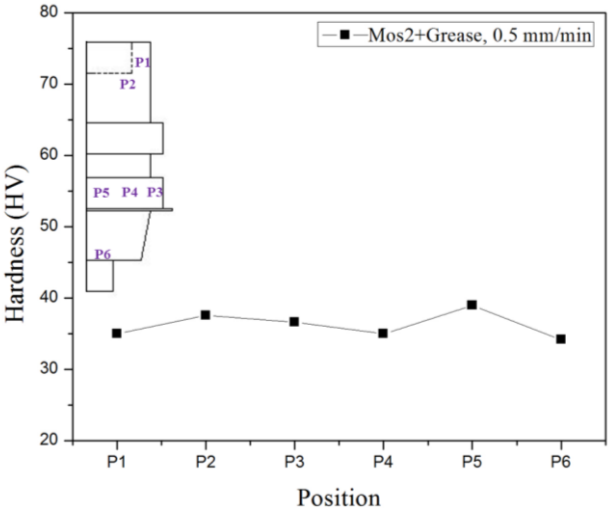

Figure 6.43 Micro hardness analyses of double collar CCH with friction factor 0.13 at 0.5 mm/min ram displacement

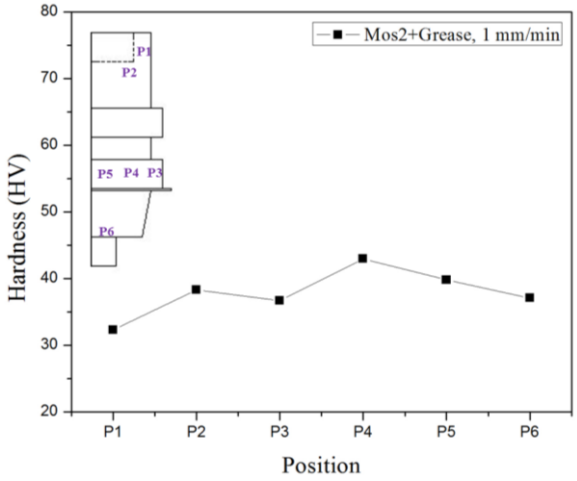

Figure 6.44: Micro hardness analyses of double collar CCH with friction factor 0.13 at 1 mm/min ram displacement

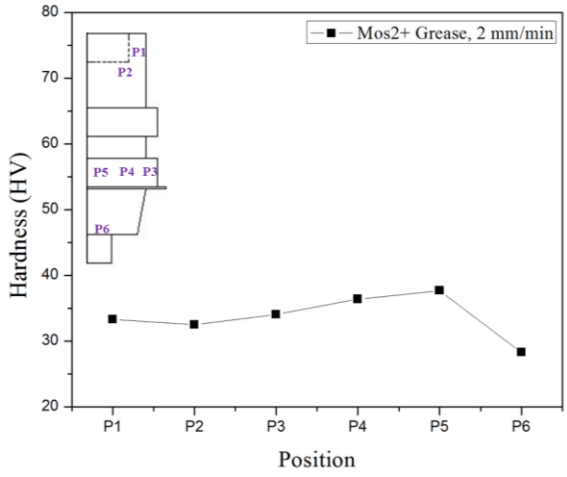

Figure 6.45: Micro hardness analyses of double collar CCH with friction factor 0.13 at 2 mm/min ram displacement

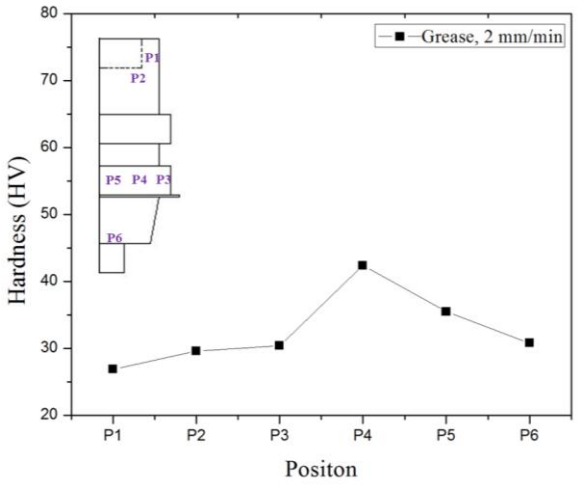

Figure 6.46: Micro hardness analyses of double collar CCH with friction factor 0.19 at 2 mm/min ram displacement

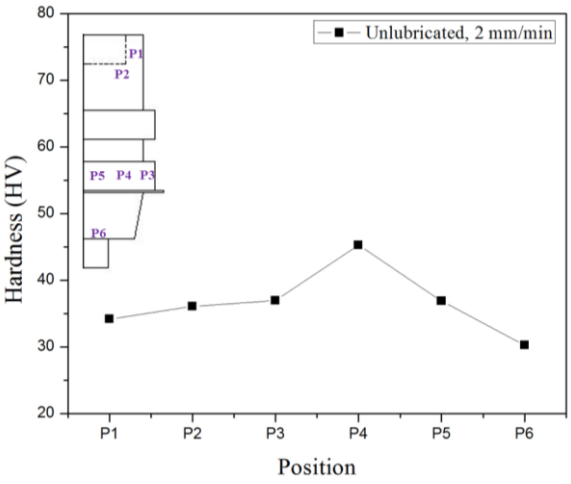

Figure 6.47: Micro hardness analyses of double collar CCH with friction factor 0.38 at 1.0 mm/min ram displacement

6.9.2.8 Residual Stress

Residual stresses measured at five points (shown in Figure 6.48) are shown in Table 6.6. As explained in section 6.9.1.8 residual stresses are compressive in nature and maximum at bottom stud and minimum at collar.

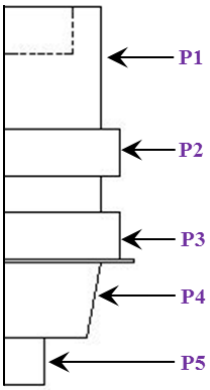

Figure 6.48: Residual stress indicating at various positions for DCCCH

Table 6.6: Residual stress values at various positions of DCCCH

Position	Residual Stress (MPa)
P1	-79.3
P2	-109.1
P3	-42.0
P4	-111.2
P5	-128.9

6.9.3 CE process of double collar collet chuck holder

6.9.3.1 Manufacturing process of double collar collet chuck holder

The double collar collet chuck holder as shown in Figure 6.49 (details dimensions are given in Figure 5.23) is manufactured by a set of dies in which the bottom die is kept open. Hence, flash provision is not engraved on the die and direct extrusion takes place at the last stage. In the present study three frictional conditions, namely, m = 0.13, 0.19 and 0.38 is considered with three ram speeds (0.5 mm/min, 1 mm/min and 2 mm/min).

Figure 6.49: Double collar collet chuck holder manufactured by CE process

6.9.3.2 Effect of friction at different ram velocities

Figures 6.50-6.52 show the load variations with ram displacement (at velocities 0.5 mm/min, 1.0 mm/min and 2.0 mm/min) at frictional conditions m=0.13, 0.19 and 0.38 respectively.

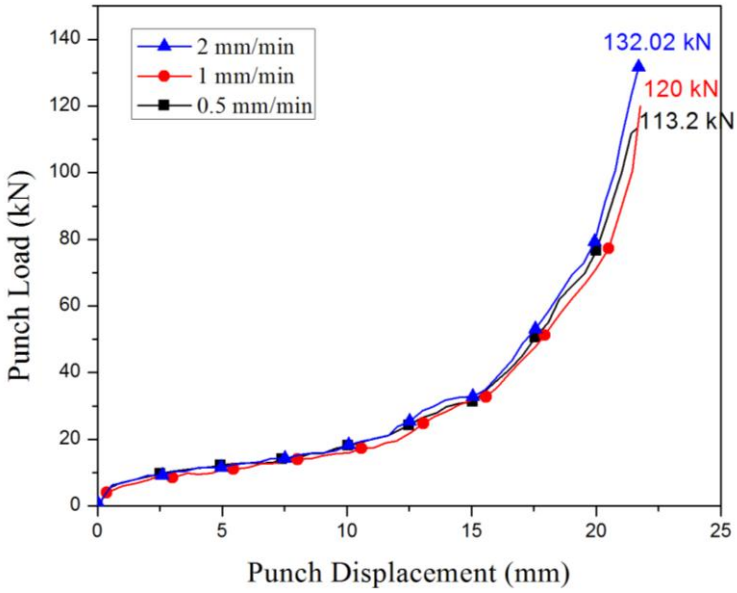

Figure 6.50: Variation of punch load with ram displacement at m = 0.13

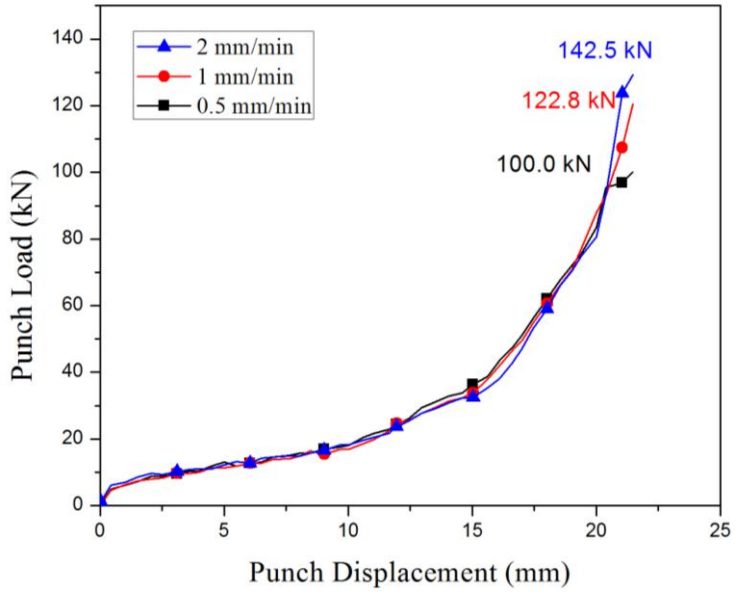

Figure 6.51: Variation of punch load with punch travel at m = 0.19

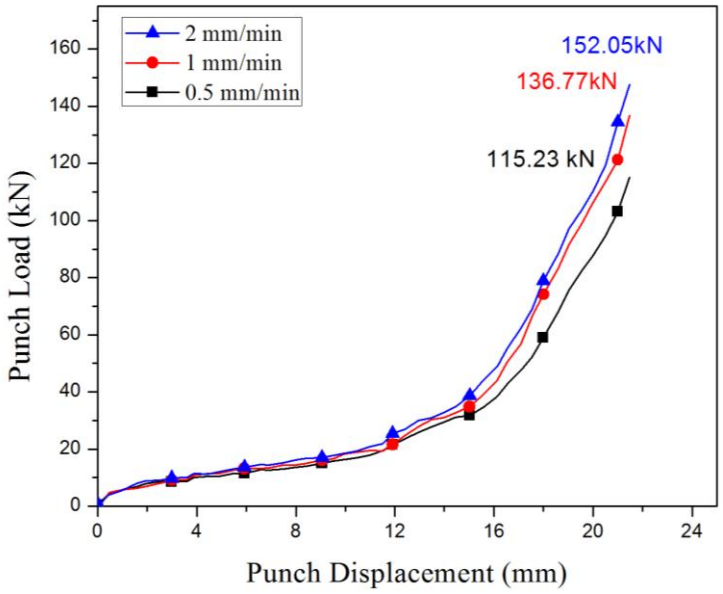

Figure 6.52: Variation of punch load with ram displacement at m = 0.38

It is evident that maximum punch load increases with ram velocity and friction because of work hardening effect. Figure 6.53 shows that minimum punch load (100 kN) was obtained with 0.13 coefficient of friction at 0.5 mm/min rate of ram displacement. The maximum load (152 kN) was obtained with 0.38 coefficient of friction at 2 mm/min.

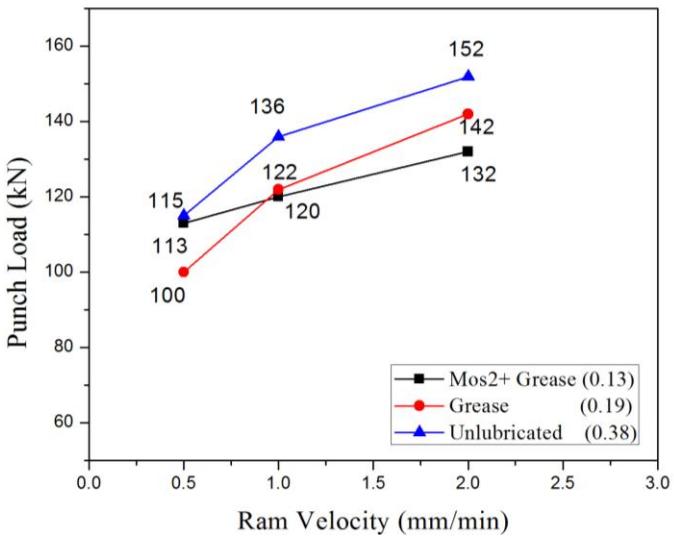

Figure 6.53: Punch load Vs Rate of ram displacement for single collar collet chuck holder

6.9.3.3 Die filling

Figure 6.54 shows the shape of the product at different punch movement, for combined extrusion process, obtained from both FEM simulation and experiment at a ram velocity of 2 mm/min with friction factor of 0.38. It was observed that the maximum displacement required for filling the die cavities is 21.4 mm.

(a) Stage I 6.71 mm punch travel

(b) Stage II 12.8 mm punch travel

(c) Stage III 18.6 mm punch travel

(d) Stage IV 21.3 mm punch travel

Figure 6.54: Die filling at different punch movement

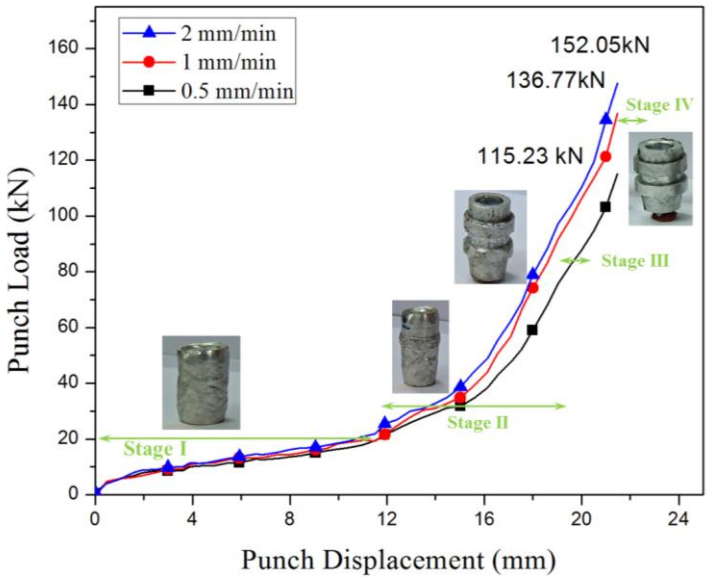

Figure 6.55: Product shape at different punch position

Referring to the Figures 6.54 - 6.55, it is seen that the whole process consists of four major stages as explained in section 6.9.2.5.

Stage I: Initial stage, in which the load gradually increases and backward extrusion takes place. The displacement takes place in the present stage is 0 - 6.71 mm.

Stage II: Second stage, in which forward and lateral extrusion takes place, which takes place during the 6.71 - 12.8 mm ram movement.

Stage III: During this stage, 12.8 - 18.6 mm of ram movement, which is a combined stage, both extrusion and forging takes place for corner filling.

Stage IV: Forward extrusion stage, between 18.6 - 21.3 mm of ram movement.

6.9.3.4 Metal flow pattern (Sectional View)

As an illustration, Figure 6.56 shows the photograph of the flow pattern for extrusion/forging process of a double collar collet chuck holder at ram velocity of 2 mm/min and friction factor of 0.38 during different punch movement obtained from experiments. The severe grid line distortions at the last two stages confirm the maximum amount of redundant work that is responsible for the steep rise in load.

(a) Stage I 6.71 mm punch travel | (b) Stage II 12.8 mm punch travel | (c) Stage III 18.6 mm punch travel | (d) Stage IV 21.3 mm punch travel

Figure 6.56: Flow pattern at different punch movement

6.9.3.5 Microscopy analysis of double collar CCH by CE process

As explained earlier, specimens are prepared and microscopic analyses are performed for five components manufactured at different working conditions (Table 6.7).

Table 6.7: Various conditions considered for experimentation of Single CCH

Component No.	Friction Factor	Ram Displacement (mm/min)
1	0.38	0.5
2	0.38	1.0
3	0.38	2.0
4	0.13	1.0
5	0.19	1.0

Figures 6.57 - 6.58 illustrates the microstructure at five different zones of the sample at m = 0.38 and ram speed of 0.5 mm/min and 1.0 mm/min respectively. Microstructural changes has been observed at this higher frictional condition where the metal sticks the die wall due to the no lubrication condition even at lower ram displacement. Similarly, Figure 6.59 illustrates the microstructures at ram speed of 2.0 mm/min and m = 0.38, shows fine sized elongated grains, indicating material experiences both shear and normal strain during the formation of cup shape at the top, collar ring at the centre and stud at the bottom. Similarly Figures 6.60 - 6.61 illustrates the grain elongations and direction changes at five zones satisfying severity of metal flow and direction change.

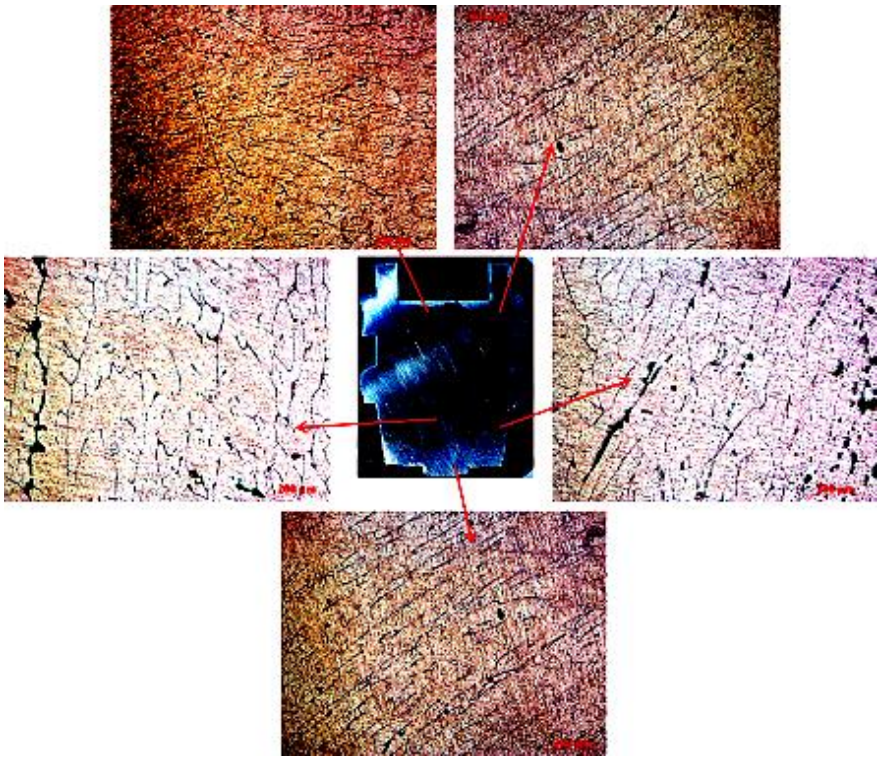

Figure 6.57: Microscopic analyses of double collar CCH with friction factor 0.38 at 0.5 mm/min ram displacement

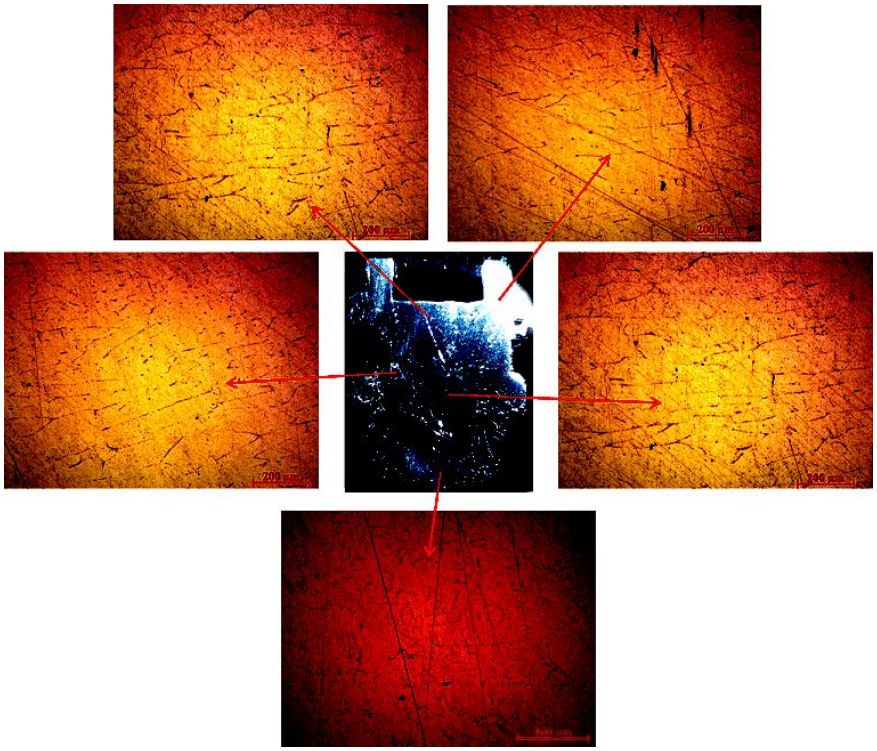

Figure 6.58: Microscopic analyses of double collar CCH with friction factor 0.38 at 1 mm/min ram displacement

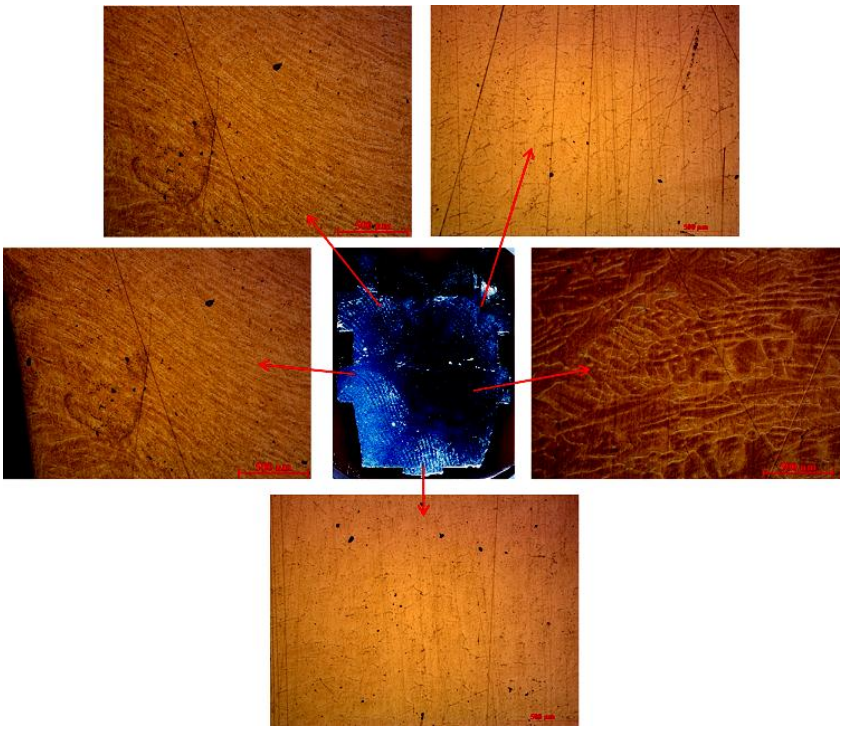

Figure 6.59: Microscopic analyses of double collar CCH with friction factor 0.38 at 2 mm/min ram displacement

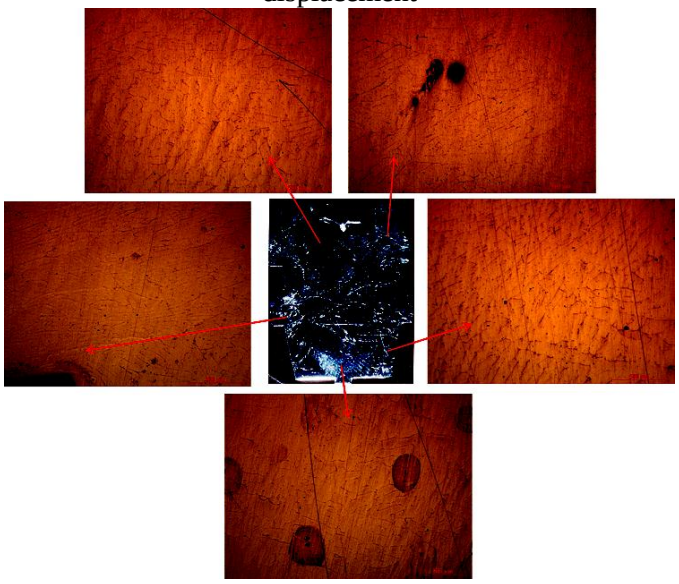

Figure 6.60: Microscopic analyses of double collar CCH with friction factor 0.13 at 1 mm/min ram displacement

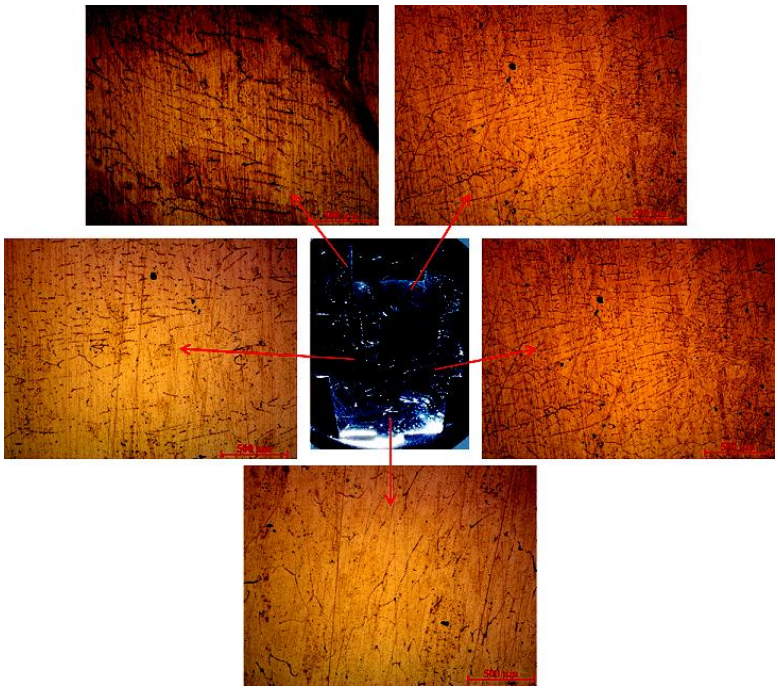

Figure 6.61: Microscopic analyses of double collar CCH with friction factor 0.19 at 1 mm/min ram displacement

6.9.3.6 Micro hardness analysis of double collar collet chuck holder by CE process

It is evident that as the grains dislocate and change its shape, there is a high tendency for change in the hardness of the component. The present analysis deals with measuring the hardness of the six components manufactured under the two working conditions (mentioned in Table 6.5) are considered. As shown in Figures 6.62 - 6.66, microhardness of the components depends on the position and metal flow conditions as explained in section 6.9.2.7. The results conclude that the component manufactured under higher ram displacement and frictional condition as shown in the Figure 6.64 gives higher hardness. At the same time, hardness vary at different location, which depend on severity in change of grain flow directions.

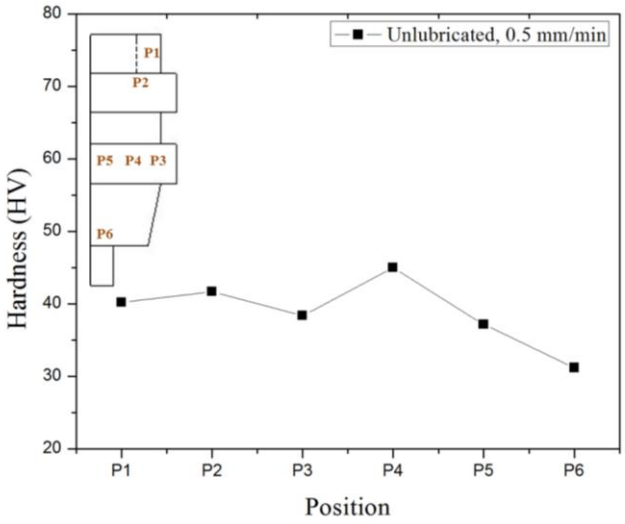

Figure 6.62: Micro-hardness analyses of double collar CCH with friction factor 0.38 at 0.5 mm/min ram displacement

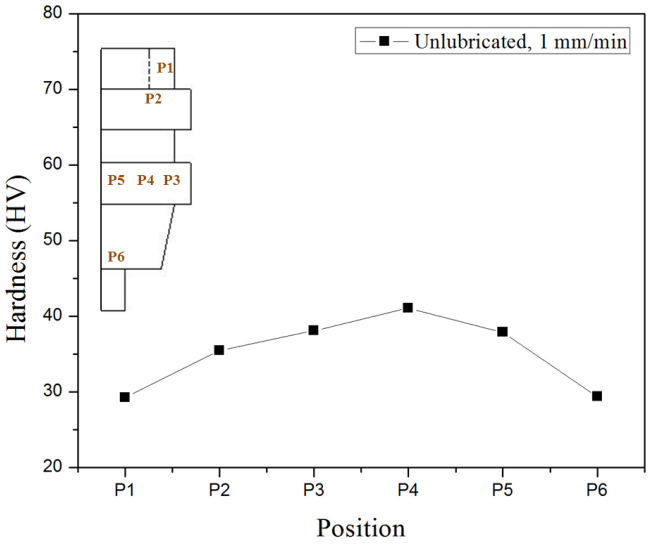

Figure 6.63: Micro-hardness analyses of double collar CCH with friction factor 0.38 at 1 mm/min ram displacement

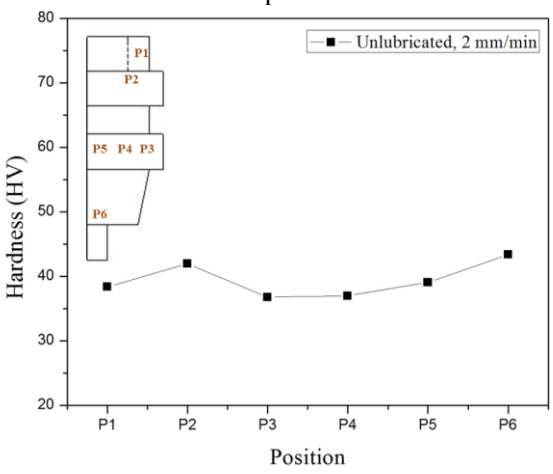

Figure 6.64: Micro-hardness analyses of double collar CCH with friction factor 0.38 at 2 mm/min ram displacement

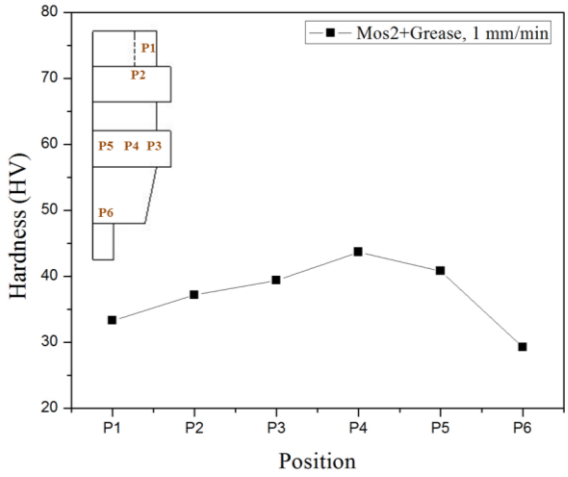

Figure 6.65: Micro-hardness analyses of double collar CCH with friction factor 0.13 at 1 mm/min ram displacement

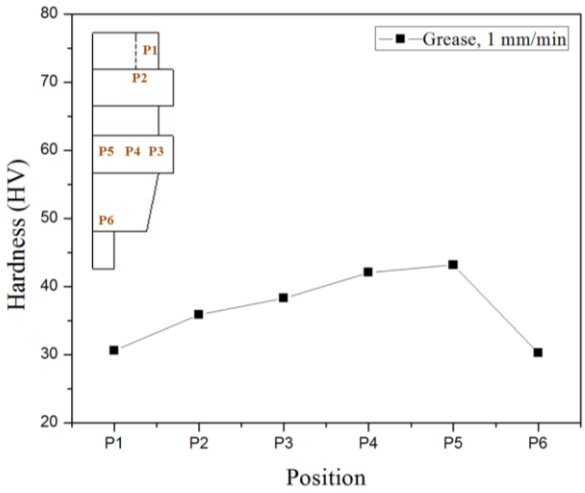

Figure 6.66: Micro-hardness analyses of double collar CCH with friction factor 0.19 at 1 mm/min ram displacement

6.9.3.7 Residual Stress

Residual stresses measured at five points (shown in Figure 6.67) are shown in Table 6.8. As explained in section 6.9.1.8 residual stresses are compressive in nature and maximum at bottom stud (pass through a constricted passage) and minimum at collar (no severe grain flow change occur).

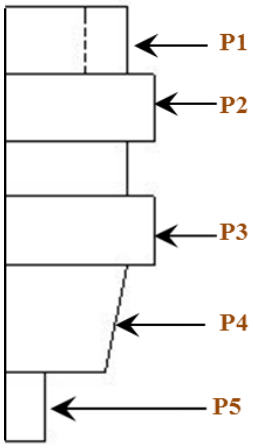

Figure 6.67: Residual stress indicating at various positions for DCCCH by CE process

Table 6.8: Residual stress values at various positions of DCCCH by CE process

Position	Residual Stress (MPa)
P1	-232.6
P2	-105.8
P3	-75.8
P4	-116.7
P5	-165.5

6.9.4 Multistage extrusion/forging of single collar collet chuck holder

The present experimental analysis is an approach of multistage extrusion/forging to manufacture a single collar collet chuck holder. The concept deals with the use of multi-stage combined extrusion-forging technique for processing a component without defects. The first product (single collar collet chuck holder) is the input specimen for the present experimentation to get the final product shown in Figure 6.68 (Detail dimensions are provided in Figure 5.32). In the present study we have considered grease (m = 0.13) as lubricant with a ram displacement of 1 mm/min for the experimental analyses.

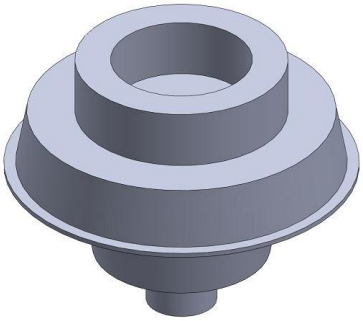

Figure 6.68: Single collar collet chuck holder manufactured by multistage CEF process

6.9.4.1 Variation of punch load with ram displacement

Figures 6.69 shows the load variation with ram displacement at ram velocity of 1.0 mm/min and frictional condition of m = 0.13. It is evident that punch load increases with ram displacement and reaches maximum value during flashing.

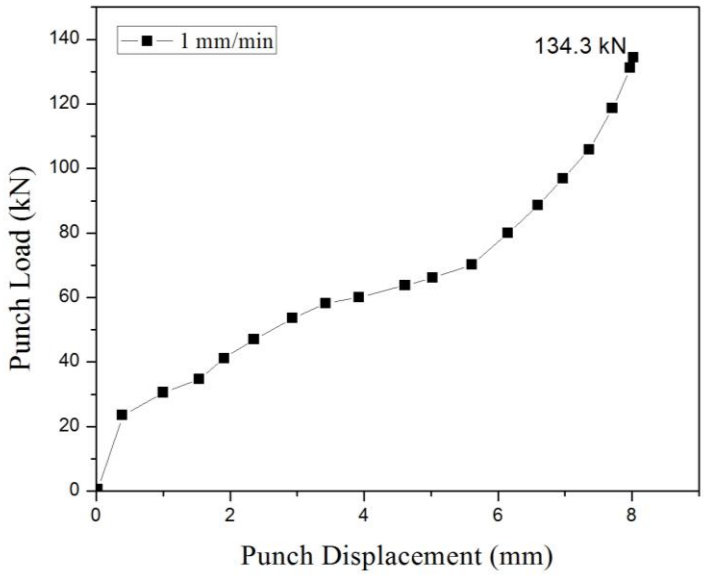

Figure 6.69: Variation of punch load with ram displacement

6.9.4.2 Die Filling

Figure 6.70 shows the shape of the product at different punch movement, for Multistage combined extrusion-forging process, obtained from experiments at a ram velocity of 1mm/min with friction factor 0.19. It was observed that the maximum displacement required for filling the die cavities was 8.2 mm.

Stage I Stage II

After 3.0 mm punch travel | After 6.0 mm punch travel | After 8.0 mm punch travel | After 8.2 mm punch travel

Figure 6.70: Die filling at different punch movement

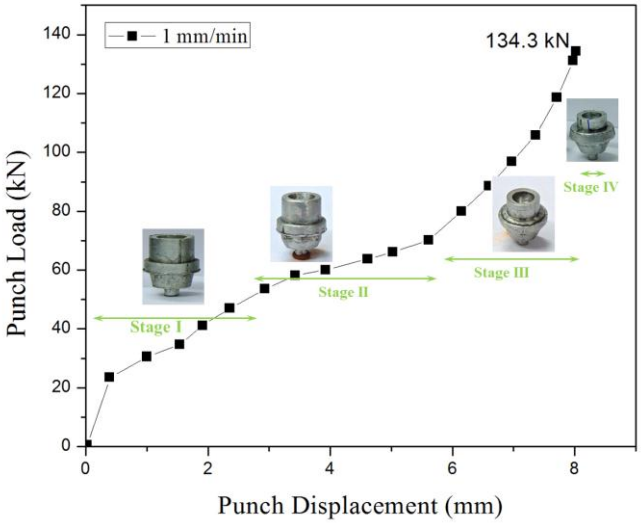

Figure 6.71: Product shape at different punch position

Referring to the Figures 6.70 - 71, it is seen that the whole process consists of two major stages. It can be explained as follows:

(iii) Initial compression stage (0 - 6.0 mm) with cavity filling by forward, bacward and lateral extrusion,

(iv) Second stage (6.0 - 8.2 mm), to form flash.

6.9.4.3 Metal flow pattern (Sectional View)

As an illustration, Figure 6.72 shows the photograph of the flow pattern for Multistage combined extrusion-forging process of a single collar collet chuck holder at ram velocity of 1 mm/min and friction factor of 0.19 during different punch movement obtained from experiments. The severe grid line distortions at the last two stages confirm the maximum amount of redundant work that is responsible for the steep rise in load.

After 3.0 mm punch travel | After 6.0 mm punch travel | After 8.0 mm punch travel | After 8.2 mm punch travel

Figure 6.72: Flow pattern at different punch movement

6.9.4.4 Microscopic analysis of Multistage extruded component

The Figures 6.73 illustrates the images of the cross-section of the multistage CEF of single collar collet chuck holder manufactured at 0.19 frictional and 1 mm/min ram displacement and examined at four different locations by optical microscope. The top right location indicate backward extrusion, grain flow is subjected to shear due to the reverse flow for the formation of cup. The centre left and centre points indicate lateral and forward extrusion where the metal is subjected to shear deformation for the formation of the collar ring and flash. The last point indicates the forward extrusion which is due to formation of the stud like element at the bottom when passed through a constricted opening. As the present product is manufactured taking first product as input, grain elongations and direction changes are not severe in comparison to that of the first product (Figure 6.18).

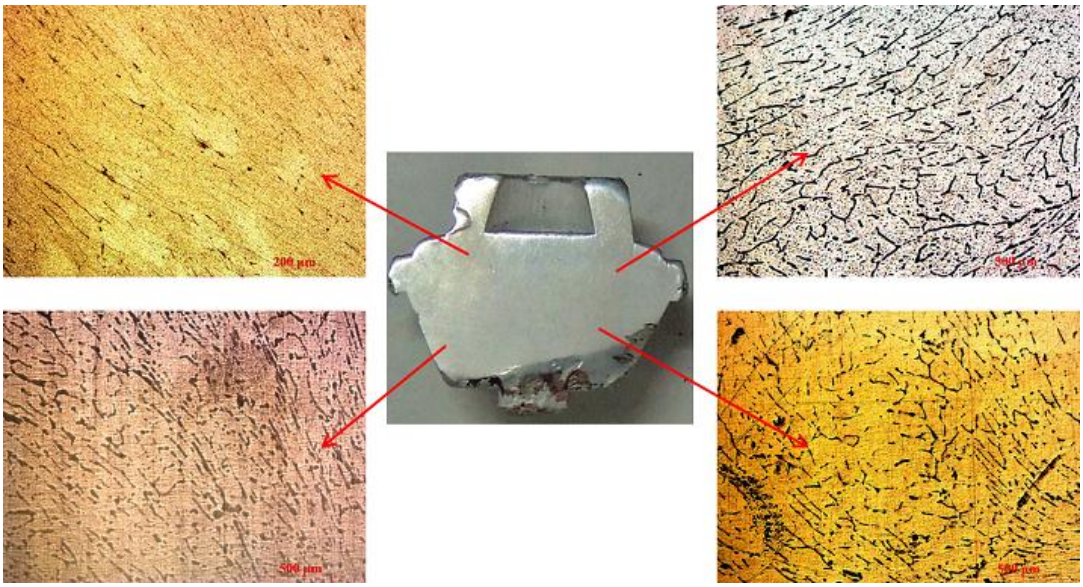

Figure 6.73: Microscopic analyses of Multistage CEF of single collar CCH with friction factor 0.19 at 1 mm/min ram displacement

6.9.4.5 Micro hardness analysis of single collar collet chuck holder

The present analysis deals with measuring the hardness at six different locations as shown in Figure 6.74. The measuring locations P1 - P6 are indicated on each component's middle cross sectional plane. An average of three readings is considered at every point. It is evident that as the grains dislocate and change its shape there is a high tendency for change in the hardness at different location, which depend on severity in change of grain flow directions. For the present product, as it is subjected to CEF processes two times, the hardness (due to work hardening) is higher than that of the input first product.

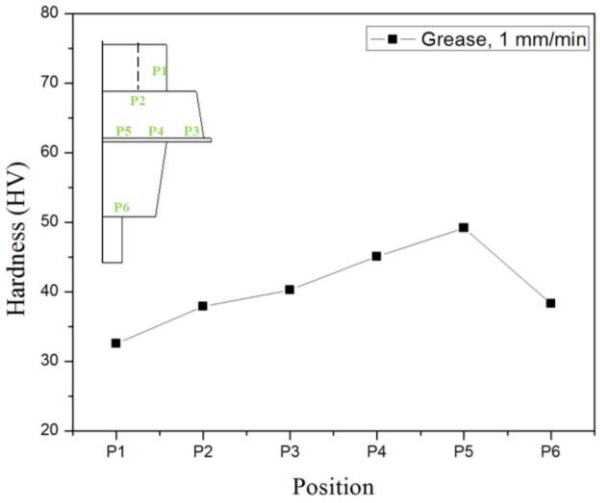

Figure 6.74: Microscopic analyses of single collar CCH with friction factor 0.19 at 1 mm/min ram displacement

6.9.4.6 Residual Stress

Residual stresses measured at five points (shown in Figure 6.75) are shown in Table 6.9. As explained in section 6.9.1.8 residual stresses are compressive in nature and maximum at bottom stud (pass through a constricted passage) and minimum at collar (minimum hindrance to flow).

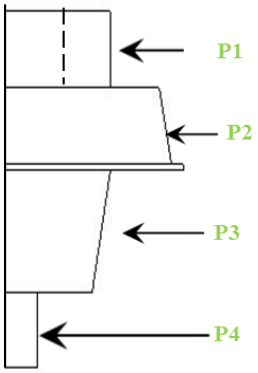

Figure 6.75: Residual stress indicating at various positions for SCCCH

Table 6.9: Residual stress values at various positions of SCCCH

Position	Residual Stress (MPa)
P1	-233.8
P2	-91.4
P3	-109.7
P4	-186.7

6.10 Conclusions

In the present research work, experimental analyses have been performed for manufacturing different types of collet chuck holders by combined extrusion-forging and combined extrusion processes. The following observations have been made based on the obtained results:

- Split dies with container and punch are successfully designed and fabricated to manufacture different type of collet chuck holders using the principle of combined/multi-stage extrusion/forging processes.
- Good numbers of experiments have been performed at various coefficients of friction along with different rate of ram displacements.
- It is observed that the complete process to get the first three components can be assumed to compose of four stages and fourth one of two stages with regard to forward/backward extrusion, forging, die corner filling, and flash formation
- From the load ~ displacement behaviour, it is seen that the forming load increases with punch movement. The rate of load increases with more redundant work when simultaneous backward, forward and lateral extrusions take place to fill the die cavities. The load increased unsteadily at last stage when corners are filled, and flash is formed.
- The minimum and maximum forming load are 149.5 kN and 219.5 kN obtained for SCCCH manufactured by CEF process. The results were obtained at 0.13 frictional conditions with 0.5 mm/min ram velocity and 0.38 frictional conditions at 2 mm/min ram velocity.
- Similarly for DCCCH manufactured by CEF and CE processes, the maximum forming loads are 199.5 kN and 152.0 kN obtained with 0.38 frictional condition at 0.2 mm/min ram velocity. The minimum forming loads are 139.5 kN and 113.2 kN obtained with 0.13 frictional condition with 0.5 mm/min ram velocity.
- Experiments are carried out for different punch movements (ram velocity) to observe the die filling and flow pattern of the metal.
- The microscopic and micro hardness analyses shown at various stages/locations validate the presence of severe plastic deformation along with the elongated and deformed grains. The Vickers's hardness was high at the central region (near the collar ring) for the component manufactured by multistage extrusion process.
- The Residual stress analysis performed for all the four components manufactured under different frictional conditions and ram velocities. All the stresses were found to be

compressive in nature. The Maximum stress was obtained at the near collar pocket region by the multistage extrusion process for a SCCCH.

The obtained experimental results have been compared with that obtained from FEM and analytical results in an elaborated manner in the next chapter.

Chapter 7

Comparison of Results and Discussion

7.1 Introduction

The primary objective of the present work is to manufacture different types of collet chuck holders using combined extrusion-forging and combined extrusion processes to obtain better mechanical properties, less material wastage by an economical way in comparison to other conventional methods currently followed in industries. To substantiate the idea, the proposed combined extrusion-forging and combined extrusion processes are analysed by upper bound method, finite element method and experiments are carried out for different types of collet chuck holders. Hence, it is imperative to compare the results obtained by different route's to validate the proposed methods of analyses.

7.2 Comparison of Results for SCCCH by CEF Process

The comparisons of results for various frictional conditions are indicated in Figures 7.1-7.3. From the load–ram displacement behaviour, we can think of the whole process consists of four stages.

In stage I, initial compression takes place where the load gradually increases when the circular punch head penetrates into the billet, leads to backward extrusion. Simultaneously, forward extrusion of taper part is also done. Due to the gradual increase in load, the grains gets compressed, and even grain elongation takes place. The load prediction by different analyses at the end of this stage varies between 14 - 19 kN, 16 - 20 kN, and 16 - 21 kN at ram velocity of 0.5 mm/min for m = 0.13; 15 - 21 kN, 17 - 21 kN, and 17 - 21 kN at ram velocity of 1.0 mm/min for m = 0.19; 13 - 21 kN, 13 - 21 kN, and 15 - 22 kN at ram velocity of 2.0 mm/min for m = 0.38.

In stage II, the metal flows in forward and lateral direction and at the end of this stage the load prediction by different analyses for the single collar collet chuck holder varies between 26 - 60 kN, 30 - 63 kN, and 30 - 77 kN at ram velocity of 0.5 mm/min for m = 0.13; 28 - 66 kN, 28 - 71 kN, and 30 - 86 kN at ram velocity of 1.0 mm/min for m = 0.19; 28 - 66 kN, 35 - 66 kN, and 38 - 80 kN at ram velocity of 2.0 mm/min for m = 0.38. Here, the formation of the bottom stud part and collar rings starts taking place.

In stage III, both extrusion and forging takes place for corner filling. In this region, the grains change its flow direction to 90 degrees or more to fill the intricate corner points that lead to shear of the metal. At the end of this stage load estimation by different methods varies between 55 - 175 kN, 66 - 178 kN, and 77 - 184 kN at ram velocity of 0.5 mm/min for m = 0.13; 58 - 198 kN, 70 - 200 kN, and 70 - 206 kN at ram velocity of 1.0 mm/min for m = 0.19; 99 - 207 kN, 107 - 209 kN, and 115 - 216 kN at ram velocity of 2.0 mm/min for m = 0.38.

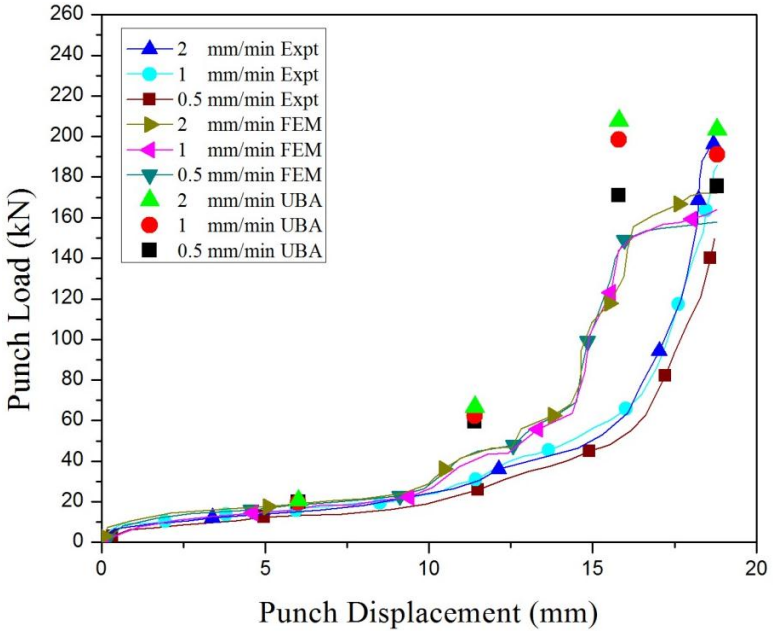

Figure 7.1: Comparison of loads at 0.13 frictional conditions at varying ram velocities

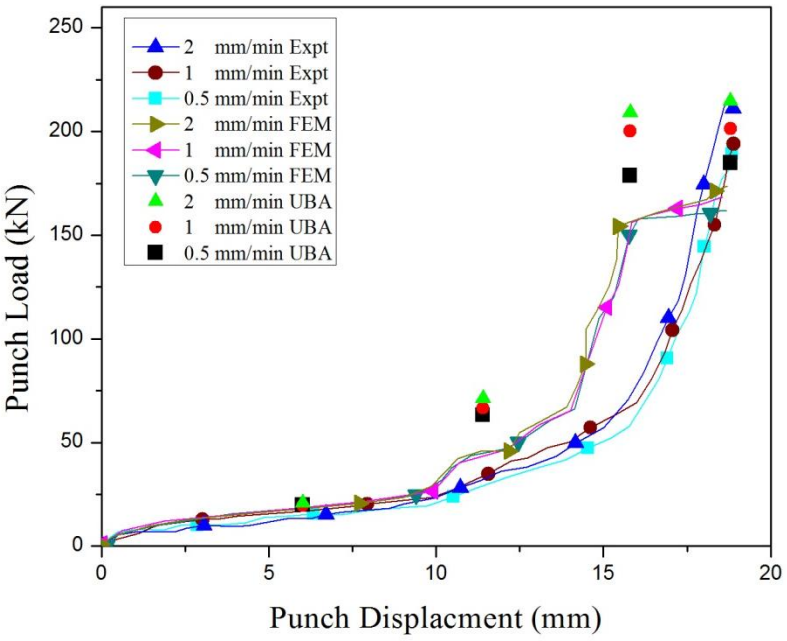

Figure 7.2: Comparison of loads at 0.19 frictional conditions at varying ram velocities

Stage IV is an unsteady state, where the last point of corner point is filled and subsequently, flash is formed. Because of severe redundant work a steep rise of the load is seen. Here, the predicted loads vary between 149 - 175 kN, 164 - 184 kN, and 172 - 214 kN at ram velocity of 0.5 mm/min for m = 0.13; 161 - 191 kN, 168 - 201 kN, and 173 - 236 kN at ram velocity of 1.0 mm/min for m = 0.19; 174 - 203 kN, 189 - 214 kN, and 195 - 252 kN at ram velocity of 2.0 mm/min for m = 0.38.

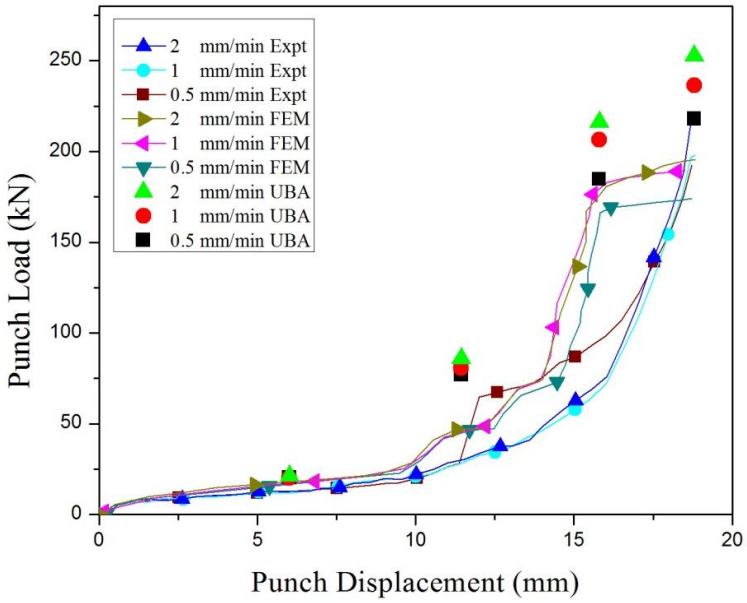

Figure 7.3: Comparison of loads at 0.38 frictional conditions at varying ram velocities

The difference between the FEM and EXPT results are ranging from 5 - 18% where the single collet chuck holders are processed under varying frictional conditions and ram velocities (Table 7.1). Similarly, the forming load difference between UBA and experimental analyses is ranging between 0.3 - 17%.

Table 7.1: Variation of forming loads for different analysis obtained for SCCCH by CEF process

The results seem to confirm the suitability of the proposed techniques for the prediction of load in combined extrusion-forging processes studied in the present work applied to collet chuck holder

7.2.1 Metal flow pattern at different punch movements

As an illustration, Figure 7.4 shows the photograph of the flow pattern for combined extrusion-forging process of a single collar collet chuck holder. at ram velocity of 0.5 mm/min and friction factor of 0.13 during different punch movement obtained both from finite element analysis and experiments. The grid distortions predict the severe plastic deformation areas located at various zone for different stages. The degree of grid distortion also confirms the load curve. It can be observed that there is a marginal change in the forming loads obtained by both simulation and experimental analysis at 6.01 mm and 11.4 mm punch movements. The variation of the load is more at 15.8 mm and 18.8 mm punch movements.

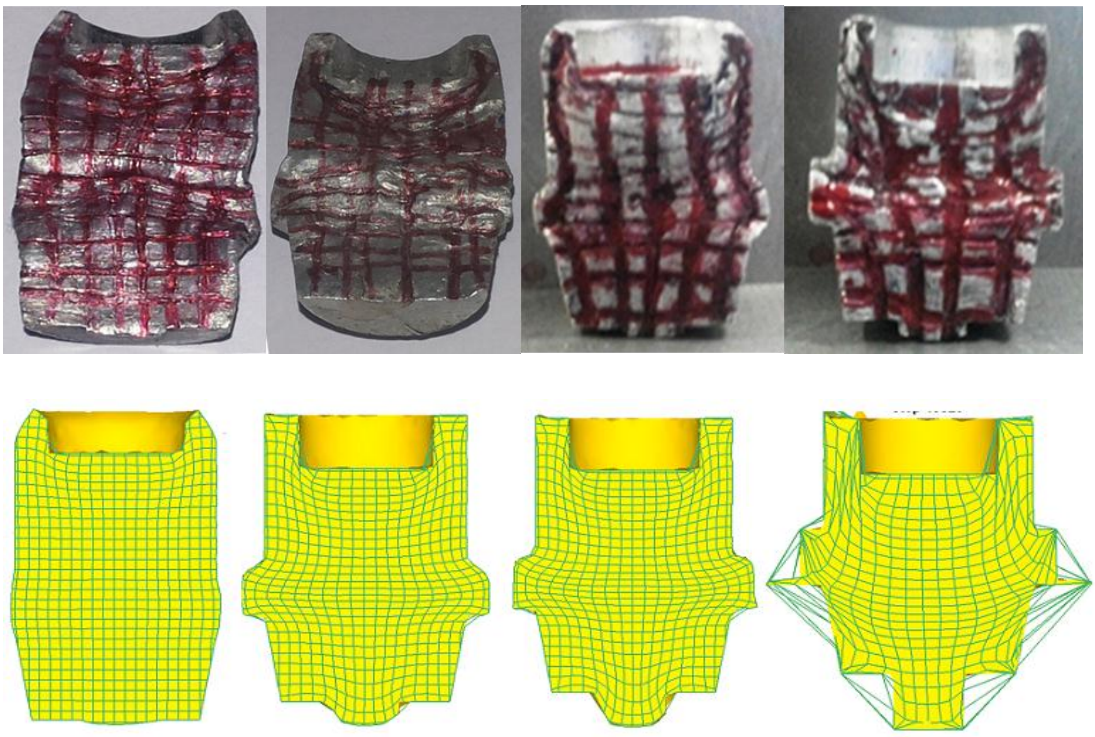

(a) Stage I 6.01 mm punch travel | (b) Stage II 11.4 mm punch travel | (c) Stage III 15.8 mm punch travel | (d) Stage IV 18.8 mm punch travel

Figure 7.4: Flow pattern at different punch movement

7.2.2 Deformed product shape at different punch movements

Progressive change in shapes of the formed product (collet chuck holder) at different punch movement for both simulation and experiments are shown in Figure 7.5 (for ram velocity = 1 mm/min and m = 0.13 as an illustration). It was observed that the numerical analysis results are well matched with the experimental observation and confirms with the load curve.

(a) Stage I 6.01 mm punch travel | (b) Stage II 11.4 mm punch travel | (c) Stage III 15.8 mm punch travel | (d) Stage IV 18.8 mm punch travel

Figure 7.5: Die filling at different punch movement at ram velocity of 1 mm/min and m=0.19

7.3 Comparison of results for DCCCH by CEF process

Table 7.2: Variation of forming loads for different analysis obtained for DCCCH by CEF process

Frictional Condition, m (friction factor)	Ram velocity (mm/min)	% Difference UBA-FEM	% Difference UBA-EXPT
0.13	0.5	6.92	15.1
	1	6.03	20.6
	2	6.18	19.3
0.19	0.5	8.31	17.7
	1	4.41	16.2
	2	4.69	14.0
0.38	0.5	9.60	15.0
	1	0.74	9.42
	2	3.00	7.29

The difference between the FEM and EXPT results are ranging from 0.7 - 10%, where the double collar collet chuck holders are processed under varying frictional conditions and ram velocities which can be noticed from the Table 7.2. Similarly the forming load differences between UBA and Experimental analyses are ranging between 15-20%. The comparison of results at various analysis processes are indicated in Figures 7.6-7.8. Similar to the first product the total process can be subdivided into four zones and the results seem to confirm the suitability of the proposed techniques for the combined extrusion-forging processes applied to collet chuck holder.

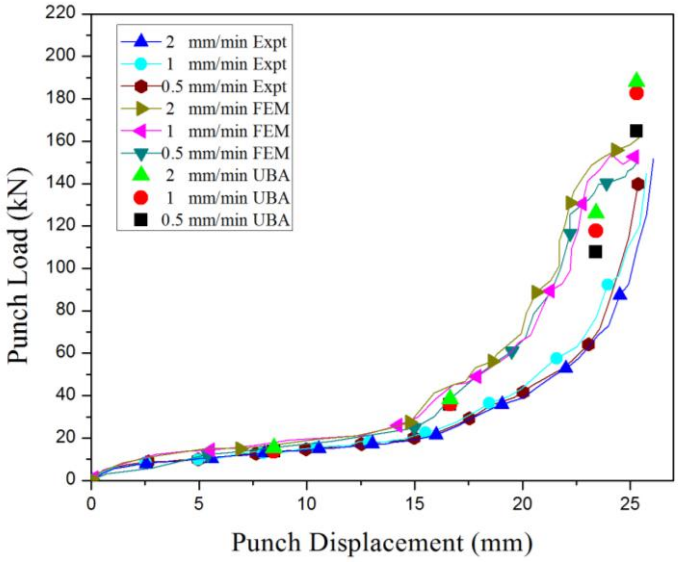

Figure 7.6: Comparison of loads at 0.13 frictional conditions at varying rams velocities

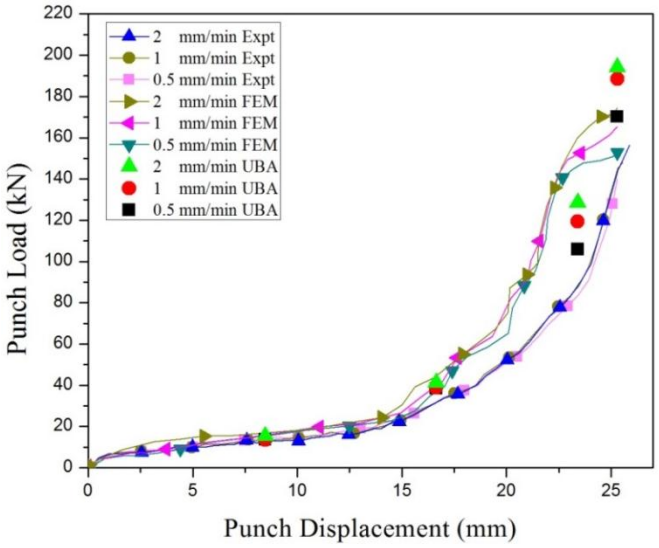

Figure 7.7: Comparison of loads at 0.19 frictional conditions at varying rams velocities

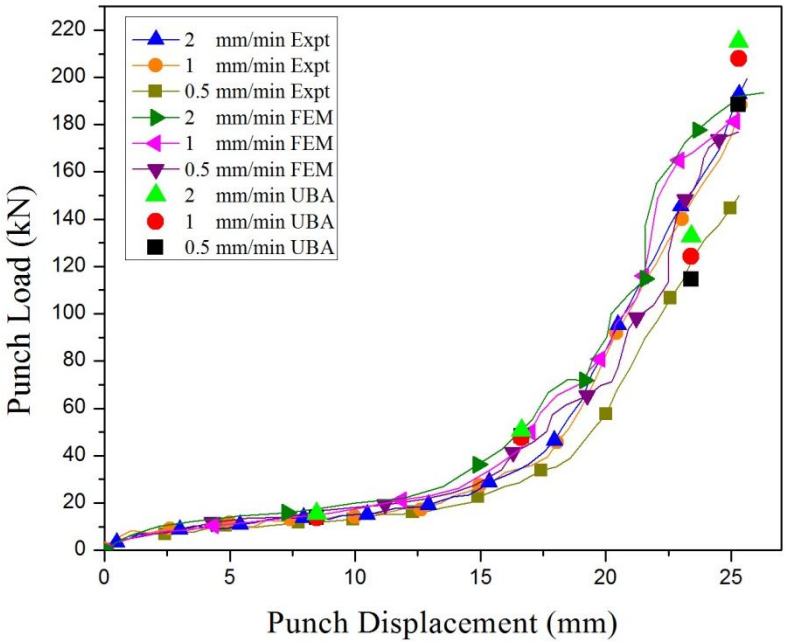

Figure 7.8: Comparison of loads at 0.38 frictional conditions at varying rams velocities

7.3.1 Metal flow pattern at different punch movements

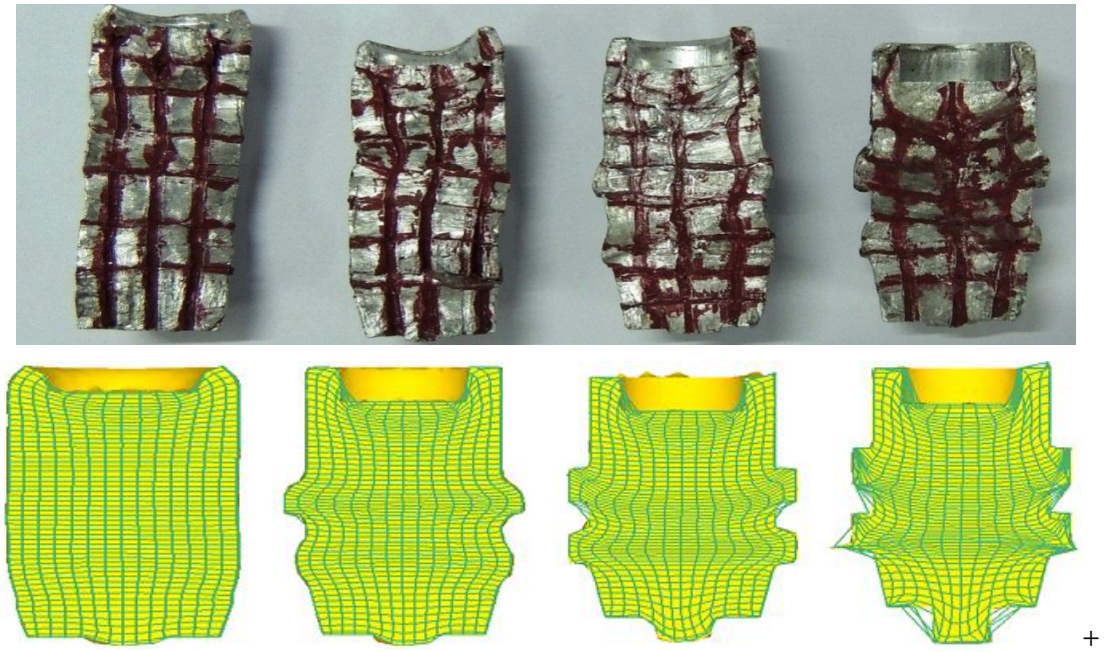

(a) Stage I 8.47 mm punch travel | (b) Stage II 16.6 mm punch travel | (c) Stage III 23.4 mm punch travel | (d) Stage IV 25.3 mm punch travel

Figure 7.9: Flow pattern at different punch movement

As an illustration, Figure 7.9 shows the photograph of the flow pattern for combined extrusion-forging process of a double collar collet chuck holder at ram velocity of 1

mm/min and friction factor of 0.19 during different punch movement obtained both from finite element analysis and experiments. The grid distortions assists to predict the severe plastic deformation located at various zone for different stages. Figure 7.9 (a-d) represents the variation of punch load with stroke at different punch movements. It can be observed that there is marginal change in the forming loads obtained by both simulation and experimental analysis at 8.47 mm and 16.6 mm punch movements. The variation of the load is more at 23.4 mm and 25.3 mm punch movements.

7.3.2 Deformed product shape at different punch movements

Progressive change in shapes of the formed product (collet chuck holder) at different punch movement for both simulation and experimental analysis are shown in Figure 7.10 (for ram velocity = 2 mm/min and m = 0.19 as an illustration). The results obtained from numerical analysis results are well matched with the experimental observation and confirms with the load curve,

(a) Stage I 8.47 mm punch travel | (b) Stage II 16.6 mm punch travel | (c) Stage III 23.4 mm punch travel | (d) Stage IV 25.3 mm punch travel

Figure 7.10: Die filling at different punch movement

7.4 Comparison of results for DCCCH by CE process

Table 7.3: Variation of forming loads for different analysis obtained for DCCCH by CE process

Frictional Condition, m (friction factor)	Ram velocity (mm/min)	% Difference FEM-EXPT	% Difference UBA-EXPT
0.13	0.5	20.8	9.58
	1	17.8	10.7
	2	14.3	7.32
0.19	0.5	30.2	22.3
	1	19.4	11.0
	2	9.00	4.93
0.38	0.5	23.8	17.6
	1	17.0	8.80
	2	14.7	4.61

The difference between the FEM and EXPT results are ranging from 14 - 30% where the double collar collet chuck holders are processed by CE route under varying frictional conditions and ram velocities which can be noticed from the Table 7.3. Similarly the forming load differences between UBA and Experimental analyses are ranging between 7 - 23%. The comparison of results of various analysis processes are indicated in Figures 7.11 - 7.13. Similar to the first product the total process can be subdivided into four zones and the results seem to confirm the suitability of the proposed techniques for the combined extrusion processes applied to collet chuck holder.

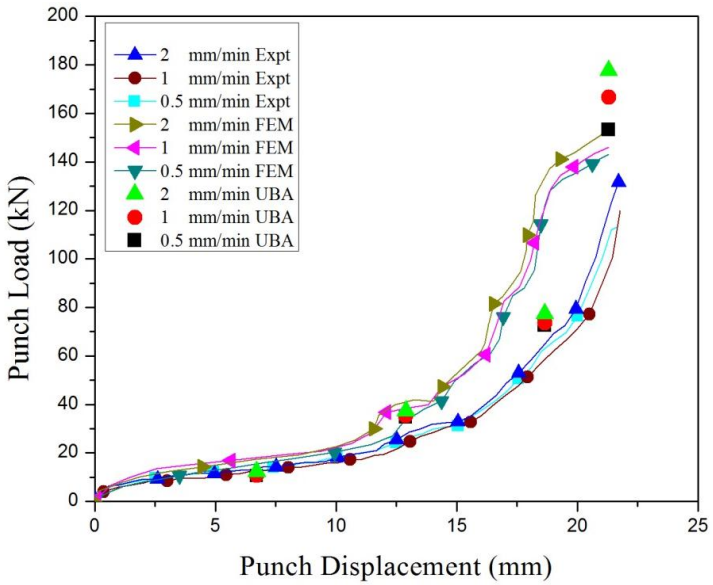

Figure 7.11: Comparison of loads at 0.13 frictional conditions at varying rams velocities

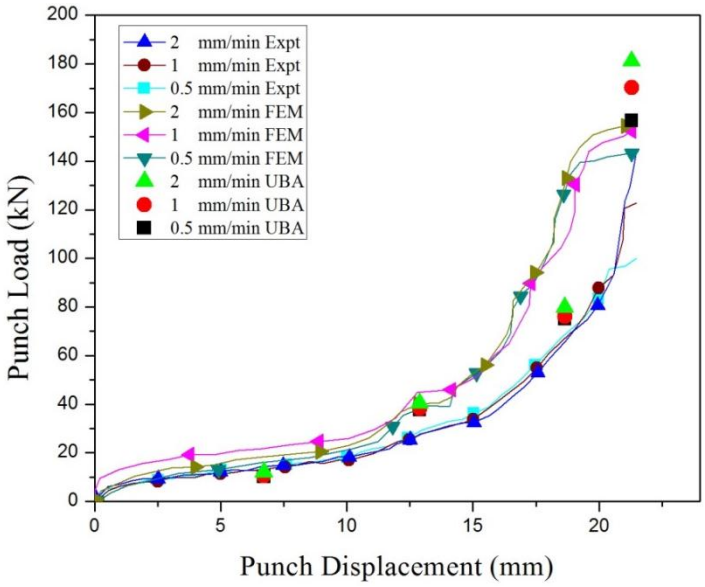

Figure 7.12: Comparison of loads at 0.19 frictional conditions at varying rams velocities

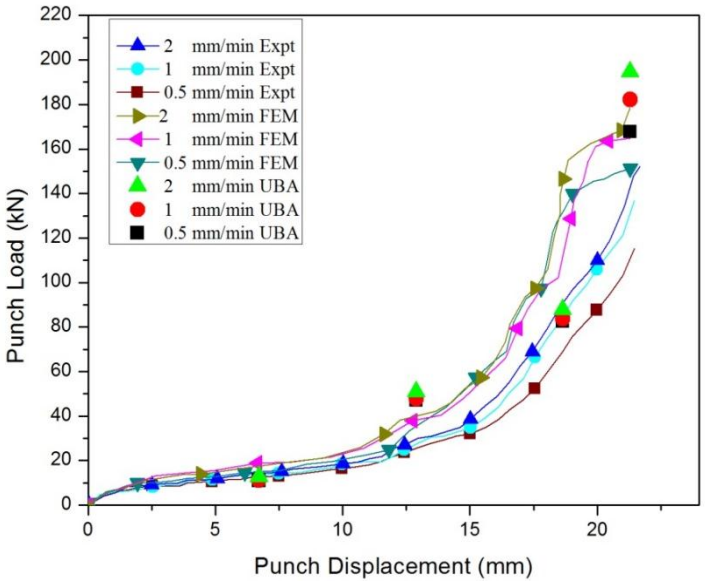

Figure 7.13: Comparison of loads at 0.38 frictional conditions at varying rams velocities

7.4.1 Metal flow pattern at different punch movements

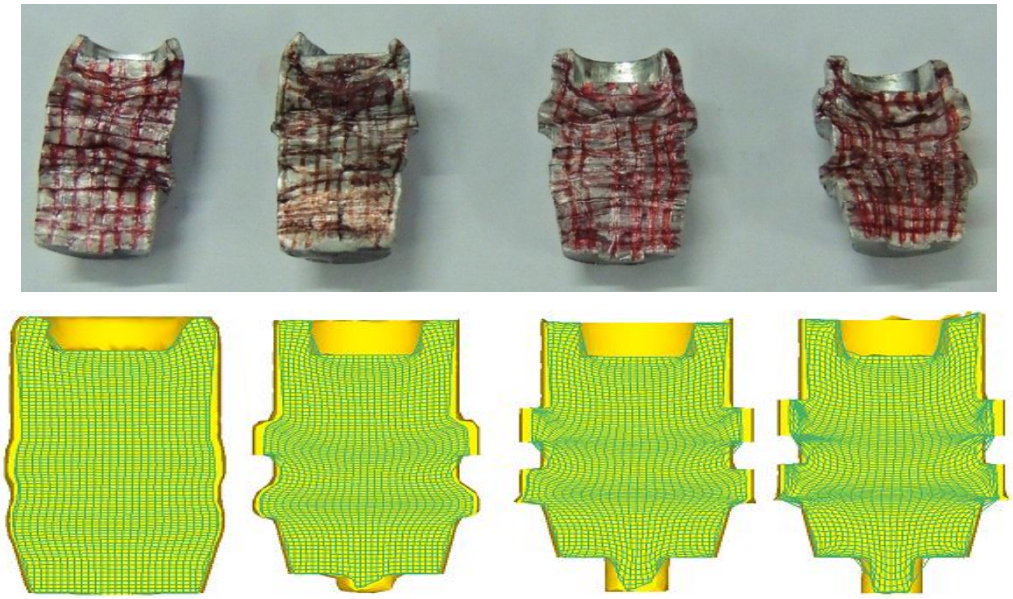

(a) Stage I 6.71 mm punch travel | (b) Stage II 12.8 mm punch travel | (c) Stage III 18.6 mm punch travel | (d) Stage IV 21.3 mm punch travel

Figure 7.14: Flow pattern at different punch movement

As an illustration, Figure 7.14 shows the photograph of the flow pattern for combined extrusion process of a double collar collet chuck holder at ram velocity of 2 mm/min and friction factor of 0.38 during different punch movement obtained both from finite element analysis and experiments. The grid distortions assists to predict the severe plastic deformation located at various zone for different stages. Figure 7.14 (a-d) represents the variation of punch load with stroke at different punch movements. It can be observed that there is marginal change in the forming loads obtained by both simulation and experimental analysis at 6.71 mm and 12.8 mm punch movements. The variation of the load is more at 18.6 mm and 21.3 mm punch movements.

7.4.2 Deformed product shape at different punch movements

Progressive change in shapes of the formed product (collet chuck holder) at different punch movement for both simulation and experimental are shown in Figure 7.15 (for ram velocity = 0.5 mm/min and m = 0.38 as an illustration). It can be noticed from the numerical analysis results which are well matched with the experimental observation and confirms with the load curve.

(a) Stage I 6.71 mm punch travel | (b) Stage II 12.8 mm punch travel | (c) Stage III 18.6 mm punch travel | (d) Stage IV 21.3 mm punch travel

Figure 7.15: Die filling at different punch movement

7.5 Multistage CEF Process

Table 7.4: Variation of forming loads for different analysis obtained for SCCCH by Multistage CEF process

Frictional Condition, m (friction factor)	Ram velocity (mm/min)	% Difference FEM-EXPT	% Difference UBA-EXPT
0.19	1	11.2	22.6

The difference between the FEM and EXPT results are ranging from 0 - 12% where the single collar collet chuck holders is processed by CE route under 0.19 frictional condition at 1 mm/min ram velocity which can be noticed from the Table 7.4. Similarly the forming load differences between UBA and Experimental analyses are ranging between 0 - 23%. The comparison of results of various analysis processes are indicated in Figures 7.16. Similar to the first product the total process can be subdivided into four zones and the results seem to confirm the suitability of the proposed techniques for the combined extrusion processes applied to collet chuck holder.

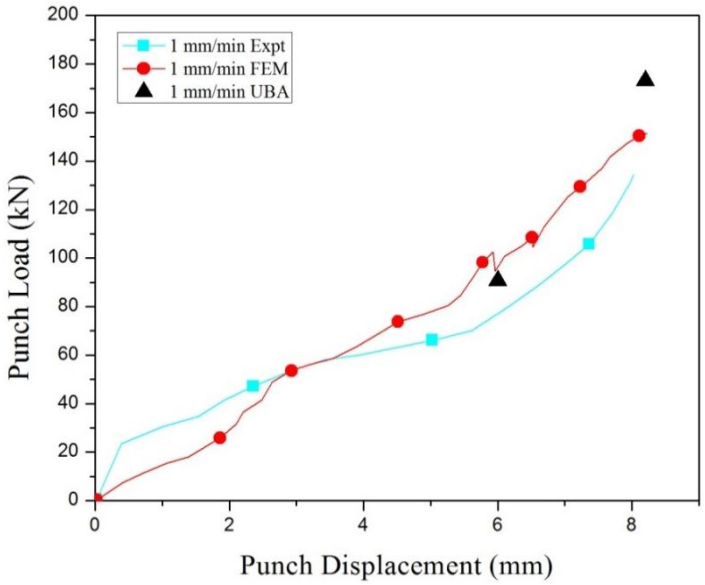

Figure 7.16: Comparison of loads at 1mm/min ram velocity with 0.19 frictional condition

7.5.1 Metal flow pattern at different punch movements

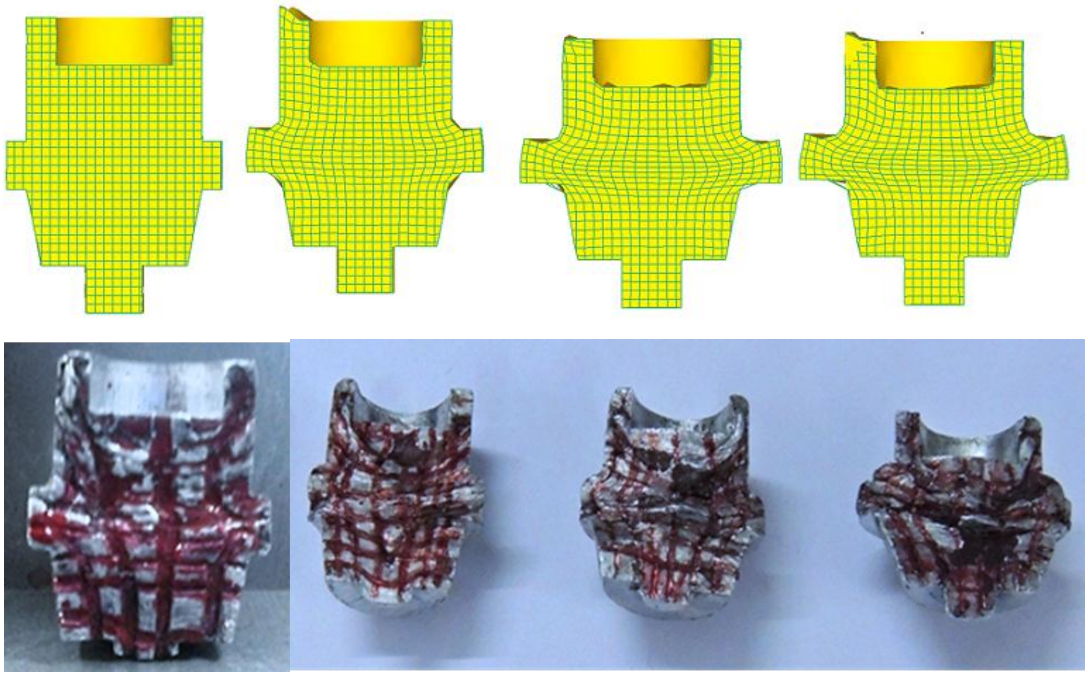

Stage I Stage II

After 3.0 mm punch travel | After 6.0 mm punch travel | After 8.0 mm punch travel | After 8.2 mm punch travel

Figure 7.17: Flow pattern at different punch movement

As an illustration, Figure 7.17 shows the photograph of the flow pattern for Multistage combined extrusion-forging process of a single collar collet chuck holder at ram velocity

of 1 mm/min and friction factor of 0.19 during different punch movement both obtained from finite element analysis and experiments. The grid distortions assists to predict the severe plastic deformation located at various zone for different stages. Figure 7.17 (a-d) represents the variation of punch load with stroke at different punch movements. It can be observed that there is marginal change in the forming loads obtained by both simulation and experimental analysis at 3.0 mm and 6.0 mm punch movements. The variation of the load is more at 8.0 mm and 8.2 mm punch movements.

7.5.2 Deformed product shape at different punch movements

Progressive change in shapes of the formed product (collet chuck holder) at different punch movement for both simulation and experimental are shown in Figure 7.18 (for ram velocity = 1 mm/min and m = 0.19 as an illustration). It can be observed from the numerical analysis results which are well matched with the experimental observation and confirms with the load curve.

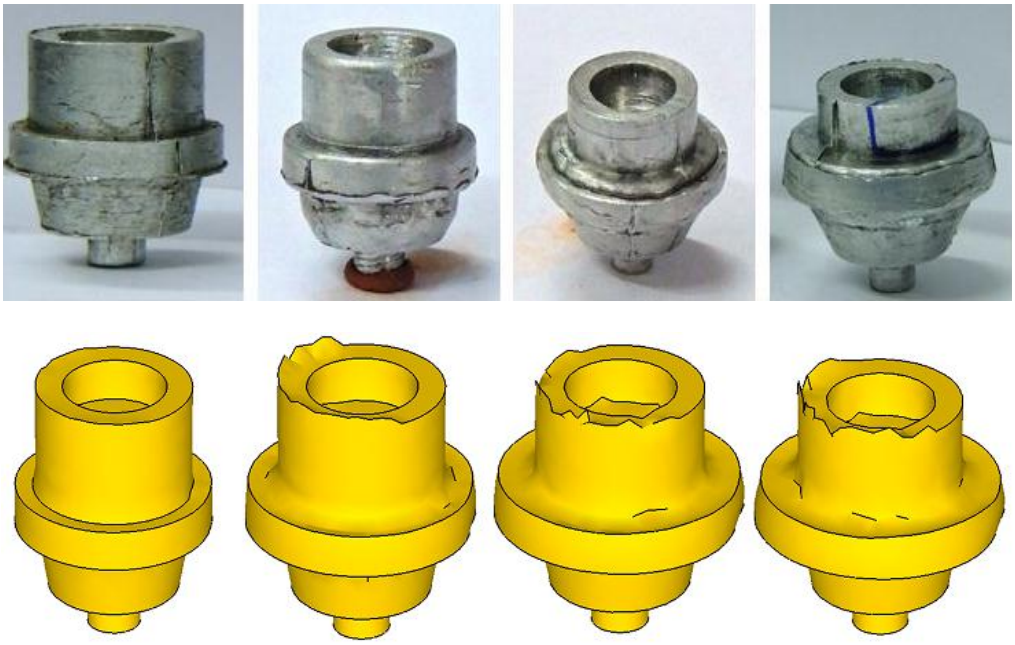

Stage I Stage II

After 3.0 mm punch travel | After 6.0 mm punch travel | After 8.0 mm punch travel | After 8.2 mm punch travel

Figure 7.18: Die filling at different punch movement

7.6 Conclusions

- The forming loads obtained by proposed upper bound technique is in good agreement with the experimental results and lies in the range of 0 - 15%, 5 - 20%, 0 - 15% and 12 - 20% for first, second, third and fourth products respectively.
- The obtained punch loads at different punch strokes proposed by the upper bound analysis are also in good agreement with FEM analysis.
- The numerical simulation results for die filling and flow pattern are in good agreement with experimental observations.
- The results confirm the suitability of the proposed techniques for the prediction of load in combined extrusion-forging processes studied in the present work applied to collet chuck holders taking care of work hardening, friction effects and redundant work.

Chapter 8

Conclusions

8.1 Introduction

In the present investigation, it is proposed to manufacture the collet chuck holder by different ways using the metal forming route of combined and/or multi-stage extrusion and/or forging. Currently, industries produce it by casting and/or by machining. In the simplest form of the combined extrusion-forging process, the forging to fill the die cavity and the extrusion through the orifice take place simultaneously; this is performed in one station only. This process has many advantages like, less material wastage, higher dimensional accuracy and surface quality, adequate mechanical and microstructural properties, etc. Due to the complexity of the process, and because of the large number of process variables, it is difficult to estimate the forming load requirement to manufacture the given component. In this direction, the present work emphasizes on estimation of forming load proposing analytical and numerical methods and validating the results performing experiments at different working conditions of ram velocities and frictions conditions.

8.2 Summary of Findings

On account of the industrial significance for collet chuck holder and combined/multi-stage extrusion/forging processes the proposed research work not only attempts to develop and optimize the process, but also makes an effort to predict the forming load, recognize the metal flow, frictional conditions, microstructural, micro-hardness & residual stress behaviour of the material. The following major observations have been outlined base on the obtained results:

- Split dies with container and punch are successfully designed and fabricated to manufacture different type of collet chuck holders using the principle of combined/multi-stage extrusion/forging. Good numbers of experiments have been performed at various coefficients of friction along with different rate of ram displacements.

- It is observed that the complete process to get the first three components can be assumed to compose of four stages and fourth one of two stages with regard to forward/backward extrusion, forging, die corner filling, and flash formation.
- From the load ~ displacement behaviour, it is seen that the forming load increases with punch movement. The rate of load increase with more redundant work when simultaneous backward, forward and lateral extrusion/forging takes place to fill the die cavities. The load increases steeply at the last stage when corners are filled, and flash is formed. The loads also increase with friction and ram velocities.
- The microscopic, micro hardness and residual stress analyses are performed for all the four components manufactured under different frictional conditions and ram velocities. The results confirm the advantage of the proposed processes to manufacture collet chuck holder.
- 3D finite element formulation is performed to analyse the effective stress, strain and total velocity to get a clear picture of metal flow direction, and stress/strain accumulation points. The data is procured for clear understanding of variation of forming loads at different regions of a component which is processed under different frictional conditions and ram velocities.
- Kinematically admissible velocity fields for four different types of collet chuck holders is proposed under varying frictional conditions and ram velocities for different zones of all stages. The minimum (175.4kN) and maximum (252.7kN) upper bound load for SCCCH manufactured by CEF process was obtained at m=0.13 with 0.5 mm/min ram velocity and m=0.38 at 2 mm/min ram velocity respectively at end of the process. Similarly for DCCCH manufactured by CEF method, the maximum forming load (215.2kN) was obtained at m= 0.38 at 0.2 mm/min ram velocity. The minimum forming load (164.6kN) was obtained at m=0.13 with 0.5 mm/min ram velocity at end of the process. The third product DCCCH processed by CE method, the maximum forming load (194.0kN) was obtained at m=0.38 at 0.2 mm/min ram velocity. The minimum forming load (153.2kN) was noticed to be same at m=0.13 and 0.19 with 0.5 mm/min ram velocity at end of the process. For multi stage process, maximum (173.1kN) upper bound load at m=0.13 with 1.0 mm/min ram velocity was obtained at end of the process.

- The forming loads obtained by proposed upper bound technique is in good agreement with the experimental results and lies in the range of 0-15%, 5-20%, 0-15% and 12-20% for first, second, third and fourth products respectively.
- It is seen that the proposed kinematically admissible velocity fields for different products adequately address the die filling and flow pattern of the metal at different punch positions and satisfactorily predict the load requirements taking care of work hardening, friction effects and redundant work.

8.3 Conclusions

- Experimental observations indicate that the collet chuck holder can be effectively manufactured by metal forming route through combined and/or multi-stage extrusion/forging to get its inherent advantages instead of following the present practice of machining and/or casting.
- The results confirm the suitability of the proposed techniques (FEA and upper bound) for the prediction of load in combined extrusion-forging processes studied in the present work applied to collet chuck holder.
- The estimated loads obtained using proposed kinematically admissible velocity fields effectively take care of work hardening, friction effects and redundant work and are remain within engineering accuracy when compared with that obtained from FEA and experiments.
- The mechanical and metallurgical studies also strengthen the appropriateness of the proposed processes for the collet chuck holders.

8.4 Contribution to Knowledge Enhancement

- The primary contribution of the current investigation is to replace the designer's 'thumb rule' based design which is predominantly followed in industries, with a methodical analysis during installation and determination of the capacity of a machine/equipment/tool/die, and processing to manufacture a complex shaped component.
- An successfully design and fabrication method for the die-punch set to perform experiments to show that the collet chuck holder can be effectively

manufactured by metal forming route of combined and/or multi-stage extrusion/forging to get its inherent advantages like, minimal material loss and better mechanical properties than machining and/or casting.

- A 3D FEM formulation for CEF and CE processes applied to collet chuck holder to explore the effects of different influencing parameters.
- Generate a database conducting numerous experiments by CEF and CE processes using lubricants such as lithium based grease and molybdenum disulphide, only grease and dry conditions at different ram velocities.
- It is shown that if a set of kinematically admissible velocity fields is taken appropriately it can effectively take care of work hardening, friction effects and redundant work, and can predict load which will are remain within engineering accuracy.
- Enhancing the metallurgical characterizing information about the final products obtained by the proposed methods.
- Open a pathway for further research in this area.

8.5 Scopes for Future Work

The present works will encourage the forthcoming investigators and have broad scope to explore various aspects of combined extrusion-forging and multi-stage forging processes. Some recommendations for future research are:

- Both processes can be explored for high strength materials such as steel, bronze, etc.
- This technique can be used for manufacturing of other complex shaped components.
- Different friction conditions (using different lubricants) and high ram velocities may be tried to get the practical results.
- Metal flow during this process may be modelled for these combined processes.
- Analysis can be extended to use taper and curved dies for extrusion.
- Analytical and computational models can be explored for all stages of the process.

References

[1] N. R. Chitkara and K. Yohngjo, "Upper bound analysis of near-net shaped forging of gear coupling form," *Int. J. Mechnaical Sci.*, vol. 38, no. 7, pp. 791–803, 1996.

[2] J. Choi, H. Y. Cho, and C. Y. Jo, "Upper-bound analysis for the forging of spur gears," *J. Mater. Process. Technol.*, vol. 104, no. 1, pp. 67–73, 2000.

[3] Y. Çan, T. Altinbalik, and H. E. Akata, "A study of lateral extrusion of gear like elements and splines," *J. Mater. Process. Technol.*, vol. 166, no. 1, pp. 128–134, 2005.

[4] A. Farhoumand and R. Ebrahimi, "Analysis of forward-backward-radial extrusion process," *Mater. Des.*, vol. 30, no. 6, pp. 2152–2157, 2009.

[5] T. Ishikawa, T. Ishiguro, N. Yukawa, and T. Goto, "Control of thermal contraction of aluminum alloy for precision cold forging," *CIRP Ann. - Manuf. Technol.*, vol. 63, pp. 289–292, 2014.

[6] P. N. Rao, "Extrusion and Other Processes," in *Manufacturing technology*, 1987th ed., New Delhi: Tata McGraw-Hill Publishing Company Limited, 1987, pp. 296–303.

[7] H. I. Lee, B. C. Hwang, and W. B. Bae, "A UBET analysis of non-axisymmetric forward and backward extrusion," *J. Mater. Process. Technol.*, vol. 113, no. 1–3, pp. 103–108, 2001.

[8] H. Jafarzadeh, S. Barzegar, and A. Babaei, "Analysis of deformation behavior in backward–radial–forward extrusion process," *Trans. Indian Inst. Met.*, vol. 68, no. 2, pp. 191–199, 2015.

[9] G. A. Lee, D. Y. Kwak, S. Y. Kim, and Y. T. Im, "Analysis and design of flat-die hot extrusion process 1. Three-dimensional finite element analysis," *Int. J. Mech. Sci.*, vol. 44, no. 5, pp. 915–934, 2002.

[10] O. C. Zienkeiwicz and Y. C. Cheung, *The Finite Element Method in Structural and Continuum Mechanics*, 1967th ed. New York: Tata McGraw-Hill Publishing Company Limited, 1967.

[11] H. W. Shin, D. W. Kim, and N. Kim, "A simplified three-dimensional finite-element analysis of the non-axisymmetric extrusion processes," *J. Mater. Process. Tech.*, vol. 38, no. 3, pp. 567–587, 1993.

[12] N. Kim and T. Altan, "Three dimensional analysis and computer simulation of shape rolling by the finite and slab element method," *Int. J. Mach. Tools Manuf.*, vol. 31, no. 3, pp. 553–563, 1991.

[13] P. A. F. Martins and M. J. M. Barata Marques, "Analysis of three-dimensional hexagonal closed-die heading by the finite-element flow formulation," *J. Mater. Process. Tech.*, vol. 38, no. 3, pp. 553–566, 1993.

[14] G. K. Lal, P. A. Balaji, and T. Sundar, "Viscoplastic deformation analysis and extrusion die design by FEM," *Trans. ASME*, vol. 58, no. 3, pp. 644–650, 1991.

[15] T. Hirai and T. Ishise, "Plastic metal flow under frictional boundary in forward extrusion die and stress distribution of the die," *Int. J. Mach. Tool Des.*, vol. 26, no. 3, pp. 217–229, 1986.

[16] Y. B. Park, J. H. Yoon, and D. Y. Yang, "Finite element analysis of steady-state three-dimensional helical extrusion of twisted sections using recurrent boundary conditions," *Int. J. Mech. Sci.*, vol. 36, no. 2, pp. 137–148, 1994.

[17] K. Mori, K. Osakada, and H. Yamaguchi, "Prediction of curvature of an extruded Bar with noncircular cross-section by a 3-D rigid-plastic finite element method," *Int. J. Mech. Sci.*, vol. 35, no. 10, pp. 879–887, 1993.

[18] Y. S. Kang and D. Y. Yang, “A numerical investigation into hot square die extrusion of an L-section considering the variation of die bearing length,” *J. Manuf. Sci. Eng.*, vol. 121, no. June 1997, pp. 225–231, 2013.
[19] G. L. Horvat and C. A. D. Cam, “Computer aided design (CAD) of forging and extrusion Dies for the production of gears by forming manufacturing,” *Gear Technol.*, no. June, 1977.
[20] S. K. Osakada, K. Iwata, and S. Fujjino, “Analysis of hydrostatic extrusion by the finite element method,” *Trans. ASME J. Eng. Ind.*, vol. 94, no. 2, pp. 697–703, 1972.
[21] J. H. Hwang, D. C. Ko, G. S. Min, B. M. Kim, and J. C. Choi, “Finite element simulation and experiment for extrusion of semi-solid Al 2024,” *Int. J. Mach. Tools Manuf.*, vol. 40, no. 9, pp. 1311–1328, 2000.
[22] B. P. P. A. Gouveia, J. M. C. Rodrigues, N. Bay, and P. A. F. Martins, “Deformation analysis of the round-to-square extrusion: A numerical and experimental investigation,” *Finite Elem. Anal. Des.*, vol. 35, no. 3, pp. 269–282, 2000.
[23] A. Minami, Y. Marumo, H. Saiki, L. Ruan, and O. Shizuma, “Effects of simulation conditions on evaluation of tool temperature in hot extrusion-forging,” *J. Mater. Process. Technol.*, vol. 177, no. 1–3, pp. 251–255, 2006.
[24] B. A. Behrens, “Finite element analysis of die wear in hot forging processes,” *CIRP Ann. - Manuf. Technol.*, vol. 57, no. 1, pp. 305–308, 2008.
[25] L. Zuyan and W. Zhongjin, “Finite-element analysis of the load of equal-cross-section lateral extrusion,” vol. 94, pp. 193–196, 1999.
[26] M. Meidert, M. Knoerr, K. Westphal, and T. Altan, “Numerical and physical modelling of cold forging of bevel gears,” *J. Mater. Process. Tech.*, vol. 33, no. 1–2, pp. 75–93, 1992.
[27] Y. T. Im, S. H. Kang, J. S. Cheon, and J. H. Lee, “Finite element simulation of tip test with an aluminum alloy,” *J. Mater. Process. Technol.*, vol. 157–158, no. SPEC. ISS., pp. 171–176, 2004.
[28] G. Li, J. Yang, J. Y. Oh, and M. Foster, “Advancements of extrusion simulation in DEFORM-3D,” *Light Met. Age*, pp. 1–5, 2009.
[29] H. Zhao, H. N. Wang, M. J. Wang, and G. Y. Li, “Simulation of extrusion process of complicated aluminium profile and die trial,” *Trans. Nonferrous Met. Soc. China (English Ed.*, vol. 22, no. 7, pp. 1732–1737, 2012.
[30] J. Zhou, L. Li, and J. Duszczyk, “3D FEM simulation of the whole cycle of aluminium extrusion throughout the transient state and the steady state using the updated Lagrangian approach,” *J. Mater. Process. Technol.*, vol. 134, no. 3, pp. 383–397, 2003.
[31] Y. V. R. K. Prasad and K. P. Rao, “Materials modeling and finite element simulation of isothermal forging of electrolytic copper,” *Mater. Des.*, vol. 32, no. 4, pp. 1851–1858, 2011.
[32] M. C. Lee, S. H. Chung, S. M. Jang, and M. S. Joun, “Three-dimensional simulation of forging using tetrahedral and hexahedral elements,” *Finite Elem. Anal. Des.*, vol. 45, no. 11, pp. 745–754, 2009.
[33] H. Haghighat and M. M. Mahdavi, “Analysis and FEM simulation of extrusion process of bimetal tubes through rotating conical dies,” *Trans. Nonferrous Met. Soc. China (English Ed.*, vol. 23, no. 11, pp. 3392–3399, 2013.
[34] A. Gavrus, H. Francillette, and D. T. Pham, “An optimal forward extrusion device proposed for numerical and experimental analysis of materials tribological properties corresponding to bulk forming processes,” *Tribol. Int.*, vol. 47, pp. 105–

121, 2012.
[35] L. Wang, Y. He, Y. Zhang, J. Cai, J. Zhou, J. Duszczyk, and L. Katgerman, “Modeling of double action extrusion-A novel extrusion process for friction characterization at the billet-die bearing interface,” *Tribol. Int.*, vol. 43, no. 11, pp. 2084–2091, 2010.
[36] S. H. Hosseini, K. Abrinia, and G. Faraji, “Applicability of a modified backward extrusion process on commercially pure aluminum,” *Mater. Des.*, vol. 65, pp. 521–528, 2015.
[37] W. Zhuang, S. Wang, J. Cao, J. Lin, and C. Hartl, “Modelling of localised thinning features in the hydroforming of micro-tubes using the crystal-plasticity FE method,” *Int. J. Adv. Manuf. Technol.*, vol. 47, no. 9–12, pp. 859–865, 2010.
[38] C.H. Lee and T. Altan, “Influence of flow stress and friction upon metal flow in Upset forging of rings and cylinders,” *Trans. ASME J. Eng. Ind.*, vol. 94, no. 3, pp. 775–782, 1972.
[39] Y. T. Lin and J. P. Wang, “A new upper-bound elemental approach technique,” *Comput. Struct.*, vol. 65, no. 4, pp. 601–611, 1997.
[40] R. Narayanasamy and K. S. Pandey, “Phenomenon of barrelling in aluminium solid cylinders during cold upset-forming,” vol. 70, pp. 17–21, 1997.
[41] G. Hirt, R. Cremer, A. Winkelmann, T. Witulski, and M. Zillgen, “Semi solid forming of aluminum alloys by direct forging and lateral extrusion,” *J. Mater. Process. Tech.*, vol. 45, no. 1–4, pp. 359–364, 1994.
[42] K. Kuzman, E. Pfeifer, N. Bay, and J. Hunding, “Control of material flow in a combined backward can-forward rod extrusion,” *J. Mater. Process.*, vol. 60, no. 96, pp. 141–147, 1996.
[43] D. Shan, F. Liu, W. Xu, and Y. Lu, “Experimental study on process of precision forging of an aluminium-alloy rotor,” *J. Mater. Process. Technol.*, vol. 170, no. 1–2, pp. 412–415, 2005.
[44] J. Monaghan, “An investigation of plane-strain lateral extrusion to form components having staggered branches,” *J. Mater. Process. Technol.*, vol. 77, no. 1–3, pp. 305–313, 1998.
[45] H. Y. Lee, J. H. Noh, and B. B. Hwang, “Surface stresses and flow modes on contact surface in a combined double cup extrusion process,” *Tribol. Int.*, vol. 64, pp. 215–224, 2013.
[46] R. K. Uyyuru and H. Valberg, “Physical and numerical analysis of the metal flow over the punch head in backward cup extrusion of aluminium,” *J. Mater. Process. Technol.*, vol. 172, no. 2, pp. 312–318, 2006.
[47] Y. W. Dong and Xianghuai, “Upper bound analysis of penetration in radial forging process,” *Int. J. Mech. Sci.*, vol. 103, pp. 1–8, 2015.
[48] M. M. El-rayes and E. A. El-danaf, “The influence of multi-pass friction stir processing on the microstructural and mechanical properties of Aluminum Alloy 6082,” *J. Mater. Process. Technol.*, vol. 212, no. 5, pp. 1157–1168, 2012.
[49] M. R. Rokni, A. Zarei-Hanzaki, H. R. Abedi, and N. Haghdadi, “Microstructure evolution and mechanical properties of backward thixoextruded 7075 aluminum alloy,” *Mater. Des.*, vol. 36, pp. 557–563, 2012.
[50] P. Garbacz, T. Giesko, and A. Mazurkiewicz, “Inspection method of aluminium extrusion process,” *Arch. Civ. Mech. Eng.*, vol. 5, pp. 2–9, 2014.
[51] V. Shatermashhadi, B. Manafi, K. Abrinia, G. Faraji, and M. Sanei, “Development of a novel method for the backward extrusion,” *Mater. Des.*, vol. 62, pp. 361–366, 2014.
[52] S. Khoddam, A. Farhoumand, and P. D. Hodgson, “Axi-symmetric forward spiral

extrusion, a kinematic and experimental study," *Mater. Sci. Eng. A*, vol. 528, no. 3, pp. 1023–1029, 2011.
[53] V. Ranatunga, J. S. Gunasekera, W. G. Frazier, and K. D. Hur, "Use of UBET for design of flash gap in closed-die forging," *J. Mater. Process. Technol.*, vol. 111, no. 1–3, pp. 107–112, 2001.
[54] J. C. Choi, Y. Choi, and S. J. Tak, "The forging of helical gears (I): Experiments and upper-bound analysis," *lnt J Mech. Sci.*, vol. 40, no. 4, pp. 325–337, 1998.
[55] D. K. Kim, J. R. Cho, W. B. Bae, Y. H. Kim, and A. N. Bramley, "An upper bound analysis of the square-die extrusion of non-axisymmetric sections," *J. Mater. Process. Technol.*, vol. 71, no. 3, pp. 477–486, 1997.
[56] C. T. Kwan, "An analysis of the closed-die forging of a general non-axisymmetric shape by the upper-bound elemental technique," *J. Mater. Process. Technol.*, vol. 123, no. 2, pp. 197–202, 2002.
[57] J. Choi, H. Cho, and J. Choi, "Upper bound analysis for forging of trochoidal gears," vol. 103, pp. 347–352, 2000.
[58] S. Kumar and S. K. Prasad, "Feature-based design of extrusion process using upper-bound and finite element techniques for extrudable shapes," *J. Mater. Process. Technol.*, vol. 155–156, no. 1–3, pp. 1365–1372, 2004.
[59] J.H. Kim and D.Y. Yang, "An analysis of upset forging of square blocks considering the three-dimensional bulging of sides," *Int. J. Mach. Tool Des. Res.*, vol. 25, no. 4, pp. 327–336, 1985.
[60] S. Jung, M. Kang, and C. Kim, "A Study on the extrusion by a two-step process for manufacturing helical gear," *Int. J. Adv. Manuf. Technol.*, vol. 41, pp. 684–693, 2009.
[61] E. M. R. Alvir, M. A. S. Pérez, and A. S. Lobera, "Mechanical solutions for drawing processes under plane strain conditions by the upper bound method," *J. Mater. Process. Technol.*, vol. 143, no. 144, pp. 539–545, 2003.
[62] A. N. Bramley, "UBET and TEUBA : Fast methods for forging simulation and preform design," *J. Mater. Process. Technol.*, vol. 116, pp. 62–66, 2001.
[63] S. Bahttacharyya, A. K. Majumdar, and S. K. Basu, "Mathematical modelling of metal extrusion process," *Trans. ASME J. Eng. Ind.*, vol. 104, pp. 65–70, 1982.
[64] J. Moller, L. Tran, D. Shrader, J. R. Douglas, and G. W. Kuhlman, "Augmented upper bound element technique for prediction of temperature and strain in forgings," *J. Mater. Process. Technol.*, vol. 152, no. 2, pp. 162–175, 2004.
[65] J. Maciejewski and Z. Mroz, "An upper-bound analysis of axisymmetric extrusion assisted by cyclic torsion," *J. Mater. Process. Technol.*, vol. 206, no. 1–3, pp. 333–344, 2008.
[66] R. S. Lee and C. T. Kwan, "Upper-bound elemental technique (UBET) with convex circular parallelepiped and convex spherical elements for three-dimensional forging analysis," *Int. J. Mach. Tools Manuf.*, vol. 37, no. 8, pp. 1053–1067, 1997.
[67] C. H. Han, M. U. Kim, and D. Y. Yang, "A generalized method for analysis of three-dimensional extrusion of arbitrarily-shaped sections," *Int. J. Mech. Sci.*, vol. 28, no. 8, pp. 517–534, 1986.
[68] C. H. Han, D. Y. Yang, and M. Kiuchi, "A new formulation for three-dimensional extrusion and its application to extrusion of clover sections," *Int. J. Mech. Sci.*, vol. 28, no. 4, pp. 201–218, 1986.
[69] C. H. Han and D. Y. Yang, "A New Formulation of Generalized Velocity Field for Axisymmetric Forward Extrusion Through Arbitrarily Curved Dies," *Trans. ASME J. Eng. Ind.*, vol. 109, pp. 161–168, 1987.
[70] R. K. Sahoo, P. K. Kar, and S. K. Sahoo, "3D upper-bound modeling for round-to-

triangle section extrusion using the SERR technique," *J. Mater. Process. Technol.*, vol. 138, no. 1–3, pp. 499–504, 2003.
[71] L. N. Patra, S. K. Sahoo, and M. Murmu, "Plastic flow through taper dies : A three-dimensional Analysis," *Int. J. Mech. Mater. Eng.*, vol. 1, no. 3, pp. 205–210, 2010.
[72] S. K. Sahoo, P. K. Kar, and K. C. Singh, "Numerical application of the upper-bound technique for round-to-hexagon extrusion through linearly converging dies," *J. Mater. Process. Technol.*, vol. 91, no. 1, pp. 105–110, 1999.
[73] P. K. Kar, S. . Sahoo, and N. S. Das, "Upper bound analysis for extrusion of T-section Bars from square billets through square dies," *Meccanica*, vol. 35, pp. 339–410, 2000.
[74] S. K. Sahoo, "An analysis of plastic flow through polygonal linearly converging dies: As applied to forward metal extrusion," *J. Mater. Process. Technol.*, vol. 132, no. 1–3, pp. 286–292, 2003.
[75] H. H. Hsu, "A study on precision forging of spur gear forms and spline by the upper bound method," *Int. J. Mech. Sci.*, vol. 44, no. 8, pp. 1543–1558, 2002.
[76] J. C. Choi and Y. Choi, "A study on the forging of external spur gears: upper-bound analyses and experiments," *Int. J. Mach. Tools Manuf.*, vol. 38, no. 10–11, pp. 1193–1208, 1998.
[77] J. C. Choi, Y. Choi, K. D. Hur, and C. H. Kim, "A study on the forging of spur gears," *Int. J. Mech. Sci.*, vol. 38, no. 12, pp. 1333–1346, 1996.
[78] V. Jayaseelan, K. Kalaichelvan, and S. Vijay Ananth, "Lubrication effect on friction factor of AA6063 in forward extrusion process," *Procedia Eng.*, vol. 97, pp. 166–171, 2014.
[79] F. Fereshteh-Saniee, I. Pillinger, and P. Hartley, "Friction modelling for the physical simulation of the bulk metal forming processes," *J. Mater. Process. Technol.*, vol. 153–154, no. 1–3, pp. 151–156, 2004.
[80] M. Sawamura, Y. Yogo, M. Kamiyama, and N. Iwata, "Measurement of friction coefficient by backward extrusion with rotating tool under severe forming conditions," *Procedia Eng.*, vol. 81, no. October, pp. 1866–1871, 2014.
[81] K. Asai and K. Kitamura, "Estimation of frictional property of lubricants for hot forging of steel using low-speed ring compression test," *Procedia Eng.*, vol. 81, no. October, pp. 1970–1975, 2014.
[82] S. M. Hafis, M. J. M. Ridzuan, R. N. Farahana, A. Ayob, and S. Syahrullail, "Paraffinic mineral oil lubrication for cold forward extrusion: Effect of lubricant quantity and friction," *Tribol. Int.*, vol. 60, pp. 111–115, 2013.
[83] L. Wang, J. Zhou, J. Duszczyk, and L. Katgerman, "Friction in aluminium extrusion - Part 1: A review of friction testing techniques for aluminium extrusion," *Tribol. Int.*, vol. 56, pp. 89–98, 2012.
[84] M. Arentoft, N. Bay, P. T. Tang, and J. D. Jensen, "A new lubricant carrier for metal forming," *CIRP Ann. - Manuf. Technol.*, vol. 58, no. 1, pp. 243–246, 2009.
[85] Y. Sagisaka, T. Nakamura, K. Hayakawa, and I. Ishibashi, "Evaluation of environmentally friendly lubricant for aluminum cold forging using friction test based on spline extrusion," *J. Manuf. Process.*, vol. 15, no. 1, pp. 167–179, 2013.
[86] R. Matsumoto, K. Hayashi, and H. Utsunomiya, "Identification of friction coefficient in high aspect ratio combined forward-backward extrusion with pulse ram motion on servo press," *Procedia Eng.*, vol. 81, no. October, pp. 1854–1859, 2014.
[87] S. Syahrullail, B. M. Zubil, C. S. N. Azwadi, and M. J. M. Ridzuan, "Experimental evaluation of palm oil as lubricant in cold forward extrusion process," *Int. J. Mech. Sci.*, vol. 53, no. 7, pp. 549–555, 2011.

[88] C. Caminaga, F. O. Neves, F. C. Gentile, and S. T. Button, “Study of alternative lubricants to the cold extrusion of steel shafts,” *J. Mater. Process. Technol.*, vol. 182, no. 1–3, pp. 432–439, 2007.
[89] N. Bay, M. Eriksen, X. Tan, and O. Wibom, “A friction model for cold forging of aluminum, steel and stainless steel provided with conversion coating and solid film lubricant,” *CIRP Ann. - Manuf. Technol.*, vol. 60, no. 1, pp. 303–306, 2011.
[90] T. Schrader, M. Shirgaokar, and T. Altan, “A critical evaluation of the double cup extrusion test for selection of cold forging lubricants,” *J. Mater. Process. Technol.*, vol. 189, no. 1–3, pp. 36–44, 2007.
[91] W. Hu, “Plane strain extrusion forging process,” Dublin City University, 1992.
[92] V. Nagpal, “A lower upper-bound approach to some metal forming problems,” Georgia Institute of Technology, 1972.
[93] E. Siebel, *Die formgebung im bildsamen zustande : Theoretische grundlagen der technischen formgebungsverfahren*. Düsseldorf : Stahleisen, 1932.
[94] R. Hill, *The Mathematical Theory of Plasticity*. Oxford University Press, 1950.
[95] H. Hencky, “Über einige statisch bestimmte fälle des gleichgewichts in plastischen körpern,” *J. Appl. Math. Mechnaics*, vol. 3, pp. 24–251, 1923.
[96] G. Hilda, *Fondements mathématiques de la théorie des corps plastiques isotropes*, Mémorial d. Paris, Gauthier-Villars, 1937.
[97] P. L. B. Oxley and W. B. Palmer, “Mechanics of orthogonal machining,” *Imeche Arch.*, vol. 173, p. 623, 1958.
[98] R. Hill, “A theoretical analysis of stresses and strains in extrusion and piercing,” *J. Iron Steel Inst.*, vol. 158, pp. 177–185, 1948.
[99] E. G. Thomsen, T. Y. Charles, and K. Shirō, *Mechanics of Plastic Deformation in Metal Processing*. Macmillan, 1965.
[100] “Prikladnaia matematika,” *Prikl. Mat. i Mekhanika*, vol. 8, p. 201, 1944.
[101] R. T. Sheild, “On the Plastic Flow of Metals under Conditions of Axial Symmetry,” *Proc. R. Soc. A*, vol. 233, no. 1193, 1955.
[102] Thomsen, G. E. Yang, and J. T. Lapsley, “Experimental stress determination within a metal during plastic flow,” *Proc. Soc. Exp. Stress Anal.*, vol. 11, pp. 59–68, 1954.
[103] E. G. Thomsen and C. T. Yang, “An experimental investigation of the mechanics of plastic deformation in metals,” *Univ. Calif. Publ. Eng.*, vol. 5, pp. 89–144, 1954.
[104] A. S. Shabaik and S. Kobayashi, “Computer application to the visioplasticity method,” *J. Eng. Ind.*, vol. 89, no. 2, pp. 339–346, 1967.
[105] J. L. Gorden and A. S. Weinstein, “A finite element analysis of the plane strain drawing problem,” in *Proceedings of the North American Metalworking Research Conference*, pp. 194–208.
[106] N. R. Chitkara and A. Aleem, “Extrusion of axi-symmetric bi-metallic tubes : Some experiments using hollow billets and the application of a generalised slab method of analysis,” *Internaltional J. Mech. Sci.*, vol. 43, pp. 2857–2882, 2001.
[107] E. Prandtl, *Über die Härte plastischer Körper, Nachrichten von der Königlichen Gesellschaft der Wissenschaften zu Göttingen*. Math.-Physik.K1, 1920.
[108] H Hencky, “Uber einige statisch bestimmte falle des gleichgewichts in plastischen korpen,” *Math. Mech.*, vol. 3, pp. 241–251, 1923.
[109] H. Geiringer, “Beit zum vollstandigen ebenen plastiziotats problem,” in *3rd Int. Congr. Appl. Mech., Stockholm*, 1930, pp. 185–190.
[110] C.C. Yih, “Stream Functions in three-dimensional flow,” *La Houlle Blanche*, vol. 12, pp. 99–107, 1957.
[111] F. Gatto and A. Giadra, “The characteristics of the three-dimensional analysis of plastic deformation according to the SERR method,” *Int. J. Mech. Sci.*, vol. 23, no.

3, pp. 129–148, 1981.
[112] W. Johnson, R. Sowerby, and R. D. Venter, *Plane-Strain Slip-Line Fields for Metal-Deformation Processes*. Theory and Bibliography, 1970.
[113] W. Johnson, "Extrusion through wedge-shaped dies. Part II," *J. Mech. Phys. Solids*, vol. 3, no. 3, pp. 218–223, 1955.
[114] W.Johnson, "Extrusion through wedge-shaped dies. part I," vol. 3, no. 1950, pp. 218–223, 1955.
[115] B.B. Basily and D.H. Sansome, "Some theoretical considerations for the direct drawing of section rod from round bar," *Int. J. Mech. Sci.*, vol. 18, no. 4, pp. 201–208, 1976.
[116] B.L. Juneja and R Prakash, "An analysis for drawing and extrusion of polygonal sections," *Int. J. Mach. Tool Des. Res.*, vol. 15, no. 1, pp. 1–18, 1975.
[117] V. Nagpal and T. Altan, "Analysis of the three dimensional metal flow in extrusion of shapes with the use of dual stream function," in *NAMRC Conference*, 1975, pp. 26–40.
[118] D. Y. Yang and C. H. Lee, "Analysis of three-dimensional extrusion of sections through curved dies by conformal transformation," *Int. J. Mech. Sci.*, vol. 20, no. 9, pp. 541–552, 1978.
[119] S. K. Sahoo, P. K. Kar, and K. C. Singh, "Direct upper bound solution to rectangular-to-polygonal extrusion through square Die," *J. Manuf. Sci. Eng.*, vol. 121, no. 2, pp. 195–202, 1999.
[120] R. K. Sahoo, P. R. Samantaray, S. K. Sahoo, B. Sahoo, and P. K. Kar, "Round-to-channel section extrusion through linearly converging die: A three-dimensional analysis," *Int. J. Adv. Manuf. Technol.*, vol. 41, no. 7–8, pp. 677–683, 2009.
[121] E. M. Rubio, M. Marin, R. Domingo, and M. A. Sebastian, "Analysis of plate drawing processes by the upper bound method using theoretical work-hardening materials," *Int. J. Adv. Manuf. Technol.*, vol. 40, no. 3–4, pp. 261–269, 2009.
[122] U. Stahlberg and J. Hou, "A UBET-simulation meant for basic understanding of the extrusion of aluminum profiles," vol. 1, no. November 1995, 2016.
[123] L. Gusel, R. Rudolf, and B. Kosec, "Analysis of a strain rate field in cold formed material using the viscoplasticity method," *Metalurgija*, vol. 48, no. 2, pp. 103–107, 2009.
[124] U. C. Paltasingh, S. K. Sahoo, P. R. Das, K. C. Nayak, and S. Potnuru, "Lateral extrusion of spur gears with involute profile: Finite element analysis and experimental investigation," vol. 3, no. 7, pp. 20–30, 2013.
[125] S. Potnuru, R. Vinjamuri, S. K. Sahoo, and S. K. Sahoo, "Three-dimensional analysis of combined forward and backward extrusion-forging process using DEFORM 3D," *Appl. Mech. Mater.*, vol. 594, pp. 791–795, 2014.
[126] S. Bingol, O. Ayer, and T. Altinbalik, "Extrusion load prediction of gear-like profile for different die geometries using ANN and FEM with experimental verification," *Int. J. Adv. Manuf. Technol.*, vol. 76, no. 5–8, pp. 983–992, 2014.
[127] H. Yamin, L. Zhouyi, and Z. Yucheng, "The study of cup-rod combined extrusion processes of magnesium alloy (AZ61A)," vol. 188, pp. 649–652, 2007.
[128] C. Giardini, E. Ceretti, and G. Maccarini, "Formability in extrusion forging: the influence of die geometry and friction conditions," *J. Mater. Process. Technol.*, vol. 54, pp. 302–308, 1995.
[129] J. Vickery and J. Monaghan, "An upper-bound analysis of a forging-extrusion process," vol. 55, pp. 103–110, 1995.
[130] J. Monghan and J. Vickery, "An investigation of the early stages of a forging / extrusion process," *J. Mater. Process. Technol.*, vol. 43, pp. 37–50, 1994.

[131] L. Brayden and J. Monaghan, “An analysis of closed-die extrusion / forging,” *J. Mater. Process. Technol.*, vol. 26, pp. 141–157, 1991.
[132] H. Choi, J. Choi, and B. Hwang, “The forming characteristics of radial-backward extrusion,” *J. Mater. Process. Technol.*, vol. 113, pp. 141–147, 2001.
[133] D. R. Narayanasamy, K. Baskaran, S. Arunachalam, and D. M. Krishna, “An experimental investigation on barreling of aluminium alloy billets during extrusion forging using different lubricants,” *Mater. Des.*, vol. 29, pp. 2076–2088, 2008.
[134] B. C. Hwang, S. J. Hong, and W. B. Bae, “An UBET analysis of the non-axisymmetric extrusion / forging process,” *J. Mater. Process. Technol.*, vol. 111, pp. 135–141, 2001.